Squeeze Film Flow of Viscoplastic Bingham Fluids

Elaheh Esmaeili

Thesis submitted to the University of Strathclyde for the degree of

Doctor of Philosophy

Chemical and Process Engineering

University of Strathclyde

December 2022

Declaration of Authenticity and Author's Rights

'This thesis is the result of the author's original research. It has been composed by the author and has not been previously submitted for examination which has led to the award of a degree.'

'The copyright of this thesis belongs to the author under the terms of the United Kingdom Copyrights Acts as qualified by the University of Strathclyde Regulation 3.50. Due acknowledgement must always be made of the use of any material contained in, or derived from, this thesis.'

Signed: Elaheh Esmaeili
Date: December 2022

Dedication

This thesis is dedicated to the loving memory of my dear father, “Baba Ali”, who passed away unbelievably three months before I started my Ph.D.

Acknowledgements

Words cannot express my deepest gratitude to my supervisor, Dr. Paul Grassia for his invaluable patience, support, and feedback throughout this research. I could not have undertaken this journey without him who generously provided motivation, knowledge, and expertise. I am lucky to have had such an incredible supervisor, who not only was able to provide me with his support, inspiration, great advice, and guidance throughout my Ph.D. but also has given me the courage to flourish as a researcher.

Additionally, this endeavour would not have been possible without the generous financial support from the University of Strathclyde and the Department of Chemical and Process Engineering.

I am also grateful to my colleagues and cohort members, Yaw, Carlos, and Maclean for their time, help, and moral support. Special thanks should also go to Carlos for his invaluable assistance in programming throughout my project.

Lastly, I would like to thank and express my deepest appreciation to my family, especially my mother, my brother and my husband for their tremendous support in my life. Their belief in me has kept my spirits and motivation high during this process. I could not have pursued this journey without their continuous encouragement and emotional support.

Contents

List of Figures

List of Tables

Nomenclature

x	Cartesian horizontal coordinate
x_c	point along plate length where flow rate is zero
x_{cf}	final point along plate length where flow rate is zero
Δx_c	difference of x_c and x_{cf}
y	Cartesian vertical coordinate
u	velocity in x coordinate direction
u_{plug}	velocity of the plug region
v	velocity in y coordinate direction
v_{top}	velocity of the upper plate
t	time
g	acceleration due to gravity
p	pressure
Q	flow rate
L	half-length of the plates
H	gap thickness
H_0	initial gap thickness
H_{c0}	initial gap thickness at the centre of the plates
H_c	gap thickness at the centre of the plates
H_f	final gap thickness
H_{cf}	final gap thickness at the centre of the plates
ΔH	difference in gap thickness from the final state
ϵ	ratio between the gap thickness at the right hand end and centre
ρ	density
μ	viscosity
μ_p	viscosity of the yield stress fluid
τ	shear stress
τ_0	yield stress

$\dot{\gamma}$	shear rate
K	consistency in Herschel-Bulkley equation
n	flow index in Herschel-Bulkley equation
θ	tilt angle
δ	rescaled tilt angle
δ_{max}	maximum rescaled tilt angle
F_{app}	applied force
F	force
F_{yield}	yield force
y_{plug}	yield surface
Od	Oldroyd number
Od_{min}	minimum Oldroyd number
Od_{max}	maximum Oldroyd number
T	torque
T_{final}	final torque
T_{yield}	yield torque
T_{steady}	steady torque
η	ratio between tilt angle and Oldroyd number

Abstract

Squeeze film flow of a viscoplastic Bingham fluid between non-parallel plates has been analysed. It is assumed that the force applied to the plates is known, therefore, their velocity must be found, and the film thickness decreases then as time proceeds. Moreover, for non-parallel plates, the position along the plates at which flow reverses direction is found as part of the solution. In the Newtonian limit, the thickness of the gap between the plates in the parallel system never quite reaches zero at any finite time, while for the non-parallel case a finite time can be obtained when the plates touch one another at a point. In squeeze flow of a viscoplastic Bingham fluid between parallel and non-parallel plates, under a fixed applied force, a final steady film thickness can sometimes be reached. This final thickness turns out to be sensitive not just to the plate tilt angle but also to the so called Oldroyd number which is defined as the ratio between yield stress and imposed stress. Nevertheless for squeeze film flow of Bingham viscoplastic fluid between non-parallel plates, the results show that other cases exist in which the lubrication force cannot always balance the applied force, leading to the plates approaching and touching at the narrowest end of the gap. Moreover torques that develop within the system have been analysed.

On the other hand, there are flows of viscoplastic Bingham fluids in which motion decays to zero in finite time typically after a load is re-

moved: a final state is thereby reached after finite time. Analogous flows of Newtonian fluids need however an infinite time for motion to decay to zero. In this thesis, a flow of a Bingham fluid squeezed between two parallel and non-parallel plates is considered with the plates subject to a constant load. This admits a final state without any motion despite the load remaining present. Asymptotic analysis close to that final state is considered, which reveals that in the squeeze film configuration, a Bingham fluid requires an infinite (rather than a finite time) to stop moving. That said, the decay of the motion of the Bingham fluid is still shown to be asymptotically much faster than that of the equivalent Newtonian fluid.

It is known that the squeeze film flows have a myriad applications, one of which can be the foam-based papermaking process. As a case in point, in this thesis, the squeeze film flow of Newtonian and non-Newtonian fluids between two parallel and non-parallel plates has been investigated in an effort to understand the behaviour of foam-fibre suspensions in the foam-formed papermaking process. Pore size distributions in foam-formed paper tend to be more uniform than in water-formed paper, so the hypothesis explored is that this distribution might reflect uniformity or non-uniformity of gaps between fibres as either foam or water is squeezed out from between them. Data we examine however tend to contradict that hypothesis, suggesting that foam rheology alone is insufficient to account for pore size distributions.

Chapter 1

Introduction

This chapter provides an introduction for this thesis and consists of three sections. In section 1.1 the background of this thesis is presented. A brief discussion of the squeeze film flow is described in the background section. Then, the motivation for the thesis is considered in section 1.2 in which the gap in knowledge and importance of this research are delineated. Finally, the layout of the thesis is outlined in section 1.3.

1.1 Background to Research

Among the different classifications of fluids that flow [1, 2], from viscous Newtonian to non-Newtonian fluids, viscoplastic fluids and in particular viscoplastic Bingham fluids are of special interest due to their specific properties. That is, some materials may not flow until a critical stress called a yield stress is exceeded [3, 4]. These are yield stress or viscoplastic materials that present a plastic response or viscous resistance when they are undergoing deformation [5, 6]. In viscoplastic Bingham materials in particular, deformation and associated viscous dissipation only take place when the shear stress is greater than the yield stress, and material will otherwise behave as a solid. Thus, when

shear stress is less than yield stress, no deformation can be seen, but when the yield stress is exceeded, any stress in excess of that yield stress is accounted for the viscous resistance of the flow [7, 8]. Although yield stress fluids are complicated to deal with as it can be challenging to compute their flow properties, there is a large number of literature articles that studied the rheological flow behaviour of these fluids in various geometries (see [4, 6, 9, 10] amongst others). One of the motivating reasons to study the rheological characteristics of viscoplastic fluids is their applications in our daily lives, from foodstuffs such as pastes, foams, sauces to cements, paints and cosmetic products [9, 11].

Another of the motivations to study the rheology of materials is to use the data obtained via rheometry devices [1, 12, 13], in development of constitutive equations, calculations of flow behaviour in varied geometries, etc.. Indeed, non-Newtonian fluids (viscoplastic fluids amongst them) are often encountered in complex geometries. Thus, observing rheological properties of non-Newtonian fluids in various geometries is useful to model the design and operation of equipment utilized in process related industries that deal with such materials [1, 12]. For instance, designing equipment in food industry requires a comprehensive knowledge to elucidate and interpret the rheological data of the materials being processed [14–16].

A rheometer [14, 17] is a device that is used to measure the rheological properties of different materials in a very specific geometry, usually classified into two main types: rotational and tube type. This then reflects that flow can be studied in various geometries, but two of the simplest are steady shear flow and extensional rheological flow. Another geometry that has drawn attention however [18, 19] is the parallel plate squeezing film flow geometry in which the data from the instrument set up will be valuable for quality control tests by comparing with other rheometer flows.

The term squeeze film refers to a system in which a material is being squeezed between two approaching plates [20, 21]. Lubricated squeeze film flow has long been studied by Stefan [22] and Reynolds [23], but originally for Newtonian fluids. The work of Stefan [22] seems to be the first which has developed a model for the squeeze film behaviour. The work done by [22] investigated the force required to separate two parallel plates laid upon one another which is called apparent adhesion, and which differs in different environments such as in air, immersed under water and other liquids. From the experiments, it is found that the apparent adhesion for the plates immersed in water is bigger than the amount acquired for plates in air. After that, Reynolds [23] developed hydrodynamic lubrication theory and established the well known equations for a viscous fluid between two circular parallel surfaces approaching each other.

Squeeze film flow experiments can be done either under constant load or constant squeezing rate [21]. Squeeze film flow between parallel plates can be employed to interrogate rheological behaviour in other flows, such as shear flow or extensional flow, since squeezing can involve elements of both [14]. The fluid used in a squeeze film system can be either Newtonian or non-Newtonian. Thus much work has been done in the area of squeeze film flow using fluids with different constitutive behaviour [18, 19, 24–28]. Indeed, due to their complex characteristics, understanding the flow behaviour and deformation of non-Newtonian fluids in different geometries is particularly instructive. As mentioned though, one of the geometries in which the steady shear and also extensional viscosity fluid properties can be relevant is the parallel lubricated squeeze film flow configuration [20, 21, 29].

One of the pioneering works that advanced knowledge in the theory of viscoplastic Bingham fluids squeezed between parallel plates is the work of Covey and Stanmore [30]. They have done both experimental and theoretical investigations in a parallel plate “plastometer” to find the fundamental rheological

properties of the non-Newtonian fluids exhibiting yield stress. They used a constant force in their rheometer instrument to figure out the yield stress and other properties of Bingham fluid flow behaviour. Other work that has been done by Muravleva [28] provides a solution for the planar squeeze film flow of a Bingham fluid where a constant velocity has been considered, and the required squeezing force for the system has then been established.

There is however a connection between the constant velocity and constant load cases: much of the solution procedure of Muravleva [28] carries over to the constant load case, but an extra step is required matching the instantaneous squeezing velocity to the given specified load. In this thesis therefore, we follow the formulation utilized by Muravleva [28], even while considering a condition in which a constant load is applied on the plates in order to figure out the squeezing rate of the system. Although the work of Covey and Stanmore [30] already considered a constant load in the squeeze film flow of a Bingham fluid, in this study, we expand that solution for a different geometry (i.e. a non-parallel squeeze film flow configuration).

1.2 Motivation for Thesis

A viscoplastic Bingham fluid [6] has a defining characteristic in which it will deform when the imposed stress exceeds the yield stress. Gels, foams, suspensions, creams, pastes, some industrial oils and muds exhibit yield stress behaviour [31]. Our everyday life is surrounded by these materials. Hence, investigation of yield stress fluid behaviour in various geometries has been long a subject of interest, due to the complex behaviour exhibited and the applications in a wide variety of industries [18].

As has been mentioned, one of the interesting geometries in which to explore yield stress fluid characteristics is the squeeze film medium in which the ma-

terial can be deformed between two plates approaching each other [28, 30]. Again as has been mentioned, squeeze film flow can be performed with a constant squeezing force or a constant displacement rate. In both situations, depending on the surface configuration and fluid properties, the gap thickness between plates will be decreased and a certain time is required to squeeze out a specified amount of the material [20, 21, 29]: for yield stress fluids in particular, the long time behaviour might however be somewhat different in the constant force or constant rate cases [28, 30]. The behaviours of the squeeze film [32] have been widely studied in many application such as machine tools, joints and gears, bearings, rolling elements, etc., and in applications such as these, yield stress fluids such as gels may present different behaviours from purely viscous fluids.

As alluded to above, much work has been done in the area of squeeze film flows using various fluids, but the focus here is on viscoplastic ones. Key references namely, works by Covey and Stanmore [30] and Muravleva [28] have likewise already been discussed. Unsteady state evolution of a system of a lubricated parallel plate squeeze film for a yield stress fluid with a constant force have been investigated by Covey and Stanmore [30]. In this system, the squeezing rate of the flow under a constant force will slow down as time proceeds and eventually stop. This is due to the fact that the applied force on the plate will be sustained by the lubrication force that develops, but over time more and more of this lubrication force is contributed by yield stress rather than viscous stress. However, the Bingham fluid squeezed between parallel plates with a constant squeezing rate as has been done by Muravleva [28] will by definition not slow down. To compensate, for flow under a constant velocity, the force required for the squeezing action to take place will necessarily increase as the film thickness between plates decreases.

The studies mentioned above refer only to parallel plate geometries. Until

now (to the knowledge of this author), there is no known work done on the squeeze film flow of a viscoplastic Bingham fluid between non-parallel plates. Hence, this research seeks to explore the yield stress fluid behaviour between non-parallel plates squeeze film configuration under a constant applied force extending the approach taken by Covey and Stanmore [30] but making use also of the work of Muravleva [28]. This work is described in Chapter 3 and also in a paper published by the present author [33].

Although the works done by [28, 30, 33] have explored the unsteady state formulation of the squeeze film theory of a yield stress fluid, the detailed solution for the unsteady approach to the final steady state has not been considered. Approach to final state is generally of interest for viscoplastic fluids, since final states can sometimes be reached in finite time and motion then ceases [34, 35], even though an analogous Newtonian fluid might require infinite time to stop. This situation to be studied here is not quite the same as [34, 35] which involve removal of a force driving flow, whereas here a driving force is maintained. Even so, with this in mind, in this thesis, further work has been established the asymptotic approach to the final state in both parallel and non-parallel squeeze film flow of a viscoplastic Bingham fluid. This then is discussed in Chapter 4.

Moreover, what has motivated the present study are applications in which a viscoplastic fluid is squeezed out of a complex shaped gap. One such example is foam-based papermaking in which a foam carrier fluid is squeezed out from a network of fibres [36]. There is no need for the fibres in the network to be aligned parallel. Often moreover, length of the fibres is significantly greater than the size of the bubbles in the foam [37], in which case it might be permitted to treat the bubbles, at least in a rough approximation, as if they were a continuum. Foam-based papermaking is in fact a very complex system [36, 38], and the problem to be solved here is admittedly just a highly idealised version of it.

The extent to which foam rheology might or might not impact on the eventual structure of paper made from a foam-based process is discussed in Chapter 5.

1.3 Layout of Thesis

This thesis includes 6 chapters. The present chapter 1 has provided an introduction which contained the background to this research, and then the motivation for it.

Chapter 2 will consider the literature review of the thesis which begins by providing materials related to non-Newtonian fluid rheology. Then the viscoplastic Bingham fluids in particular and their properties and applications are reviewed. After that, the squeeze film flow theory in general and yield stress fluids squeezed between parallel and non-parallel plates are discussed. Finally, the last part of the chapter presents one of the potential applications of the squeeze film flow theory which is the foam-based papermaking process. We propose a hypothesis for how squeeze film flow in the process of making paper using a yield stress fluid such as foam might influence the properties of the paper eventually produced.

Chapter 3 will focus on the methodology of this research which develops numerical solution for squeeze film flow of viscoplastic Bingham fluids between non-parallel plates. The discussion will highlight the underlying physics and and analyse the mathematics of the equations. The final steady state situation reached after viscoplastic Bingham fluid is squeezed between non-parallel plates has been established in this chapter as well. Finally, section 3.3 discusses the results from the squeeze film flow system of viscoplastic Bingham fluids between the non-parallel plates.

Chapter 4 will consider one of the interesting characteristics of yield stress flu-

ids regarding how they come to a stop while the driving force is maintained. Specifically the chapter will investigate the asymptotic behaviour of the viscoplastic Bingham fluid approaching the final steady state situation when it is squeezed between parallel and subsequently non-parallel plates. Then, section 4.4 will consider the results obtained from equations derived from different systems (parallel or non-parallel) on the approach to final state.

Chapter 5 will consider the implications from the proposed hypothesis related to how foam rheology might influence the foam-formed papermaking process. This is included as an application of squeeze film flow of yield stress fluids which is reviewed in chapter 2.

Finally, chapter 6, will discuss the conclusions and potential research areas for the future.

Appendix A presents the squeeze film flow theory of Newtonian fluids between parallel and non-parallel fluids to provide the fundamental background for the concepts discussed in chapter 3. Furthermore, in appendix B, the principal equations, important effects and results of viscoplastic Bingham fluid squeezed between parallel plates are outlined in detail again to give insights into the discussion in chapter 3. The author's published paper is provided in appendix C.

Chapter 2

Literature Survey

This chapter covers some fundamental concepts of fluid mechanics which starts with rheology in section 2.1. Then in section 2.2 we review the viscoplastic Bingham fluids and their properties. After that, squeeze film flow theory will be discussed in section 2.3. Following that, in section 2.4 we specifically describe the squeeze film flow of viscoplastic materials. Finally, we outline a particular application in which the literature that we have reviewed thus far may be relevant, namely the foam-based papermaking process. This is discussed in section 2.5, along with some more general background on foams (which are viscoplastic fluids).

2.1 Rheology

The word rheology was first introduced by Bingham in 1928 [14, 39]. Rheology [12, 40] is defined as the "study of deformation and flow of matter". It is also described [41] as the investigation of the behaviour of materials in response to an applied stress or strain.

Elastic behaviour has been described by Hooke's law [12, 42] for solid materials. Viscous behaviour has been described by Newton's law [12, 43] for

liquids. Based on these two laws, there has been a distinction between solids and liquids. In Hooke's law, the strain (i.e. displacement) of an elastic object is proportional to the stress applied on that object. Meanwhile, in Newton's law, the required stress or force per unit area is proportional to the shear rate (i.e. shear strain rate) of a liquid. In fact, in both laws, linearity [12] is assumed between stress and strain or rate thereof. Thus, linearity applies to both Hookean solids and Newtonian viscous liquids. However, many materials that do not follow the aforementioned laws: these are called non-Newtonian or complex materials [12, 44]. Based on the definition provided by Crochet et al. [1], any fluids that exhibit behaviour which cannot be predicted by the Navier-Stokes equations (applicable to purely viscous fluids) are called non-Newtonian fluids.

Understanding the rheological properties of complex materials is of paramount importance in a wide variety of applications and industries such as food industry, engineering, materials science, etc.. Significant growth of rheology as a discipline has been seen in food industries in particular, due to the biological nature of foods rendering them very often complex [3]. The information from rheological properties of materials is used by researchers and industry alike to design operational equipment for processes [1]. There are also different instruments that are able to measure the rheological properties of materials which are called rheometers [14].

2.2 Viscoplastic Bingham Fluids

Viscoplastic fluids or so called yield stress materials are considered to be important class of non-Newtonian fluids. Our everyday life is surrounded by yield stress materials from food products such as pastes, gels, foams, to cosmetic products to muds, slurries, coatings, paints, cements, and various other household and industrial products [9, 45, 46]. One of the other applications of yield

stress materials is that they can be used as lubricants [47, 48] in hydrodynamic bearing devices to transport loads between two moving parts. Thus, it is useful to understand the rheological behaviour of yield stress materials in different applications.

Mathematical equations used to describe the rheological properties of materials may be called rheological models or constitutive models [3]. A Newtonian model for instance can be used to describe the rheological data of Newtonian viscous fluids. A Newtonian fluid [49] is characterised by having a linear relationship between the shear stress τ and shear rate $\dot{\gamma}$,

$$\tau = \mu\dot{\gamma} \tag{2.1}$$

where μ here represents the (constant) viscosity of a Newtonian fluid, whereas a non-Newtonian fluid has a more complex relation [14]. The fluids of interest in the present work, viscoplastic fluids (also known as yield stress materials as we have said) fall under the category of non-Newtonian fluids, such that their effective viscosity (i.e. ratio of stress to shear rate) changes with the shear rate.

For many non-Newtonian fluids, particularly viscoplastic ones, the measured flow curves e.g. from a rheometer are often fitted using the Herschel-Bulkley law [14, 50] which relates the shear stress τ and shear rate $\dot{\gamma}$ by,

$$\begin{cases} \tau = \tau_0 + K\dot{\gamma}^n & \text{for} \quad |\tau| > \tau_0 \\ \dot{\gamma} = 0 & \text{for} \quad |\tau| \leqslant \tau_0 \end{cases} \tag{2.2}$$

where τ_0 is yield stress (i.e. stress needed for the material to flow at all, the defining characteristic of viscoplasticity), $n > 0$ is flow index and K is called consistency.

For Newtonian fluids and Bingham viscoplastic fluids, the consistency term (i.e. K) is replaced by a viscosity term (denoted μ) and n is set to unity. For Newtonian fluids in addition, yield stress (i.e. τ_0) is zero. Meanwhile for power-law fluids that are classified into shear thinning or pseudo-plastic ($0 < n < 1$) and shear thickening or dilatant ($1 < n < \infty$), the yield stress τ_0 is likewise zero [14, 49]. The curves of shear stress versus shear rate for typical fluids explained above is depicted in Figure 2.1.

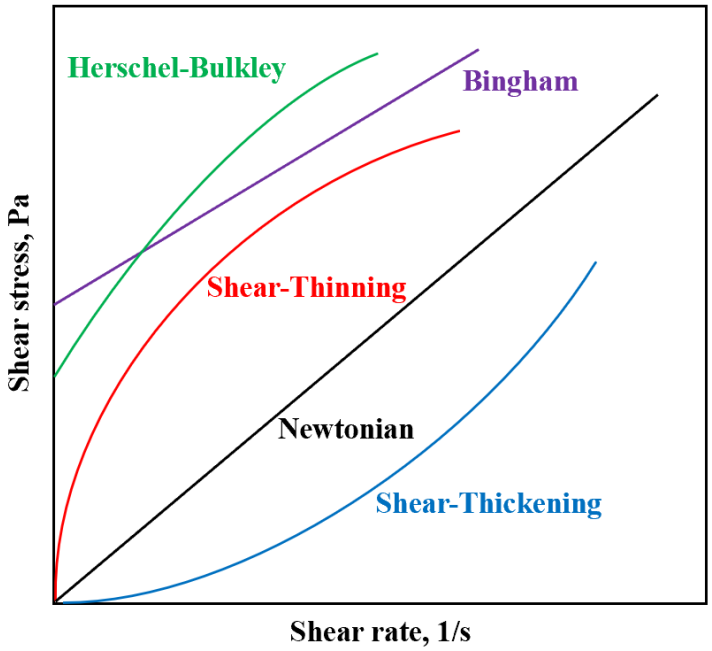

Figure 2.1: Shear stress against shear rate curves for different fluids [5, 14, 51].

As alluded to above, if a yield stress material has a flow index of unity [52], then the Herschel-Bulkley expression is reduced to a Bingham model equation [12, 39]

$$\begin{cases} \tau = \tau_0 + \mu_p \dot{\gamma} & \text{for} \quad |\tau| > \tau_0 \\ \dot{\gamma} = 0 & \text{for} \quad |\tau| \leqslant \tau_0 \end{cases} \tag{2.3}$$

in which μ_p is the "plastic" viscosity of a Bingham viscoplastic or yield stress material [7]. As is clear from the above equation, a yield stress material has an intermediate liquid/solid characteristic in which there is no flow when the shear stress is less than the yield stress, and it has a liquid-like behaviour if the shear

stress is larger than the yield stress [9, 14, 39, 46, 53]. As well as being difficult to start moving, viscoplastic fluids also stop moving easily. There are cases for instance in which viscoplastic fluid flows are known to stop moving in finite time [34, 35] (e.g. upon removal of a driving force), whereas an equivalent Newtonian fluid might require (at least in principle) an infinite time to stop.

Non-Newtonian fluids such as those discussed above have been studied in different geometries [1] such as steady shear flow, contraction flow, extensional flow, squeeze film flows, etc.. There is moreover a review by Bird et al. [54] in which the rheology and flow of viscoplastic Bingham fluids in particular have been investigated. In what follows, we specifically expand upon one particular geometry, namely lubricated squeeze film flows.

2.3 Squeeze Film Flows

Squeeze film flows [21] are flows in which a material is compressed between two approaching parallel or nearly parallel plane surfaces. They have myriad applications, including in areas such as engineering, biology, food industries, rheometry devices, compression moulding, papermaking, etc. [21, 55–57].

Squeeze flow tests can be carried out either using a specified shear rate (constant displacement rate) or a specified shear stress (constant load). Thus, results can be in the form of relations between force-height, force-time and height-time depending on how the test is done [21, 30, 55, 57]. The relation between the load-carrying capacity and the rate of approach, is the focal point of most squeeze film analyses.

The squeeze film flow for a sample is shown schematically in Figure 2.2. In Figure 2.2a, the material is confined between two plates, the lower plate is fixed and the upper plate is moving downward subject to a constant applied

force, $\hat{F}_{app}$ and this squeezes the sample. Figure 2.2b shows the sample after being pushed by the upper plate.

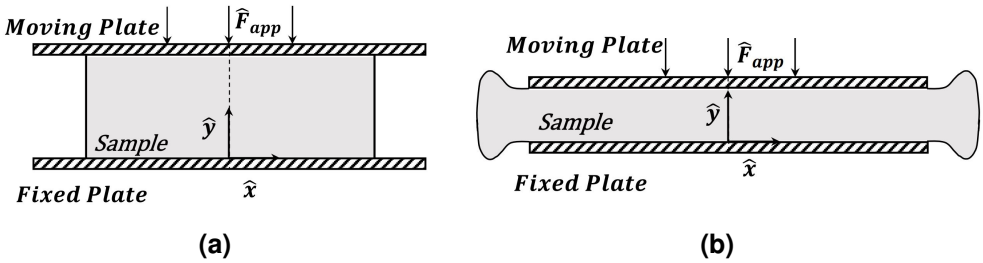

Figure 2.2: Geometry of squeeze film flow.

An early review on the subject of squeeze films was provided by Moore [21], who revised even earlier classical works of Stefan [22] and Reynolds [23]. Squeeze film flows of Newtonian and non-Newtonian fluids have been studied experimentally, theoretically and numerically. In particular, there is another comprehensive review by Engmann et al. [57] on squeeze flow theory and its applications in which a wide variety of materials (such as Newtonian, viscoelastic and viscoplastic) with different boundary conditions (i.e. perfect slip, no slip and partial slip) at the sample-plate interfaces have been investigated.

Assuming a no slip condition between the sample and the plates, at fixed applied force (i.e. constant load), the shear rate in the squeeze film tends to fall as time proceeds (even the Newtonian case implies that in fact, see appendix A). For one class of non-Newtonian fluid, so called viscoelastic fluids, this then means that elastic effects are likely to become less important over time [58] (viscoelastic fluids behave closer to Newtonian as shear rate falls). On the other hand, for a pseudo-plastic power law fluid say, it implies that the effective viscosity rises as time proceeds (the flow necessarily slows down relative to a Newtonian case) [55, 57, 59]. The same is true for viscoplastic fluids: effective viscosity (ratio of stress to strain rate) rises and the impact of yield stress is greater as time proceeds. Squeeze flow can thereby be used to gain insights into different rheologies [5, 60, 61].

In summary, squeeze flows are applicable in many industrial processes [62]. Meanwhile understanding deformation and flow of non-Newtonian fluids is of utmost importance as many fluids (including e.g. foams, emulsions and suspensions) utilised in industrial processes are non-Newtonian [19]. As a result, understanding squeeze flows of non-Newtonian fluids is important. Indeed there are several published articles, as discussed in more detail below, investigating squeeze film flow of complex non-Newtonian fluids either experimentally or numerically.

One such complex fluid for instance would be an electrorheological (ER) fluid used in vibration control devices, dampers, automotive and aerospace industries [63, 64]. An experimental study of squeeze flow of ER silica suspensions was carried out by Chu et al. [65] to evaluate the ER rheological properties and also squeeze flow performance. Theory for squeeze flow of an elastic Oldroyd fluid meanwhile has been considered by Phan-Thien and Tanner [66]. Further to this, temperature dependence and viscoelastic effects of an elastic Oldroyd fluid using squeeze flow between infinite plates have been studied numerically by Debbaut [62], By virtue of a finite element method, a fountain flow was observed at the outer border of the sample. However, rather than considering a fixed applied force (i.e. constant load) the required force for squeeze action was determined in that case with a constant squeeze velocity applied. In yet another study, the thermo-hydrodynamic properties of a non-Newtonian power law fluid by applying squeeze flow was investigated [67]. A complex interrelation between squeezing dynamics and rheology of the fluid has been established. Consequently, the results would be beneficial for industries which involve designing engineering devices including squeezing and extrusion of non-Newtonian fluids such as these. In what follows, we focus however on squeezing of a viscoplastic Bingham fluid.

2.4 Viscoplastic Bingham Squeeze Film Flows

Viscoplastic Bingham or yield stress materials [4, 10, 68] are of special interest in squeeze film situations [56, 57, 69], since they flow as a fluid when the imposed stress is bigger than the yield stress but can be treated as a plug-like solid when the imposed stress is less than the yield stress. Since, as already mentioned, the flow slows down over time under constant load, more and more of the fluid is expected to enter that plug-like regime. Indeed as shown in Figure 2.3, the squeeze film flow field for a viscoplastic fluid is often considered to be divided into two regions [19, 28, 70], yielded (fluid) and plug (unyielding) region. The surface which separates yielded and plug regions is called the yield surface [71].

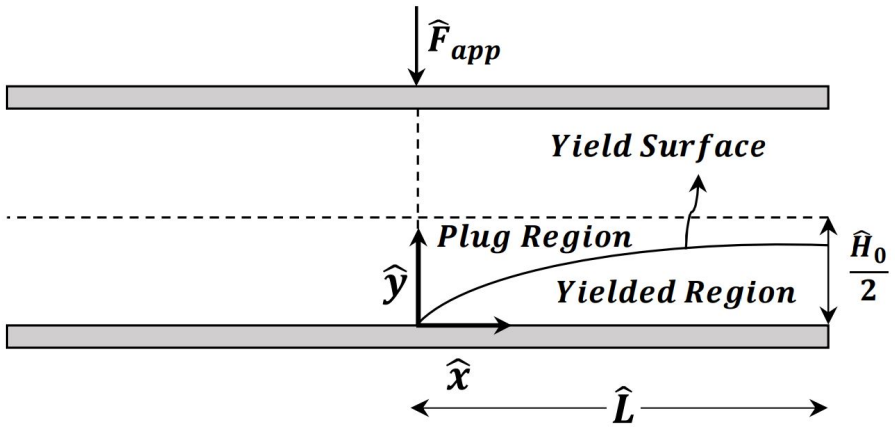

Figure 2.3: Schematic representation of the flow structure showing yielded and plug regions. The sketch shows the case for the initial film thickness, $\hat{H} = \hat{H}_0$, but generalizes to any other $\hat{H}$ at subsequent time.

During squeeze film flow under constant load, as time proceeds, the yield surface would be expected to shift so that, as mentioned, more and more of the flow domain is in the plug region and less of it is in the yielded region, until the yielded region disappears and the flow has stopped altogether, even whilst the squeeze film can remain at a finite thickness [30, 52, 56].

These flows are however less simple than might first appear. When coupled with conventional lubrication theory applicable in small aspect ratios, they lead

to an apparent paradox (the so called “lubrication paradox”) [19, 25, 31, 70]. It is predicted that the plug region in Figure 2.3 has a variable velocity at different locations in x direction. Hence there is predicted to be a non-zero strain rate in the normal direction even in the (supposedly non-yielding) plug region, albeit this is of much smaller magnitude than the shear strain rate in the yielded region. The paradox has however been resolved by Walton and Bittleston [72]. That analysis revealed [72, 73] that the yielded region was in fact what was termed a “fully-plastic” region, in which even the dominant shear stress component exceeded the yield stress. On the other hand, the plug region was revealed to be merely a “pseudo-plug”. When normal stresses (in addition to shear stresses) as well as perturbations over and above the leading order horizontal flow are taken into account, the “pseudo-plug” was found to be at a stress condition just slightly in excess of the yield stress. This then admitted the required non-zero strain rate there, which as mentioned, is smaller than the shear strain rate in the “fully-plastic” region. The “fully-plastic” and “pseudo-plug” regions were separated by what was termed a “fake yield surface”. For the present work however it is sufficient to consider just the leading order horizontal flow and the pressure field that is associated with it. For simplicity then we continue to use the terminology “yielded”, “plug” and “yield surface” rather than the terms “fully-plastic” “pseudo-plug” and “fake yield surface” [72, 73].

As already alluded to above, squeeze film flow between parallel plates say can be considered either with constant rate or constant load. The work done by Covey and Stanmore [30], investigated the behaviour of a yield stress material between two parallel plates with a constant load, theoretically and experimentally. However, this work did not deal with the non-parallel plate geometry, to be discussed in chapter 3 onward. Nonetheless it was one of the early works that advanced the study of Bingham fluid behaviour in parallel plate plastometers.

Following on from this, other research has been undertaken in this area: e.g.

squeeze film flow in different geometries, with various applications in mind and using various (viscoplastic) fluid types and materials [5, 19, 27, 28, 74]. The work of Muravleva [28] for instance provided an asymptotic solution for the two-dimensional planar squeeze film flow of a viscoplastic medium and analytical solutions for the flow fields have been compared to numerical computations. We will make use of these solutions. Nonetheless the work done by Muravleva [28] and likewise by Smyrnaios and Tsamopoulos [19], again only investigated the squeeze flow of a viscoplastic fluid between parallel plates with a constant squeezing rate. This requires in particular that larger squeezing forces are applied as time proceeds, with the squeezing force needing to become arbitrarily large as the gap narrows.

Few studies though have investigated non-parallel squeeze film flows. The squeeze film flow, albeit of a viscous Newtonian fluid, between inclined plates has been considered theoretically and experimentally by Moore [75]. The squeezing or sinkage rate (i.e. the velocity of the inclined plate) and film thickness changes with varying the loading force and time were established. Flow of two viscoplastic fluid types on an inclined plane (and opposed to between inclined plates) has been studied by De Kee et al. [76] theoretically and experimentally. Two models were utilized (i.e. Herschel-Bulkley and another model proposed by Kee et al. [77]) to determine the yield stress of two viscoplastic fluids. The work done by Koblitz et al. [78] has carried out the two-dimensional numerical simulation of the squeeze film flow of a viscoplastic fluid between two approaching circular cylinders. In another study conducted by Vajravelu et al. [79], the peristaltic flow of a Herschel–Bulkley fluid was examined in an inclined tube.

These studies have not however used the aforementioned calculation procedure of Covey and Stanmore [30] (originally developed by [30] for parallel squeeze films) to establish under constant load conditions what the final

steady state of a viscoplastic Bingham fluid might be in a non-parallel squeeze film system. Instead they have tended to use different geometries and even different fluids. Thus, in the present work (see chapter 3 onward), non-parallel squeeze flow of a viscoplastic Bingham fluid with an assumption of a fixed squeezing force (arguably more realistic than constant squeezing rate which requires an ever increasing force) is developed. In the present work, the final steady state of the system is identified, and it is also considered how the squeezing rate varies with time (up to the final state). A number of features specific to non-parallel plates i.e. identifying the position along the plates at which flow direction reverses as well as evolution of torque, will also be described in subsequent chapters.

2.5 Foam and Papermaking

Foam (i.e. gas bubbles dispersed in a liquid phase) is relevant to this thesis as it is a typical example of a viscoplastic fluid. Some of the properties of foam, along with their relevance to applications which helped to motivate the present study (specifically foam-based papermaking and pressing/squeezing flows that occur during papermaking) are discussed below.

2.5.1 Physics of Foam

A two-phase system of liquid and gas in which gas bubbles are surrounded by liquid films is called aqueous foam. This liquid phase consists of a liquid, mainly water and a surfactant which stabilises the films and allows foams to exist. Moreover, surfactants are concentrated at the gas-liquid interfaces and help to decrease the surface tension reducing the surface energy cost. Surfactant molecules can also prevent the rupture of liquid films through increasing the viscoelasticity of the interfaces and producing colloidal forces between bubbles

that can oppose film thinning [80, 81].

Generally speaking, the thickness of the liquid films enclosing gas bubbles can be in the range of 10 nanometre to a few microns [80]. A foam film can reach a stable configuration when there exists a balance between the pressure difference across the gas-liquid interface and the net surface tension force acting on the interface in the presence of film curvature. When a foam drains to equilibrium, the pressure in the gas bubbles is different from the pressure of the liquid and this difference is due to capillary and disjoining pressures, whereas, the pressure in the liquid can be defined by the hydrostatic laws at least in a static foam [82].

Foams can be categorized into two regimes of wet and dry in terms of the relative proportion of liquid and gas. Although finding a precise boundary for these two regimes is not straightforward, a foam with gas content below around 80 percent can be treated effectively as liquid (it tends to deform much like a liquid would), thus it can be called wet foam [83]. Meanwhile dry foams contain little liquid thus, having very thin liquid films and also very thin liquid-filled channels at which different films meet. For a wet foam, gas bubbles are almost spherical with little contact between them due to the presence of a thick layer of liquid separating the gas bubbles [84]. Bubbles in dry foam however are not spherical, and make direct contact with numerous neighbours.

Now, based on the properties explained for viscoplastic Bingham fluids in section 2.2, foams particularly dry foams, can be classified as yield stress materials. The reason is that bubbles in a wet foam are unjammed, but in dry foam they are jammed together such that their motion is constrained by neighbouring bubbles [85]. If just a small amount of stress is applied, the jammed foam deforms like an elastic solid, and bubbles retain their neighbours [86]. If instead large stress is applied however, bubbles can change their neighbours

and yielding occurs [86].

2.5.2 Foam Generation

Foam can be produced in different ways, such as, blowing or injecting gas into the liquid phase through a nozzle or a porous plug (which is called the sparging process), shaking or beating the liquid and nucleation of gas bubbles in a supersaturated liquid phase [80]. Therefore, each method has specific application. For instance, most everyday foams can be produced by shaking and beating the liquid or even the nucleation method, while blowing or sparging methods can be used to produce foams for laboratory or industrial applications. The foam generation method used in the system of interest to us, foam-based papermaking, is mechanical mixing of water and surfactant with gas within a vessel [83].

To summarise the discussion to date, foams are ubiquitous, have interesting physics (including yield stress behaviour), are straightforward to generate, and have different applications such as fire fighting, enhancing oil recovery, food and drinks applications, and so on [80]. Here however our focus is to be on foam-based (also known as foam-formed) papermaking, as described in more detail below.

2.5.3 Rationale for the Foam-formed Papermaking Process

Although technology has revolutionized the way people communicate, there is still a tremendous demand for using paper at offices, producing books, newspapers, packaging etc.. Paper therefore remains an important commodity, combining wood as raw material and significant volumes of water during the papermaking process. Given the extremely large volume of paper production [87], even small percentage increases in the efficiency of the papermaking

process translate into massive sustainability gains.

Increasingly however, many communities around the globe are confronting the problems of water stress and/or water scarcity. There is an extreme competition for water worldwide [88]. Climate change, global population rise, the expansion of cities, dietary changes, and the emerging biofuels industry are factors putting the world's water supplies under pressure. Therefore, seeking a new holistic approach to water management is needed.

Reducing the water footprint of the papermaking process will help significantly to alleviate the aforementioned issues [89]. Recently, there has been an increasing interest in so called foam-forming technology which helps saving energy and raw materials in the papermaking industry. Replacing water by foam as a carrier for the fibres utilized in papermaking will lead to sustainability gains through using less water. Given that foam is typically just several percent by volume water, using foam in lieu of water in the papermaking process will not only decrease the water consumption considerably but also the required energy for the paper drying process [82, 90].

To summarize, foam-forming is of great advantage to the papermaking industry in comparison with water-forming. Using foam instead of water in papermaking have been considered as a sustainable solution which reduces water use in the process significantly [91]. Accordingly, research on the papermaking process using foams and investigation of the final properties of papers that are formed with foams has been increasing over the years: a recent review can be found in [36]. Some of the main research advances in the field are discussed in the next section.

2.5.4 Properties of Foam-formed Paper

Foam-forming can provide the possibilities to control the structure of subsequent paper sheets [92]. It has been reported that there is a different behaviour while producing paper sheets, specifically in the wet-pressing step, between water and foam-forming processes. At this stage, a higher "thickness recovery" (applying a load, then removing it and measuring how much thickness recovers after removing the load) is observed for the foam-formed papers rather than water-formed ones [93]. One possible explanation of this behaviour is the unique structure of fibre networks made by foam which is able to remove plastic deformation of fibres and subsequently reduce the stresses on the fibres during the pressing stage [93].

Subsequent to wet-pressing, one of the most important properties of paper which directly affects the drying, coating and printing processes, is pore size distribution which is more uniform with also bigger pores on average for foam made papers compared to water-formed sheets [83]. In addition to that, one of the effective controlling factors on pore size distribution of final fibre networks is the type of fibre used in the papermaking process [83, 89]. In what follows, we consider not only pore sizes but also bubble sizes, fibre types as well as mechanical properties.

2.5.4.1 Bubble Sizes

It is observed that during foam generation, adding fibres often leads to a decrease in the bubble size due to the effect of fibres in enhancing the shear forces that drive bubble break up [84]. Moreover, different fibre types can change the bubble size considerably [94]. For instance, using natural wood fibres (which contain a substantial proportion of sub-micron fine fibrillar particles and have rough surfaces and broad size distributions) reduce the bubble size

significantly. The possible explanation suggested by Al-Qararah et al. [94] for this behaviour is that these fine particles can be adsorbed on the interfaces of foam bubbles and as a result, help to stabilize those interfaces. Meanwhile, using short regenerated cellulose fibres [94] (regenerated fibres have smoother surfaces than the natural wood fibres and their length varies from 0.35 mm to 10 mm) can boost the foam bubble size slightly in comparison with the bubble size in pure foam without fibres. It is proposed by Al-Qararah et al. [94] that these regenerated fibres are able to stick to those bubbles with diameter equal to fibre length. Therefore, fibres not only decrease the shear forces driving break up but also protect the interfaces of bubbles.

2.5.4.2 Pore Sizes

Bubble size distributions aside, it is noticed that there is a direct relationship between the proportion of large pores in paper structures and foam-fibre interactions in which the proportion of large pores is greater for the sheets produced by foam-forming [89]. As has been mentioned already, foam-forming can be applied to manufacture fibrous structures typically with more uniform pore size distribution than papers made by traditional water-forming. One of the possible reasons for producing these uniform fibre networks can be explained by the reduced flocculation of fibres as their movement is confined in the foam [82, 93].

One study which considered pore size distribution in detail was the work of Al-Qararah et al. [83]. This used foams to produce paper and studied the subsequent structure of paper thereby made. According to the approach they used for making paper, firstly foam was generated through mechanical mixing of water containing surfactant with gas. Then a suspension of fibres and aqueous foam is transferred to a screen and finally foam is removed using vacuum. This technique can provide many advantages. For instance, in the foam-fibre

suspension medium, foam bubbles have the property to enclose fibres and thus fibre transport is blocked and this gives less agglomeration in the web of sheets. In addition, Al-Qararah et al. [83] showed that this method reduces the energies required for de-watering and incorporating air drying of the foam-fibre suspension will provide bulky fibrous network structures.

A typical pore size distribution found by Al-Qararah et al. [83] is shown in Figure 2.4. This will be discussed in more detail in the next subsection.

2.5.4.3 Relationship between Fibre Types, Bubble Sizes and Pore Sizes

The link between properties of foam and subsequent pore structure in foam-formed fibre networks was studied by Al-Qararah et al. [83]. They found a different pore size distribution in sheets made with foam-forming compared to water-formed ones. The impacts of different parameters such as, type and concentration of surfactant, different types of fibres, rotational speed of mixer and air content of the foam upon the pore size distribution of sheets made by either foam or water were investigated. The results indicate that pore size distribution might indeed be affected by the properties of the foam.

Thus, foam-forming is recognized as a technique in which the characteristic form of pore size distribution can be controlled. Meanwhile this distribution cannot be manipulated so easily for the case of water-forming, consequently, the proportion of large pores is fairly small [95].

The average bubble radius of the foams used in the experiment of Al-Qararah et al. [83] was approximately 30 micron (i.e. 60 micron bubble diameter) and fibre length was about 1.6 mm, so fibres were much larger than bubbles. Average pore size was also a similar order of magnitude to, but slightly larger, than bubble size (see Figure 2.4). Moreover based on the results shown in Figure 2.4, more large pores are observed in the foam-formed sample, while there

are typically smaller pores on average in the sample made by water. Indeed Al-Qararah et al. [83] suggested that there may be an effect of foam bubbles in which they act like “ghost particles” during foam-forming. Since pores could not be smaller than the “ghost particles” this then would be a plausible reason for forming larger pores when using foams, albeit not the only possible explanation. They also stated that geometric restrictions caused by bubbles not only affect the location and orientation of fibres, but can also influence their bending.

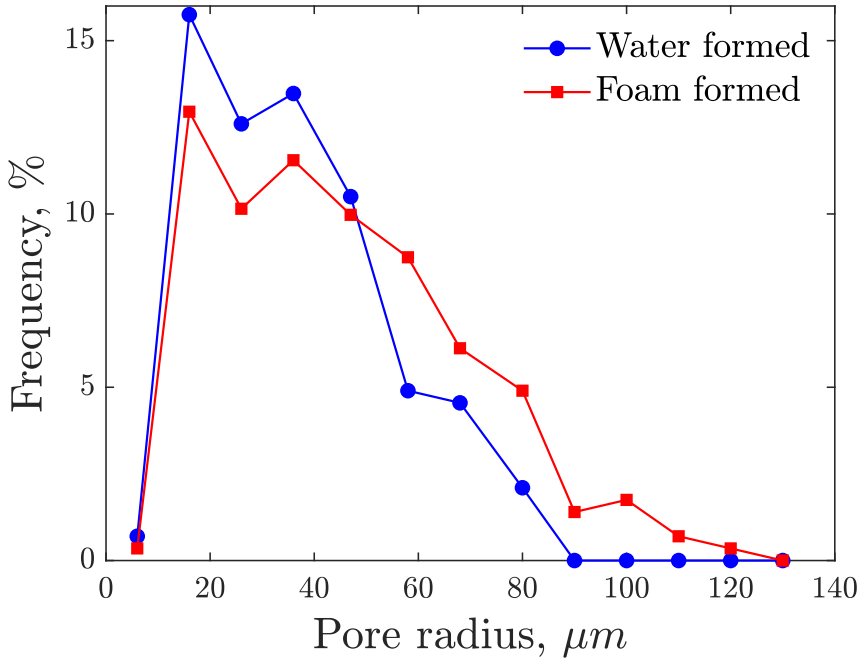

Figure 2.4: Pore size distribution of water and foam-formed samples with the average bubble radius of 30 μm for foams [83].

Subsequent studies have considered pore size distributions as well. The work of Al-Qararah et al. [89], focussed on achieving a micro-structure of fibre networks made from foam used as a suspending medium. A wider pore size distribution accessing larger pores is achieved for the case of foam-formed sheets compared to water-formed ones. The impact of different types of fibres on pore size distribution of resulting fibre networks was studied. It was concluded that using flexible fibres leads to smaller pore size distribution, while

the pore size of the stiff fibre networks can be influenced by the bubble size distribution of foam, although data in [83] suggest that bubble size distribution has only limited impact on pore size, compared at least to the impact that fibre type has.

Returning to consider [89], in addition, fibres can reorient and bend during the interaction with bubbles due to the geometric restrictions caused by bubbles. Moreover, it was mentioned along the same lines as [83], that bubbles can potentially behave like “ghost particles” during foam-forming, limiting how small pores are allowed to become and thus, leaving more large pores in the sheet structures once the sheet is formed. It is possible to speculate however that foam rheology (or even foam-fibre suspension rheology) might be a surrogate measurement for bubble size, which suggests that rheology of foam-fibre suspensions might be of interest, a point we will return to later.

Meanwhile [92] and the follow up study [96] modified the process of foam-formed papermaking and explored a new technique to produce lightweight fibrous networks using foams. Their approach involves slowly draining (and thereby drying) the foam-fibre suspension until all foam has disappeared. This method was able to result in very thin fibrous structures. Moreover using this method, the properties of resulting structures such as, strength, density and thickness could be effectively controlled by manipulating the initial liquid fraction of the foam and initial fibre concentration. The follow up study [96] examined both bubble size distributions and pore size distributions and found they were comparable, lending some support to the notion of ghost particles. This work of Burke et al. [92, 96] (i.e. carrier fluid draining slowly away from the fibres) differs however from industrial-scale papermaking in which carrier fluid generally needs to be separated rapidly from the fibres via pressing.

2.5.4.4 Mechanical Properties

In work carried out by by Jarvinen et al. [93], the compression behaviour of foam-formed and water-formed wet sheets has been studied. The experimental results obtained from their work suggest that the solid contents (i.e. solid mass fraction) in paper produced using foam are higher compared to water-formed papers which is due to the better sheet formation and usage of higher consistency for the fibres (consistency is the mass fraction of the solid fibres in the water suspension before mixing the foam) and also the low surface tension of the aqueous phase in the case of foams. They also found that permeability of fibre networks made by foam-forming leads to achieving a uniform de-watering process. According to the work of Alimadadi and Uesaka [97], which investigated the structures and mechanical properties of three dimensional fibre network structure made by foam-forming, using foams in papermaking process helps in boosting bulk and softness features of papers produced from long and fine fibres at higher consistencies.

The effects of utilizing foam-forming on producing lightweight three dimensional fibre structures has been studied by Burke et al. [92], albeit with carrier fluid being separated from fibres via drainage rather than pressing (see section 2.5.4.3). They found that fibre concentration and initial liquid fraction of the foam-fibre suspension have direct impact on compressive strength and density of the fibrous structures. There is a linear relationship between density of the final product and fibre concentration of the initial suspension which for densities less than a specific amount, samples cannot behave stably mechanically. Their results showed that the compressive strength of samples increases linearly with the sample's density. They also suggested that adding bonding agents can help enhance the compressive strength of fibre networks.

2.5.5 Foam-formed Papermaking from a Rheological Viewpoint

In order to gain insights into the properties of foam-formed paper, and in order to process the foam-fibre suspensions that are utilised in foam-formed papermaking, it is helpful to understand their rheology. Although foam rheology has been studied extensively, foam-particle systems have received less attention [98]. Flows of particles suspended in fluid occur in a number of contexts [99–102] amongst them papermaking. Therefore, at the most basic level we need to understand the case of single fibre in fluid [103], before tackling multiple fibres. Yet more complexity is anticipated of fibres suspended in a foam (non-Newtonian fluid), as opposed to in a Newtonian fluid which is simpler [104].

In the context of foam-based papermaking, a previous study has treated just a single fibre (as a chain of approximately 50 disks tethered together and interact with enclosing bubbles), with both the fibre and the foam bubbles surrounding it as discrete objects [37]. Fibres are likely to undergo a tumbling motion, in the same way that rigid rods would in a shear flow [103, 105]. Even though the work of Langlois and Hutzler [37] resolved both fibres and foam bubbles, in reality the fibres (at least in their longest dimension) are many times larger than the foam bubbles. According to the study of Haffner et al. [90, 91], the fibres (average length 2.3 mm, average diameter 35 micron) are an order of magnitude larger than the bubbles (average bubble diameter 170 micron to 220 micron depending on the system). That then suggests using a discrete model for the fibres but a continuum model for the foam, as is considered next.

2.5.5.1 Discrete Objects within Continuum Fluids

The objective is to study the foam-fibre system rheology but to describe the system using a discrete model for each fibre as per [106], but a continuum

description of the foam, the latter treated as a yield stress material, with the foam yield stress being sensitive both to bubble size and foam liquid fraction [107, 108]. This approach should be more computationally efficient than the fully discrete models used hitherto, and should then meet the objective of studying foam-mediated interactions between a collection of fibres (as opposed to just a single fibre as per the previous study of Langlois and Hutzler [37]): clearly it is important to consider more than one single fibre in the context of papermaking.

The study of elongated objects such as fibres moving in continuum fluids has a long history. The work of Jeffery [103] for instance calculated the angular motion and dissipation for a small ellipsoidal particle in a viscous fluid. Properties of the bulk stress in a suspension of non-spherical particles immersed in a Newtonian fluid have been studied by Batchelor [104]. The work of Keiller and Hinch [109] found the constitutive equation for a suspension of rods in a Newtonian fluid as a Newtonian term, plus a non-Newtonian contribution from the rods. Additional complexity arises here because fibre suspensions are typically classified into three concentration regimes: dilute, semi-dilute, and concentrated [110, 111], based on their volume fraction.

The dilute regime is such that the fibres within the suspension are sufficiently far apart that they are free both to rotate and translate without contacting one another. The transition to semi-dilute occurs when hydrodynamic interaction between fibres is the predominant phenomenon albeit with little actual fibre contact: a fibre is likely to have neighbouring fibres within a distance on the order of one fibre length away, but because the fibres are long, slender objects with varying orientations, they are not necessarily in direct contact. As they move through the foam, fibres produce flow fields which in turn influence the motion of other nearby fibres. Even when the volume fraction occupied by the fibres remains comparatively small (i.e. semi-dilute), owing to their elongated

shape, they can actually interact via the fluid flow field and hence influence the flow very strongly. In the concentrated regime however, fibre-fibre interactions dominate and this can eventually lead to solid-like jamming behaviour typical of sufficiently concentrated suspensions [112]. All of the above studies however concern fibres or rods moving in Newtonian fluids. Any non-Newtonian behaviour arises thereby from the presence of the fibres, but not however from the carrier fluid.

Fibres (or solid objects more generally) that are moving through viscoplastic yield stress materials have been modelled by [113–115]: techniques used involve finite element, finite difference or even spectral methods. In addition to those sorts of techniques, fibres in a purely viscous liquid can be described by a so called boundary element technique which uses analytic formulae for describing what is happening throughout the bulk of the liquid, and so only needs to be solved around the boundaries of the domain [116]. This reduces the dimensionality of the problem, speeding up the solution technique immensely. Unfortunately however, the analytical approaches [104] underpinning the boundary element technique lose their validity in the case of fibres suspended in foam (as a result of the greater complexity, i.e. non-linearity of the viscoplastic fluid rheology compared to simple viscous liquids). Nonetheless boundary element techniques for objects suspended in and moving through simple viscous liquids could still be used to validate say a finite element technique applied to objects in those same simple liquids. Then that finite element technique could be extended to fibres suspended in a viscoplastic fluid such as foam for instance.

It is clear from the above discussion that modelling flows involving a collection of fibres in a viscoplastic fluid (such as would occur in foam-based papermaking) remains a challenging task. To a large extent, the challenge here is that obtaining mechanistic understanding of how foam-fibre suspensions behave

during the foam based papermaking process involves incorporating foam-fibre interactions and foam-mediated fibre-fibre interactions into the description. Obtaining such understanding is however far from straightforward though because foams are themselves considered to be complex fluids [117]. Nevertheless the first step toward understanding all of this must be to understand the properties of the underlying elements, namely the fibres and the foam, and ultimately how these govern the processing of and properties of foam-formed paper.

As we have mentioned earlier, an important step in the papermaking process is pressing. In what follows therefore we consider a system which is specifically subject to pressing. Section 2.5.6 proposes a hypothesis for how a system might evolve during pressing if foam behaves like a continuum fluid (even though surrounding fibres remain discrete), and how the continuum fluid properties then affect the characteristics of a resulting fibre network structure. Pressing however is effectively a squeeze film flow, so the hypothesis links back to the discussion given earlier on viscoplastic squeeze flows.

2.5.6 Hypothesis

As just mentioned above, one interesting application of squeeze film flow with viscoplastic fluids is foam-formed papermaking. As has been alluded to, foam-forming technology for manufacturing paper is a novel technique in which the paper sheets are made from a suspension of pulp fibres in foam, rather than a suspension of pulp fibres in water. The properties of foam bubbles along with foam rheology potentially play a role in producing a fibre network with improved characteristics compared to water-formed papers, including more uniform pore size distribution, increased strength, different density, etc. [36, 83, 96, 118].

As we have already discussed, pore size distribution is amongst the most commonly measured properties [119], and from it one can deduce an average pore

size and also a measure of polydispersity, i.e. standard deviation of pore size divided by the average. A hypothesis commonly made in the foam-formed papermaking literature is the aforementioned “ghost particle” hypothesis, namely that the pore size distribution is simply inherited from the bubble size distribution of the foam used to make the paper [89, 120].

During any papermaking process, regardless of whether the pulp fibres are suspended in water (as in conventional papermaking) or suspended in foam, a step typically arises in which the fibres must be pressed together and the carrier fluid squeezed out [38]. As a model for contrasting water-forming versus foam-forming, the present work investigates the effect of squeeze film flow of water as a Newtonian fluid versus that of foam as a viscoplastic Bingham fluid between two parallel and non-parallel fibres. Treating fibres as discrete but the foam between them as a continuum recognises that fibre lengths often far exceed bubble diameters [37, 106] as has been mentioned. In such a model, bubble sizes then impact the squeezing behaviour, but not in the form of “ghost particles”. Instead bubble sizes impact only to the extent that yield stress of a foam treated as a viscoplastic fluid scales typically as the ratio between surface tension and bubble size [80, 107, 108]. Thus, yield stress is a surrogate for bubble size.

Using a model like that enables us to predict how rheological properties of foam might affect the size of the voids or pores between fibres during the foam-forming process. The investigation of non-parallel squeeze flows is of particular interest to study the potential impact of foam rheology on producing either more or less uniformity in the size of voids: if fibres are non-parallel, a void or gap at one end of a fibre would have a different size from an adjacent void at the other end. Of course any model predictions that we make also need to be checked against data for the properties of foam-formed papers, a point we return to towards the end of the thesis (see chapter 5).

A hypothesis then to explain larger pore sizes could be that the foam might behave as a “continuum viscoplastic fluid” during foam-forming, with the properties of the continuum fluid (i.e. in particular yield stress) being a function of the underlying bubble size. The fact that, compared to a simple viscous liquid, the presence of a yield stress makes it more difficult to push fibres together could then account for voids, i.e. pores in the foam-formed papers, remaining larger. As already noted in the context of e.g. the work of Al-Qararah et al. [83] and also Haffner [90], fibre lengths are considerably larger than bubble sizes, so in the first approximation at least, it should be permissible to consider a model in which the fibres are discrete, but the foam is treated as a continuum viscoplastic fluid.

From Figure 2.4, it can be clearly seen that foam gives bigger pores on average than water. A question however arises in this regard is that what would be the main reason producing larger pores in foam-formed papers rather than papers made by water. Is it due to the “ghost particle” mechanism or is it due to “continuum foam rheology”, e.g. associated with yield stress of the foam?

If the “ghost particle” mechanism is correct, then smaller bubbles might be expected to lead to smaller pores. Likewise, if the “ghost particle” mechanism is correct, more uniform bubble sizes would be expected to lead to more uniform pores. On the other hand, if “continuum foam rheology” plays a role, we know that smaller bubbles should produce higher yield stress [80, 107, 108], and this could actually leave a larger gap between the fibres. Moreover, if “continuum foam rheology” is relevant and if fibres are tilted (i.e. non-parallel case), then differences in a final gap size after squeezing between one end of the tilted fibre and the other might give an indication of polydispersity of eventual pore sizes: again these differences in gap size between ends of a fibre should be sensitive to yield stress.

The difficulty here however is that it is not clear a priori exactly how non-parallel fibres behave when a non-Newtonian viscoplastic fluid is squeezed between them, so what the squeeze film implications might be of coupling non-parallel fibres with complex rheology (and in particular how such coupling might affect pore size distribution) still needs to be determined. This then is the problem we will tackle. The implications that follow from the aforementioned “continuum foam rheology” hypothesis now need to be deduced: the effect of squeezing film for the cases of either foam or water between two non-parallel squeezed fibres will therefore be investigated in the chapters to follow.

Chapter 3

Squeeze Film Flow of Viscoplastic Bingham Fluid between non-Parallel Plates

3.1 Introduction

In this section, the squeeze film flow of a yield stress fluid between non-parallel plates is investigated. The general analysis is based on the work of Covey and Stanmore [30] Muravleva [28], but now for tilted plates, and compared to [28] a different situation is considered. In [28], squeezing force is analysed with a constant squeezing velocity, whereas here we are investigating a constant squeezing force to find the rate of squeeze action, as was done by Covey and Stanmore [30], albeit for parallel plates. Squeeze film flows of Newtonian and non-Newtonian fluids between parallel plates have been known and investigated significantly [5, 30]. We have reviewed the squeeze film flow of Newtonian fluid between parallel and non-parallel plates in appendix A. Moreover, the analysis of Covey and Stanmore [30] for the squeeze film flow of a viscoplastic Bingham fluid between parallel plates is reviewed in appendix B. The

present chapter focusses on the methodology and results for a Bingham fluid with non-parallel plates which is one of the novel contributions of this thesis.

In what follows, this chapter describes in detail the methodology 3.2 by which squeeze film flow of a viscoplastic Bingham fluid squeezed out from between non-parallel plates is considered. Section 3.2.1 discusses the assumptions considered to develop the equations and mathematical model needed to investigate the behaviour of a yield stress fluid in squeeze film flow. Then section 3.2.2 describes the squeeze film flow problem between non-parallel plates. Then section 3.2.3 considers final steady states of the non-parallel squeeze film system of a yield stress fluid. Finally, section 3.3 will discuss the results associated with the squeeze film flow of viscoplastic Bingham fluid between non-parallel plates.

3.2 Methodology

In this section the mathematical method used to investigate the squeeze film flow of viscoplastic Bingham fluid between non-parallel plates is described. The parallel case has already been tackled by Covey and Stanmore [30], but for the convenience of the reader we give the details of the parallel squeeze film methodology in appendix B. In what follows, to make the analysis easier to carry out, whether non-parallel or parallel, a number of assumptions have been made as discussed below.

3.2.1 Squeeze Film Flow Assumptions

In squeeze film flows (i.e. lubrication flows [23]), inertia effects tend to be negligible in comparison with the dominant effects of pressure and viscous forces, thus the Reynolds number for the flow is small. We are simplifying the three-dimensional problem of squeezing two fibres together (see e.g. section 2.5) by

the simple two-dimensional problem of squeezing two plates together. Hereafter we will refer to plates rather than fibres. In all systems considered here, the lower plate is fixed, and the upper plate approaches to the lower plate under the influence of externally applied force with a non-inertial squeeze motion. The following assumptions are imposed:

1. Planar (i.e. two-dimensional) geometry is considered, i.e. we consider a squeeze film between plates. This assumption is made for mathematical simplicity even though in a papermaking application for instance (again see section 2.5), fibres are not planar in reality. Instead, fibre-fibre interaction is a complicated three-dimensional process. However, by considering plates rather than fibres, the system can be simplified into a two-dimensional planar geometry.

2. Inertial and gravitational terms are negligible compared to the pressure and viscous forces.

3. There is a no slip condition at boundaries between the liquid and the plates.

4. The thickness of the squeeze film is assumed to be small in comparison with the plate dimensions which means that the velocity component in the direction of flow is bigger than the velocity component perpendicular to the plane of plate. Therefore, the outflow velocity gradient in the direction along the squeeze film flow is smaller than the velocity gradient across the gap between the plates.

3.2.2 Squeeze Film Flow of Viscoplastic Bingham Fluid between non-Parallel Plates

This section considers the squeeze flow of viscoplastic Bingham fluid between non-parallel plates. The analysis for a parallel, Newtonian squeeze film is well known in the literature [23]. However for completeness we have presented it in appendix A.1. Moreover, the behaviour of a Newtonian fluid squeezed between non-parallel plates is reviewed in appendix A.2 to facilitate comparison with the non-parallel viscoplastic Bingham case, particularly with regard to possible final steady states. The solution of squeeze film flow of a Bingham viscoplastic in the parallel case has been investigated by Covey and Stanmore [30] and we provide the mathematical procedure in the appendix B.1 again to support the non-parallel plate case which is discussed in the present section.

We consider a gap of initial thickness $\hat{H}_{c_0}$ at the centre of the plates of length $2\hat{L}$. In Figure 3.1 the top plate is moving downward with a time-varying velocity $\hat{v}_{top}$ under a constant applied force $\hat{F}_{app}$ (per unit distance transverse to the two-dimensional plane) thereby displacing the fluid, while the bottom plate is stationary. Moreover θ is the angle between the upper surface and the horizontal coordinate (it is assumed that the angle θ is small).

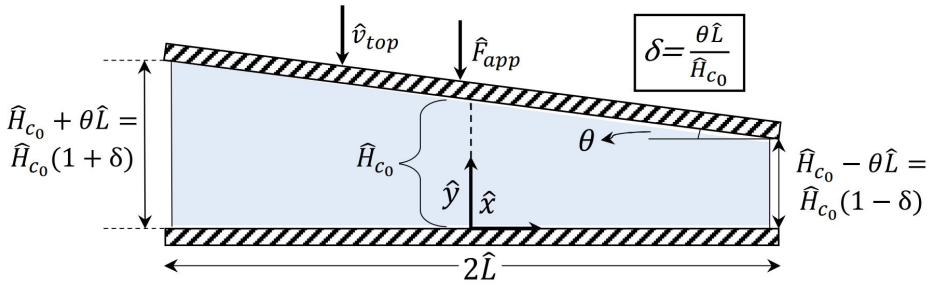

Figure 3.1: Geometry of squeeze film flow between non-parallel plates.

The flow of a non-Newtonian fluid is governed by the momentum and continuity

equations [121] in dimensional form as follow:

$$\rho\left(\frac{\partial \hat{u}}{\partial \hat{t}}+\hat{u}\frac{\partial \hat{u}}{\partial \hat{x}}+\hat{v}\frac{\partial \hat{u}}{\partial \hat{y}}\right)=-\frac{\partial \hat{p}}{\partial \hat{x}}+\left(\frac{\partial \hat{\tau}_{xx}}{\partial \hat{x}}+\frac{\partial \hat{\tau}_{xy}}{\partial \hat{y}}\right)+\rho\, g_x \tag{3.1}$$

$$\rho\left(\frac{\partial \hat{v}}{\partial \hat{t}}+\hat{u}\frac{\partial \hat{v}}{\partial \hat{x}}+\hat{v}\frac{\partial \hat{v}}{\partial \hat{y}}\right)=-\frac{\partial \hat{p}}{\partial \hat{y}}+\left(\frac{\partial \hat{\tau}_{xy}}{\partial \hat{x}}+\frac{\partial \hat{\tau}_{yy}}{\partial \hat{y}}\right)+\rho\, g_y \tag{3.2}$$

$$\frac{\partial \hat{u}}{\partial \hat{x}}+\frac{\partial \hat{v}}{\partial \hat{y}} \tag{3.3}$$

Now, using those assumptions as made in section 3.2.1, governing lubrication equations [25] for a viscoplastic Bingham fluid are

$$-\frac{\partial \hat{p}}{\partial \hat{x}}+\frac{\partial \hat{\tau}_{xy}}{\partial \hat{y}}=0 \tag{3.4}$$

$$\frac{\partial \hat{p}}{\partial \hat{y}}=0 \tag{3.5}$$

$$\frac{\partial \hat{u}}{\partial \hat{x}}+\frac{\partial \hat{v}}{\partial \hat{y}}=0. \tag{3.6}$$

Here $\hat{u}$ and $\hat{v}$ are velocities in $\hat{x}$ and $\hat{y}$ directions, $\hat{p}$ is pressure and $\hat{\tau}_{xy}$ denotes shear stress of the viscoplastic Bingham fluid which satisfies the Bingham material model (see e.g. [39, 68]). As discussed in chapter 2 (see section 2.2), the Bingham model describes the behaviour of a viscoplastic material which is characterized by two parameters namely a viscosity and yield stress. If yield stress is bigger than the magnitude of stresses, the Bingham material will behave as a solid. Meanwhile the material can be considered as a viscous Newtonian fluid when the stresses exceed the yield stress [6, 8, 30, 39, 47].

It should be noted that the stress and strain rate are tensors and when all the components of the stress tensor (shear components and normal compo-

nents together) and strain rate tensor (shear strain rate components and normal strain rate components) are taken into account, the components can be combined together into a quantity called the second invariant [73]. For the fluid to yield, it is the second invariant of stress which must exceed the yield stress, rather than any single component of the stress tensor needing to exceed the yield stress. Of course when one component of the stress tensor dominates all the others, then it is that particular component which dominates the yielding [39]. Indeed, in this thesis, based on the squeeze film flow assumptions, we only consider the shear stress and shear strain rate components of stress tensor and strain rate tensor, respectively.

Now for a viscoplastic Bingham fluid, shear stress is

$$\begin{cases} \hat{\tau}_{xy} = \pm\tau_0 + \mu_p\hat{\dot{\gamma}} & \text{for} \quad |\hat{\tau}_{xy}| > \tau_0 \\ \hat{\dot{\gamma}} = 0 & \text{for} \quad |\hat{\tau}_{xy}| \leqslant \tau_0. \end{cases} \tag{3.7}$$

Here τ_0 is yield stress, $\hat{\dot{\gamma}} = \partial\hat{u}/\partial\hat{y}$ is shear rate and μ_p is Bingham fluid viscosity after yielding occurs. Here the $\pm\tau_0$ term is positive if $\hat{\dot{\gamma}} > 0$ and it is negative if $\hat{\dot{\gamma}} < 0$. The dimensional variables are denoted with a hat symbol and their dimensionless analogues (described later on) will have the hat symbol dropped.

3.2.2.1 Non-dimensionalization of Equations

We cast equations in dimensionless form. Horizontal lengths are scaled by $\hat{L}$, and vertical lengths are scaled by $\hat{H}_{c_0}$. Horizontal velocities are scaled by $\tilde{u} \equiv (\hat{F}_{app}/\mu)(\hat{H}_{c_0}^2/\hat{L}^2)$, and vertical velocities are scaled by $\tilde{v} \equiv \hat{H}_{c_0}\tilde{u}/\hat{L}$. Times are scaled by $\hat{H}_{c_0}/\tilde{v} \equiv \hat{L}/\tilde{u}$ and shear stress $\hat{\tau}_{xy}$ is scaled by $\mu\tilde{u}/\hat{H}_{c_0}$. Finally pressures are scaled by $\hat{F}_{app}/\hat{L}$: note that this has the correct units of pressure since $\hat{F}_{app}$ is taken as applied force per unit distance transverse to the two-dimensional calculation domain. Now the dimensionless analogue of equation

(3.4) becomes

$$-\frac{\partial p}{\partial x}+\frac{\partial \tau_{xy}}{\partial y}=0 \tag{3.8}$$

$$\frac{\partial p}{\partial y}=0 \tag{3.9}$$

$$\frac{\partial u}{\partial x}+\frac{\partial v}{\partial y}=0. \tag{3.10}$$

The dimensionless film thickness H is a function of both time t and x coordinate. We define δ as a rescaled angle, $\delta = \theta\hat{L}/\hat{H}_{c_0}$. Geometrically δ is the thickness change between the middle of the plate and one of the ends divided by the initial thickness in the middle. Thus, the dimensionless squeeze film thickness which varies with x-coordinate and time t, can be determined

$$H(x,t) = H_c(t) - \delta\, x \tag{3.11}$$

where $H_c(t)$ is film thickness at the centre of the plates.

We can define a dimensionless group, the Oldroyd number (Od) which represents the relative importance of yield stress effects and imposed stress [71]. In our system, Oldroyd number can be defined as follows

$$Od = \frac{\text{Yield stress}}{\text{Imposed stress}} = \frac{\tau_0 \hat{L}^2}{\hat{H}_{c_0}\hat{F}_{app}}. \tag{3.12}$$

Suppose we make shear rate $\hat{\dot{\gamma}} \equiv \partial\hat{u}/\partial\hat{y}$ dimensionless on the scale $\tilde{u}/\hat{H}_{c_0}$. We deduce a dimensionless analogue of the constitutive equation

$$\begin{cases} \tau_{xy} = \pm Od + \dot{\gamma} & \text{for} \quad |\tau_{xy}| > Od \\ \dot{\gamma} = 0 & \text{for} \quad |\tau_{xy}| \leqslant Od. \end{cases} \tag{3.13}$$

Here the $\pm Od$ term is positive if $\dot{\gamma} > 0$ and is negative if $\dot{\gamma} < 0$. Now, integrating

equation (3.8), and applying the boundary condition in which at $y = H(x,t)/2$, we have $\tau_{xy} = 0$, shear stress can be written, at least in regions in which the fluid is yielding, as below

$$\tau_{xy} = \frac{\partial p}{\partial x}\left(y - \frac{H(x,t)}{2}\right) = \pm Od + \dot{\gamma} = \pm Od + \frac{\partial u}{\partial y}. \tag{3.14}$$

In the non-parallel geometry, the point along the plates at which flow reverses such that the flow rate to either right or left is zero needs to be determined. This point will be denoted as x_c. The domain for solving the problem is divided into two sections $x > x_c$ and $x < x_c$ and we consider these in what follows.

3.2.2.2 Squeeze Film Flow for Domain $x > x_c$

For the domain in which $x > x_c$, considering the fact that at the yield surface (denoted $y = y_{plug}$), shear rate is zero and shear stress is Od, using equation (3.14), pressure gradient with respect to x will be found

$$\frac{\partial p}{\partial x} = \frac{Od}{\left(y_{plug} - \frac{H(x,t)}{2}\right)}. \tag{3.15}$$

By substitution of equation (3.15) into (3.14), and from the Bingham fluid rheology, it is found that (in the yielded region $0 \leq y \leq y_{plug}$), $\tau_{xy} = \partial u/\partial y + Od$, thus, integrating and using the boundary condition in which at $y = 0$, $u = 0$, the velocity profile in the x direction for yielded and plug regions will be obtained

$$\begin{cases} u = \dfrac{Od}{2(y_{plug} - \frac{H(x,t)}{2})}y^2 - \dfrac{Od}{(y_{plug} - \frac{H(x,t)}{2})}y_{plug}y & \text{for} \quad y \leqslant y_{plug} \\ u_{plug} = -\dfrac{Od}{2(y_{plug} - \frac{H(x,t)}{2})}y_{plug}^2 & \text{for} \quad y_{plug} < y < \dfrac{H}{2}. \end{cases} \tag{3.16}$$

Now we note $\mathrm{d}Q/\mathrm{d}x = v_{top}$, i.e. downward motion of the plates v_{top} necessarily causes the volumetric flow Q along the gap to change, since the fluid is incompressible. In general there is a location x_c at which there is neither flow

to left or right, thus at that point, $Q = 0$. Integrating then gives the equation for flow rate Q which is established from the velocity profile for both plug and yielded regions as follow

$$Q = 2\left(\int_0^{y_{plug}} u\,\mathrm{d}y + \int_{y_{plug}}^{\frac{H(x,t)}{2}} u_{plug}\,\mathrm{d}y\right) = v_{top}(x - x_c). \tag{3.17}$$

Substitution of equation (3.16) into (3.17), taking the integral and making some manipulations, the final equation for y_{plug} for the domain $x > x_c$ will be generated. If $H(x,t)$ is substituted using equation (3.11) a cubic equation for y_{plug} now results

$$y_{plug}^3 - \frac{3}{2}(H_c(t) - \delta x)y_{plug}^2 - 3\frac{v_{top}(x - x_c)}{Od}y_{plug} + \frac{3}{2}\frac{v_{top}(H_c(t) - \delta x)(x - x_c)}{Od} = 0. \tag{3.18}$$

3.2.2.3 Squeeze Film Flow for Domain $x < x_c$

In the domain, $x < x_c$, the flow and the shear stress have opposite sign from what they have for $x > x_c$. Working through the computation, we deduce

$$y_{plug}^3 - \frac{3}{2}(H_c(t) - \delta x)y_{plug}^2 + 3\frac{v_{top}(x - x_c)}{Od}y_{plug} - \frac{3}{2}\frac{v_{top}(H_c(t) - \delta x)(x - x_c)}{Od} = 0. \tag{3.19}$$

3.2.2.4 Solving for y_{plug}

The next step is to solve for the yield surface, y_{plug}, which is a function of position x, based on the two obtained equations (3.18) and (3.19) for domains $x > x_c$ and $x < x_c$ respectively. To do so, a standard numerical method such as the Newton-Raphson technique is employed. Following an analogous procedure to that used for parallel plates (discussed in the appendix B, section B.1.1), assuming small values of $|x - x_c|$ and y_{plug}, a first guess for y_{plug} can be obtained. Specifically, based on the observation that at $x = x_c$ there can be no

fluid motion either to left or right, hence there is no strain rate $\partial u/\partial y$ at any y. Hence at $x = x_c$, we must have $y_{plug} = 0$. For the domain $x > x_c$ but close to $x = x_c$, it follows that y_{plug} must be small, i.e. $y_{plug} \ll H(x, t)/2$. The integral within (3.17) then evaluates to $u_{plug}H(x, t)$ which we set equal to $v_{top}(x - x_c)$, with $u_{plug} \approx y_{plug}^2 Od/H(x, t)$ via (3.16). We can use analogous assumptions for the domain $x < x_c$, therefore, the initial guess for y_{plug} is

$$\begin{cases} y_{plug} = \sqrt{v_{top}(x - x_c)/Od} & \text{for} \quad x > x_c \\ y_{plug} = \sqrt{v_{top}(x_c - x)/Od} & \text{for} \quad x < x_c. \end{cases} \tag{3.20}$$

These only apply if they predict $y_{plug} \ll H(x, t)/2$. More generally we can have y_{plug} values up to $H(x, t)/2$. Nevertheless once we have the correct y_{plug} value at any given x, we can readily find it at a nearby x, using one y_{plug} value as an initial guess for the next. We end up with y_{plug} values for all x, provided H_c, v_{top} and x_c are given, and provided Od and δ are specified. The technique for finding v_{top}, x_c and ultimately squeeze film thickness H versus time t is described next.

3.2.2.5 Computing Film Thickness versus Time

So far, the computational procedure for the constant load (i.e. constant applied force) and constant rate systems have been similar. In this section, we proceed to find the force as a function of velocity, and hence the velocity required to deliver a constant load, and so we start to see a deviation between the constant load and constant rate systems.

Now, after finding y_{plug}, for the domain $x > x_c$, we can integrate the pressure gradient equation (3.15) to find the pressure as

$$p = \int_x^1 \frac{Od}{\frac{H(x,t)}{2} - y_{plug}} \, \mathrm{d}x. \tag{3.21}$$

Meanwhile for the pressure profile in the domain $x < x_c$, we have

$$p = \int_{-1}^{x} \frac{Od}{\frac{H(x,t)}{2} - y_{plug}} \, \mathrm{d}x. \tag{3.22}$$

The value of x_c needs to be chosen to ensure p is continuous at $x = x_c$. Once that is achieved (for any selected v_{top}) the value of v_{top} then needs to be chosen so as to ensure $\int_{-1}^{1} p(x)\,\mathrm{d}x = 1$, the integral being readily computed numerically by quadrature. All this says is that in the dimensionless system considered here, the constant load is set to unity. We then evolve $H_c(t)$ according to $\mathrm{d}H_c(t)/\mathrm{d}t = -v_{top}$, with $H(x, t)$ then given by equation (3.11). To start the iteration at initial time, we need guesses of x_c and v_{top}. However we have guesses corresponding to the Newtonian case (see equations (A.21) and (A.22) in the appendix A), and in general we expect that the Newtonian v_{top} provides an upper bound for the velocity in the viscoplastic Bingham fluid case. Once we have x_c and v_{top} values initially, we can then use x_c and v_{top} values at one time step as initial guesses for the subsequent time step.

The algorithm flowchart used to compute v_{top} and x_c is shown in Figure 3.2.

3.2.2.6 Computing Torque

In addition to computing film thickness versus time, the numerical scheme outlined above also allows us to track another quantity namely torque T. The scheme balances a lubrication force developed between the plates to an external applied force (which as mentioned is unity in the dimensionless system). However if the plates are tilted, a lubrication torque also develops. To keep the tilt angle fixed (as is assumed here), an external applied torque would be needed to balance it assuming applying a fixed downwards force on the plate, and imposing a zero rotation rate. That said, it turns out that the signs of torques that we compute, were they able to act, would try to rotate the plates

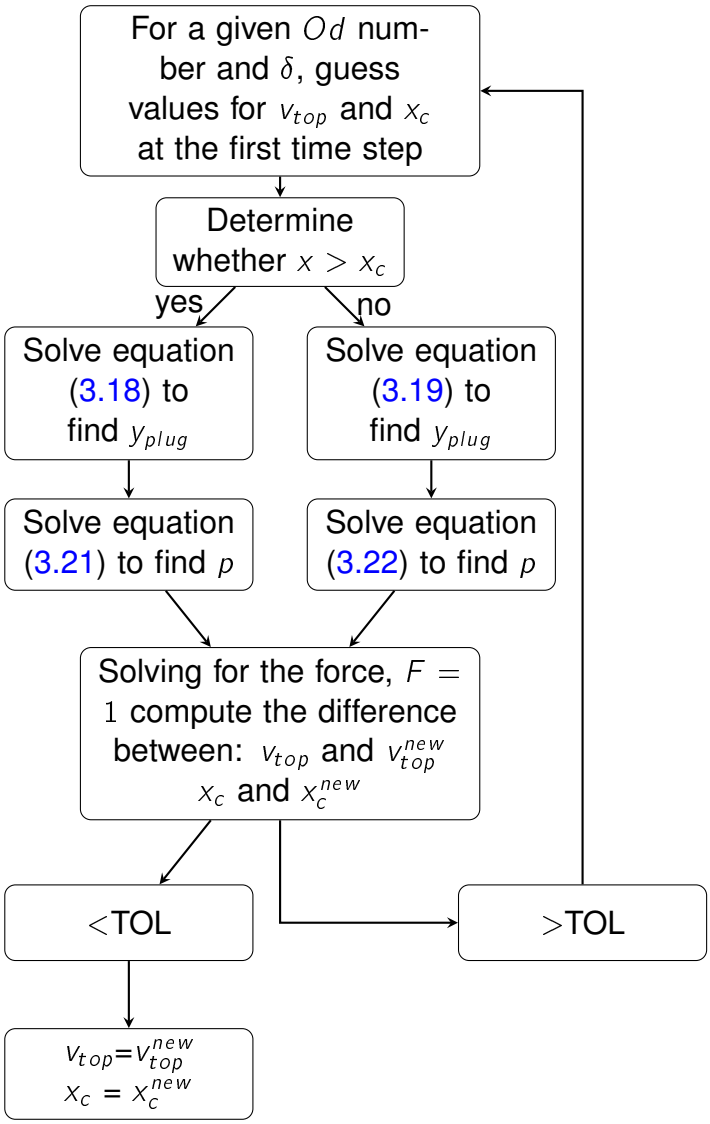

Figure 3.2: Algorithm flowchart used to compute v_{top} and x_c, TOL is the tolerance needed for the convergence of the code. This value was set at 10^{-4}.

closer to parallel. In fact, there is another option of imposing a fixed load and no torque. We can however quantify the lubrication torque (per unit distance normal out of the two-dimensional plane) via

$$T = \int_{-1}^{1} x\, p(x)\, \mathrm{d}x. \tag{3.23}$$

Since p versus x is computed numerically at any instant in time, this torque can also be evaluated by quadrature.

Here we have considered a zero rotation rate. However, there is another option of imposing a fixed load and no torque (e.g. by pushing down the plate with a certain weight at the centre point). In that case, there is a new constraint (torque = 0) which would have to be imposed by adding an (a priori unknown) angular rotation Ω to the plate, as well as the (unknown) plate speed v_{top}. We now have an equation $\mathrm{d}Q/\mathrm{d}x = v_{top} - \Omega x$, where v_{top} represents downward motion and Ω represents anticlockwise rotation. This integrates to $Q = Q_0 + v_{top}x - \Omega x^2/2$, where Q_0 is an a priori unknown flow rate at $x = 0$. This is a quadratic equation which, in the domain of interest namely $-1 < x < 1$, might have no solutions for $Q = 0$, exactly one solution for $Q = 0$, or two solutions for $Q = 0$. Therefore, once we include rotation, the kinematics of the flow field becomes more complicated. In that case, the definitive answer would require more analysis with additional equations (i.e. a torque balance) and possibly a less straightforward picture for the flow reversals (as the flow kinematics is more complex when rotation is included).

It is possible to consider a hypothetical case in which there is rotation about $x = 0$ but no squeezing. If Ω is the rotation rate, then we know that vertical velocity of the plate at location x is Ωx. If the rotation leads the plate to move upwards locally (as happens for positive x assuming Ω is positive), then Q (the horizontal fluid flux) decreases with x. If the rotation causes the plate to move

downwards locally (as happens for negative x), then Q (the horizontal fluid flux) increases with x. In short we have $\mathrm{d}Q/\mathrm{d}x = -\Omega\, x$ from which it follows $Q = Q_0 - \Omega\, x^2/2$, where Q_0 is as above the a priori unknown flux at $x = 0$ (which needs to be calculated as part of the solution of the problem).

Now there are different possible scenarios. If $Q_0 > 0$, there are two flow reversals (and hence two places in which shear stress switches sign) and if moreover $2Q_0/\Omega < 1$ they are both in the domain $-1 < x < 1$. However if $Q_0 < 0$, there is no flow reversal (and hence no place in which shear stress switches sign). Thus the kinematics with rotation is more complicated than in the case of squeezing with no rotation. Of course in general we have both squeezing (velocity v_{top}) and rotation (angular velocity Ω) together, and both of them affect Q.

As we have stated therefore, depending on Q_0 and depending on the relative size of v_{top} and Ω then, over the domain of interest $-1 < x < 1$, we might have no places in which flow changes sign, exactly one place in the domain in which flow changes sign (as per the case of squeezing without rotation), or two places in which flow changes sign.

In other words, there might be no values of x_c, exactly one value of x_c or exactly two values of x_c. Perhaps, in all practical cases, we always end up with a situation in which there is exactly one value of x_c in the domain of interest (as per the case of squeezing without rotation), but this is not yet certain. The problem surely could be tackled (starting with the Newtonian case, and then tackling the non-linear viscoplastic Bingham case after that). However the rotating, torque-free case is not presented here. Instead we focus on the non-rotating case.

The question we now ask is whether the plates ever come to rest at a finite film thickness (as is known to happen for a viscoplastic Bingham fluid in a parallel

plate geometry as described in appendix B section B.1.4) or whether their right hand ends manage to touch (as happens for a Newtonian fluid between non-parallel plates as demonstrated in section A.2). The question is addressed in the next section.

3.2.3 Final Steady State for the Case of Viscoplastic Bingham Fluid between non-Parallel Plates

This section develops the final steady state solution for the system. The analogous approach for a yield stress fluid system in a parallel plate configuration is provided in appendix B.1 and more specifically in section B.1.4 . In the parallel plate system, a final steady state with a finite gap thickness is always found to exist. However in a non-parallel plate system, a final steady state with a finite gap does not always exist. If there is no such final steady state, then the plates eventually touch.

3.2.3.1 Conditions for Final Steady State to Exist

In the final steady state, the plug region fills the entire gap and the yield surface is at $y_{plug} = 0$. On the yield surface, there is a point now denoted $x = x_{cf}$ at which the dimensionless shear stress changes sign from $-Od$ to $+Od$. This x_{cf} is the final value of x_c (which typically denotes the point at which flow changes sign). However there is no flow at all in the final steady state, so what changes sign is now the shear stress.

We integrate the equation $\partial p/\partial x = \mp Od/((H_{cf} - \delta x)/2)$ applicable in the final steady state. Here H_{cf} is the assumed final thickness at the centre of the plates. Thus for $x > x_{cf}$, the pressure profile is determined

$$p(x) = \frac{2Od}{\delta} \ln \frac{H_{cf} - \delta x}{H_{cf} - \delta}. \tag{3.24}$$

For $x < x_{cf}$, the pressure profile is

$$p(x) = \frac{2Od}{\delta} \ln \frac{H_{cf} + \delta}{H_{cf} - \delta x}. \tag{3.25}$$

Since the pressure profile has to be continuous at $x = x_{cf}$, equations (3.24) and (3.25) should be equal at this point

$$\frac{2Od}{\delta} \ln \frac{H_{cf} - \delta x_{cf}}{H_{cf} - \delta} = \frac{2Od}{\delta} \ln \frac{H_{cf} + \delta}{H_{cf} - \delta x_{cf}}. \tag{3.26}$$

Simplifying equation (3.26), a quadratic equation can be obtained

$$x_{cf}^2 - 2\frac{H_{cf}}{\delta} x_{cf} + 1 = 0. \tag{3.27}$$

Solving the quadratic equation (3.27) gives x_{cf} as a function of H_{cf} and δ

$$x_{cf} = \frac{H_{cf}}{\delta} - \sqrt{\frac{H_{cf}^2}{\delta^2} - 1}. \tag{3.28}$$

The force applied over the entire plate length can be calculated utilising the pressure profiles obtained above

$$F = \int_{-1}^{x_{cf}} p(x)\mathrm{d}x + \int_{x_{cf}}^{1} p(x)\mathrm{d}x = \frac{2Od}{\delta} \left(\left(x_{cf} - \frac{H_{cf}}{\delta} \right) \ln \frac{H_{cf}^2 - \delta^2}{(H_{cf} - \delta x_{cf})^2} + 2x_{cf} \right). \tag{3.29}$$

Substituting the obtained x_{cf} from equation (3.28) into (3.29), considerable simplification results, because the argument of the logarithmic term turns out to be unity, so the logarithm itself vanishes. Assuming the plates have stopped moving then, the force applied over the entire plate length turns out to be

$$F = 4\frac{Od}{\delta} \left(\frac{H_{cf}}{\delta} - \sqrt{\frac{H_{cf}^2}{\delta^2} - 1} \right) = \frac{4Od}{\delta} x_{cf}. \tag{3.30}$$

This force generated by the pressure profile must now be matched to the unit force applied to the plates, and conditions determined in which physically

meaningful solutions for H_{cf} or equivalently for x_{cf} are obtained. Setting $F = 1$ we need to find combinations of Od and δ that admit solutions with $H_{cf} > \delta$ or equivalently with $x_{cf} < 1$. It is clear that to achieve this we require $4Od/\delta > 1$. Provided this condition is satisfied, the gap at the right hand end $H_{cf} - \delta$ is then finite.

3.2.3.2 Final Steady State Torque Calculation

As well as computing a force in the final steady state, we can also compute a torque. For a Bingham fluid in a non-parallel system this can be obtained by taking the integral of equation (3.23) using pressure profiles provided in equations (3.24) and (3.25). For comparison, analysis of torque for a Newtonian fluid (albeit at unsteady state) has been done in the appendix A, section A.2.2, but here we focus on the final steady state Bingham case. We find

$$T_{steady} = \frac{Od}{2\delta^3}\left(2(H_{cf}^2 - \delta^2 x_{cf}^2)\ln\frac{(H_{cf} - \delta\, x_{cf})^2}{H_{cf}^2 - \delta^2} + 4\,\delta\, x_{cf} H_{cf} + 2\delta^2(x_{cf}^2 - 1)\right) \tag{3.31}$$

where T_{steady} is the final steady state torque and x_{cf} is a known function of H_{cf}/δ from equation (3.28). As before the logarithmic term vanishes (its argument is unity) and after some further algebra using equation (3.27), the final steady state torque reduces to

$$T_{steady} = \frac{2Od}{\delta} x_{cf}^2. \tag{3.32}$$

However, from equation (3.30) applicable in the final steady state we already know $(Od/\delta)x_{cf} = \frac{1}{4}$. Hence final torque is

$$T_{final} = x_{cf}/2. \tag{3.33}$$

This indicates that T_{final} depends on the film thickness at the right hand end $H_{cf} - \delta$ relative to the film thickness at the centre H_{cf}. For instance, a final state with a gap on the right hand end that is not too narrow relative to the centre (i.e. small δ / H_{cf}, hence small x_{cf}) leads to small T_{final}. However a much narrower gap with plates almost touching when they stop (i.e. δ / H_{cf} close to unity, hence x_{cf} close to unity) leads to $T_{final} = \frac{1}{2}$. Note that this is only half the torque of the Newtonian system when it touches (see section A.2.2 in appendix A).

There is another way to interpret the torque obtained in equation (3.32). Rather than obtaining it at the final thickness H_{cf}, we can find torque at any instantaneous H_c. This allows us to estimate (at any instant) a yield stress contribution to both force and torque, the total force and torque being a sum of yield stress contributions and viscous contributions. This approach will be discussed in section 3.2.3.6. However, when a final steady state is reached, there is no motion even though the driving force is maintained, hence no viscous contribution, and so total force and torque arise entirely from yield stress contributions.

3.2.3.3 Maximum and Minimum Oldroyd Number

To proceed we next define a parameter called η which involves the ratio between the tilt angle and the Oldroyd number

$$\eta = \delta / (4Od). \tag{3.34}$$

Note that the bracketed term in equation (3.30) is always less than unity for any $H_{cf}/\delta > 1$, i.e. $x_{cf} < 1$ always. Hence in order to satisfy the constraint $F = 1$, it is essential to have $\eta < 1$. In other words for a specified Od there is a maximum δ at which a final steady state solution with a finite thickness could exist (or equivalently for any δ, there is a minimum Oldroyd number, Od_{min}, for

a final steady state with a finite gap thickness to exist)

$$Od_{min} = \delta/4. \tag{3.35}$$

If $Od < Od_{min}$, the plates rather than reaching final steady state instead must touch as they do in the Newtonian limit $Od \to 0$. It is only in the limit of parallel plates with $\delta \to 0$ that Od_{min} falls to zero. When plates are tilted, the narrow end of the gap is more effective at supplying force to the plates than the wider end is. The issue with increasing δ however is that the gap only remains narrow over a limited domain of x close to its right hand end. An increase in δ therefore must be accompanied by an increase in Od (effectively an increase in yield stress of the fluid) to ensure that equation (3.30) in the absence of any fluid motion is still able to satisfy $F = 1$.

If $\eta > 1$, there is no final steady state in which the yield stresses in the fluid are able to balance the imposed unit force on the plates. The plates must always keep moving until their right hand ends touch, as happens in the Newtonian limit for instance. Moving plates always have $y_{plug} > 0$, and this leads to larger pressures p and larger forces F (due to those pressures) than a stationary plate case can deliver (via equation (3.30)). Hence moving plates can achieve $F = 1$ even with $\eta > 1$ even though stationary plates cannot.

In addition to Od_{min} given above, there is a maximum Oldroyd number, Od_{max}, at which $H_{cf} = 1$: at this Od_{max}, the plates will not move at all. Inserting $H_{cf} = 1$ in equation (3.30) and rearranging, Od_{max} which depends on δ turns out to be

$$Od_{max} = \frac{1 + \sqrt{1 - \delta^2}}{4}. \tag{3.36}$$

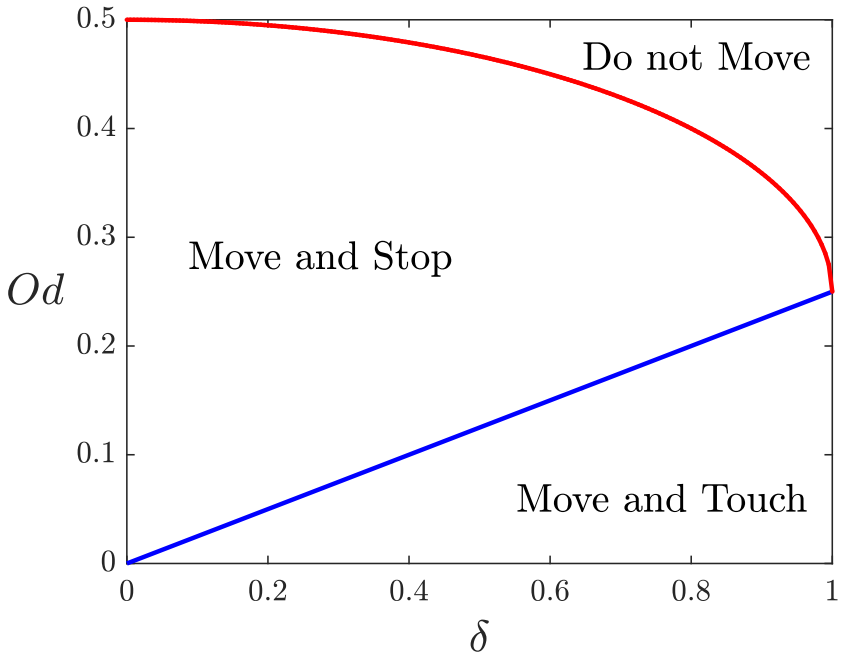

Figure 3.3: Phase diagram in the Od versus δ plane for squeeze flow of viscoplastic Bingham fluid between non-parallel plates. In the "move and stop" and "do not move" regions, $\eta < 1$. In the "move and touch" region, $\eta > 1$.

3.2.3.4 Phase Diagram for Permitted States of System

Figure 3.3 shows the phase diagram in the Od versus δ plane in which there are three regions, "do not move"; "move and stop"; "move and touch". Although (at any fixed δ) there is both a Od_{min} and Od_{max} for the plates to move and stop, in the case of fixed Od, there is only a maximum δ value, δ_{max} say. However what happens at that δ_{max} depends on the value of Od. If $Od < \frac{1}{4}$, then δ_{max} corresponds to the plates moving and touching. However if $Od > \frac{1}{4}$, then δ_{max} corresponds to the plates not moving at all.

Generally speaking, the data for the unsteady state evolution are sensitive to both δ and Od number. However the final fate of the system (i.e. whether the plates stop without touching or whether instead they move and touch) is only dependent on the η value. Indeed, if $\eta < 1$, such that the final film thickness is non-zero, the final steady state is approached but an arbitrarily long time is needed to reach it at least in principle (see chapter 4; qualitatively this is similar

to the viscoplastic Bingham case in a parallel system). However, if $\eta > 1$, the gap falls to zero at the right hand end and a non-parallel viscoplastic Bingham system will behave instead more like a Newtonian non-parallel case. In the Newtonian case, the right hand ends of the plates touch in a finite time (see section A.2).

3.2.3.5 Computing Final Film Thickness

Having now identified the domain for which final steady state solutions are possible, we proceed to analyse the final steady state solutions further. Returning to equation (3.30) assuming $\eta < 1$, and imposing $F = 1$ we deduce

$$H_{cf} = \frac{\delta^2}{8Od} + 2Od. \tag{3.37}$$

For any Od number less than the maximum, a final H_{cf} less than unity can be determined. Now using this H_{cf} value, the point x_{cf} at which the viscoplastic stress switches sign can be defined. This can be determined via equation (3.28) and/or (3.30), and the result is

$$x_{cf} = \delta/(4Od) \equiv \eta. \tag{3.38}$$

Note that this final state viscoplastic x_{cf} in general differs from the instantaneous Newtonian x_c given by equation (A.21). Note also that as $\eta \to 1$, meaning the plates almost touch at their right hand ends once they have stopped moving, we find that $x_{cf} \to 1$, i.e. shearing in the final steady state is entirely towards the left. Furthermore, as already mentioned, in the non-parallel case, torques can develop, and it turns out that final states with the largest x_{cf} also exhibit the largest torques. Indeed based on equation (3.33), torque is just $x_{cf}/2 = \eta/2$.

Rearranging equation (3.37) in terms of η gives $H_{cf}/(2Od)$ which is the aver-

age film thickness in the final steady state (at the centre of the plates) relative to the parallel case. This satisfies

$$\frac{H_{cf}}{2Od} = \eta^2 + 1. \tag{3.39}$$

Another important quantity, $(H_{cf} - \delta)/2Od$, which is the minimum film thickness (at the right hand end) in the final steady state relative to the parallel case, can be obtained

$$\frac{H_{cf} - \delta}{2Od} = (1 - \eta)^2. \tag{3.40}$$

The ratio between equation (3.40) and equation (3.39), $(H_{cf} - \delta)/H_{cf}$, is a measure of uniformity or otherwise of gap thicknesses such that it is zero if polydisperse (the gaps at either end of the plates have different sizes) and unity if monodisperse (the gaps at either end have, in relative terms at least, the same thickness)

$$\frac{H_{cf} - \delta}{H_{cf}} = \frac{(1 - \eta)^2}{\eta^2 + 1}. \tag{3.41}$$

To summarise, equations (3.39) and (3.40) give final film thicknesses in a tilted case relative to a parallel one. Meanwhile equation (3.41) tells us about the uniformity of final film thicknesses in the tilted case. These quantities depend on η, but not on Od and δ individually.

3.2.3.6 Yield Force and Yield Torque Calculation

For the Bingham parallel system presented in section B.1.3 of the appendix B, we discuss a so called “yield force” contribution to the total force (the remainder of the total force being viscous force). The yield force is the force that would be developed with a given plate separation in the hypothetical case in which motion is stopped. Typically early on in the evolution, when plate separations are still quite large, yield force can be relatively small, meaning that total force is primarily viscous. However (see e.g. Figure B.6) we show that over time

eventually all the force becomes yield force. In this present section we explore the analogous behaviour for the non-parallel system.

Of course in the non-parallel case, in addition to defining a “yield force”, we can also define a “yield torque”. Again these both correspond at any given plate separation to the situation that occurs in the hypothetical case in which motion is stopped. The formulae we need are just (3.30) and (3.32), but using now the instantaneous H_c, albeit still computing x_c for this H_c value using (3.28). Thus at any instantaneous film thickness, a yield stress contribution to the force using equation (3.30) can be deduced

$$F_{yield} = Od \Big/ \left(\frac{H_c}{4} + \sqrt{\frac{H_c^2}{16} - \frac{\delta^2}{16}} \right). \tag{3.42}$$

Here we have multiplied the numerator and denominator of (3.30) by $(H_c/\delta) + \sqrt{(H_c^2/\delta^2) - 1}$ and then simplified. What the yield force corresponds to is computing force via $\int_{-1}^{1} p \, \mathrm{d}x$ as usual, but replacing the pressure field in (3.22) via an analogous pressure field as if the instantaneous $H(x, t) = H_c - \delta x$ were the final state (essentially dropping y_{plug} from (3.22)). Then considering the total force to be unity in our dimensionless system, viscous force would be $F_{viscous} = 1 - F_{yield}$.

Similarly, at any instantaneous film thickness, a yield stress contribution to the torque using equation (3.32) can be deduced

$$T_{yield} = \frac{2Od}{\delta} \left(\frac{H_c}{\delta} - \sqrt{\frac{H_c^2}{\delta^2} - 1} \right)^2. \tag{3.43}$$

What the yield torque corresponds to is computing torque via (3.23) as usual, but replacing the pressure field (3.22) as if the instantaneous $H(x, t) = H_c - \delta x$ were the final state. Effectively then we use (3.32) but substitute (3.28) again as if the instantaneous $H(x, t)$ were the final state. Then the viscous torque

will be the difference between total torque, T and yield torque, T_{yield} as follow $T_{viscous} = T - T_{yield}$.

Of course the yield force and yield torque are not the same as the total force and total torque, since the totals include viscous contributions as well. Typically we can expect the yield force and yield torque to start out quite small, and only grow to match the total force and total torque in a situation in which the plates move and stop. On the other hand, if the plates instead move and touch (which can happen in a non-parallel system but not a parallel one), the yield force and yield torque might never match the total force and total torque.

In methodology section, the equations needed to investigate the behaviour of a viscoplastic Bingham fluid in squeeze film flow with non-parallel plates have been developed in both final steady state and unsteady state situations. Now that the formulation and mathematical modelling of the squeeze flow of Bingham fluids between non-parallel plates is complete, predictions from the various equations that we have derived will be analysed in the next section 3.3.

3.3 Results and Discussion for Squeeze Flow of Viscoplastic Bingham Fluids between non- Parallel Plates

The results we discuss in the thesis are organised as follows. Section A.3 (in the appendix A) deals with the results obtained from the squeeze flow of Newtonian fluid between parallel and non-parallel plates. Then section B.2 (in the appendix B) considers the results of investigating the squeeze flow of a Bingham fluid between parallel plates. In this section (main results section presented below) considers a Bingham fluid and non-parallel plates, with sections A.3 and and B.2 being included in the appendix for comparison.

In the present section, results for a viscoplastic Bingham fluid in a non-parallel plate scenario are presented. We consider yield surfaces (section 3.3.1), film thicknesses (section 3.3.3), forces (section 3.3.4), torques (section 3.3.5) and final steady states (section 3.3.6). As already alluded to, sections A.3 and B.2 focus primarily on results for the Newtonian fluid between parallel and non-parallel plates, and a viscoplastic Bingham fluid in a parallel plate configuration, respectively. Those results are useful for comparing and contrasting with the viscoplastic non-parallel case.

3.3.1 Yield Surface

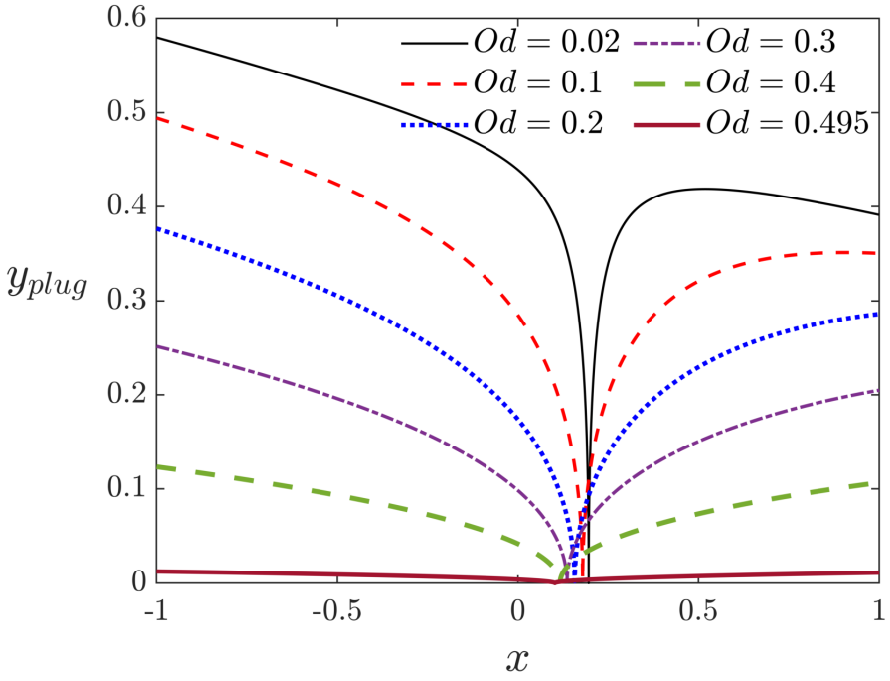

Figure 3.4: Yield surfaces as functions of x corresponding to $H_c = 1$ and $\delta = 0.2$ for different Oldroyd numbers. Note that $Od = 0.495$ is close to the maximum Od number for the particular $\delta = 0.2$, so that $y_{plug} \ll 1$ when $H_c = 1$ in this case.

The yield surface, y_{plug} versus x for $H_c = 1$ and $\delta = 0.2$ is shown in Figure 3.4 (see Table 3.1 for relevant data). This shows that y_{plug} for $x > x_c$ is not necessarily a monotonically increasing function of x, because y_{plug} has a maximum value of $H(x,t)/2$ and $H(x,t)$ is a decreasing function of x. Note that for $\delta = 0.2$, the maximum Od just slightly above $Od \approx 0.495$ is determined

(via equation (3.36)). Close to this maximum Od number, y_{plug} is small.

For small Od however, y_{plug} is close to $H(x,t)/2$ (except very close to $x = x_c$ where $y_{plug} = 0$). For x just slightly greater than x_c, the value of y_{plug} increases very sharply at first (a consequence of the square root law in equation (3.20)), but for values of $Od = 0.1$ or less, y_{plug} reaches a maximum at a certain x, then, starts to decrease gradually.

The yield surface, y_{plug} versus x corresponding to $H_c = 1$ for different δ values and a constant $Od = 0.3$ is shown in Figure 3.5 (see Table 3.2 for relevant data). It is seen that, by increasing δ, the value of x_c increases and the yield surface becomes increasingly asymmetrical, tending to be thicker on the left hand side and thinner on the right hand side due to the geometrical constraint. For even larger δ however, y_{plug} can be small even on the left hand side, despite the wider gap there. This is due to v_{top} turning out to be small for these larger δ. Indeed by rearranging equation (3.36), a maximum value of δ (for the plates to move at all) just above 0.97 can be obtained for $Od = 0.3$.

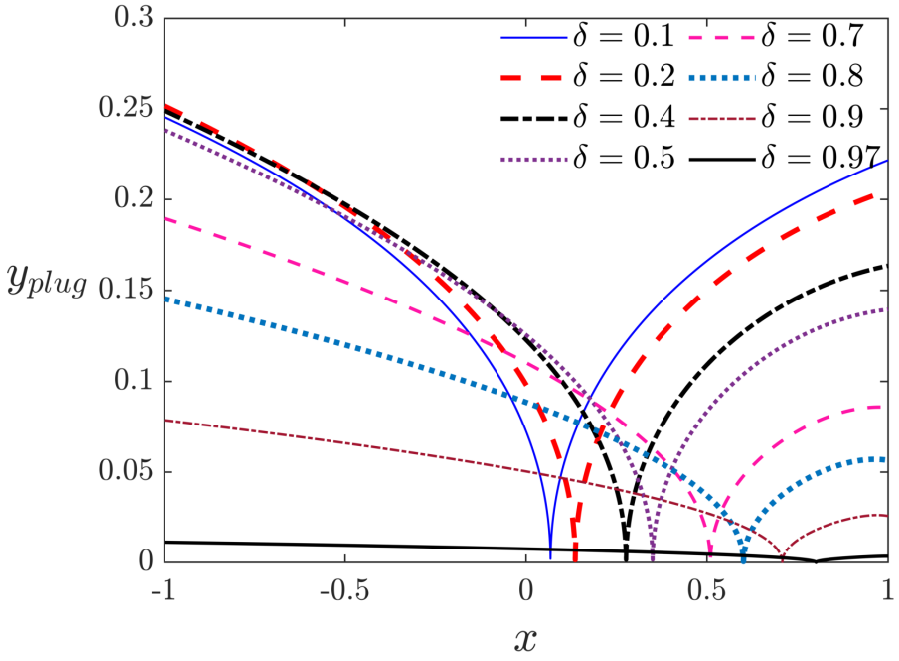

Figure 3.5: Yield surfaces as functions of x corresponding to $H_c = 1$ and $Od = 0.3$ for different δ values.

Note that Figure 3.4 and Figure 3.5 tell us the locations of the plug region and yielded region, but not the velocities within each of those regions. Data for these velocities are however reported in next section.

Note moreover that Figure 3.4 and Figure 3.5 just consider one instant of time, i.e. the initial instant at which $H_c = 1$. The shapes of the yield surfaces can also be computed at later times with $H_c < 1$. However results are not presented here, because qualitatively the shapes are similar to those already seen in Figure 3.4 and Figure 3.5. The narrower the gap, the more impact the yield stress has upon the system, to the point that motion might stop altogether (as per section 3.2.3). Hence decreasing H_c at fixed Od is similar, as far as shapes of yield surfaces are concerned, to increasing Od at fixed H_c. Likewise the narrower the gap, the more impact a given tilt angle has upon the ratio of the film thickness between the right hand end and the centre. Hence decreasing H_c at fixed δ is similar, as far as shapes of yield surfaces are concerned, to increasing δ at fixed H_c. Instead of focussing on how y_{plug} varies with varying H_c, we therefore focus in what follows on how film thickness varies with time. Before that however we consider, as already mentioned, some velocity profiles.

3.3.2 Velocity Profiles

In this section we report some additional results for a Bingham fluid squeezed between non-parallel plates to supplement those already given in section 3.3.1. Figure 3.4 and Figure 3.5 plot values of shapes of yield surfaces for various combinations of Od and δ. To compute these shapes it is necessary to know v_{top} and x_c. Relevant values are reported in Table 3.1 and Table 3.2.

In addition to computing shapes of yield surfaces as Figure 3.4 and Figure 3.5 already do, it is also of interest to know the velocity fields both in the yielded and plug regions. These velocity fields are influenced by the shapes of the

Od	v_{top}	x_c
0.495	6×10^{-5}	0.1023
0.4	0.0064	0.1168
0.3	0.0248	0.1360
0.2	0.052	0.1573
0.1	0.0853	0.1793
0.02	0.1145	0.1961

Table 3.1: Values of v_{top} and x_c for the case $\delta = 0.2$ and various Od. These v_{top} and x_c values correspond to the initial instant at which $H_c = 1$, and are needed to compute yield surfaces.

δ	v_{top}	x_c
0.1	0.06774	0.0260
0.2	0.0248	0.1360
0.4	0.01995	0.2763
0.5	0.01654	0.3498
0.7	0.00851	0.5096
0.8	0.00447	0.6009
0.9	0.00115	0.7083
0.97	2×10^{-5}	0.8013

Table 3.2: Values of v_{top} and x_c for the case $Od = 0.3$ and various δ. These v_{top} and x_c values correspond to the initial instant at which $H_c = 1$, and are needed to compute yield surfaces.

yield surface (i.e. by the y_{plug} values) and hence are influenced in turn by the v_{top} and x_c values as given in Table 3.1 and Table 3.2. Figure 3.6 shows the plots of velocity profiles u versus y at various x values. Provided $x > x_c$, these can be computed using equation (3.16). If $x < x_c$, the profile is given by the negative of equation (3.16).

In Figure 3.6 we consider the case $\delta = 0.2$ and $Od = 0.3$, a parameter combination occurring in both Figure 3.4 and Figure 3.5. Velocity profiles at the initial instant of time are plotted at $x = 0.2$, $x = 0.6$ and $x = 1.0$, and also at

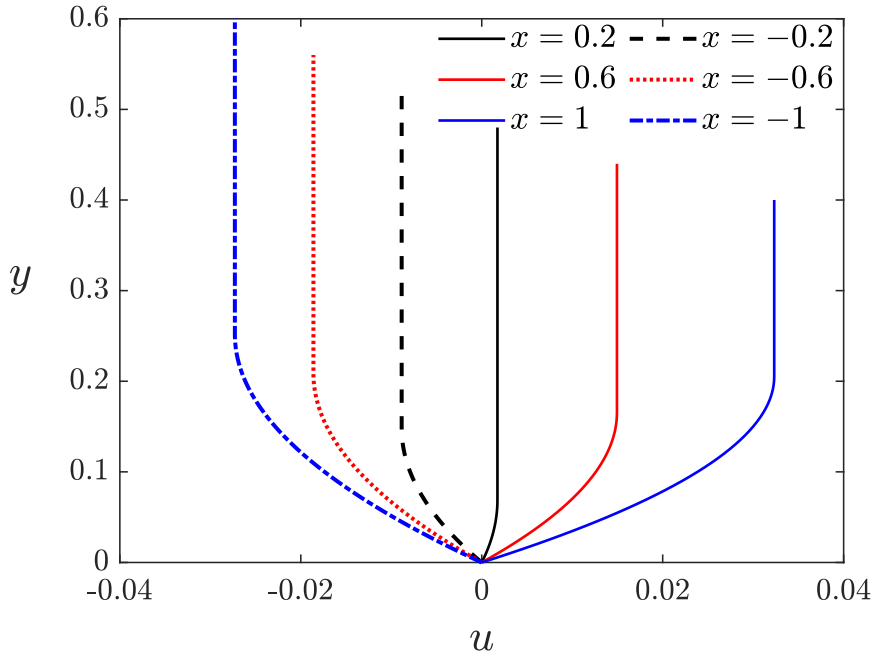

Figure 3.6: Velocity profiles for the case $Od = 0.3$ and $\delta = 0.2$ at different x locations.

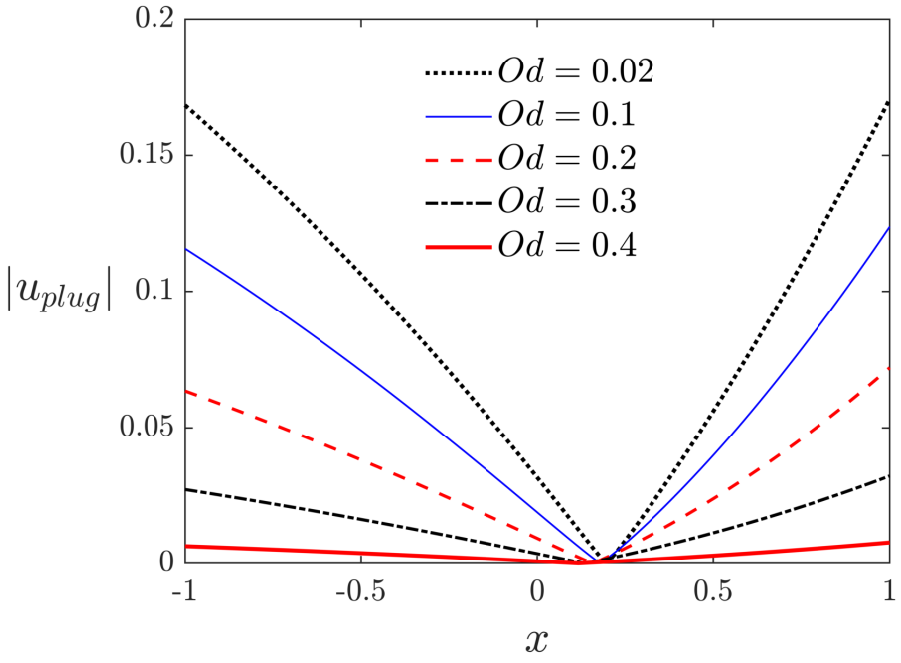

Figure 3.7: Profiles of $|u_{plug}|$ versus x for $\delta = 0.2$ and various Od. Data are determined at the initial instant (such that $H_c = 1$).

$x = -0.2$, $x = -0.6$ and $x = -1.0$. According to Table 3.1 and Table 3.2 the value of x_c is $x_c \approx 0.1360$. What we see then, as x moves away from x_c in either direction, is that velocities generally increase in magnitude and also a

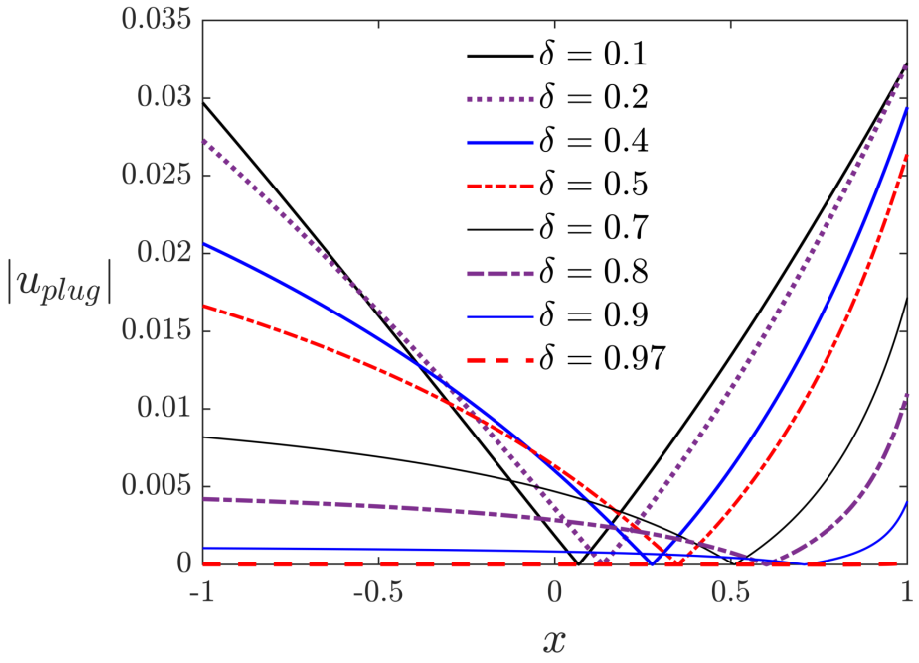

Figure 3.8: Profiles of $|u_{plug}|$ versus x for $Od = 0.3$ and various δ. Data are determined at the initial instant (such that $H_c = 1$).

higher proportion of the flow profile is in the yielded region and less of it is in the plug region.

Another effect evident in Figure 3.6 is that, at any given value of $|x|$, there is more flux to the left than to the right (owing to x_c being positive). However this does not always manifest in a higher u_{plug} value on the left as Figure 3.7 and Figure 3.8 show. The larger flux to the left is also delivered over a larger vertical distance, and this impacts on the velocity. Notice that Figure 3.6 indicates how u varies with y at specified x, whereas Figures 3.7 and 3.8 indicate how u in the plug region varies with x. At first sight it might appear that we can use these figures to compare $\mathrm{d}u/\mathrm{d}y$ and $\mathrm{d}u/\mathrm{d}x$. However this overlooks the fact (see section 3.2.2.1) that x and y are already scaled differently. If a direct comparison were made, removing the effect of that different scaling, derivatives of u in the y direction would always be must greater than those in the x direction.

3.3.3 Film Thickness versus Time Results

Changes of film thickness with respect to time for a constant $\delta = 0.2$ and various Od numbers are shown in Figure 3.9. For the maximum $Od \approx 0.495$, the plates never move at all, whereas, for very small Od numbers (i.e. according to equation (3.35) for $Od < 0.05$ with this particular δ), the plates move and touch one another, and for all values of Od number in between, the plates move and stop at a final film thickness without touching one another at the right hand end (see also Figure 3.3). Assuming the plates move and stop without touching, equation (3.37) implies final film thickness is dependent not just on Od, but also on the ratio between tilt angle δ and Od number which appears in the definition of η in equation (3.34).

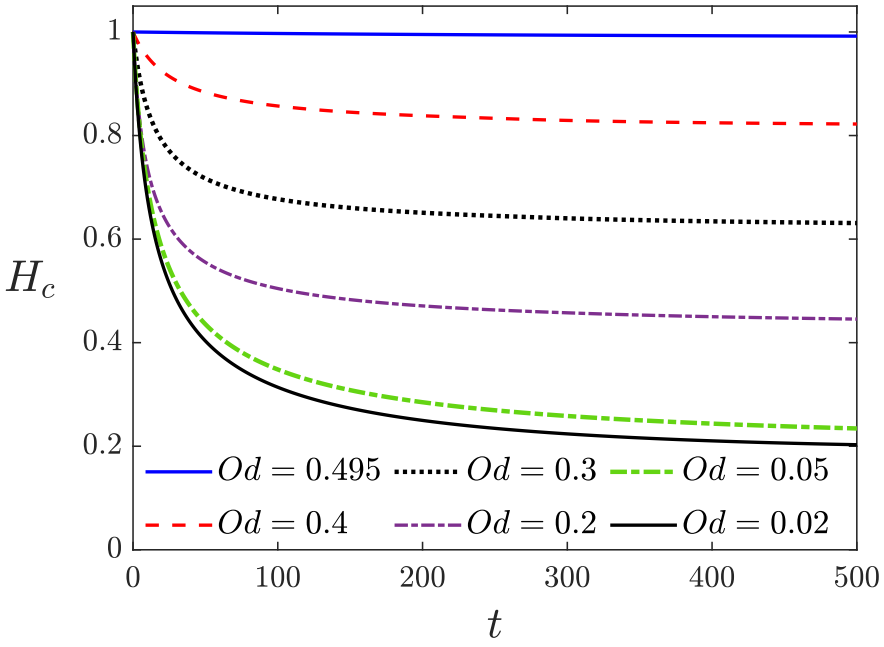

Figure 3.9: Film thickness versus time for a constant $\delta = 0.2$ and different Oldroyd numbers.

Film thickness versus time for different δ values and a constant $Od = 0.3$ is shown in Figure 3.10. As δ increases, the final thickness H_{cf} increases. For any value of Od, there is a maximum value of δ beyond which the system stops moving. Using equation (3.36), the maximum δ value for a given Od number

can be estimated (i.e. for $Od = 0.3$, a δ_{max} just slightly above 0.97 is achieved). All the δ values here are therefore less than the maximum. Hence, for all values of δ shown, the plates move, but also stop at final thickness since the value of η (see equation (3.34)) is also less than unity. However, for some cases (e.g. $\delta = 0.97$ or $\delta = 0.9$) the plates barely move before stopping.

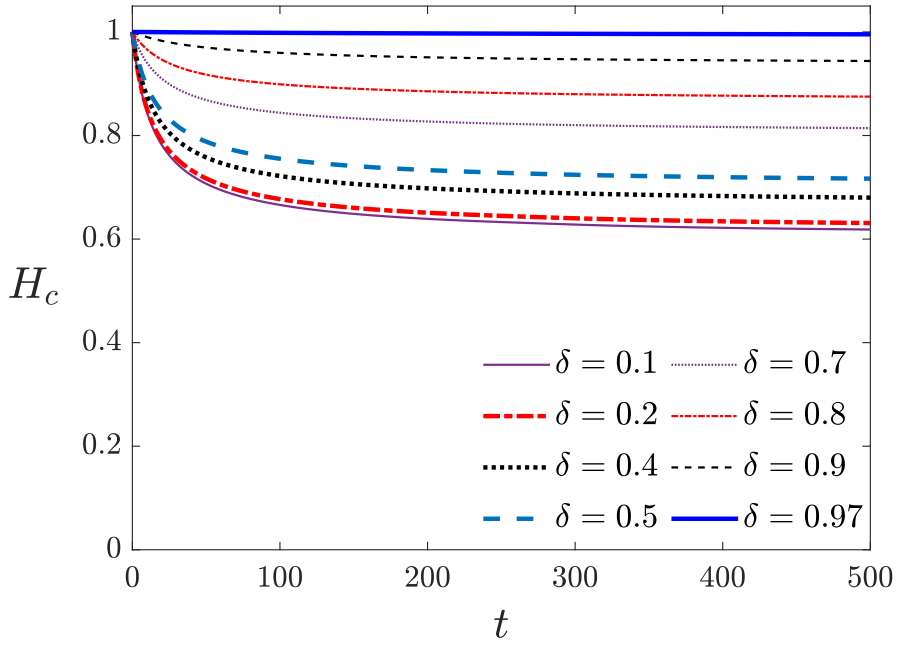

Figure 3.10: Film thickness versus time corresponding to $Od = 0.3$ and different δ values.

A general comparison of film thickness versus time for squeeze film flow of a viscoplastic Bingham fluid with a constant $Od = 0.3$ between parallel non-parallel plates with different δ values is depicted in Figure 3.11. In addition to that, changes of thickness at right hand ends of the plates (i.e. $H_c - \delta$) versus time for the two non-parallel cases are shown in the figure.

The difference between the final film thickness in the parallel case and the $\delta = 0.2$ non-parallel case is very small indeed, in line with the prediction of (3.37) which suggests this difference is second order in η and hence in δ. The difference with respect to the system with $\delta = 0.5$ is larger. Nonetheless, both the non-parallel systems shown here behave at least quantitatively analogous

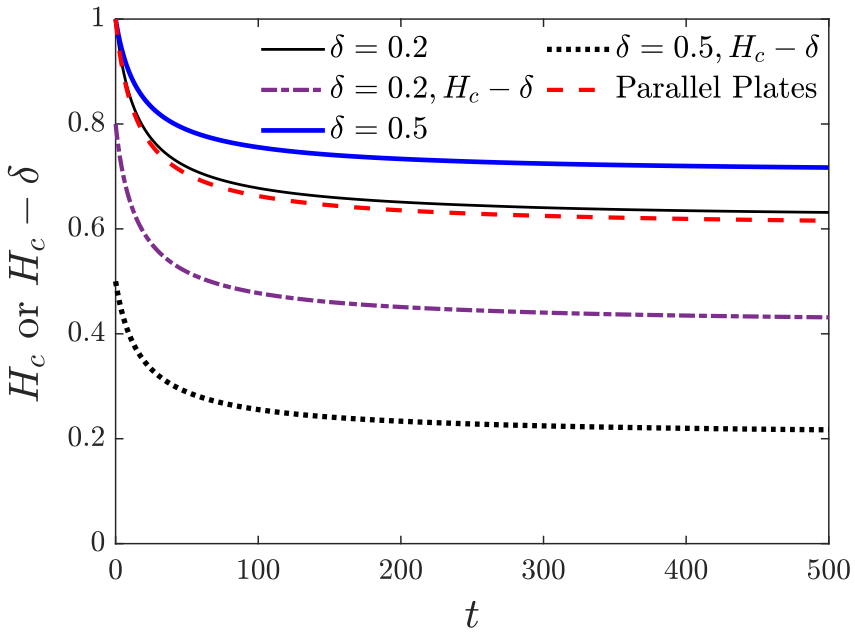

Figure 3.11: Film thickness versus time corresponding to $Od = 0.3$ for parallel plates and non-parallel plates with δ values $\delta = 0.2$ and $\delta = 0.5$.

to the parallel case, with the gap at the right hand ends of the plates never reaching zero thickness as seen for the curves of $H_c - \delta$ (contrast this with section A.3 in appendix A and in particular Figure A.2).

In Figure 3.11 the parallel H_{cf} always lies between the non-parallel H_{cf} and the non-parallel $H_{cf} - \delta$, but is always further from the latter. This follows from equation (3.40) which suggests $H_{cf} - \delta$ is a first order quantity in η and hence first order in δ.

3.3.4 Contributions to the Force

The force contributions (comprised of yield force and viscous force contributions summing to unity) as time proceeds for different Od values and $\delta = 0.2$ are shown in Figure 3.12. The analogous result for the Bingham fluid in a parallel system has been provided in the appendix B, section B.2.5.

For bigger Od numbers in the move and stop region (i.e. $Od = 0.2$, $Od = 0.1$), after relatively short times, yield force dominates the viscous force which is sim-

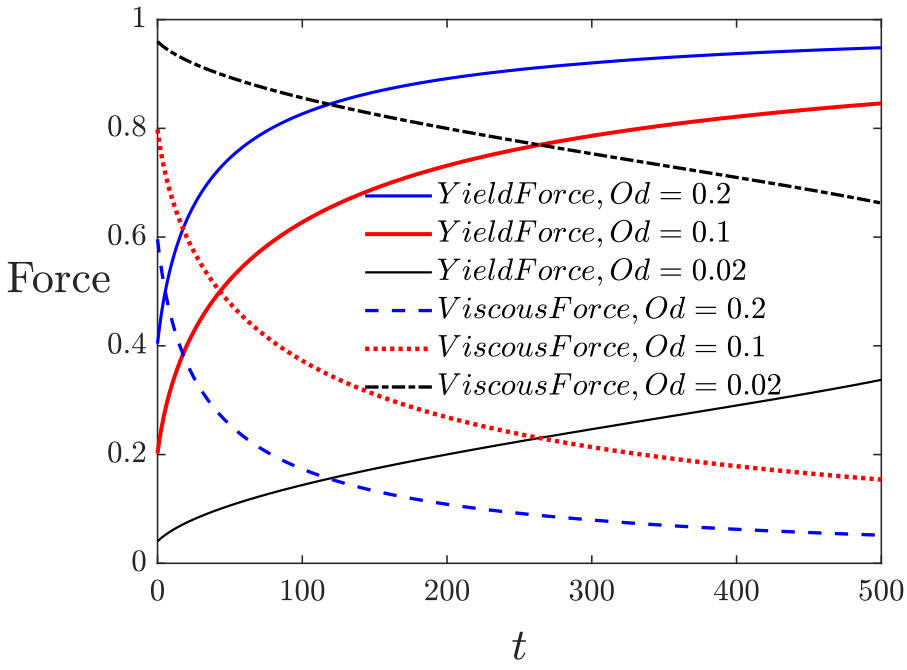

Figure 3.12: Force contributions to the squeeze flow versus time for different Oldroyd numbers and $\delta = 0.2$ in the non-parallel geometry.

ilar to the behaviour of the Bingham parallel system. However, for the smallest Od number considered (i.e. $Od = 0.02$) which is in the move and touch region, the yield force starts small, and despite it growing, it never approaches anywhere near unity. In fact when the plates eventually touch at right hand end of the gap the yield force, can only ever reach $(4Od)/\delta$.

3.3.5 Torque Results

Figure 3.13 shows the numerically computed total torque (T; see the definition in section 3.2.2.6) and also yield torque (T_{yield}; see section 3.2.3.6) versus time for different Od numbers and a constant $\delta = 0.2$. From the figure, for each Od value the total torque is bigger than the yield torque and as time proceeds, the total torque and yield torque come closer together. For the largest Od number plotted (i.e. $Od = 0.2$), in fact total and yield torques are close together for almost all times. However, for the smallest Od number plotted (i.e. $Od = 0.05$), the yield torque starts off very small as mostly viscous torque is present initially

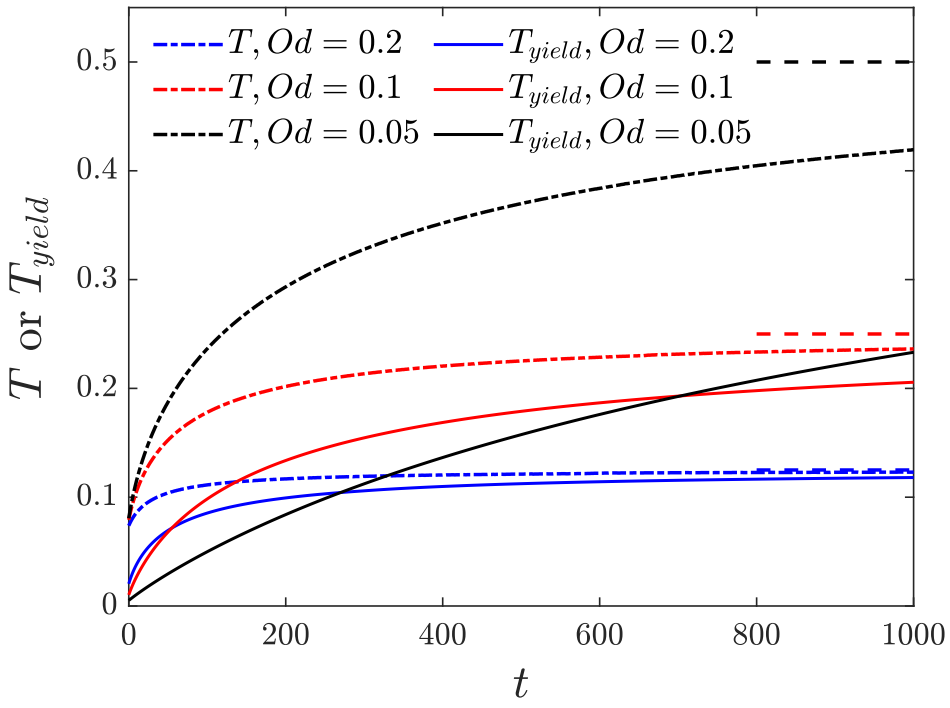

Figure 3.13: Numerically computed total torque and also yield torque versus time for different Od numbers and $\delta = 0.2$. The horizontal dashed lines are the final torques attained in the limit of long times.

and only by increasing the time, do the total and yield torques come closer together. Note that case $Od = 0.05$ with $\delta = 0.2$ has $\eta = 1$ so is on the boundary between the move and stop region and the move and touch region. Any smaller Od number will be in the move and touch region, and in such cases, the yield torque will never reach the same value as the total torque.

Another important point is that as Od decreases, the torque overall increases, whereas the yield torque starts off smaller but finishes larger due to the fact that the smaller the Od number, the greater the nonuniformity (average film thickness relative to film thickness on the right hand end) in the final steady state. This leads to a greater value of x_{cf}, and thus a larger final yield torque. Indeed the predicted final torque for each Od value is found via equation (3.33) and then given x_{cf} from equation (3.38), the final torque is found to be $T_{final} = \delta/(8Od)$. As seen in Figure 3.13, the curves for each Od value are approaching the predicted final torque, although in the $Od = 0.05$ case, the

approach is seen to be rather slow.

This completes the discussion of torque in the Bingham fluid case, although a comparison between torques for Newtonian and Bingham fluids both as functions of x_c has been discussed in section A.3.3 of appendix A, (e.g. see Figure A.4).

3.3.6 Final Steady States

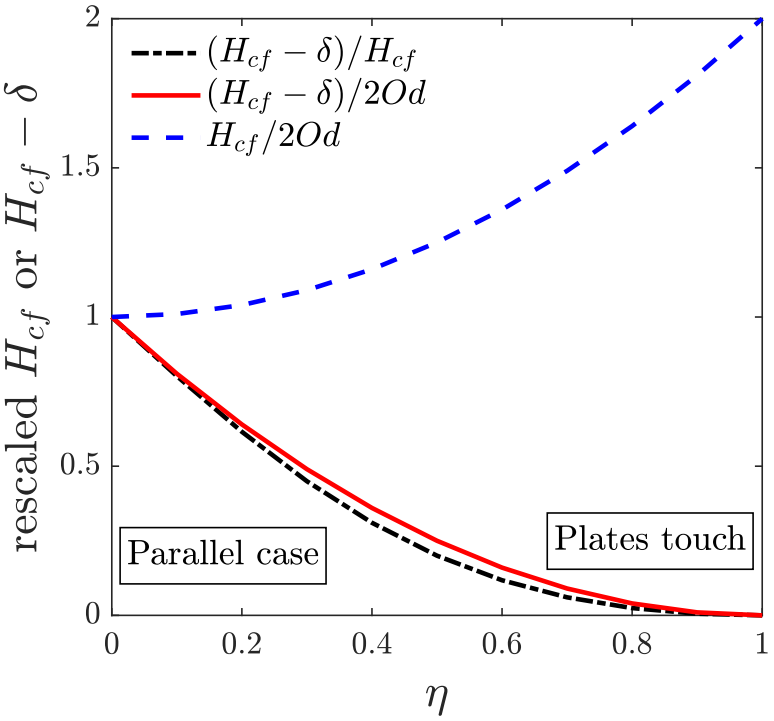

Figure 3.14: Final film thicknesses in terms of $\eta = \delta/(4Od)$ values. The parallel case is $\eta = 0$ and the plates touch at $\eta = 1$.

In Figure 3.14 plots are shown of $H_{cf}/(2Od)$ the average film thickness in the final steady state relative to the parallel case, $(H_{cf}-\delta)/(2Od)$ the minimum film thickness in the final steady state relative to the parallel case, and $(H_{cf}-\delta)/H_{cf}$ which is a measure of how uniform or nonuniform of film thicknesses are, specifically $(H_{cf}-\delta)/H_{cf}$ measures the ratio of the narrowest point to the average film thickness. All these quantities are plotted in terms of η (see equations (3.39)–(3.41)), recalling that they are indeed functions only of η and

not of Od and δ individually. In the case of the ratio $(H_{cf} - \delta)/H_{cf}$ in particular, note that as η increases, this ratio becomes smaller and hence the more polydisperse the system becomes in terms of film thickness, since the narrowest gap at the right hand end is then much thinner than the average thickness.

3.4 Summary

Planar non-Newtonian squeeze film flows between non-parallel plates has been investigated and equations which model the changes of film thickness versus time have been generated.

From the results shown in appendix A, for both Newtonian parallel and non-parallel plates, the film thickness decreases as time increases and both systems have the same behaviour initially. For the parallel plates though the thickness of the gap between the plates never quite reaches zero at any finite time (as it needs infinite time to achieve that), while for the non-parallel case a finite time can be obtained when the plates touch one another at one point at least.

In squeeze flow theory of a Bingham fluid between parallel and non-parallel plates we considered a system squeezed by a fixed applied force (unlike the work of [28] which considered a fixed squeezing rate). Under a fixed applied force, a final film thickness can be found which is very sensitive to Oldroyd number. A maximum Oldroyd number can be found such that film thickness is constant without any squeezing whatsoever, due to the fact that the whole flow field is in a plug region. However, decreasing Oldroyd number allows the system to yield, thereby reduce the film thickness as time increases. In a parallel system, for any finite Oldroyd number, the two plates never touch even at infinite time.

How the non-parallel system behaves depends however upon the ratio be-

tween the tilt angle, δ and the Oldroyd number, Od which is defined as η. If this ratio is small (i.e. $\eta < 1$), the behaviour is analogous to a Bingham fluid in a parallel configuration: squeezing stops while the gap is still finite. If this tilt angle to Oldroyd number ratio becomes too large (i.e. $\eta > 1$) however, the behaviour is more akin to a Newtonian fluid in a non-parallel configuration: the plates touch one another at a point. It is in the narrow part of the gap in which a Bingham fluid is best able to resists squeezing, but for a large tilt angle, the gap can only remain narrow over a very limited distance.

Chapter 4

Asymptotic Behaviour Approaching the Final State of Viscoplastic Bingham Fluid Squeezed between Parallel & non-Parallel Plates

4.1 Introduction

Viscoplastic fluids (i.e. fluids that exhibit a yield stress including as examples gels, muds, pastes, emulsions and foams) form one of the classes of fluids of interest in the field of non-Newtonian fluid mechanics [10]. Even more generally, viscoelastoplastic fluids may exhibit yield stress behaviour also [122]. Nonetheless the archetype of yield stress fluids remains the viscoplastic Bingham fluid which has been first modelled by [39]. There is a large volume of published studies exploring the rheological behaviour of yield stress fluids in general and Bingham fluids in particular [4, 10, 68, 123–126]. It was already

identified by [39] that a viscoplastic material will only start to flow after an imposed stress exceeds a yield stress. A corollary of this however is that, when the material is flowing but the stress is decaying over time, the flow will necessarily stop once stress everywhere falls below the yield stress. Via techniques of [127], a remarkable characteristic of Bingham fluids is therefore that, in finite time, they can stop dead (and their velocity can hence go to zero) due to the aforementioned yield stress effects [34, 35]. This typically happens when the cause of the flow (the driving force) is removed, so that the flow slows and eventually ceases. Meanwhile, for Newtonian fluids in analogous flows [128], the velocity fields go to zero only in the limit of infinite time. In view of this difference, a number of quantitative and qualitative analyses have been performed to establish the finite time decay of viscoplastic Bingham fluids in various geometries and under various conditions [129–132].

Returning to consider fluids in general (not just viscoplastic ones), there are of course many different geometries in which rheology can be studied [12], e.g. steady shear flows, oscillatory shear flows, extensional flows, flows through channel expansions and contractions. One particularly simple geometry to set up however is a squeeze film flow, originally studied by [23] in the context of lubrication theory [133], but also useful for studying interactions between a fluid and the solid that bounds it [134, 135]. Squeeze film flows have moreover been investigated using various types of fluids [21, 57], Newtonian or non-Newtonian. In a squeeze film situation, fluid inertia tends to be insignificant [133], so if a driving force (e.g. a load on the squeeze film) were to be removed, the flow would in principle stop immediately (regardless of the fluid's rheology). Hence a driving force must be applied to continue to have any flow. That said, absence of flow does not necessarily imply absence of a driving force, if the fluid in question happens to be viscoplastic.

It is possible also to distinguish between a squeeze film flow with a constant

squeezing rate (see e.g. [28]) or with a constant applied squeezing force (also known as a constant load case, see e.g. [56]). In the latter case, flow tends to slow down over time even for a Newtonian fluid [23]. This happens because, as the gap becomes narrow, pressures can develop within it that are sufficient to match the applied force despite having a lower shear stress and hence a lower flow velocity along the gap also.

In the case of squeeze film flows of yield stress fluids, many of the results in literature (see e.g. [19, 28, 78]) are for constant rate rather than constant load. A question of interest in studies like those is therefore how the load must vary as the constant rate squeezing proceeds. To determine this, it is necessary to establish, given the kinematics associated with the constant rate squeezing, how the stress field varies both across and along the gap. The stresses then determine lubrication pressures and lubrication forces that ultimately match the varying load. The stresses are however such that fluid in certain regions of the gap (typically close to the plates) is in a yielded plastic region, whereas fluid elsewhere in the gap (typically midway across and midway along the gap) is more plug-like [28]. A yield surface between these regions must be found as part of the solution of the problem.

This however leads to an apparent paradox, the so called “lubrication paradox” for yield stress fluids [25, 31, 70]: different parts of the supposedly plug-like region at different locations along the gap need to move at different velocities. It cannot truly be a plug. One way to resolve this is to consider a so called biviscosity model rather than a yield stress fluid per se [19]. In other words, a fluid can be considered which has a certain viscosity at high shear rates, but with a much higher (albeit still finite) viscosity at low shear rates.

It is however possible to resolve the paradox [72] even for a yield stress fluid, without resorting to biviscosity models. Stress is a tensor, and the dominant

component of that tensor in a typical lubrication flow is a shear stress coupling the directions along the flow direction and across the gap. In the yielded plastic region, this component alone, although not itself as large as the lubrication pressures, is still large enough to exceed the yield criterion for stress. However the conditions for yielding can involve all components of the stress tensor, not just the aforementioned shear stress one. In the nominal plug region, that particular component of the stress tensor is insufficient to produce yielding on its own. Nonetheless, it has been found by [73] that when all components of the tensor are considered, even the nominal plug region very slightly exceeds the yield criterion [72]. Hence even that region deforms, albeit with a much lower strain rate than in the aforementioned plastic region. The nominal yield surface then separates a rapidly strained region from a much more slowly strained one. Sometimes the terms “fully plastic region”, “pseudo-plug region” and “fake yield surface” are used (see [72, 73] for full details), reflecting the fact that even the nominally plug-like region also yields to a certain extent. However, as was also the case in [33], distinctions like those are not central to the arguments that follow.

One issue with constant rate studies though is that it is not possible to interrogate long time behaviour. For constant rate, by definition, we always know exactly what the plate separation is at any instant in time, and we know that there is always a finite time at which the plates come into contact. Hence we cannot ask questions about how yield stresses in particular might cause flow to come to a stop, nor about how the squeeze film flow behaves if and when it is close to stopping. To address questions like those, a constant load (i.e. constant applied squeezing force) must be considered. In fact the solution procedure for determining the squeeze film flows of yield stress fluids at constant rate [28] can be readily adapted to the constant load case also, merely with an extra step of identifying the instantaneous squeezing rate for any instan-

taneous gap thickness. Despite the similarity in procedure, what is however different is the final state of the system, i.e. whether the plates touch at the end of the process or not.

Squeeze film flow of a yield stress fluid between parallel plates and subject to a constant applied squeezing force has been studied by [30]. As already alluded to, the shear stress decays as the gap between the plates decreases: in more and more of the gap, the shear stress decays below the yield stress. The study of [30] accordingly identified that for a viscoplastic Bingham fluid, the flow can cease at a finite final gap thickness even through the load is not removed. In that final state, the gap between the plates remains finite, and yield stresses alone cause sufficient pressure to develop so as to balance the applied force. This feature which makes yield stress fluids attractive for lubrication applications, potentially also mitigating against complications associated with lubricating gaps with rough surfaces[136].

The work of [30] was recently extended by [33]. This showed that the final steady state of a viscoplastic Bingham fluid squeezed between non-parallel plates is qualitatively similar to the parallel plate case, provided the tilt angle remains less than a certain threshold value, albeit the threshold value itself is sensitive to yield stress. This then echoes a more general finding of [137], namely that static (i.e. non-flowing) states of yield stress fluids can be rather common in many different geometries, and are not always trivial to analyse.

Returning specifically to the squeeze film case, although the final steady states under constant load are known, and although [30, 33] also considered unsteady state evolution numerically, what these works did not consider are the details of how the unsteady state solution approaches the final state. Specifically it was not established whether the unsteady state reaches the final state in finite time and then stops dead, or whether this final state is only reached

in the limit of infinite time. This therefore is the question we address in this chapter. What we will find is that the viscoplastic Bingham fluids do not actually stop dead in a squeeze film, but instead they take an infinite time to reach the final state. However, the way in which they approach the final state is faster than for a Newtonian fluid. In yield stress fluids, what we will demonstrate is that the difference between instantaneous gap thickness at any time t and final gap thickness decays proportionally to t^{-1}, whereas for a Newtonian fluid this decays instead proportionally to $t^{-1/2}$.

Thus what we discover in this chapter is that, for a yield stress fluid, there is more than one way to cut off motion quickly. One way, as already alluded to, is cutting off motion in finite time (e.g. by removing a driving force). The other way is still to require infinite time for motion to stop, but even so, for motion to decay faster than for the analogous Newtonian fluid. This chapter explores the latter type of behaviour specifically for a viscoplastic Bingham fluid squeezed between parallel plates in section 4.2. Similar results also apply for a non-parallel plate case discussed in section 4.3, whereas the mathematical analysis is rather more complicated. The results associated with the approach to the final state in parallel and non-parallel cases are discussed in sections 4.5 and 4.6, respectively. The analysis that we used for the parallel case is based on the methodology of [30] which is outlined in appendix B but now focussing specifically on the asymptotic behaviour. Meanwhile, the analysis for the non-parallel case is based on chapter 3.

4.2 Methodology: Asymptotic Behaviour for the Case of a Bingham Viscoplastic Fluid between Parallel Plates Approaching Final State

In this section the behaviour of a Bingham fluid in parallel squeeze film geometry near the final state will be developed. The methodology to be adopted is summarised as follows. In section 4.2.1 we identify parameter values for the squeezed parallel plate system. After that section 4.2.2 considers a yield surface within the squeeze film. Section 4.2.3 then identifies the final state of the squeeze flow. Following that in section 4.2.4, gap thicknesses close to a final state are discussed. After this section however, novel aspects of the methodology are introduced. Section 4.2.5 for instance determines lubrication pressure and lubrication force close to a final state. This then enables us to determine, close to that final state, the speed of approach of the plates enclosing a squeeze film (section 4.2.6) and subsequently the evolution of the gap between them (section 4.2.7).

4.2.1 Parallel Plates System

As alluded already, the case of a Bingham fluid squeezed between parallel plates is discussed in detail in appendix B. In the system studied here depicted in Figure 4.1 say, we have parallel plates of length $2\hat{L}$, with a viscoplastic Bingham fluid in between them. A fixed force $\hat{F}_{app}$ (or more specifically, since we consider a two-dimensional system, force per unit length in the direction normal to the two-dimensional plane) is applied on the upper plate. This moves downward with a time varying velocity, $\hat{v}_{top}$. The initial thickness of the gap between the plates is $\hat{H}_0$ and the instantaneous thickness is $\hat{H}$.

We use governing momentum, continuity and Bingham model equations [25,

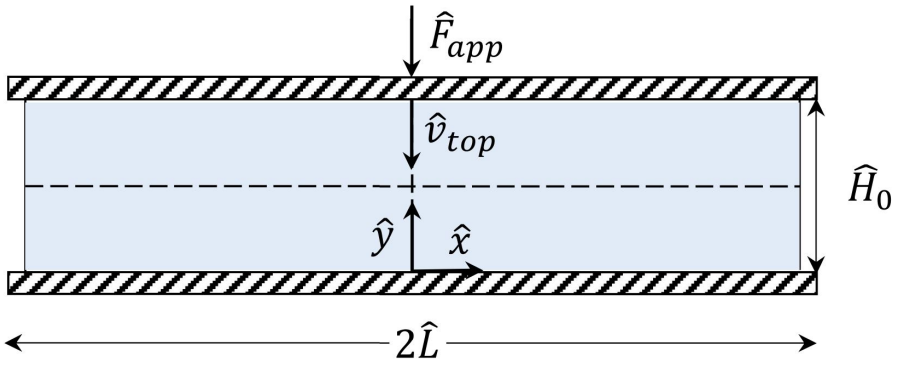

Figure 4.1: Geometry of squeeze film flow between parallel plates.

39, 121] provided in chapter 3. We cast parameters in dimensionless form based on section 3.2.2.1.

The lubrication force that develops in the gap between the plates must match the applied force. In order of magnitude terms, we estimate the lubrication pressure as being order $\hat{F}_{app}/\hat{L}$ and the gradient of the pressure as being order $\hat{F}_{app}/\hat{L}^2$. Momentum balance requires that the pressure gradient should match the divergence of the shear stress. If the shear stress has a typical value τ, then in order of magnitude terms its divergence (at least in the initial configuration with gap thickness $\hat{H}_0$) will be order $\tau/\hat{H}_0$. It follows then that τ will be an order $\hat{H}_0\hat{F}_{app}/\hat{L}^2$ quantity. Note specifically that we use the initial $\hat{H}_0$ and not some other time varying $\hat{H}$ here.

Suppose now that the Bingham fluid has a yield stress τ_0. As was the case in chapter 3, an Oldroyd number can be defined based on equation (3.12) (i.e. $Od \equiv \tau_0\hat{L}^2/(\hat{H}_0\hat{F}_{app})$). Effectively, as alluded to already, this is the ratio between the yield stress τ_0 and the typical imposed shear stress $\hat{H}_0\hat{F}_{app}/\hat{L}^2$, at least assuming a shear stress corresponding to the initial gap thickness. If $Od \ll 1$, then the yield stress is much smaller than the typical shear stress needed to balance applied force. The system must yield, leading then to viscous stresses over and above the yield stress. However as the gap narrows, the shear stress τ required to balance the applied force falls likewise, becom-

ing only order $\hat{H}\hat{F}_{app}/\hat{L}^2$ instead of $\hat{H}_0\hat{F}_{app}/\hat{L}^2$. Eventually τ falls to a value commensurate with the yield stress τ_0.

4.2.2 Determining the Yield Surface

We now work towards identifying the location of the yield surface, which recall separates plastic and plug regions. The analysis follows the approach of [28]. The procedure to find the yield surface is explained in detail in section B.1. It requires first converting from dimensional variables to dimensionless ones (relevant scales are given in chapter 3 and also in Table A.1). We use the same notation for dimensional variables and dimensionless ones, merely with the hat symbol dropped in the case of dimensionless variables. The equation for the yield surface $y_{plug}(x)$ is then as follows

$$y_{plug}^3 - \frac{3}{2}H(t)y_{plug}^2 - 3\frac{v_{top}|x|}{Od}y_{plug} + \frac{3}{2}\frac{v_{top}|x|H(t)}{Od} = 0. \tag{4.1}$$

One issue with solving the above equation for y_{plug} is that v_{top} is a priori unknown. In order to determine the plate velocity v_{top}, in general we need to proceed iteratively as it is discussed in section B.1.1. For any assumed value of v_{top} and any position x along the plates and any given Oldroyd number Od, it is possible to identify the location of a yield surface $y_{plug}(x)$. In any case once the yield surface is identified for an assumed v_{top}, it is possible to deduce the lubrication pressure field developed in the gap (obtained via equation (B.2), i.e. $\mathrm{d}p/\mathrm{d}x = Od/(y_{plug} - (H/2))$), and hence the lubrication force: further details of pressures and lubrication forces that we compute are given later on, see section 4.2.5. The value of v_{top} then generally needs to be adjusted iteratively until the lubrication force balances the applied force. In fact in the dimensionless system considered here, forces have been scaled in such a fashion that the dimensionless applied force is effectively unity.

Another complication however is that equation determining y_{plug} for any given v_{top}, x and Od, is a cubic equation that is rather awkward to solve [33]. Here however we are specifically interested in systems approaching close to their final state. In this limit, small v_{top} is expected. For small v_{top}, the second and fourth terms on the left hand side of equation (4.1) dominate, with the first and third terms becoming smaller (which is easily verified a posteriori). It then follows that

$$y_{plug} \approx \sqrt{|x| v_{top}/Od}. \tag{4.2}$$

For small v_{top} what this equation means is that $y_{plug}(x)$ is small, i.e. the yield surface at $y_{plug}(x)$ and its symmetric partner at $H - y_{plug}(x)$ are both close to the plates. Most of the gap is then in the plug region, and most of the fluid flux out of the gap is carried by the plug, with very little flux contribution from the plastic region. This approximate formula for $y_{plug}(x)$ was originally obtained for a general v_{top} but just in the neighbourhood of $x = 0$. However when v_{top} is small, as happens when the final state is approached, this same formula for y_{plug} applies now for a general x.

4.2.3 Final State

In the present formulation similar to [30] but unlike [28], a constant squeezing force is applied to determine the squeezing rate. Squeezing must however eventually stop. For any given Oldroyd number, a final gap thickness (denoted H_f) can be obtained. Indeed, for large enough values of Od, we will see that even the initial state, which is non-dimensionalized here such that $H = 1$, leads to no motion.

When motion comes to a stop that is equivalent to having $y_{plug} \to 0$ (or equivalently $y_{plug} \ll H/2$) for all x values. Thus, the plug region now fills essentially the entire gap. Putting $y_{plug} = 0$ and $H = H_f$ in pressure gradient equation

(B.2), (i.e. $\mathrm{d}p/\mathrm{d}x = Od/(y_{plug} - (H/2))$)

$$\left|\frac{\mathrm{d}p}{\mathrm{d}x}\right| = \frac{2Od}{H_f}, \tag{4.3}$$

with $\mathrm{d}p/\mathrm{d}x$ being positive if $x < 0$ and negative if $x > 0$. In addition, $p = 0$ at $x = \pm 1$.

Force is obtained by integrating the pressure profile

$$F = \int_{-1}^{1} p(x)\,\mathrm{d}x = \int_{-1}^{0} \frac{2Od}{H_f}(1+x)\,\mathrm{d}x + \int_{0}^{1} \frac{2Od}{H_f}(1-x)\,\mathrm{d}x = \frac{2Od}{H_f}. \tag{4.4}$$

Inserting $F = 1$ in the above equation, we find

$$H_f = 2Od. \tag{4.5}$$

Thus at any given Od the final steady state thickness is just twice the Od number. For small Od, it is possible to squeeze plates really quite close together before they stop moving. As Od increases though, the plates stop moving at a rather larger H_f. Moreover a maximum Oldroyd number equal to $\frac{1}{2}$ is found in order for any squeezing to take place whatsoever: as $Od \to \frac{1}{2}$, there can be no plate motion even at the initial plate separation $H = 1$.

Systems with $Od \geq 1/2$ do not yield at all, but systems with $Od < 1/2$ evolve from $H = 1$ initially to $H_f = 2Od$ at steady state. Newtonian systems, which have Od zero by definition, permit the plates to approach arbitrarily close together, i.e. $H_f \to 0$.

Having determined the final state, what we describe next is how to perturb the system for H close to H_f.

4.2.4 Gap Thicknesses Close to the Final State

Thus far we have identified the final state of the squeeze film flow, but have not determined how rapidly flow comes to a stop. To determine that, what needs to be established is how v_{top} varies as a function of H. We then know that

$$\frac{\mathrm{d}H}{\mathrm{d}t} = -v_{top}, \tag{4.6}$$

the negative sign here arising from the sign convention that plates approaching one another are considered to have positive v_{top}. After finding v_{top} for any given H, we can solve for how H evolves with time t. Clearly v_{top} is identically zero in the final state when $H = H_f$, but the question here is how v_{top} behaves for $H > H_f$, and in particular for H just slightly greater than H_f. Based on arguments presented in [130, 137], the flow of yield stress fluids tends to slow to a stop more quickly than Newtonian fluids do. This then could also impact on the functional form of v_{top} versus H.

For parallel plates with a Newtonian system (originally tackled by [23] but summarised in dimensionless form in [33], see also appendix A), final gap thickness H_f is zero, and velocity $\mathrm{d}H/\mathrm{d}t$ turns out to be $-H^3/8$. The Newtonian solution for H is then

$$H = (1 + t/4)^{-1/2} \tag{4.7}$$

meaning that at long times

$$H \sim 2t^{-1/2}. \tag{4.8}$$

For parallel plates with a viscoplastic yield stress fluid, final gap thickness H_f is non-zero as we have seen. It is convenient then to write

$$H(t) \equiv H_f + \Delta H(t), \tag{4.9}$$

where $\Delta H(t)$ (the difference in gap thickness from the final state) must even-

tually decay towards zero. For a Bingham fluid, we will show shortly as one of the main novel contributions of this work (see section 4.2.6), that in the asymptotic limit when ΔH is small, the value of $\mathrm{d}\Delta H/\mathrm{d}t$ is proportional to $-\Delta H^2$. This still takes an infinite time for ΔH to reach zero, and hence an infinite time for H to reach the final state H_f (see section 4.2.7). However because it involves a quadratic ΔH^2 not a cubic $H^3/8$, the approach is faster than the purely viscous Newtonian case. In addition, in the viscoplastic Bingham fluid case, the value of $\mathrm{d}\Delta H/\mathrm{d}t$ also turns out (again see section 4.2.6) to depend on Oldroyd number Od, and part of our aim here is to elucidate how Od impacts upon the time to approach the steady state.

4.2.5 Determining the Pressure Field and Lubrication Force

Having found a formula for y_{plug} (equation (4.1) or more specifically equation (4.2) close to the final state), we can now determine the pressure field in the gap. Pressure for $x > 0$ obeys equation (B.2), (i.e. $\mathrm{d}p/\mathrm{d}x = Od/(y_{plug} - (H/2))$) and for $x < 0$, it is similar, merely with opposite sign. Physically this is simply a momentum balance, with pressure gradient matched to the divergence of the shear stress. The divergence of the shear stress is then computed on the basis that shear stress vanishes on the centreline of the gap, but equals the yield stress on the yield surface [28].

Close to the final state, in the asymptotic limit of small ΔH and small v_{top}, we Taylor expand the pressure gradient, for $x > 0$

$$\frac{\mathrm{d}p}{\mathrm{d}x} \approx -\frac{2Od}{H_f}\left(1 - \frac{\Delta H}{H_f} + \frac{2y_{plug}(x)}{H_f}\right) \tag{4.10}$$

with an analogous equation for $x < 0$, solely with opposite sign. This equation implies that having finite ΔH makes the magnitude of the pressure gradient slightly smaller (meaning the lubrication pressure is less able to resist

the imposed pressure). Meanwhile having finite y_{plug} makes the magnitude of the pressure gradient slightly bigger (meaning the lubrication pressure is more able to resist the imposed pressure).

Integrating equation (4.10), after substituting from equation (4.2) and imposing conditions that $p = 0$ at $x = \pm 1$, we find

$$p(x) \approx \frac{2Od}{H_f}\left((1-|x|) - \frac{\Delta H}{H_f}(1-|x|) + \frac{4\sqrt{v_{top}/Od}}{3H_f}(1-|x|\sqrt{|x|})\right).$$

In the above equation, the first term is dominant and gives the final pressure field, making a positive contribution to the pressure. The second term has a negative contribution to the pressure due to the fact that when the gap is still thick, the pressure may be rather weak, but it can become stronger and support the force applied on the system when the gap thickness is smaller. The third term has a positive contribution to the pressure, since the system is able to yield in order to increase the pressure to sustain the applied force. We integrate this pressure field $p(x)$ over the whole domain $-1 \leq x \leq 1$ to find the lubrication force F which is comprised of three terms as follows

$$F \approx \frac{2Od}{H_f} - \frac{2Od}{H_f^2}\Delta H(t) + \frac{16Od}{5H_f^2}\sqrt{\frac{v_{top}}{Od}}. \tag{4.11}$$

4.2.6 Determining Speed of Approach of the Plates

In equation (4.11) the lubrication force F, must match the applied force, which is normalised to unity in the dimensionless system being considered here. However the first term on the right hand side, which is the force in the final state, is also necessarily unity (as equation (4.4) already found). In order to keep $F = 1$, the second and third terms on the right hand side are required to be equal. Thus

$$v_{top} \approx \frac{25}{64}Od\,\Delta H(t)^2. \tag{4.12}$$

We recall also (see equation (4.6)) that $\mathrm{d}H(t)/\mathrm{d}t = -v_{top}$ and hence

$$\frac{\mathrm{d}\Delta H(t)}{\mathrm{d}t} \approx -\frac{25}{64} Od\, \Delta H(t)^2. \tag{4.13}$$

As already stated earlier, the value of $\mathrm{d}\Delta H/\mathrm{d}t$ is indeed proportional to $-\Delta H(t)^2$.

The above equation is well known in chemistry and chemical engineering albeit in a different context. It is in fact entirely analogous to the equation that arises for the evolution of reactant concentration for a second order reaction [138] provided reactants are supplied in stoichiometric amounts (neither of them in excess). This then leads to a relatively slow decay because both reactants become exhausted simultaneously, thereby slowing the reaction rate significantly. This is then a rather slower decay than the late-time exponential decay which arises when one reactant is supplied in excess, meaning that just one of them becomes exhausted. On the other hand, the decay is still faster than for a third order reaction in stoichiometric amounts, which is the analogue of equations (4.7) and (4.8). We also observe that the Oldroyd number Od within equation (4.13) is analogous to a second order kinetic rate constant. Hence decreasing Od tends to slow down the decay.

4.2.7 Evolution of the Plate Separation

The gap between the plates $H(t)$ can now be determined remembering here that $\Delta H(t) \equiv H(t) - H_f$ with H_f given by equation (4.4). The solution of equation (4.13) for ΔH versus t is obtained as

$$\Delta H \approx \frac{\Delta H_1}{(25/64) Od\, (t - t_1)\, \Delta H_1 + 1} \tag{4.14}$$

where ΔH_1 is any value at which ΔH is small, and then t_1 is the time at which ΔH reaches ΔH_1. Equation (4.14) cannot be extrapolated for t values much

earlier than t_1, because ΔH would then be predicted to grow, whereas the derivation leading up to equation (4.13) was an asymptotic analysis that assumed small ΔH. On the other hand, for $t > t_1$, the equation should be reliable. Moreover in the limit when $t \gg t_1$ and $(25/64)Od\,(t - t_1)\,\Delta H_1 \gg 1$, we find a very simple formula

$$\Delta H \sim 64/(25Od\,t). \tag{4.15}$$

It follows then that the approach to the final state for the yield stress fluid requires an infinite time and, at any instant in time, the state of the system is sensitive only to the value of Od number (i.e. ratio between yield stress and imposed stress).

In addition to the analytical approximations described above, we can also compute $\Delta H(t) \equiv H(t) - H_f$ versus t numerically (details of the numerical procedure are already discussed in appendix B and [33] so are not reproduced here). If we plot those data on a log-log graph, then based on equation (4.15) a slope -1 is expected for long times. Although this is still an algebraic decay (rather than an exponential one), even so it is faster than the decay of the Newtonian case, given by equation (4.7) and then reducing to equation (4.8), namely $H \sim 2t^{-1/2}$ in the long time limit. Plotting the Newtonian system on a log-log graph will give a slope of $-1/2$, indicating a more gradual decay than happens for a slope of -1.

4.3 Methodology: Asymptotic Behaviour of Viscoplastic Bingham Fluid between non-Parallel Plates on the Approach to Final State

The method to analyse the approach to a final state in the parallel case with a yield stress fluid is outlined in previous section. In this section the fluid behaviour will be established in the tilted, i.e. non-parallel case. The methodology is summarised and discussed as follows. In section 4.3.1 the equation for the yield surface in the squeeze film is developed. Then in section 4.3.2 the approach to determine the pressure profiles and lubrication forces is discussed. After that, we establish the speed of approach of the plates enclosing a squeeze film (section 4.3.3) and finally the evolution of the gap between them is presented in section 4.3.4.

4.3.1 Determining the Yield Surface

There are a few subtleties in the non-parallel case, i.e. the need to perturb x_c (which is the separation point between leftward and rightward flow) away from x_{cf} (the final limiting value of that point). In the parallel case x_c always vanishes on symmetry grounds, so the issue does not arise.

In the non-parallel system, a significant change is that H_f in equation (4.10) becomes a function of x. Hence the equation for the pressure gradient for $x > x_c$ domain considering equations (3.15) and (4.9) after some algebra reduces to

$$\frac{\mathrm{d}p}{\mathrm{d}x} \approx -\frac{2Od}{H_f(x)}\left(1 - \frac{\Delta H(t)}{H_f(x)} + \frac{2y_{plug}(x)}{H_f(x)}\right) \tag{4.16}$$

where $H_f(x) = H_{cf} - \delta\, x$. Recall that H_{cf} (as it is already described in chapter 3) is the final thickness at the centre of the plates. Like equation (4.10) this assumes $\Delta H/H_f \ll 1$ and $y_{plug}/H_f \ll 1$. For $x < x_c$ there is a sign change

in the above equation. Either way though $y_{plug}(x)$ is approximated by equation (3.20) (i.e. $\sqrt{|x - x_{cf}|\, v_{top}/Od}$), remembering here that x_c is close to x_{cf} (as we are near the final state).

Note that for investigating the yield stress behaviour close to final state in the non-parallel case, the system should be in the "move and stop" region described in Figure 3.3. Thus, the Od number should be greater than the value $\delta/4$ and, at long enough times, that then leads to small values of v_{top} and y_{plug}. By contrast, if the plates touch, there needs to be some regions in which y_{plug} is a significant fraction of film half-thickness $H/2$ to keep the pressures in equations (3.21)–(3.22) and hence the associated lubrication forces higher than they would be in a static state. Since H is a function of x (tending to zero at the right hand end if the plates touch), then y_{plug} can be considerable compared with $H/2$ at least near $x = 1$. Indeed the complication in the "move and touch" region at $x = 1$ is that both y_{plug} and H_f are zero. However, in the "move and stop" region as considered here, since the system comes eventually to a stop with H_f always finite, there is a finite minimum value of $H_f(x)$ when $x = 1$. Moreover, close to the final state, a small v_{top} and hence a small $y_{plug}(x)$ can be obtained (much smaller than $H_f(x)/2$, the half-thickness of the gap).

4.3.2 Determining Pressure Profile and Lubrication Force

By integrating equation (4.16), starting from 1 down to x, and from -1 up to x, the pressure fields are obtained. For the $x > x_c$ domain, the pressure field is

$$p = 2Od\left[\frac{1}{\delta}\ln\frac{H_{cf}-\delta x}{H_{cf}-\delta} + \frac{\Delta H}{\delta}\left(\frac{1}{H_{cf}-\delta x} - \frac{1}{H_{cf}-\delta}\right)\right.$$
$$+ 2\sqrt{\frac{v_{top}}{Od}}\left(-\frac{\sqrt{x-x_{cf}}}{\delta(H_{cf}-\delta x)} + \frac{\sqrt{1-x_{cf}}}{\delta(H_{cf}-\delta)}\right.$$
$$\left.\left. + \frac{1}{\delta^{3/2}\sqrt{H_{cf}-\delta x_{cf}}}\left(\tanh^{-1}\sqrt{\frac{\delta(x-x_{cf})}{H_{cf}-\delta x_{cf}}} - \tanh^{-1}\sqrt{\frac{\delta(1-x_{cf})}{H_{cf}-\delta x_{cf}}}\right)\right)\right]. \quad (4.17)$$

For the $x < x_c$ domain, the pressure profile is

$$p = 2Od\left[\frac{1}{\delta}\ln\frac{H_{cf}+\delta}{H_{cf}-\delta x} + \frac{\Delta H}{\delta}\left(\frac{1}{H_{cf}+\delta} - \frac{1}{H_{cf}-\delta x}\right)\right.$$
$$+ 2\sqrt{\frac{v_{top}}{Od}}\left(\frac{\sqrt{x_{cf}-x}}{\delta(H_{cf}-\delta x)} - \frac{\sqrt{1+x_{cf}}}{\delta(H_{cf}+\delta)}\right.$$
$$\left.\left. - \frac{1}{\delta^{3/2}\sqrt{H_{cf}-\delta x_{cf}}}\left(\tan^{-1}\sqrt{\frac{\delta(1+x_{cf})}{H_{cf}-\delta x_{cf}}} - \tan^{-1}\sqrt{\frac{\delta(x_{cf}-x)}{H_{cf}-\delta x_{cf}}}\right)\right)\right]. \quad (4.18)$$

The pressures need to match at $x = x_c$. The pressure profile contains a main term which is the pressure at final state (i.e. no motion) and perturbations due to ΔH and y_{plug} being non-zero: the term involving y_{plug} has been written in terms of v_{top} using equation (3.20). We also however need to account for x_c not being quite the same as the value of x_{cf}. The second and third terms in the above (i.e. terms involving ΔH and y_{plug}) can be evaluated at x_{cf}, but the leading terms should be evaluated at $x_c = x_{cf} + \Delta x_c$ (where Δx_c is a perturbation). Since terms involving ΔH and y_{plug} are already small, considering x_c as being x_{cf} rather than $x_c = x_{cf} + \Delta x_c$ in those terms will not have any effect on the pressure field. This however is not valid for the leading order pressure term, as shifting x_c by a small amount away from x_{cf} would possibly lead to the final pressure failing to meet up.

However the leading order contributions to the leading order pressure terms at $x = x_{cf}$ for both $x > x_c$ and $x < x_c$ domains are equal by definition. Hence that can be subtracted from the leading order expression and the remaining contribution to the pressure will be on the order of Δx_c. Therefore, the above equations once pressures are matched will be reduced to

$$2Od\left[\frac{2\Delta x_c}{H_{cf}-\delta x_{cf}}+\frac{\Delta H}{\delta}\left(\frac{2H_{cf}}{H_{cf}^2-\delta^2}-\frac{2}{H_{cf}-\delta x_{cf}}\right)+2\sqrt{\frac{v_{top}}{Od}}\left(-\frac{\sqrt{1+x_{cf}}}{\delta(H_{cf}+\delta)}\right.\right.$$
$$\left.\left.-\frac{\sqrt{1-x_{cf}}}{\delta(H_{cf}-\delta)}+\frac{1}{\delta^{3/2}\sqrt{H_{cf}-\delta x_{cf}}}\left(\tanh^{-1}\sqrt{\frac{\delta(1-x_{cf})}{H_{cf}-\delta x_{cf}}}+\tan^{-1}\sqrt{\frac{\delta(1+x_{cf})}{H_{cf}-\delta x_{cf}}}\right)\right)\right]$$
$$=0. \quad (4.19)$$

The prefactor for ΔH and y_{plug} perturbation terms are constants (independent of time) and can be denoted as D and E, respectively.

$$D=\left(\frac{2H_{cf}}{H_{cf}^2-\delta^2}-\frac{2}{H_{cf}-\delta x_{cf}}\right) \quad (4.20)$$

$$E = \left(\frac{1}{\delta^{3/2}\sqrt{H_{cf}-\delta x_{cf}}}\left(\tanh^{-1}\sqrt{\frac{\delta(1-x_{cf})}{H_{cf}-\delta x_{cf}}}+\tan^{-1}\sqrt{\frac{\delta(1+x_{cf})}{H_{cf}-\delta x_{cf}}}\right)\right.$$
$$\left.-\frac{\sqrt{1-x_{cf}}}{\delta(H_{cf}-\delta)}-\frac{\sqrt{1+x_{cf}}}{\delta(H_{cf}+\delta)}\right). \quad (4.21)$$

Then equation (4.19) becomes

$$2Od\left[\frac{2\Delta x_c}{H_{cf}-\delta x_{cf}}+\frac{\Delta H}{\delta}D+2\sqrt{\frac{v_{top}}{Od}}E\right]=0. \quad (4.22)$$

Now that we have derived the pressure profiles, we need to integrate equations (4.17) and (4.18) over x to obtain the force,

$$
\begin{aligned}
F = 2Od\Bigg[&\Big(\frac{1}{\delta}(x_c - \frac{H_{cf}}{\delta})\ln\frac{H_{cf}^2-\delta^2}{(H_{cf}-\delta x_c)^2} + \frac{2x_c}{\delta}\Big) \\
&+ \frac{\Delta H}{\delta}\Big(\frac{1}{\delta}\ln\frac{(H_{cf}-\delta x_c)^2}{H_{cf}^2-\delta^2} + \frac{2H_{cf}x_c - 2\delta}{H_{cf}^2-\delta^2}\Big) \\
&+ 2\sqrt{\frac{v_{top}}{Od}}\Bigg(\frac{(1-x_c)\sqrt{1-x_{cf}}}{\delta(H_{cf}-\delta)} - \frac{(1-x_c)}{\delta^{3/2}\sqrt{H_{cf}-\delta x_{cf}}}\tanh^{-1}\sqrt{\frac{\delta(1-x_{cf})}{H_{cf}-\delta x_{cf}}} \\
&+ \frac{1}{\delta^{5/2}}\Bigg(3\sqrt{\delta(1-x_c)} + \frac{\delta(1-x_c)-3(H_{cf}-\delta x_{cf})}{\sqrt{H_{cf}-\delta x_{cf}}}\tanh^{-1}\sqrt{\frac{\delta(1-x_{cf})}{H_{cf}-\delta x_{cf}}}\Bigg) \\
&- \frac{(1+x_c)\sqrt{1+x_{cf}}}{\delta(H_{cf}+\delta)} + \frac{(1+x_c)}{\delta^{3/2}\sqrt{H_{cf}-\delta x_{cf}}}\tan^{-1}\sqrt{\frac{\delta(1+x_{cf})}{H_{cf}-\delta x_{cf}}} \\
&+ \frac{1}{\delta^{5/2}}\Bigg(3\sqrt{\delta(1+x_c)} - \frac{\delta(1+x_c)+3(H_{cf}-\delta x_{cf})}{\sqrt{H_{cf}-\delta x_{cf}}}\tanh^{-1}\sqrt{\frac{\delta(1+x_c)}{H_{cf}-\delta x_{cf}}}\Bigg)\Bigg)\Bigg].
\end{aligned}
\tag{4.23}
$$

Here the two pressure profiles have been integrated from -1 to x_c and from x_c to 1. In the perturbation terms involving ΔH and y_{plug} (or equivalently involving v_{top}), x_c will be replaced by x_{cf}. Moreover, the leading order force expression at $x_c = x_{cf}$ is 1 by definition, a result that follows based on equation (3.30). Note that the leading order contribution to the force is insensitive to Δx_c also, as x_{cf} in practice is chosen in exactly such a way that the leading order term from Δx_c is zero (a result that turns out to follow from final pressures necessarily matching at x_{cf}, so locally near x_c it does not matter which branch of the pressure formula we integrate). Imposing the condition that $F = 1$ leads to the sum of second and third terms (i.e. perturbation) terms becoming zero. Now, balancing those second and third terms at $x_c = x_{cf}$

$$
\frac{\Delta H}{\delta}M = 2\sqrt{\frac{v_{top}}{Od}}N \tag{4.24}
$$

where M and N are as follow

$$M = \left(\frac{1}{\delta}\ln\frac{(H_{cf}-\delta x_{cf})^2}{H_{cf}^2-\delta^2}+\frac{2H_{cf}x_{cf}-2\delta}{H_{cf}^2-\delta^2}\right) \tag{4.25}$$

$$\begin{aligned} N = \Bigg[& -\frac{(1-x_{cf})\sqrt{1-x_{cf}}}{\delta(H_{cf}-\delta)}+\frac{(1-x_{cf})}{\delta^{3/2}\sqrt{H_{cf}-\delta x_{cf}}}\tanh^{-1}\sqrt{\frac{\delta(1-x_{cf})}{H_{cf}-\delta x_{cf}}} \\ & -\frac{1}{\delta^{5/2}}\left(3\sqrt{\delta(1-x_{cf})}+\frac{\delta+2\delta x_{cf}-3H_{cf}}{\sqrt{H_{cf}-\delta x_{cf}}}\tanh^{-1}\sqrt{\frac{\delta(1-x_{cf})}{H_{cf}-\delta x_{cf}}}\right) \\ & +\frac{(1+x_{cf})\sqrt{1+x_{cf}}}{\delta(H_{cf}+\delta)}-\frac{(1+x_{cf})}{\delta^{3/2}\sqrt{H_{cf}-\delta x_{cf}}}\tan^{-1}\sqrt{\frac{\delta(1+x_{cf})}{H_{cf}-\delta x_{cf}}} \\ & -\frac{1}{\delta^{5/2}}\left(3\sqrt{\delta(1+x_{cf})}-\frac{\delta-2\delta x_{cf}+3H_{cf}}{\sqrt{H_{cf}-\delta x_{cf}}}\tan^{-1}\sqrt{\frac{\delta(1+x_{cf})}{H_{cf}-\delta x_{cf}}}\right)\Bigg]. \end{aligned} \tag{4.26}$$

4.3.3 Determining the Speed of the Approach to Final State

Using the expression (4.24), v_{top} can be found as a function of ΔH

$$v_{top} = (\frac{\Delta H M}{2\delta N})^2 Od. \tag{4.27}$$

Substituting v_{top} in equation (4.19) (or equivalently equation (4.22)), Δx_c as a function of ΔH will be acquired

$$\Delta x_c = -\frac{(H_{cf}-\delta x_{cf})\Delta H}{2\delta}(D+\frac{ME}{N}) \tag{4.28}$$

Using H_{cf}, x_{cf} and η definitions from equations (3.37), (3.38) and (3.34), modifying all the parameters in terms of η and Od, we have

$$D = \frac{2\eta^2}{Od(1-\eta^2)^2} \tag{4.29}$$

$$E = \frac{1}{8Od^2\eta}\left[\frac{1}{\sqrt{2\eta(1-\eta^2)}}\left(\tanh^{-1}\sqrt{\frac{2\eta}{1+\eta}} + \tan^{-1}\sqrt{\frac{2\eta}{1-\eta}}\right) - \frac{1}{(1-\eta)\sqrt{1-\eta}} - \frac{1}{(1+\eta)\sqrt{1+\eta}}\right] \quad (4.30)$$

$$M = \frac{\eta}{Od(\eta^2-1)} \quad (4.31)$$

$$N = \frac{1}{8Od^2\eta}\left[-\frac{1}{\sqrt{1-\eta}} + \sqrt{\frac{1-\eta}{2\eta(1+\eta)}}\tanh^{-1}\sqrt{\frac{2\eta}{1+\eta}} - \frac{1}{2\eta}\left(3\sqrt{1-\eta} + \frac{(1+\eta)^2-4}{\sqrt{2\eta(1-\eta^2)}}\tanh^{-1}\sqrt{\frac{2\eta}{1+\eta}}\right) + \frac{1}{\sqrt{1+\eta}} + \sqrt{\frac{1+\eta}{2\eta(1-\eta)}}\tan^{-1}\sqrt{\frac{2\eta}{1-\eta}} - \frac{1}{2\eta}\left(3\sqrt{1+\eta} + \frac{4-(1-\eta)^2}{\sqrt{2\eta(1-\eta^2)}}\tan^{-1}\sqrt{\frac{2\eta}{1-\eta}}\right)\right] \quad (4.32)$$

Now Δx_c follows

$$\Delta x_c = \frac{\eta^2-1}{\eta}\Delta H(D + \frac{ME}{N}) \quad (4.33)$$

where it turns out Δx_c is a negative quantity since the final value of x_c which is denoted as x_{cf} is the largest possible value that can be obtained over the course of this evolution, and hence x_c is always less than x_{cf}. Geometrically this follows because the tilt has more impact (i.e. the ratio between the gap at the right hand end of the plates to the gap at the left hand end of the plates is further from unity) when the gap is thinner. Equation (4.33) indicates how much x_c is evolving on the approach to the final state. Since x_c evolves over time, this equation then gives the final asymptotic approach of x_c to its final value.

4.3.4 Evolution of the Plate Separation

The centre point of the plates (denoted H_c) located at $x = 0$, now satisfies $\mathrm{d}H_c/\mathrm{d}t = -v_{top}$, but $H_c = H_{cf} + \Delta H$ and since H_{cf} is constant, then from

equation (4.27), v_{top} is a known function of ΔH^2, thus, similar to the parallel plates system, a relation for $\mathrm{d}(\Delta H)/\mathrm{d}t$ follows

$$\Delta H = \frac{\Delta H_1}{(\frac{M}{2\delta N})^2 Od(t - t_1)\Delta H_1 + 1}. \tag{4.34}$$

When writing $\delta \equiv 4\,Od\,\eta$ in the expression $(M/2\delta N)^2$ that expression becomes solely a function of η. We will consider this expression further in next section 4.4. Note however that in the limit $\eta \to 0$ (parallel case) it reduces to $25/64$ as per equation (4.14). For much stronger tilt with $\eta \to 1$, we have instead $M \sim -1/(2Od(1-\eta))$, and

$$N \sim \frac{1}{8Od^2}\left(-\frac{1}{\sqrt{1-\eta}} + \frac{1}{\sqrt{1-\eta}}\frac{\pi}{2} - \frac{1}{2}\left(\frac{2}{\sqrt{1-\eta}}\frac{\pi}{2}\right)\right) \sim -\frac{1}{8Od^2}\frac{1}{\sqrt{1-\eta}} \tag{4.35}$$

so that $M/(2\delta N) \sim 2Od/(\delta\sqrt{1-\eta}) \sim 1/(2\sqrt{1-\eta})$. Here we have used the fact that δ approaches $4Od$ when $\eta \to 1$. Finally we deduce, in the $\eta \to 1$ limit, that

$$(\frac{M}{2\delta N})^2 \sim \frac{1}{4(1-\eta)}. \tag{4.36}$$

Computing time for the plates to touch, i.e. $\eta > 1$, in the viscoplastic Bingham case in instances when the plates move and touch, is a difficult task to do. Details of this are expanded upon below.

Numerical schemes are not typically well suited at distinguishing between situations in which plates move and touch in finite time, and those which move and nearly touch in finite time, but then require an infinite time to touch in actuality. To distinguish between these situations therefore, we require an asymptotic analytical approximation, at least close to point of plates touching.

In the Newtonian case, it is possible to obtain this asymptotic approximation (as per appendix A). However even the Newtonian case is non-trivial as sec-

tion A.2.1 explains. Near the point of touching, there is a very large relative difference between the widest part of the gap (on the left hand end of the gap) and the narrowest part of the gap (on the right hand end). Since pressure gradients vary inversely with gap thickness, the pressure field is highly skewed towards the narrow end of the gap. A consequence of this turns out to be that at the instant the plates touch, the approach velocity is not finite, but has instead tended towards zero (albeit it is a logarithmic decay to zero velocity such that time for plates to touch remains finite). Knowing that there is (zero) velocity at the instant when the plates touch is, on its own, no help for determining time for the plates to touch. It is necessary to know how the velocity behaves asymptotically on the approach to touching.

The viscoplastic Bingham case (the rheology now being non-linear) in cases for which the plates move and touch is even harder to tackle than the Newtonian "move and touch" case. The equation we have to solve in general is $\mathrm{d}p/\mathrm{d}x = \pm Od/((H/2) - y_{plug})$.

In the case when the plates move and stop (without touching), it is possible to obtain an analytic approximation of the approach rate and it turns out to take an infinite time for the plates to come to a stop. The reason why an analytical approximation is possible in that case (as it is discussed in section 4.3.1) is that at long enough times, y_{plug} is uniformly small compared with $H/2$. Almost all the flow is in the plug region, and a simplified approximate analytic formula for y_{plug} then follows.

However, the case when the plates move and touch is more challenging. We have the same equation as above to solve. In some parts of the gap, y_{plug} remains small compared to $H/2$. However in other parts of the gap, y_{plug} must become comparable with $H/2$. (Otherwise the plates would simply move and stop, instead of move and touch). Thus in the move and touch case there is no

simplified approximate analytical formula for y_{plug} that applies uniformly over the entire length of the plates. As a consequence, there is no easy way to estimate the pressure field for plates that nearly touch, and hence no easy way to obtain an analytical estimate for the approach velocity for nearly touching plates either.

Therefore, finding time for the plates to touch relies on a very delicate (and a priori unknown) asymptotic behaviour involving very small velocities that nonetheless significantly perturb pressure fields in very narrow gaps. We know the plates move and touch solely due to the absence of a steady state in which they move and stop. However, we do not know the details of the final approach to the move and touch state, nor therefore whether the time required to achieve it is finite or infinite. To summarise, if plates were to move and touch and meet with finite velocity, it would be easy to compute numerically the time for them to touch. However that situation does not arise, not even for a Newtonian case. Instead in the Newtonian case there is a logarithmic singularity and velocity falls to zero at the instant of touching. We then only manage to determine time to touch, owing to an analytic formula for the singular behaviour. A non-Newtonian move and touch case is harder still, as the nonlinearity prevents us from determining the exact nature of any singularity.

To recapitulate, the asymptotic formulae for the approach to the final state of the squeeze film system of a viscoplastic Bingham fluid between parallel and non-parallel plates have been formulated and developed here. In next section results for a squeeze film on the approach to the final state will be compared with the asymptotic formulae.

4.4 Results for Asymptotic Behaviour Approaching Final State of Viscoplastic Bingham Fluid Squeezed between Parallel and non-Parallel Plates

Yield stress fluids will deform and flow similar to a liquid if the local stresses become greater than the yield stress. However, they will behave as an elasto-plastic solid when yield stress exceeds the shear stress [39, 45, 54]. What is interesting about yield stress fluids however is not just how they flow, but also how they stop flowing. Specifically yield stress fluids stop flowing much faster than viscous Newtonian fluids do. It is known that motion of Bingham fluids can decay to zero in finite time [34, 35] when a driving force is removed. Here however, we have analysed a system with a different behaviour in which an infinite time is required for a yield stress fluid to stop flowing while maintaining a constant driving force. Nonetheless, the stopping of the flow for a yield stress fluid is much faster than a viscous Newtonian fluid.

In this section, the results acquired for the asymptotic approach to the final steady state situation for parallel and non-parallel squeeze film geometries are considered to investigate the behaviour of the viscoplastic Bingham fluid rheology. This is done in sections 4.5 and 4.6, respectively.

In the parallel geometry [33], the approach to the final state for the yield stress fluid takes an infinite time and its rate depends only on the value of Oldroyd number Od (i.e. ratio between yield stress and imposed stress). However, for non-parallel configuration, the asymptotic analysis for the approach to the final state still requires infinite time, but depends not just on the the Oldroyd number but on the tilt angle as well.

4.5 Results: Approach to Final State of Squeeze Flow of Viscoplastic Bingham Fluid for Parallel Plates

In what follows, sections 4.5.1–4.5.3 deal with evolution of squeeze film gap thickness, and sections 4.5.2–4.5.4 deal with difference between gap thickness and final gap thickness.

4.5.1 Squeeze Film Gap Thickness versus Time

Figure 4.2 shows the profiles of gap thickness (computed numerically using the procedures of appendix B, section B.1.2 and [33]) versus logarithmic time for a viscoplastic Bingham fluid with different Od values, and also for a Newtonian fluid with $Od = 0$. As seen, for small Oldroyd numbers, the curves will stay close to the Newtonian curve (i.e. $Od = 0$) up to a comparatively long time. Meanwhile the curves for larger Od numbers deviate from the Newtonian graph sooner. In addition to that, gap thickness for each Od number eventually approaches $H_f \equiv 2Od$ at long enough time. Note though that this value is approached sooner as Od increases.

4.5.2 Difference in Gap Thickness versus Time

Figure 4.3 presents both numerical and analytical ΔH (i.e. the difference in gap thickness from the final state) on a logarithmic scale in terms of logarithmic time for different Oldroyd numbers. Here the numerical ΔH is computed using the methodology of explained in appendix B, whereas the analytical ΔH is obtained using equation (4.14). Values of ΔH_1 and t_1 to use within equation (4.14) were themselves read off from the numerical data: see values in Table 4.1. Equation (4.14) is however insensitive to which combination of ΔH_1 and t_1 is

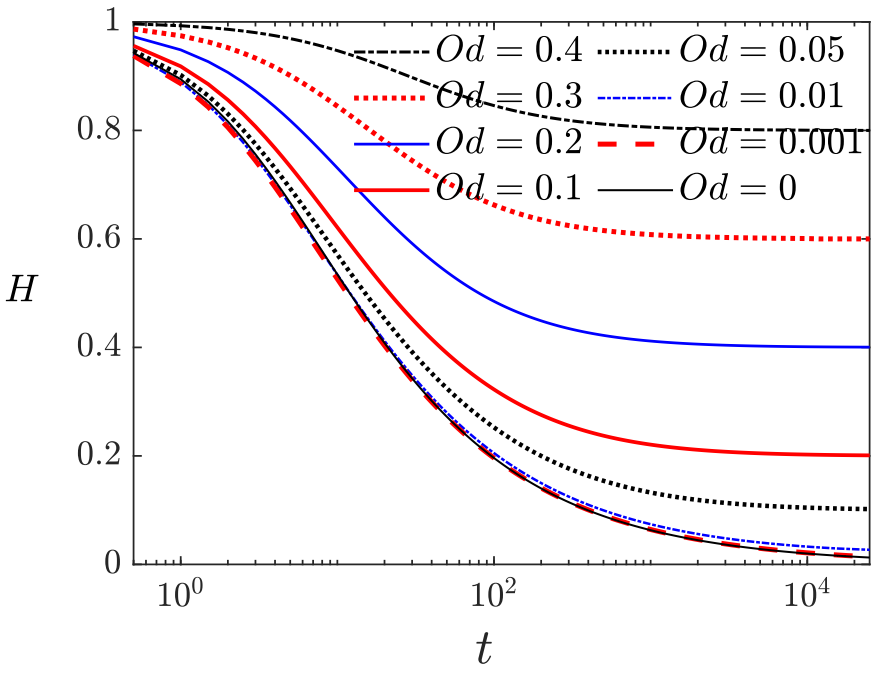

Figure 4.2: Gap thickness H against logarithmic time t for different Od values.

chosen, provided we select a combination with ΔH_1 rather smaller than H_f. This is certainly the case in Table 4.1 when $Od = 0.2$, $Od = 0.1$ or $Od = 0.05$. For $Od = 0.01$ or $Od = 0.001$ this is more difficult to achieve however, as it would require very long t_1 values, so we have opted in those cases for ΔH_1 values just slightly smaller than H_f.

Od	ΔH_1	$\Delta H_1/H_f$	t_1	$Od^2\, t_1$
0.001	0.0013	0.65	40000	0.04
0.01	0.01277	0.6385	10000	1
0.05	0.01044	0.1044	4000	10
0.1	0.00913	0.04565	2500	25
0.2	0.00483	0.012075	2500	100

Table 4.1: Values of ΔH_1 and t_1 used for each Od.

Gap thickness for $Od = 0$ (i.e. Newtonian fluid) decreases with a slope of $-1/2$ in Figure 4.3, at least at long times. Meanwhile subtracting H_f from H to obtain ΔH moves the curves for the viscoplastic Bingham fluid below the Newtonian case.

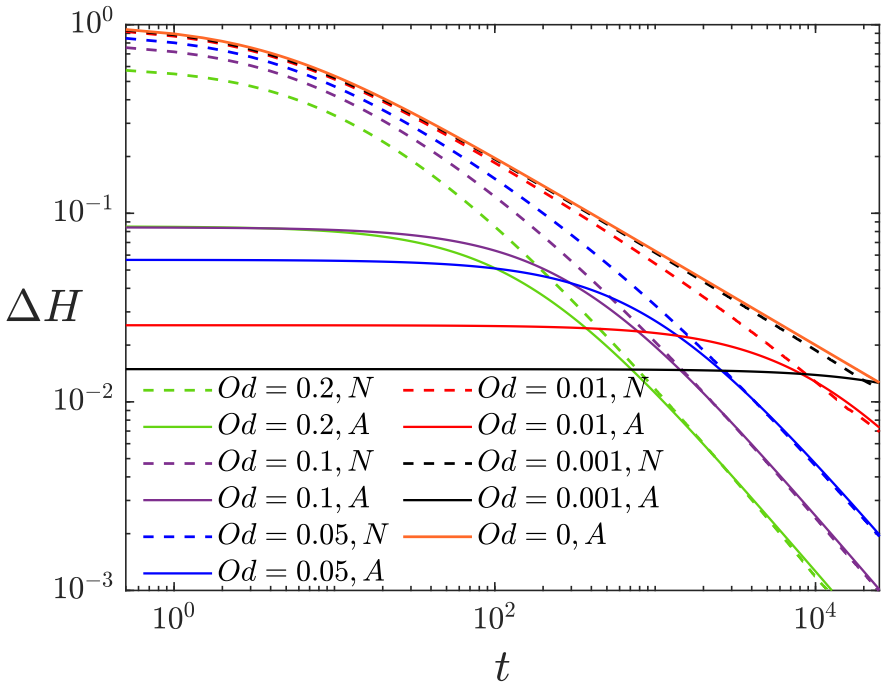

Figure 4.3: Numerical (N) and Analytical (A) values of logarithmic ΔH against logarithmic t for different Od values.

In the Bingham fluid case, by plotting numerical and analytical ΔH values against time, we see that discrepancies arise at early times, but for times greater than t_1, the analytical predictions and numerical data tend to agree. As Od decreases however, we need to select longer and longer times before agreement is attained. Indeed for $Od = 0.001$, the numerical and analytical data are only just starting to agree at the very largest timescales we have considered.

For $Od = 0.2$, $Od = 0.1$, $Od = 0.05$, we see in Figure 4.3 good agreement between numerical and analytical formulae for ΔH less than about 2×10^{-2}, which matches with the notion that $\Delta H / H_f$ needs to be small for the analytical formulae to work well, remembering here that $H_f = 2Od$. Smaller Od values e.g. $Od = 0.01$ and $Od = 0.001$, in principle should require even smaller ΔH values before the analytical formula starts to be reliable. Judging the quality of the analytical formula for these smaller Od is however less straightforward for the following reason. By construction we fit the analytical formula to the

numerical data at t_1 and ΔH_1, and so what we must verify is that the formula continues to fit well for $t \gg t_1$ and $\Delta H \ll \Delta H_1$, but that then needs data out to very long times. Nonetheless, as Table 4.1 makes apparent, when Od is small, meaning that H_f is also small, it is not easy to reach a ΔH_1 that is itself much smaller than H_f.

From Figure 4.3, ΔH for all values of Od number decays towards zero as time proceeds, and moreover the curves at long times appear to acquire a slope of -1 as expected based on equation (4.15). For bigger Od numbers, this regime is attained sooner. For small Od on the other hand, the curves follow the Newtonian case (slope $-1/2$) for quite some time, before deviating towards a slope -1.

4.5.3 Gap Thickness versus Rescaled Time

The timescale that is of interest in this system is order $1/Od^2$, which can be deduced as follows. For small enough Od, systems should start off following Newtonian behaviour (equation (4.7) and eventually equation (4.8), $H \sim 2t^{-1/2}$). However that behaviour must cease once equation (4.8) predicts H values comparable with H_f (with $H_f \equiv 2Od$ itself given by equation (4.5)). This of course happens when $t \sim 1/Od^2$. We can however rescale time (from t to $Od^2\, t$) in an effort to obtain a universal behaviour for different Od values. We also rescale the gap thickness (plotting H/H_f instead of just H). Thus Figure 4.4 presents rescaled logarithmic gap thickness H/H_f against rescaled logarithmic time $Od^2\, t$ for various Od numbers.

As seen, each curve now starts off at a different location for each Oldroyd number, but at sufficiently large $Od^2\, t$ they all collapse together onto a single master curve. In fact since the initial H is unity whereas $H_f \equiv 2Od$, it follows that the initial H/H_f is $(2Od)^{-1}$. Therefore, as Od decreases, the initial H/H_f is

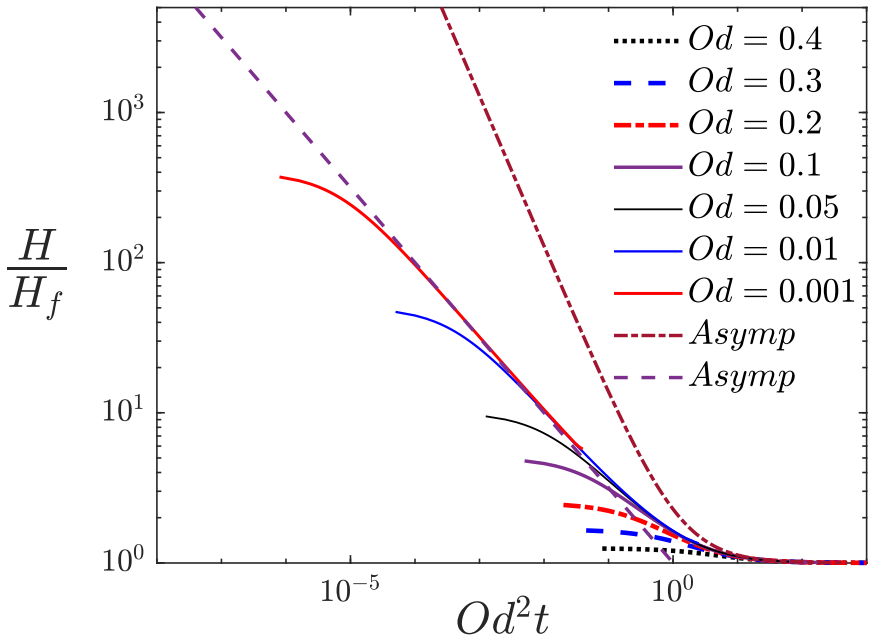

Figure 4.4: Logarithmic ratio of gap thickness to final state gap thickness H/H_f in terms of rescaled logarithmic time, $Od^2\,t$ for different Od values. Long time asymptotic formulae given respectively by equations (4.37) (dash-dot curve) and (4.38) (dashed line) are also plotted.

larger, whilst the master curve is likewise attained at a larger H/H_f value and hence at a smaller $Od^2\,t$. Using equations (4.5), (4.9) and (4.15) a possible asymptotic form for a master curve can be deduced

$$H/H_f \sim 1 + 32/(25Od^2\,t), \tag{4.37}$$

which is plotted within Figure 4.4. Obviously though this formula presents issues for the case $Od \ll 1$, because we then also need very long times t to prevent $Od^2\,t$ from being vanishingly small. If times are not sufficiently long, then the $Od \ll 1$ case should follow instead the Newtonian equations (4.7)–(4.8), not equation (4.15). If a system with $Od \ll 1$ satisfies, at least temporarily, equation (4.8) instead of equation (4.15), we can deduce an asymptotic formula

$$H/H_f \sim (Od^2\,t)^{-1/2}. \tag{4.38}$$

This is also plotted in Figure 4.4.

What is apparent is that equation (4.37) does not give a good fit to H/H_f over a wide domain of H/H_f values, whereas equation (4.38) evidently does, particularly when Od is small. The issue with equation (4.37) is that the analysis leading to it is based on an assumption that ΔH is rather smaller than H_f and hence $H/H_f \equiv 1 + \Delta H/H_f$ can never be much larger than unity if the formula is to be valid.

4.5.4 Difference in Gap Thickness versus Rescaled Time

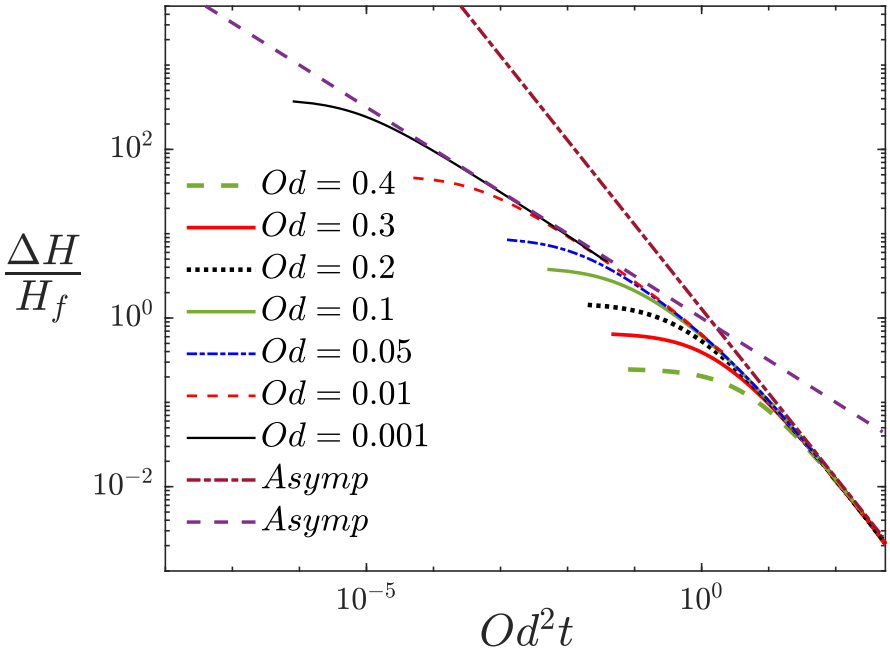

Figure 4.5: Numerical values of rescaled logarithmic $\Delta H/H_f$ in terms of rescaled logarithmic time, $Od^2\,t$ for different Od values. Long time asymptotic formulae given respectively by equations (4.38) (dashed line) and (4.39) (dash-dot line) are also plotted.

Figure 4.5 shows the rescaled logarithmic gap thickness $\Delta H/H_f$ (computed numerically) against rescaled logarithmic time $Od^2\,t$ for different Oldroyd numbers. Recall also the basis for this rescaling: the characteristic timescale to approach close to the final state is expected to be on the order of $1/Od^2$.

In Figure 4.5, all of the plots do appear to collapse together at sufficiently long

times. At very short times of course there are discrepancies: the value of ΔH can never exceed $1 - 2Od$ and so the value of $\Delta H/H_f$ can never exceed $(2Od)^{-1} - 1$. Focussing on asymptotics at much longer times though, the analogue of equation (4.37) is

$$\Delta H/H_f = 32/(25Od^2\, t). \tag{4.39}$$

This is plotted on Figure 4.5. It does fit the data when $Od^2\, t$ is sufficiently large and $\Delta H/H_f$ is sufficiently small. On the other hand, it does not fit the data well for larger $\Delta H/H_f$. To attain large values of $\Delta H/H_f$ (well in excess of unity) we require small Od. Data with small Od (e.g. $Od = 0.001$, $Od = 0.01$) do collapse together in Figure 4.5 but they collapse onto the Newtonian formula given by equation (4.38), also plotted on Figure 4.5. Even though equation (4.38) gives H/H_f rather than $\Delta H/H_f$, they are essentially the same when $\Delta H/H_f$ is large.

A conclusion we draw here is that Figure 4.4 shows that equation (4.37) is not valid over a wide domain of H/H_f values (even though equation (4.39) is valid over, in relative terms, a wide domain of $\Delta H/H_f$ values as Figure 4.5 shows).

4.6 Results: Approach to Final State of Squeeze Flow for a Viscoplastic Bingham Fluid for non-Parallel Plates

In a non-parallel configuration, the approach to the final steady state situation is qualitatively the same as the parallel case (i.e. it takes an infinite time to reach the final film thickness). Whereas the behaviour of Bingham fluid in the parallel system is dependent on the Oldroyd number, in the tilted case, it is reliant also on the ratio between tilt angle δ and Od number which is defined

as η. Specifically we have $\eta = \delta/(4Od)$. In what follows, the difference of gap thickness and final gap thickness with respect to time and rescaled difference in gap thickness against rescaled time are discussed in sections 4.6.1 and 4.6.2, respectively.

4.6.1 Difference in Gap Thickness versus Time

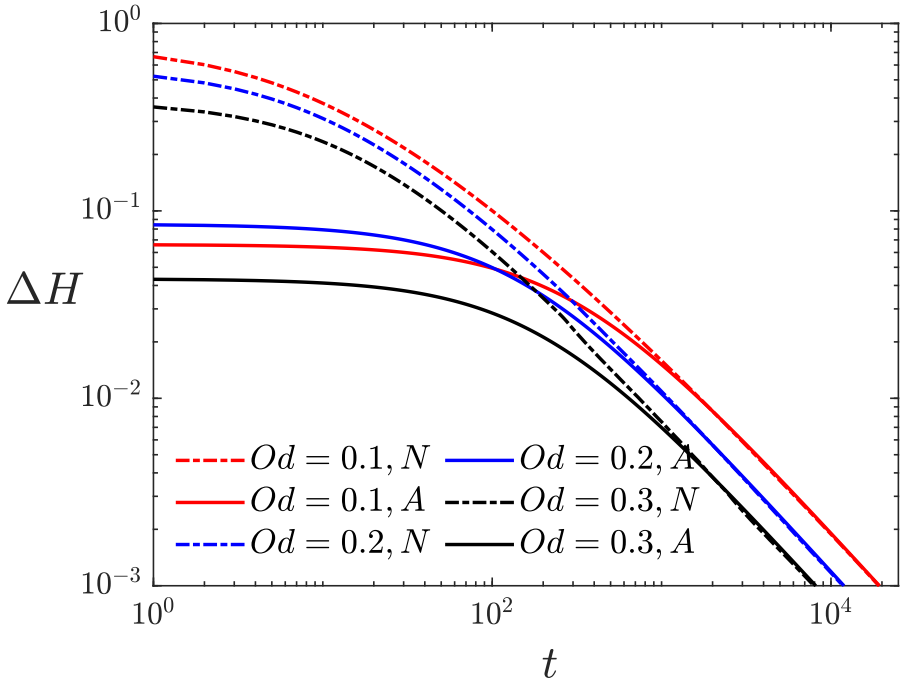

Figure 4.6: Numerical (N) and Analytical (A) values of logarithmic ΔH in terms of logarithmic t for $\delta = 0.2$ and different Od values.

Figure 4.6 shows the logarithmic numerical and analytical difference in gap thickness relative to the final gap thickness for different Oldroyd numbers and a constant tilt angle (i.e. $\delta = 0.2$). The numerical ΔH is computed via the equation $\Delta H = H_c(t) - H_{cf}$ where $H_c(t)$ is calculated numerically through the procedure described in chapter 3, section 3.2.2.5. The analytical ΔH is also computed using analytical equation (4.34) derived in section 4.3.4 in which the ΔH_1 and t_1 have been selected from the numerical values such that for $t > t_1$, and $\Delta H < \Delta H_1 < H_{cf}$. Selected values of ΔH_1 and t_1 for different Od numbers have been provided in Table 4.2.

Od	ΔH_1	$\Delta H_1/H_f$	t_1	$Od^2\, t_1$
0.1	0.0252	0.1008	584	5.84
0.2	0.046	1.08	2500	8
0.3	0.003794	0.00615	2000	180

Table 4.2: Values of ΔH_1 and t_1 used for each Od and a fixed $\delta = 0.2$.

As can be seen from the Figure 4.6 there is a good agreement between numerical and analytical data for ΔH and for all values of Od, the curves will decay to zero. However, for bigger Od values this decay takes place faster compared with the smaller Od numbers.

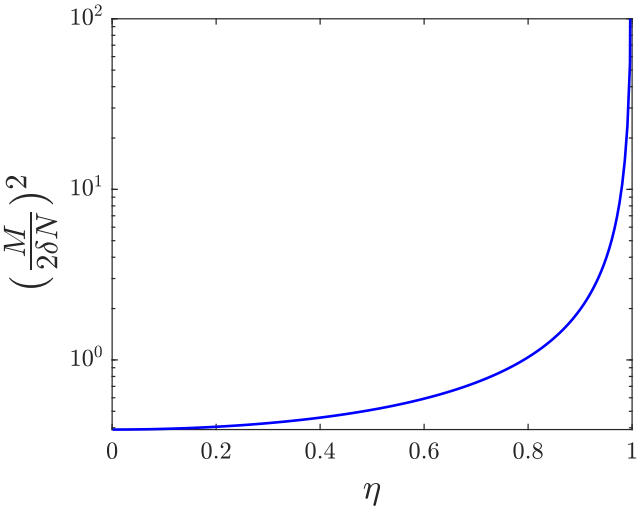

(a) $(\frac{M}{2\delta N})^2$ versus η

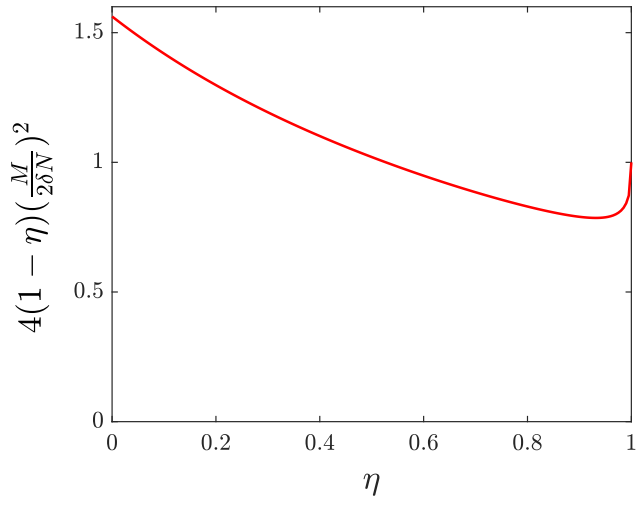

(b) $4(1-\eta)(\frac{M}{2\delta N})^2$ versus η

Figure 4.7: Plots of $(\frac{M}{2\delta N})^2$ and $4(1-\eta)(\frac{M}{2\delta N})^2$ with respect to η.

The behaviour of the yield stress fluid in non-parallel system depends on both Od number and tilt angle δ and recall we defined the ratio of tilt angle and Oldroyd as a parameter called $\eta \equiv \delta/(4Od)$. Thus it is rational to investigate the results based on η rather than Od number or δ individually. Figure 4.7(a) depicts a function $(M/(2\delta N))^2$ in terms of η: at large times, equation (4.34) shows ΔH is decaying to $1/(Od\, t\, f(\eta))$ in which $f(\eta) \equiv (M/(2\delta N))^2$ is a sharply increasing function of η. Thus the decay would be much faster when η is larger: in the limit as $\eta \to 1$ it is possible to show that $f(\eta)$ is proportional to $(1-\eta)^{-1}$ so that $f(\eta)(1-\eta)$ approaches a finite limit. This function is also shown in Figure 4.7(b).

Moreover (see Figure 3.3), if η increases and reaches a value close to 1, then the plates are more likely to move and (almost) touch, at least provided Od is not too large (otherwise they do not move at all). Then, the fact that the moving system is decaying very quickly means that it reaches the final state much more quickly. On the other hand, the gap at the right hand side of the plates at steady state will decrease as η increases. One way to account for this is to rescale data, as discussed below.

4.6.2 Rescaled Difference in Gap Thickness and its Variation with Rescaled Time

As is discussed for parallel plates case in section 4.5.3, the rescaled time for the approach to the final state will be $Od^2 t$. Thus, Figure 4.8 shows the rescaled gap thickness $\Delta H/H_{cf}$ (i.e. $\Delta H/H_{cf}$ is the deviation from the final state relative to the final state) against logarithmic rescaled time for a constant Od number (i.e. $Od = 0.3$) and different values of η. Figure 4.9 shows similar data but plotting $\Delta H/(H_{cf} - \delta)$, i.e. normalised by the gap on the right hand end in the final state, rather than the gap at the centre.

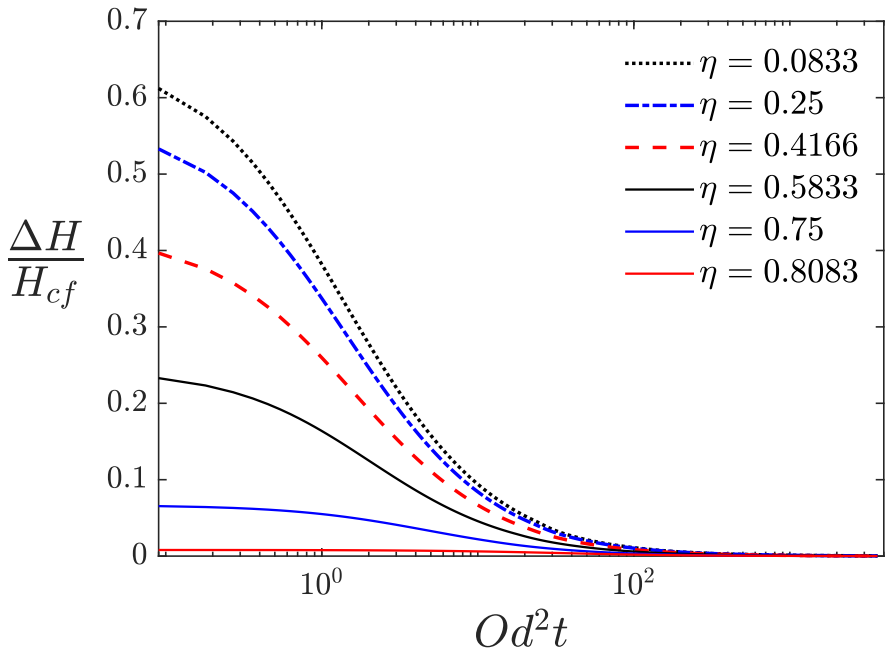

Figure 4.8: Size of ΔH relative to the final gap width H_{cf} against logarithmic rescaled time Od^2t for $Od = 0.3$ and different η values. These are numerical data.

When we consider ΔH against time, ΔH decays more quickly in the non-parallel case (as has been demonstrated with the asymptotic analysis; it decays like $1/(Od\,t\,f(\eta))$ as already mentioned). The value of ΔH also tends to start off smaller if the plates are non-parallel. Meanwhile H_{cf} grows as the plates deviate further and further from parallel. As a result, in Figure 4.8 at initial times, all of the curves start comparatively far away from each other. Then at later times they approach each other as $\Delta H/H_{cf}$ approaches zero. However, even at these later times, the curves with smaller η are always higher up than those with larger η.

The gap at the centre in the final state can however be very different from the gap at the right hand end. For a highly tilted system, ΔH might be small in absolute terms and small relative to H_{cf}, but it might be quite large compared to the gap at the right hand side $H_{cf} - \delta$. We are in a situation here in which the gap at the right hand end is quite small as well. We have a small deviation from the final state (i.e. ΔH) and also a small final gap on the right and that is

why we investigate the ratio between those.

Figure 4.9 shows the deviation from the final state relative to the final gap width at the right hand side of the plates, $\Delta H/(H_{cf}-\delta)$ with respect to the rescaled time, Od^2t for fixed $Od = 0.3$ number and different η values. For these parameter values, the initial value of $\Delta H/(H_{cf}-\delta)$ is non-monotonic in η. As can be seen, for all values of η, all the curves will eventually approach zero at long times.

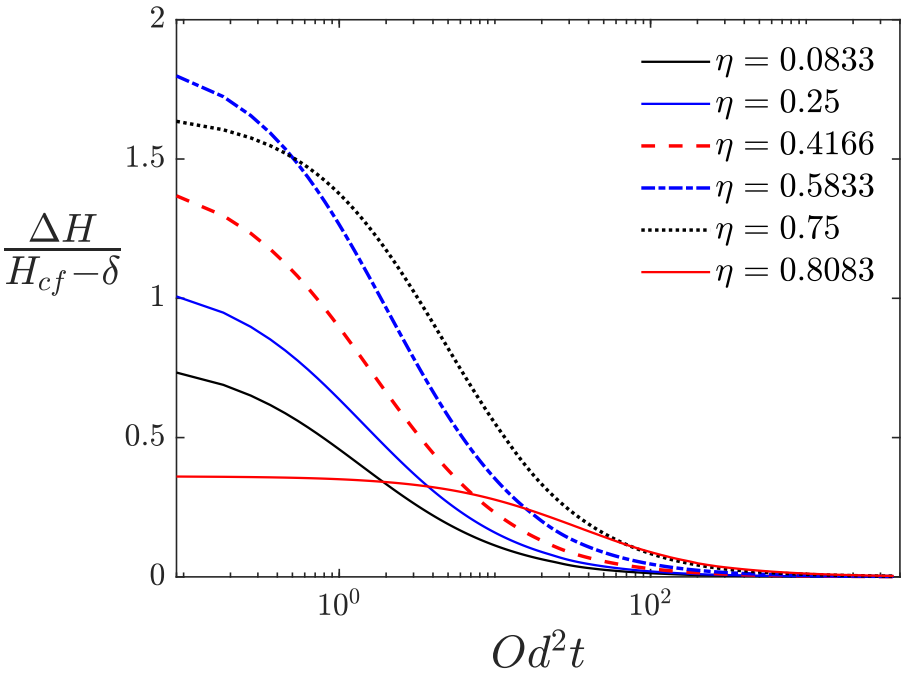

Figure 4.9: Size of ΔH relative to the final gap width at the right hand side of the plates $(H_{cf}-\delta)$ against logarithmic rescaled time Od^2t for $Od = 0.3$ and different η values. These are numerical data.

For η close to 0 (i.e. the parallel geometry) the curves in both Figures 4.8 and 4.9 are broadly the same but for η close to 1 they are rather different since the gap at the centre is then very different from the gap on the right hand side. Comparing Figure 4.8 and 4.9 recall (see section 3.2.3.5) that we have $H_{cf} = 2Od(1+\eta^2)$ and so by changing η, then the value of H_{cf} is not varying dramatically. Meanwhile since $H_{cf}-\delta = 2Od(1-\eta)^2$, varying η will change $H_{cf}-\delta$ significantly particularly when η is relatively close to 1. For small η values, $H_{cf}-\delta$ is around $2Od$ but for larger η, it is much smaller. At long times

$\Delta H/(H_{cf}-\delta)$ is $1/(2Od^2\, t\, f(\eta)\,(1-\eta)^2)$ and the increase in $f(\eta)$ with η is offset by the decrease in $(1-\eta)^2$.

4.7 Summary

In the present squeeze film system assuming constant load and focussing particularly on late times, the Bingham viscoplastic fluids do not stop dead, but rather they take an infinite time to reach the final steady state. However, the way they reach the final state is faster than a Newtonian fluid does. In yield stress fluids, the difference in film thickness from the final one decays on the order of t^{-1}, whereas for a Newtonian fluid the decay is on the order of $t^{-1/2}$. Thus, there is more than one way to cut off one motion quickly. One way is cutting off a motion in finite time by removing the driving force. The other way is to cut off the motion in infinite time while maintaining the driving force but faster than the Newtonian fluids.

Viscoplastic fluids are of interest because they stop much more suddenly than Newtonian fluids do. Indeed these types of fluids have been studied in the past due to the fact that they have the capacity to stop dead in finite time upon removal of a driving force. In this work we looked at a squeeze film system with a different behaviour in which yield stress fluids stop only in infinite time but they still decay faster than Newtonian fluids do. The decay in the motion of squeezed yield stress fluids depend on the Oldroyd number. For instance, for larger Od numbers, the decay is faster than for smaller Od numbers, as the smaller values of Od lead to the fluid behaving similar to a Newtonian fluid.

Chapter 5

Squeeze Film Flow Applications in Papermaking

5.1 Introduction

In the present work, the squeeze film flow of Newtonian and non-Newtonian fluids between two parallel and non-parallel plates has been analysed in an effort to understand the behaviour of foam-fibre suspensions in the foam-formed papermaking process. Relative to conventional water-based papermaking which involves using large flows of water, the process of making paper with foam-forming utilises foam instead of water as a carrier for the fibres. Therefore, it leads to significant sustainability gains by reducing the water footprint of the process [118]. The foam forming technique can produce a paper with more uniform pore size distribution than a water-formed paper [83]. The squeeze flow theory can help to establish the extent to which foam rheology plays a role in establishing the more uniform pore size distribution of foam-formed papers as opposed to papers made with water. The hypothesis to be explored is that, during the course of the papermaking process, as fibres are pushed together to remove the carrier fluid, the foam might be behaving as a contin-

uum viscoplastic fluid, albeit with the viscoplastic fluid properties being related to underlying bubble size. Thus, if the hypothesis were to be borne out, investigation of squeeze film flow would give an insight into whether non-uniformity of the gap between two fibres being pushed together is reflected in the subsequent level of uniformity or non-uniformity of pore sizes of foam-formed paper, and if so, how the non-uniformity of the gap depends on the fluid rheology.

5.2 Foam-formed Papermaking as a Squeeze Film Process

Foam-forming has aroused interest [82] and provides many advantages compared with water-forming. For instance, as already mentioned, reduction of water footprint is realised in the process of making foam-formed paper, which leads to sustainability gains and reduction of energy especially in the drying process [82].

In this thesis, as alluded to earlier, the squeeze film flows of a Newtonian and a non-Newtonian fluid between two parallel and non-parallel plates have been investigated in order to establish the effects of non-Newtonian rheology in the papermaking process. Thus, this should achieve a general insight into the mechanism of fluid-mediated interaction between fibres using different types of fluids (from Newtonian to yield stress fluids). According to the study of [83], pore size distribution of papers made using foam-forming is bigger and more uniform than the pore size distribution of papers made using water. In order to explore a possible reason of this uniform structure, a hypothesis was proposed implying that foam can behave like a continuum fluid with rheology properties which affects the properties of fibre networks structure. The notion (see section 2.5.6 for discussion) is that the squeeze film gap size after squeezing (i.e. after pressing the foam-formed paper pulp to remove the foam carrier fluid prior

to a drying step) might correlate with the typical pore size in the eventual paper, whereas the similarity or difference in final gap size from one side of a tilted fibre to the other might correlate with uniformity or non-uniformity of pore sizes. To the extent that foam rheology (or in other words Oldroyd number) influences squeeze film gap sizes, it could then also influence pore sizes. Therefore, exploring this hypothesis potentially gives insights into pore size distribution that could result due to squeezing fluids with different rheology [28].

5.3 Results and Discussion

The way in which this work has represented the foam as a continuum fluid is convenient due to the fact that the foam structural properties influence primarily the yield stress, and the only place in which the yield stress enters is in the Oldroyd number. The implication of this approach is that the obtained results can easily be compared with the experimental data. For instance, an experimentalist can change the size of bubbles and our established approach then makes the process of comparison effective and straightforward because that parameter (i.e. bubble size) which the experimentalist changes in a laboratory would need to be incorporated in the Oldroyd number definition. In other words, changing of foam structural and hence rheological properties is a characteristic which is incorporated in this work and makes it straightforward to compare with experiments. Therefore, we would be able to make a prediction with the model and then compare the results against experimental data.

To the extent that gap thicknesses and gap non-uniformities as predicted here might correlate with pore sizes and pore size variations in foam-formed paper, the model explored here makes predictions for how pore size distribution might be sensitive to foam rheology. The predictions are distinct from those of the ghost particle hypothesis advanced by [83], so a suitably designed experiment

could distinguish between these models. The prediction of the present model is that smaller bubbles (with larger yield stress [80, 107, 108] and hence larger Oldroyd numbers) lead to larger gaps (hence larger pores). Moreover larger Oldroyd numbers lead to smaller $\eta \equiv \delta/(4Od)$ (i.e. larger Od reduces the influence of tilt angle δ) and hence gives more monodisperse pores (less relative difference in gap size between one side of the fibre and the other). In addition to that, Newtonian fluids between plates on the point of touching have more torque than viscoplastic fluids between plates on the point of touching (see Figure A.4). Moreover, larger Od number keeps the gap wider, thus there is not such a big relative difference in gap size from one side of the gap to the other: this also tends to reduce the impact of torque.

The aforementioned ghost particle hypothesis predicts instead that larger bubbles would give larger pores, and also that polydisperse bubbles are needed to give polydisperse pores: the predictions are distinct as has been mentioned. Note moreover that finding pore size being similar to bubble size for one set of bubble sizes (see e.g. Figure 2.4) is not in itself sufficient to prove the ghost particle hypothesis. It would be necessary to look at different sets of bubble sizes and to see how pore size changed, with the ghost particle hypothesis and the foam rheology hypothesis then predicting opposite trends for pore size.

At least some of the literature [83, 120] on foam-formed papers however suggests that even though foam bubble size is sensitive to surfactant type (as one might expect), it is relatively insensitive to fibre type (i.e. whether fibres are flexible or rigid). That same literature shows that pore size in the foam-formed papers tends to be sensitive to fibre type (i.e. flexible versus rigid) but relatively insensitive to surfactant type (hence insensitive to bubble size). This suggests then that pore size distribution in foam-formed papers is sensitive to solid mechanics of the fibres (differing amounts of fibre-fibre flocculation for the different fibre types might also play a role, see e.g. [82, 93]), and less sen-

sitive to the properties of the foam. It is not then relevant to apply either the ghost particle or the viscoplastic foam rheology models to predict pore sizes in foam-formed paper. So the model explored here is arguably not useful for foam-formed papers but it might still be useful for other applications involving squeeze film flows of viscoplastic materials.

Chapter 6

Conclusions and Future Work

6.1 Conclusions

Historically squeeze film flows have been investigated extensively using various types of fluids [21, 57]. One of the interesting fluids to consider is a viscoplastic Bingham fluid which has been modelled first by [39]. There is a large volume of published studies exploring the rheological behaviour of viscoplastic Bingham fluids [4, 10, 68, 123, 126]. Squeeze film flow of a yield stress fluid between parallel plates has been studied by [30] in which they have formulated the final state of a viscoplastic Bingham fluid. We considered a viscoplastic Bingham fluid squeezed between non-parallel plates (extending the work of [30] which considered merely the parallel geometry) under a fixed applied force (unlike the work of [28] which considered a fixed squeezing rate and parallel plates). We have also investigated the torque for the tilted plates as well as establishing the final state of a viscoplastic Bingham fluid squeezed between non-parallel plates [33].

Under a fixed applied force, a final film thickness can be found at which the plates stop moving. The final thickness is sensitive to Oldroyd number. A max-

imum Oldroyd number can be found beyond which the film thickness remains constant always without any squeezing whatsoever, due to the fact that the whole solution domain is in a plug region even at the initial instant. However, decreasing Oldroyd number allows the system to yield, and thereby reduces the film thickness as time increases. In a parallel system though for any finite Oldroyd number, the two plates never touch even at infinite time. How the non-parallel, viscoplastic system which is considered here behaves depends, however, upon the ratio between the tilt angle, δ and the Oldroyd number, Od, this ratio appearing in the definition of a parameter $\eta \equiv \delta/(4Od)$.

If this ratio is small (i.e. $\eta < 1$), the behaviour is analogous to a viscoplastic Bingham fluid in a parallel configuration: squeezing stops while the gap is still finite. If this tilt angle to Oldroyd number ratio becomes too large (i.e. $\eta > 1$) however, the behaviour is more akin to a Newtonian fluid in a non-parallel configuration: the plates touch one another at a point. It is in the narrow part of the gap in which a viscoplastic Bingham fluid is best able to resist squeezing, but for a large tilt angle, the gap can only remain narrow over a very limited distance. Hence, with sufficient tilt, the applied force overcomes the yield stress even in the narrow part of the gap and drives the plates to touch. Moreover larger Oldroyd numbers lead to smaller η and hence more monodisperse film thicknesses.

Changing Oldroyd number also impacts on torque. Decreasing Od number increases the torque value, and torque also increases as time proceeds. In particular the torque is comprised of viscous and yield stress components. As Od decreases, the yield torque component is typically very small at early times as viscous torque dominates the yield torque. Then, as time proceeds and the system approaches a final state, the yield torque tends to dominate the viscous torque due to the fact that fluid is not moving in the final state.

A remarkable characteristic of viscoplastic Bingham fluids is that they can stop dead and their velocities can go to zero in finite time due to the yield stress effects [34, 35, 127]. Meanwhile, in Newtonian fluids the velocity fields only go to zero at infinite time [128]. Thus viscoplastic fluids (e.g. gels, muds, pastes, emulsions, suspensions, foams) are of interest because, amongst other properties, they can stop flowing much more suddenly than the Newtonian fluids do. As mentioned, studies on these types of fluids in the past have identified that they have the capacity to stop dead in finite time, if a driving force or a load is removed. However viscoplastic fluids can also stop moving even when a load is maintained. In this thesis we looked at a squeeze film problem to explore such behaviour. What we have found is that yield stress fluids in a squeeze film require infinite time to stop, but even so their motion still decays faster than what happens with Newtonian fluids. Specifically we see a decay in the difference between instantaneous squeeze film gap thickness and final gap thickness scaling inversely with time. The Newtonian analogue however scales inversely with only square root of time.

The decay towards the final thickness in yield stress fluids depends also on the Oldroyd number Od, which measures the ratio between the yield stress and the initial applied stress. For larger Od numbers i.e. larger yield stresses, the decay towards the final state is faster than for smaller Od numbers. This implies an advantage of selecting fluids with larger Od in lubrication applications: squeeze films approach a final gap thickness more rapidly, and then remain at that thickness. On the other hand, smaller values of Od lead to the system behaving, for quite some time, similar to a Newtonian fluid with its slower decay. It is then only at very long times that the faster than Newtonian decay in rate of squeezing becomes evident. Although many of the results presented here concern parallel squeeze films, it turned out they also extend to the non-parallel case, albeit the calculations were less simple to perform than for the

parallel case.

The model explored here also makes predictions (distinct from those of the so called ghost particle hypothesis advanced by [83]) for how the pore size distribution of a foam-formed porous medium (e.g. foam-formed paper) might be sensitive to foam rheology: a suitably designed experiment could therefore distinguish between these models. The prediction of the present model is that smaller bubbles (which have larger yield stress and hence larger Oldroyd numbers) lead to larger gaps (hence larger pores). Moreover larger Oldroyd numbers leads to more monodisperse pores. What we discovered though based on literature [83, 94] is that pore size distribution in foam-formed papers is sensitive to the fibre types so that it is sensitive to solid mechanics of the fibre. In circumstances like that it is not relevant to use either ghost particle or the foam rheology models, as these are sensitive only to the properties of the foam. So the model explored here is not useful for foam-formed papers but it might be useful for other applications of squeezed yield stress fluids.

6.2 Future Work

Although we have obtained model predictions for squeezed yield stress fluids it is worth reflecting on the limitations of the model, that would need to be overcome in future work. We have considered a two dimensional planar system (squeezing plates together): squeezing together fibres is however a three dimensional problem, and it is likely to be easier for fluid to escape in that case since it can flow in various directions. Moreover we have ignored rotation of the plates. In reality the pressure field induced in the squeeze film, places not just a force on the plates (that balances the applied force) but also, as we have discussed, a torque. By balancing torque in addition to force it should be possible to deduce both a plate squeezing rate and a plate rotation rate. Rotation

does however lead to a slightly more complicated flow field in the squeeze film (specifically equation (3.17) no longer applies; this is a complication, because depending on the values of rotation rate, squeezing rate and flow rate midway along the plates, it can be shown that there might be a single x location at which there is flow neither to left or right as in the non-rotating case, or there might be two such x locations, or no such location – this needs to be explored further to establish which case is realized in practice). Here of course, rather than computing rotation, we have computed instead the torques that develop in the absence of rotation. Nevertheless the signs of those torques suggest that had rotation been permitted, it would have been such as to move the configuration closer to parallel as time evolved.

Although the analysis discussed in chapter 4 is for a non-rotating case, it raises interesting questions regarding what might happen in a rotating case. From [31, 126] we know that yield stress fluids have a habit of stopping more quickly that viscous fluids do, and we know that there are solutions for final states with non-zero tilt (which balance fluid lubrication force to imposed force, albeit they do not necessarily balance torque). We expect that rotation (needed to balance torque) will tend to reduce the amount of tilt (possibly at a different rate in a yield stress fluid than in a viscous fluid though).

Now the question that is raised is whether the rotating system can ever stop moving even with non-zero tilt. In other words, for a given Oldroyd number, are there combinations of film thickness and tilt angle that balance imposed force but simultaneously have zero net torque? For instance, if an arbitrarily oriented tilted particle is inserted into a strong enough gel (i.e. a fluid with high enough yield stress), the tilted particle should stay there without moving. However that is not a problem for attempting to balance torque, because there is no constraint that the shear stress at the tilted particle surface must equal the yield stress. Any shear stress less than the yield stress will do and will

keep the particle in place.

For the case of our system however the tilted fibre was moving and then stops. Hence, at the point where it stops, the shear stress at the fibre must be the yield stress, not some lower value. Otherwise there would not have been motion up to this point. Since the y derivative of the shear stress matches the x derivative of the pressure, imposing a (shear stress) equal to a (yield stress) condition at the fibre surface seems like a strong constraint (much stronger that the aforementioned case of the arbitrarily oriented particle placed in a gel). Therefore it probably still is the case in this system that the fibre must rotate to parallel if torque is to balance as motion also ceases.

Bibliography

[1] M. J. Crochet, A. R. Davies, and K. Walters. *Numerical simulation of non-Newtonian flow*. Elsevier, 2012.

[2] R. C. Baker. Review: Internal fluid flow: The fluid dynamics of flow in pipes and ducts. by AJ Ward-Smith. *Journal of Fluid Mechanics*, 113: 530–533, 1981.

[3] M. A. Rao. *Rheology of fluid and semisolid foods: Principles and applications*. Springer Science & Business Media, 2010.

[4] P. Coussot. Yield stress fluid flows: A review of experimental data. *Journal of non-Newtonian Fluid Mechanics*, 211:31–49, 2014.

[5] R. L. Peek Jr. Parallel plate plastometry. *Journal of Rheology*, 3(3): 345–372, 1932.

[6] P. Coussot. *Rheometry of pastes, suspensions, and granular materials: applications in industry and environment*. John Wiley & Sons, 2005.

[7] H. A. Barnes. The yield stress – a review or 'panta rei' – everything flows? *Journal of non-Newtonian Fluid Mechanics*, 81:133–178, 1999.

[8] G. W. S. Blair. On the nature of "yield-value". *Physics*, 4(3):113–118, 1933.

[9] P. Coussot. Rheophysics of pastes: A review of microscopic modelling approaches. *Soft Matter*, 3(5):528–540, 2007.

[10] P. Coussot, A. Y. Malkin, and G. Ovarlez. Introduction: Yield stress – or 100 years of rheology. *Rheologica Acta*, 56(3):161–162, 2017.

[11] Q. Barral, G. Ovarlez, X. Chateau, J. Boujlel, B. Rabideau, and P. Coussot. Adhesion of yield stress fluids. *Soft Matter*, 6(6):1343–1351, 2010.

[12] H. A. Barnes, J. F. Hutton, and K. Walters. *An Introduction to Rheology*. Elsevier, Amsterdam, 1st edition, 1989.

[13] R. I. Tanner and K. Walters. *Rheology: An historical perspective*, volume 7. Elsevier, 1998.

[14] J. F. Steffe. *Rheological methods in food process engineering*. Freeman Press, 1996.

[15] A. Leighton, A. Leviton, and O. E. Williams. The apparent viscosity of ice cream: I. The sagging beam method of measurement. II. Factors to be controlled. III. The effects of milkfat, gelatin and homogenization temperature. *Journal of Dairy Science*, 17(9):639–650, 1934.

[16] J. Mewis and N. J. Wagner. Current trends in suspension rheology. *Journal of non-Newtonian Fluid Mechanics*, 157(3):147–150, 2009.

[17] R. P. Chhabra. Non-Newtonian fluids: An introduction. In *Rheology of complex fluids*, pages 3–34. Springer, 2010.

[18] E. J. O'Donovan and R. I. Tanner. Numerical study of the Bingham squeeze film problem. *Journal of non-Newtonian Fluid Mechanics*, 15 (1):75–83, 1984.

[19] D. N. Smyrnaios and J. A. Tsamopoulos. Squeeze flow of Bingham

plastics. *Journal of non-Newtonian Fluid Mechanics*, 100(1–3):165–189, 2001.

[20] J. D. Jackson. A study of squeezing flow. *Applied Scientific Research, Section A*, 11(1):148–152, 1963.

[21] D. F. Moore. A review of squeeze films. *Wear*, 8(4):245–263, 1965.

[22] M. Stefan. Experiments on apparent adhesion. *The London, Edinburgh, and Dublin Philosophical Magazine and Journal of Science*, 47(314): 465–466, 1874.

[23] O. Reynolds. IV. On the theory of lubrication and its application to Mr. Beauchamp Tower's experiments, including an experimental determination of the viscosity of olive oil. *Philosophical Transactions of the Royal Society of London*, 177:157–234, 1886.

[24] J. D. Sherwood, G. H. Meeten, C. A. Farrow, and N. J. Alderman. Squeeze-film rheometry of non-uniform mudcakes. *Journal of non-Newtonian Fluid Mechanics*, 39(3):311–334, 1991.

[25] S. D. R. Wilson. Squeezing flow of a Bingham material. *Journal of non-Newtonian Fluid Mechanics*, 47:211–219, 1993.

[26] M. J. Adams, B. Edmondson, D. G. Caughey, and R. Yahya. An experimental and theoretical study of the squeeze-film deformation and flow of elastoplastic fluids. *Journal of non-Newtonian Fluid Mechanics*, 51(1): 61–78, 1994.

[27] M. J. Adams, İ. Aydin, B. J. Briscoe, and S. K. Sinha. A finite element analysis of the squeeze flow of an elasto-viscoplastic paste material. *Journal of non-Newtonian Fluid Mechanics*, 71(1-2):41–57, 1997.

[28] L. Muravleva. Squeeze plane flow of viscoplastic Bingham material. *Journal of non-Newtonian Fluid Mechanics*, 220:148–161, 2015.

[29] W. Hai. A review of porous squeeze films. *Wear*, 47(2):371–385, 1978.

[30] G. H. Covey and B. R. Stanmore. Use of the parallel-plate plastometer for the characterisation of viscous fluids with a yield stress. *Journal of non-Newtonian Fluid Mechanics*, 8(3–4):249–260, 1981.

[31] I. A. Frigaard and D. P. Ryan. Flow of a visco-plastic fluid in a channel of slowly varying width. *Journal of non-Newtonian Fluid Mechanics*, 123 (1):67–83, 2004.

[32] J. R. Lin. Squeeze film characteristics between a sphere and a flat plate: Couple stress fluid model. *Computers & Structures*, 75(1):73–80, 2000.

[33] E. Esmaeili, P. Grassia, and C. A. Torres Ulloa. Squeeze film flow of viscoplastic Bingham fluid between non-parallel plates. *Journal of non-Newtonian Fluid Mechanics*, 305:104817, 2022.

[34] R. R. Huilgol, B. Mena, and J. M. Piau. Finite stopping time problems and rheometry of Bingham fluids. *Journal of non-Newtonian Fluid Mechanics*, 102(1):97–107, 2002.

[35] M. Chatzimina, G. C. Georgiou, E. Argyropaidas, I.and Mitsoulis, and R. R. Huilgol. Cessation of Couette and Poiseuille flows of a Bingham plastic and finite stopping times. *Journal of non-Newtonian Fluid Mechanics*, 129(3):117–127, 2005.

[36] T. Hjelt, J. A. Ketoja, H. Kiiskinen, A. I. Koponen, and E. Pääkkönen. Foam forming of fiber products: A review. *Journal of Dispersion Science and Technology*, 43:1–37, 2020.

[37] V. J. Langlois and S. Hutzler. Dynamics of a flexible fibre in a sheared

two-dimensional foam: Numerical simulations. *Colloids and Surfaces A: Physicochemical and Engineering Aspects*, 534:105–111, 2017.

[38] J. Lehmonen, E. Retulainen, J. Paltakari, K. Kinnunen-Raudaskoski, and A. Koponen. Dewatering of foam-laid and water-laid structures and the formed web properties. *Cellulose*, 27(3):1127–1146, 2020.

[39] E. C. Bingham. *Fluidity and plasticity*, volume 2. McGraw-Hill, 1922.

[40] D. V. Boger and K. Walters. *Rheological phenomena in focus*. Elsevier, 2012.

[41] M. A. Rao and J. F. Steffe. *Viscoelastic properties of foods*. Elsevier Applied Science New York, 1992.

[42] R. W. Soutas-Little. *Elasticity*. Courier Corporation, 2012.

[43] Isaac Newton and NW Chittenden. *Newton's principia: The mathematical principles of natural philosophy*. Geo. P. Putnam, 1850.

[44] N. Chandran, C. Sarathchandran, and S. Thomas. Introduction to rheology. In *Rheology of Polymer Blends and Nanocomposites*, pages 1–17. Elsevier, 2020.

[45] T. C. Papanastasiou and A. G. Boudouvis. Flows of viscoplastic materials: Models and computations. *Computers & Structures*, 64(1-4): 677–694, 1997.

[46] D. Bonn and M. M. Denn. Yield stress fluids slowly yield to analysis. *Science*, 324(5933):1401–1402, 2009.

[47] J. A. Tichy. Hydrodynamic lubrication theory for the Bingham plastic flow model. *Journal of Rheology*, 35(4):477–496, 1991.

[48] S. G. E. Lampaert and R. A. J. van Ostayen. Lubrication theory for Bingham plastics. *Tribology International*, 147:106160, 2020.

[49] K. Walters and W. M. Jones. Measurement of viscosity. In *Instrumentation Reference Book*, pages 45–52. Elsevier, 2003.

[50] W. H. Herschel. Consistency of rubber benzene solutions. *Industrial & Engineering Chemistry*, 16(9):927–927, 1924.

[51] H. A. Barnes and K. Walters. The yield stress myth? *Rheologica Acta*, 24(4):323–326, 1985.

[52] G. H. Meeten. Effects of plate roughness in squeeze-flow rheometry. *Journal of non-Newtonian Fluid Mechanics*, 124(1–3):51–60, 2004.

[53] B. Géraud, L. Jørgensen, L. Petit, H. Delanoë-Ayari, P. Jop, and C. Barentin. Capillary rise of yield-stress fluids. *EPL (Europhysics Letters)*, 107 (5):58002, 2014.

[54] R. B. Bird, G. C. Dai, and B. J. Yarusso. The rheology and flow of viscoplastic materials. *Reviews in Chemical Engineering*, 1(1):1–70, 1983.

[55] O. H. Campanella and M. Peleg. Squeezing flow viscometry for nonelastic semiliquid foods: Theory and applications. *Critical Reviews in Food Science and Nutrition*, 42(3):241–264, 2002.

[56] G. H. Meeten. Yield stress of structured fluids measured by squeeze flow. *Rheologica Acta*, 39(4):399–408, 2000.

[57] J. Engmann, C. Servais, and A. S. Burbidge. Squeeze flow theory and applications to rheometry: A review. *Journal of non-Newtonian Fluid Mechanics*, 132(1–3):1–27, 2005.

[58] G. Brindley, J. M. Davies, and K. Walters. Elastico-viscous squeeze films. Part I. *Journal of non-Newtonian Fluid Mechanics*, 1(1):19–37, 1976.

[59] O. H. Campanella and M. Peleg. Squeezing flow viscosimetry of peanut butter. *Journal of Food Science*, 52(1):180–184, 1987.

[60] P. J. Leider and R. B. Bird. Squeezing flow between parallel disks. I. Theoretical analysis. *Industrial & Engineering Chemistry Fundamentals*, 13(4):336–341, 1974.

[61] P. J. Leider. Squeezing flow between parallel disks. II. Experimental results. *Industrial & Engineering Chemistry Fundamentals*, 13(4):342–346, 1974.

[62] B. Debbaut. Non-isothermal and viscoelastic effects in the squeeze flow between infinite plates. *Journal of non-Newtonian Fluid Mechanics*, 98 (1):15–31, 2001.

[63] Y. Tian, S. Wen, and Y. Meng. Compressions of electrorheological fluids under different initial gap distances. *Physical Review E*, 67(5):051501, 2003.

[64] A. K. El Wahed, J. L. Sproston, R. Stanway, and E. W. Williams. An improved model of ER fluids in squeeze-flow through model updating of the estimated yield stress. *Journal of Sound and Vibration*, 268(3): 581–599, 2003.

[65] S. H. Chu, S. J. Lee, and K. H. Ahn. An experimental study on the squeezing flow of electrorheological suspensions. *Journal of Rheology*, 44(1):105–120, 2000.

[66] N. Phan-Thien and R. I. Tanner. Lubrication squeeze-film theory for the Oldroyd-B fluid. *Journal of non-Newtonian Fluid Mechanics*, 14:327–335, 1984.

[67] P. Kaushik, P. K. Mondal, S. Pati, and S. Chakraborty. Heat transfer and

entropy generation characteristics of a non-Newtonian fluid squeezed and extruded between two parallel plates. *Journal of Heat Transfer*, 139 (2):022004, 2017.

[68] D. Bonn, M. M. Denn, L. Berthier, T. Divoux, and S. Manneville. Yield stress materials in soft condensed matter. *Reviews of Modern Physics*, 89:035005, 2017.

[69] B. Rabideau, C. Lanos, and P. Coussot. An investigation of squeeze flow as a viable technique for determining the yield stress. *Rheologica Acta*, 48:517–526, 2009.

[70] G. G. Lipscomb and M. M. Denn. Flow of Bingham fluids in complex geometries. *Journal of non-Newtonian Fluid Mechanics*, 14:337–346, 1984.

[71] J. G. Oldroyd. Two-dimensional plastic flow of a Bingham solid: A plastic boundary-layer theory for slow motion. *Mathematical Proceedings of the Cambridge Philosophical Society*, 43(3):383–395, 1947.

[72] I. C. Walton and S. H. Bittleston. The axial flow of a Bingham plastic in a narrow eccentric annulus. *Journal of Fluid Mechanics*, 222:39–60, 1991.

[73] N. J. Balmforth and R. V. Craster. A consistent thin-layer theory for Bingham plastics. *Journal of non-Newtonian Fluid Mechanics*, 84(1):65–81, 1999.

[74] D. K. Gartling and N. Phan-Thien. A numerical simulation of a plastic fluid in a parallel-plate plastometer. *Journal of non-Newtonian Fluid Mechanics*, 14:347–360, 1984.

[75] D. F. Moore. On the inclined non-inertial sinkage of a flat plate. *Journal of Fluid Mechanics*, 20(2):321–330, 1964.

[76] D. De Kee, R. P. Chhabra, M. B. Powley, and S. Roy. Flow of viscoplastic fluids on an inclined plane: Evaluation of yield stress. *Chemical Engineering Communications*, 96(1):229–239, 1990.

[77] D. De Kee, G. Turcotte, K. Fildey, and B. Harrison. New method for the determination of yield stress. *Journal of Texture Studies*, 10(3):281–288, 1980.

[78] A. R. Koblitz, S. Lovett, and N. Nikiforakis. Viscoplastic squeeze flow between two identical infinite circular cylinders. *Physical Review Fluids*, 3(2):023301, 2018.

[79] K. Vajravelu, S. Sreenadh, and V. R. Babu. Peristaltic transport of a Herschel–Bulkley fluid in an inclined tube. *International Journal of non-Linear Mechanics*, 40(1):83–90, 2005.

[80] D. Weaire and S. Hutzler. *The Physics of Foams*. Clarendon Press, Oxford, 1999.

[81] M. Alimadadi. *Foam-formed Fiber Networks: Manufacturing, Characterization, and Numerical Modeling: With a Note on the Orientation Behavior of Rod-like Particles in Newtonian Fluids*. PhD thesis, Mid Sweden University, 2018.

[82] A. Jäsberg, P. Selenius, and A. Koponen. Experimental results on the flow rheology of fiber-laden aqueous foams. *Colloids and Surfaces A: Physicochemical and Engineering Aspects*, 473:147–155, 2015.

[83] A. M. Al-Qararah, T. Hjelt, K. Kinnunen, N. Beletski, and J. Ketoja. Exceptional pore size distribution in foam-formed fibre networks. *Nordic Pulp & Paper Research Journal*, 27(2):226–230, 2012.

[84] A. M. Al-Qararah, T. Hjelt, A. Koponen, A. Harlin, and J. Ketoja. Bub-

ble size and air content of wet fibre foams in axial mixing with macro-instabilities. *Colloids and Surfaces A: Physicochemical and Engineering Aspects*, 436:1130–1139, 2013.

[85] G. Katgert, B. P. Tighe, and M. van Hecke. The jamming perspective on wet foams. *Soft Matter*, 9:9739–9746, 2013.

[86] H. M. Princen. Rheology of foams and highly concentrated emulsions: I. Elastic properties and yield stress of a cylindrical model system. *Journal of Colloid and Interface Science*, 91:160–175, 1983.

[87] US Environmental Protection Agency. Paper and paperboard: Material-specific data, 2018. www.epa.gov/facts-and-figures-about-materials-waste-and-recycling/paper-and-paperboard-material-specific-data.

[88] C. Chartres and S. Varma. *Out of water: From abundance to scarcity and how to solve the world's water problems*. FT Press, 2010.

[89] A. M. Al-Qararah, A. Ekman, T. Hjelt, J. Ketoja, H. Kiiskinen, A. Koponen, and J. Timonen. A unique microstructure of the fiber networks deposited from foam–fiber suspensions. *Colloids and Surfaces A: Physicochemical and Engineering Aspects*, 482:544–553, 2015.

[90] B. Haffner, F. F. Dunne, S. R. Burke, and S. Hutzler. Ageing of fibre-laden aqueous foams. *Cellulose*, 24(1):231–239, 2017.

[91] B. Haffner, F. F. Dunne, and S. Hutzler. Stability of foams containing fibres. In *EUFOAM 2016, Dublin, Ireland, 3rd–6th July*, 2016.

[92] S. R. Burke, M. E. Möbius, T. Hjelt, and S. Hutzler. Properties of lightweight fibrous structures made by a novel foam forming technique. *Cellulose*, 26(4):2529–2539, 2019.

[93] M. Järvinen, R. Pihko, and J. Ketoja. Density development in foam form-

ing: Wet pressing dynamics. *Nordic Pulp & Paper Research Journal*, 33 (2):226–236, 2018.

[94] A. M. Al-Qararah, T. Hjelt, A. Koponen, A. Harlin, and J. Ketoja. Response of wet foam to fibre mixing. *Colloids and Surfaces A: Physicochemical and Engineering Aspects*, 467:97–106, 2015.

[95] K. Niskanen. *Paper Physics*. Finnish Paper Engineers' Association, Paperi ja Puu Oy, Helsinki, Finland, 2008.

[96] S. R. Burke, M. E. Möbius, T. Hjelt, J. Ketoja, and S. Hutzler. Analysis of the foam-forming of non-woven lightweight fibrous materials using X-ray tomography. *SN Applied Sciences*, 3(2):1–15, 2021.

[97] M. Alimadadi and T. Uesaka. Exploring one-more dimension of paper: Properties of 3D-oriented fiber network. In *Progress in Paper Physics 2014 Seminar, North Carolina State University, Raleigh, NC, USA, 8th–11th September*, 2014.

[98] N. N. Thondavadi and R. Lemlich. Flow properties of foam with and without solid particles. *Industrial & Engineering Chemistry Process Design and Development*, 24(3):748–753, 1985.

[99] R. G. Cox and S. G. Mason. Suspended particles in fluid flow through tubes. *Annual Review of Fluid Mechanics*, 3:291–316, 1971.

[100] J. J. Stickel and R. L. Powell. Fluid mechanics and rheology of dense suspensions. *Annual Review of Fluid Mechanics*, 37:129–149, 2005.

[101] M. Maxey. Simulation methods for particulate flows and concentrated suspensions. *Annual Review of Fluid Mechanics*, 49:171–193, 2017.

[102] E. Guazzelli and O. Pouliquen. Rheology of dense granular suspensions. *Journal of Fluid Mechanics*, 852:P1, 2018.

[103] G. B. Jeffery. The motion of ellipsoidal particles immersed in a viscous fluid. *Proceedings of the Royal Society of London. Series A*, 102(715): 161–179, 1922.

[104] G. K. Batchelor. The stress system in a suspension of force-free particles. *Journal of Fluid Mechanics*, 41:545–570, 1970.

[105] J. E. Butler and B. Snook. Microstructural dynamics and rheology of suspensions of rigid fibers. *Annual Review of Fluid Mechanics*, 50:299–318, 2018.

[106] V. J. Langlois, F. F. Dunne, and S. Hutzler. Simulation of the dynamics of a foam-fibre dispersion. In *EUFOAM 2016, Dublin, Ireland, 3rd–6th July*, 2016.

[107] H. M. Princen. Rheology of foams and highly concentrated emulsions. II. Experimental study of the yield stress and wall effects for concentrated oil-in-water emulsions. *J. Colloid Interface Sci.*, 105:150–171, 1985.

[108] H. M. Princen and A. D. Kiss. Rheology of foams and highly concentrated emulsions. IV. An experimental study of the shear viscosity and yield stress of concentrated emulsions. *J. Colloid Interface Sci.*, 128:176–187, 1989.

[109] R. A. Keiller and E. J. Hinch. Corner flow of a suspension of rigid rods. *Journal of non-Newtonian Fluid Mechanics*, 40(3):323–335, 1991.

[110] M. Doi and N. Y. Kuzuu. Nonlinear elasticity of rodlike macromolecules in condensed state. *Journal of Polymer Science: Polymer Physics Edition*, 18(3):409–419, 1980.

[111] M. Doi. Rheology of concentrated suspensions of slender rods. *Advances in Colloid and Interface Science*, 17:233–239, 1982.

[112] F. Boyer, E. Guazzelli, and O. Pouliquen. Unifying suspension and granular rheology. *Physical Review Letters*, 107:188301, 2011.

[113] P. Saramito and A. Wachs. Progress in numerical simulation of yield stress fluid flows. *Rheologica Acta*, 56:211–230, 2017.

[114] D. R. Hewitt and N. J. Balmforth. Taylor's swimming sheet in a yield-stress fluid. *Journal of Fluid Mechanics*, 828:33–56, 2017.

[115] D. R. Hewitt and N. J. Balmforth. Viscoplastic slender-body theory. *Journal of Fluid Mechanics*, 856:870–897, 2018.

[116] F. R. Cunha, A. J. Sousa, and M. Loewenberg. A mathematical formulation of the boundary integral equations for a compressible Stokes flow. *Computational & Applied Mathematics*, 22(1):53–73, 2003.

[117] I. Cantat, S. Cohen-Addad, F. Elias, F. Graner, R. Höhler, O. Pitois, F. Rouyer, and A. Saint-Jalmes. *Foams: Structure and dynamics*. OUP Oxford, 2013.

[118] D. Whyte, B. Haffner, A. Tanaka, T. Hjelt, and S. Hutzler. Interactions of fibres with simple arrangements of soap films. *Colloids and Surfaces A: Physicochemical and Engineering Aspects*, 534:112–119, 2017.

[119] A. Koponen, A. Jäsberg, T. Lappalainen, and H. Kiiskinen. The effect of in-line foam generation on foam quality and sheet formation in foam forming. *Nordic Pulp & Paper Research Journal*, 33(3):482–495, 2018.

[120] A. M. Al-Qararah, A. Ekman, T. Hjelt, H. Kiiskinen, J. Timonen, and J. Ketoja. Porous structure of fibre networks formed by a foaming process: A comparative study of different characterization techniques. *Journal of Microscopy*, 264(1):88–101, 2016.

[121] R. B. Bird, W. E. Stewart, and E. N. Lightfoot. *Transport Phenomena*. John Wiley and Sons, 2007.

[122] S. Bénito, C. H. Bruneau, T. Colin, C. Gay, and F. Molino. An elasto-visco-plastic model for immortal foams or emulsions. *The European Physical Journal E*, 25(3):225–251, 2008.

[123] P. P. Mosolov and V. P. Miasnikov. Variational methods in the theory of the fluidity of a viscous-plastic medium. *Journal of Applied Mathematics and Mechanics*, 29(3):545–577, 1965.

[124] P. P. Mosolov and V. P. Miasnikov. On stagnant flow regions of a viscoplastic medium in pipes. *Journal of Applied Mathematics and Mechanics*, 30(4):841–854, 1966.

[125] P. P. Mosolov and V. P. Miasnikov. On qualitative singularities of the flow of a viscoplastic medium in pipes. *Journal of Applied Mathematics and Mechanics*, 31(3):609–613, 1967.

[126] I. A. Frigaard. Stratified exchange flows of two Bingham fluids in an inclined slot. *Journal of non-Newtonian Fluid Mechanics*, 78(1):61–87, 1998.

[127] R. Glowinski. *Numerical methods for nonlinear variational problems*. Springer-Verlag, Berlin, Heidelberg, New York, Tokyo, 1984.

[128] T. Papanastasiou, G. Georgiou, and A. N. Alexandrou. *Viscous fluid flow*. CRC Press, 2021.

[129] A. Wachs and I. A. Frigaard. Particle settling in yield stress fluids: Limiting time, distance and applications. *Journal of non-Newtonian Fluid Mechanics*, 238:189–204, 2016.

[130] I. Karimfazli, I. A. Frigaard, and A. Wachs. A novel heat transfer switch using the yield stress. *Journal of Fluid Mechanics*, 783:526–566, 2015.

[131] K. Alba and I. A. Frigaard. Dynamics of the removal of viscoplastic fluids from inclined pipes. *Journal of non-Newtonian Fluid Mechanics*, 229: 43–58, 2016.

[132] I. Palabiyik, B. Olunloyo, P. J. Fryer, and P. T. Robbins. Flow regimes in the emptying of pipes filled with a Herschel-Bulkley fluid. *Chemical Engineering Research and Design*, 92(11):2201–2212, 2014.

[133] O. Pinkus, B. Sternlicht, and E. Saibel. *Theory of hydrodynamic lubrication*. McGraw-Hill, 1962.

[134] P. Rognon and C. Gay. Soft dynamics simulation. 1. normal approach of two deformable particles in a viscous fluid and optimal-approach strategy. *The European Physical Journal E*, 27(3):253–260, 2008.

[135] P. Rognon and C. Gay. Soft dynamics simulation. 2. elastic spheres undergoing a t1 process in a viscous fluid. *The European Physical Journal E*, 30(3):291–301, 2009.

[136] B. Lorenz and B. N. J. Persson. Time-dependent fluid squeeze-out between solids with rough surfaces. *The European Physical Journal E*, 32 (3):281–290, 2010.

[137] I. Karimfazli and I. A. Frigaard. Flow, onset and stability: Qualitative analysis of yield stress fluid flow in enclosures. *Journal of non-Newtonian Fluid Mechanics*, 238:224–232, 2016.

[138] K. J. Laidler. *Chemical kinetics*. McGraw Hill, New York, 2nd edition, 1987.

[139] J. O. Wilkes and S. G. Birmingham. *Fluid Mechanics for Chemical Engineers with Microfluidics and CFD*. Pearson Education, 2006.

Appendix A

Squeeze Film Flow of Newtonian Fluid between Parallel & non-Parallel Plates

A.1 Methodology: Squeeze Film Flow of Newtonian Fluid between Parallel Plates

In this section, the analysis for a parallel, Newtonian squeeze film will be reviewed. Geometry of the squeeze film flow specifically between parallel plates is shown in Figure 4.1.

We consider a gap of initial thickness $\hat{H}_0$ between plates of length $2\hat{L}$. In Figure 4.1 the top plate is moving downward with a time-varying velocity $\hat{v}_{top}$ under a constant applied force $\hat{F}_{app}$ (per unit distance transverse to the two dimensional plane) thereby displacing the fluid, while the bottom plate is stationary.

To solve the system, the continuity and Navier-Stokes equations are required. The general dimensional form of these equations in Cartesian $\hat{x}$ and $\hat{y}$ coor-

dinates for an incompressible and Newtonian fluid in planar geometry can be written as below [139]. Here dimensional variables are denoted with a hat symbol.

$$\rho\left(\frac{\partial \hat{u}}{\partial \hat{t}}+\hat{u}\frac{\partial \hat{u}}{\partial \hat{x}}+\hat{v}\frac{\partial \hat{u}}{\partial \hat{y}}\right)=-\frac{\partial \hat{p}}{\partial \hat{x}}+\mu\left(\frac{\partial^2 \hat{u}}{\partial \hat{x}^2}+\frac{\partial^2 \hat{u}}{\partial \hat{y}^2}\right)+\rho\, g_x \tag{A.1}$$

$$\rho\left(\frac{\partial \hat{v}}{\partial \hat{t}}+\hat{u}\frac{\partial \hat{v}}{\partial \hat{x}}+\hat{v}\frac{\partial \hat{v}}{\partial \hat{y}}\right)=-\frac{\partial \hat{p}}{\partial \hat{y}}+\mu\left(\frac{\partial^2 \hat{v}}{\partial \hat{x}^2}+\frac{\partial^2 \hat{v}}{\partial \hat{y}^2}\right)+\rho\, g_y \tag{A.2}$$

$$\frac{\partial \hat{u}}{\partial \hat{x}}+\frac{\partial \hat{v}}{\partial \hat{y}}=0. \tag{A.3}$$

Here, $\hat{u}$ and $\hat{v}$ are velocities in the $\hat{x}$ and $\hat{y}$ directions, respectively, $\hat{p}$ is pressure ρ is fluid density, μ is Newtonian viscosity, and g_x and g_y denote components of gravity acceleration.

A.1.1 Nondimensionalization of Equations

In this work we use the dimensionless form of the continuity and Navier-Stokes equations. The horizontal lengths are scaled on $\hat{L}$, and vertical lengths are scaled on $\hat{H}_0$. Meanwhile horizontal velocities are scaled on an as yet unspecified scale $\tilde{u}$, and vertical velocities are scaled on $\tilde{v} \equiv \hat{H}_0\tilde{u}/\hat{L}_0$. Times are scaled on $\hat{H}_0/\tilde{v} \equiv \hat{L}/\tilde{u}$. Finally pressures are scaled on $\hat{F}_{app}/\hat{L}$: note that this has the correct units of pressure since $\hat{F}_{app}$ is taken as applied force per unit distance transverse to the two dimensional calculation domain. The dimensionless variables are summarised in Table A.1.

We now set

$$\tilde{u}=\frac{\hat{F}_{app}}{\mu}\frac{\hat{H}_0^2}{\hat{L}^2}. \tag{A.4}$$

The governing lubrication equations for squeeze film flow of a Newtonian fluid

Nondimensionalization of variables
$\hat{x} = \hat{L}x$
$\hat{y} = \hat{H}_0 y$
$\hat{H}(\hat{t}) = \hat{H}_0 H(t)$
$\hat{u}(\hat{x},\hat{y}) = \tilde{u}\, u(x,y)$
$\hat{v}(\hat{x},\hat{y}) = \tilde{v}\, v(x,y) = (\hat{H}_0/\hat{L})\tilde{u}\, v(x,y)$
$\hat{v}_{top}(\hat{t}) = \tilde{v}\, v_{top}(t) = (\hat{H}_0/\hat{L})\tilde{u}\, v_{top}(t)$
$\hat{t} = (\hat{H}_0/\tilde{v})\, t = (\hat{L}/\tilde{u})\, t$
$\hat{p}(\hat{x}) = (\hat{F}_{app}/\hat{L})\, p(x)$

Table A.1: Table of dimensionless variables.

based on the assumptions made in chapter 3 are [23]

$$-\frac{\partial \hat{p}}{\partial \hat{x}} + \mu \frac{\partial^2 \hat{u}}{\partial \hat{y}^2} = 0 \tag{A.5}$$

$$\frac{\partial \hat{p}}{\partial \hat{y}} = 0 \tag{A.6}$$

$$\frac{\partial \hat{u}}{\partial \hat{x}} + \frac{\partial \hat{v}}{\partial \hat{y}} = 0. \tag{A.7}$$

Dimensionless analogues of these equations, making variables dimensionless on scales identified in Table A.1 are

$$\frac{\partial p}{\partial x} = \frac{\partial^2 u}{\partial y^2} \tag{A.8}$$

$$\frac{\partial p}{\partial y} = 0 \tag{A.9}$$

$$\frac{\partial u}{\partial x} + \frac{\partial v}{\partial y} = 0. \tag{A.10}$$

The solution of equations (A.8), (A.9) and (A.10) now follows a standard procedure for a Newtonian squeeze film [21, 55]. From equation (A.9) we find that the pressure is a function of x coordinate, thus, $p = p(x)$. Using the no slip boundary conditions $u = 0$ at $y = 0$ and $y = H(t)$, equation (A.8) can be solved to obtain the velocity u in the horizontal direction

$$u = \frac{1}{2}\frac{\partial p}{\partial x} y(y - H(t)). \tag{A.11}$$

Via the continuity equation (A.10), the vertical velocity component at the top of the film, v_{top} can be determined

$$v_{top} = -\frac{H(t)^3}{12}\frac{\partial^2 p}{\partial x^2}. \tag{A.12}$$

Note the sign convention adopted here: we define v_{top} to be a positive quantity, so that $v_{top}(t) \equiv -v|_{y=H(t)}$. The flow rate between the plates can be expressed as

$$Q \equiv \int_0^{H(t)} u \, \mathrm{d}y = \int_0^{H(t)} \frac{1}{2}\frac{\partial p}{\partial x} y(y - H(t)) \, \mathrm{d}y = -\frac{H(t)^3}{12}\frac{\partial p}{\partial x}. \tag{A.13}$$

We also know that, $Q = v_{top}x$, in which recall v_{top} is considered as a positive quantity. Thus, using also boundary conditions in which at $x = -1$ and $x = 1$, $p = 0$, we can obtain the pressure distribution in the squeeze film

$$p(x) = \frac{6v_{top}}{H(t)^3}(1 - x^2). \tag{A.14}$$

We now define F as the force (per unit distance out of the two-dimensional plane) that this pressure field places on the upper plate. This is obtained by integration of the pressure field along the plates

$$F = \int_{-1}^{1} p(x) \, \mathrm{d}x = \frac{8v_{top}}{H(t)^3}. \tag{A.15}$$

We can define the velocity of the upper plate, v_{top} as a derivative of film thickness, $H(t)$. With our sign convention

$$v_{top} = -\mathrm{d}H(t)/\mathrm{d}t. \tag{A.16}$$

The force F imposed by the pressure field on the plate must balance the applied force that sets up the squeeze film flow in the first place. However because of the way we have non-dimensionalized the system (the relevant scales were given earlier), this applied force is simply unity. It then follows from equation (A.15) that $v_{top} = H(t)^3/8$. Via equation (A.16) it then follows

$$t = 4\left(\frac{1}{H(t)^2} - 1\right). \tag{A.17}$$

This rearranges to

$$H(t) = (1 + t/4)^{-1/2}. \tag{A.18}$$

A.2 Methodology: Squeeze Film Flow of Newtonian Fluid between non-Parallel Plates

Now, we will investigate the behaviour of squeeze film flow between two non-parallel plates, still for a Newtonian fluid. In the parallel case, section A.1, on symmetry grounds, it was found that the dimensionless flow rate Q vanishes at the half way point along the plates, i.e. at $x = 0$. However, we cannot use that same assumption for non-parallel plates. Therefore, we must find the point at which the flow rate will be zero. This point will be denoted as x_c. The flow rate Q can still be defined in terms of the integral of the horizontal velocity equation (A.11) over the film thickness which gives equation (A.13). However the flow rate for non-parallel plates is $Q = v_{top}(x - x_c)$ where, as before, the sign convention is such that v_{top} is positive. Moreover, H within that equation

now depends on x (not just on t). Hence, using the equations (A.13) and (3.11), the pressure gradient is

$$\frac{\partial p}{\partial x} = \frac{12 v_{top}(x_c - x)}{(H_c(t) - \delta x)^3}. \tag{A.19}$$

Here $H_c(t)$ is the separation at the centre of the plates, and δ is the rescaled tilt angle. Note that when H_c is close to δ and also x is close to unity, such that the gap at the right hand end of the plates is narrow, large pressure gradients are seen near $x = 1$. This means that as x decreases from unity, sharp rises in pressure are seen in the narrow part of the gap. Integration of equation (A.19) using the boundary conditions in which at $x = -1$ and $x = 1$, the pressure is equal to zero, the pressure distribution and also x_c can be determined after some algebra

$$p(x) = \frac{6 v_{top}(1 - x^2)}{H_c(t)^3 \left(1 - \frac{\delta}{H_c(t)} x\right)^2} \tag{A.20}$$

with

$$x_c = \delta / H_c(t). \tag{A.21}$$

Note that in the limit of $\delta \to 0$ this reduces back to the parallel plate case as we expect. On the other hand for a fixed δ, as $H_c(t)$ falls over time, it is clear that x_c grows. When $H_c(t)$ falls towards the value δ, the plates come into contact at the right hand end, since in that case $H|_{x\to 1} \equiv H_c(t) - \delta$ approaches zero. In that limit, $x_c \to 1$, implying that all the flux $Q = v_{top}(x - x_c)$ is to the left with $x < x_c$ and none of it flows out the narrow gap to the right. Returning to a general value of $\delta / H_c(t)$, the force F which the pressure distribution places on the upper plate can be obtained by integrating equation (A.20) which leads to

$$F = \frac{24 v_{top}}{H_c(t)\delta^2} \left(\frac{H_c(t)}{2\delta} \ln \frac{1 + \frac{\delta}{H_c(t)}}{1 - \frac{\delta}{H_c(t)}} - 1 \right). \tag{A.22}$$

A differential equation for $H_c(t)$ versus t can now be derived by recognising that this force F due to the pressure field must be balanced to the unit force imposed externally on the plate. Setting $F = 1$ and $v_{top} = -\mathrm{d}H_c(t)/\mathrm{d}t$ leads to after some algebra

$$t = \frac{12}{\delta^3}\Bigg((H_c - \delta)\ln(1 - \frac{\delta}{H_c}) - (1 - \delta)\ln(1 - \delta) \\ - (H_c + \delta)\ln(\frac{\delta}{H_c} + 1) + (\delta + 1)\ln(\delta + 1)\Bigg). \quad \text{(A.23)}$$

This is an implicit equation for H_c given t. It is easy to check by inspection that $H_c \to 1$ as $t \to 0$. At other times, we cannot in general invert this expression to obtain an explicit analytic formula for H_c in terms of t. However there is still a limiting case that we can analyse as discussed below.

A.2.1 Asymptotic Behaviour in Limit $\delta/H_c \to 1$

In this section, the special case in which the two plates touch at one end is considered. In equation (A.23), if we take the limit $\delta/H_c \to 1$, a final time t_f at which the plates touch (i.e. H_c equals δ) can be calculated:

$$t_f = \frac{12}{\delta^3}\Bigg(-(1 - \delta)\ln(1 - \delta) - 2\,\delta\ln(2) + (\delta + 1)\ln(\delta + 1)\Bigg). \quad \text{(A.24)}$$

Details of how t_f behaves are deferred until section A.3. For now however we note that t_f is finite, i.e. the plates touch in finite time, unlike the parallel case given by equation (A.18) which requires infinite time for the plates to touch.

Hence, for non-parallel geometry and at the final time, what happens at this point geometrically is that according to Figure A.1 (b), the gap thickness on the right is much smaller compared to the gap thickness on the left, meaning that the gap at right end is almost closed and flow moves towards the left end.

By way of contrast, Figure A.1 (a) shows the case with the same δ but with instantaneously a rather thicker gap. In relative terms, the gap thickness on the right and left are comparable, so the non-parallel plates case can be considered as almost a parallel case and flow can move towards both the left and right ends of plates. The present section however focusses on the case of Figure A.1 (b), i.e. close to the final time.

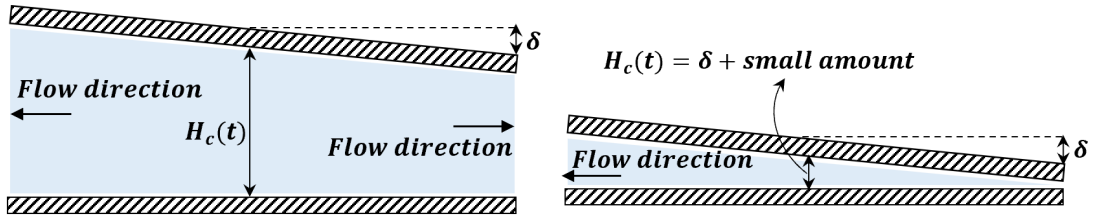

(a) thick gap but small slope **(b)** small gap

Figure A.1: Two types of geometries obtained for non-parallel squeeze film flow

Of interest also is to find out how H_c varies with time close to this final time. Within equation (A.22) we know that the term $\ln(1 - \delta/H_c(t))$ goes to infinity when $H_c(t)$ approaches δ. Hence, consulting equation (A.22) with $F = 1$ and $v_{top} = -\mathrm{d}H_c(t)/\mathrm{d}t$, it follows that $\mathrm{d}H_c(t)/\mathrm{d}t$ approaches zero at $t = t_f$, even though the final time is already obtained as a finite quantity.

Therefore, an asymptotic analysis is required to establish the behaviour of film thickness for times close to the final time. A parameter called ϵ (the gap thickness on the right relative to the gap thickness in the centre) is defined such that $\epsilon(t) \equiv 1 - \delta/H_c(t)$ with $\epsilon \ll 1$ in cases of interest. In this limit $\epsilon \ll 1$ we have $H_c(t) \approx \delta + \delta\,\epsilon(t)$. It follows via equation (A.22) that

$$\delta \frac{\mathrm{d}\epsilon(t)}{\mathrm{d}t} \approx \frac{\mathrm{d}H_c(t)}{\mathrm{d}t} \approx \frac{\delta^3}{24 \ln \epsilon}. \tag{A.25}$$

As expected $\mathrm{d}H_c(t)/\mathrm{d}t$ approaches zero in the limit as $\epsilon \to 0$, but the approach to zero is exceedingly slow, so tiny velocities are only reached for exceedingly small ϵ.

When ϵ is small this gives at leading order

$$t \approx t_f - \frac{24}{\delta^2}\epsilon \ln(1/\epsilon) \quad \text{for} \quad \epsilon \ll 1. \tag{A.26}$$

Starting then from any time t at which ϵ is small but finite, the subsequent time interval $t_f - t$ that must elapse for the plates to touch scales not proportionally to ϵ but rather proportionally to $\epsilon \ln(1/\epsilon)$ which is significantly greater than ϵ. The time interval $t_f - t$, whilst shrinking as ϵ shrinks, is therefore surprisingly long.

To summarize, even though having a very narrow gap tends to imply a very slow approach to the final state (e.g. $v_{top} = H(t)^3/8$ in the parallel case), in the tilted case, the gap only manages to be exceedingly narrow over a very short distance in x (at the far right hand end), so v_{top} is large enough that plates still touch in finite time. That said, the approach to the final state still remains surprisingly slow.

A.2.2 Torque Calculation

Tilted systems are associated with non-zero torques. In this section the analysis for investigating the torque is considered. Torque (per unit distance out of the two-dimensional plane) is evaluated as an integral along the plates $\int_{-1}^{1} x\, p(x)\, \mathrm{d}x$. Thus, for Newtonian fluid in the non-parallel system, we can compute a dimensionless torque that is analogous to the dimensionless force formula, equation (A.22). Since v_{top} is defined by setting the dimensionless lubrication force to unity, we can evaluate v_{top} and substitute it in, to obtain a torque expression wholly in terms of $\delta/H_c(t)$. Equivalently the torque can be expressed in terms of x_c since by equation (A.21), $\delta/H_c(t)$ is the same as x_c in

the Newtonian case. We find

$$T = \int_{-1}^{1} x\, p(x) \mathrm{d}x = \frac{H_c(t)^2 \left((3 - \frac{\delta^2}{H_c(t)^2}) \ln \frac{1+\frac{\delta}{H_c(t)}}{1-\frac{\delta}{H_c(t)}} - 6\frac{\delta}{H_c(t)} \right)}{4\delta^2 \left(\frac{H_c(t)}{2\delta} \ln \frac{1+\frac{\delta}{H_c(t)}}{1-\frac{\delta}{H_c(t)}} - 1 \right)}. \tag{A.27}$$

In the limit of $x_c \to 0$ (i.e. $\delta / H_c(t)$ to zero), this gives zero torque (as expected). Also in the limit of $x_c \to 1$ (i.e. $\delta / H_c(t)$ to unity), it gives unit torque. Physically this implies that the lubrication pressure field (and hence the lubrication force) is highly concentrated in the neighbourhood of $x_c = 1$.

A.3 Results: Newtonian Fluid Squeezed between Parallel & non-Parallel Plates

In the main body of the thesis, chapter 3, section 3.3 focussed primarily on results for the viscoplastic Bingham fluid in non-parallel plate configurations. In the present section, in the interests of completeness and for comparison, analogous results for a Newtonian fluid are presented.

A.3.1 Film Thickness versus Time

In Figure A.2 changes of film thickness versus time are shown. For parallel plates (equation (A.18)), film thickness decreases with time and the most rapid changes occur at early times and then film thickness changes slowly with subsequent time. Indeed, in the parallel case, the plates only come into contact in the limit of infinite time which means that theoretically the film thickness never quite reaches zero [21, 55].

However, in the case of non-parallel plates, H_c reaches its final value δ when time is still finite. The parallel case can be a good approximation to the non-parallel case for sufficiently large values of film thickness, i.e. provided H_c

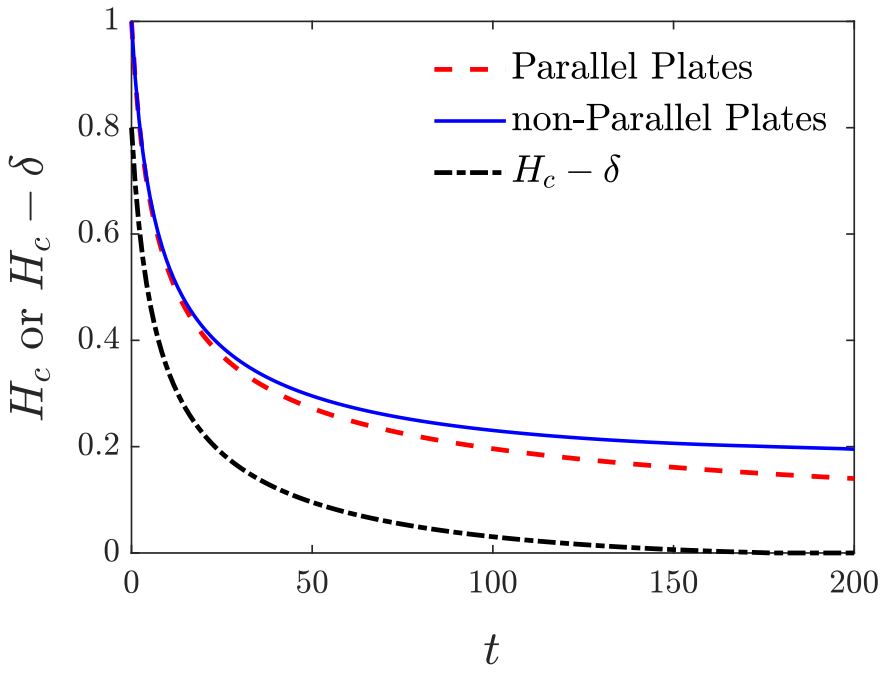

Figure A.2: Profile of film thickness versus time. For non-parallel plates, δ was set to 0.2.

much larger than δ. It is only when H_c falls to comparable magnitude to δ that the non-parallel case differs notably from the parallel one. In that situation, the film thickness on the right hand end $H_c - \delta$ is much smaller in relative terms than the film thickness at the centre H_c.

Furthermore, for small times, the parallel and non-parallel plate formulae are almost the same because δ is small and it cannot be seen easily that the plates are not parallel: in relative terms, the gap thickness on the left and right hand side are nearly the same (see Figure A.1 (a)).

However for times close to the final time as shown in Figure A.1 (b), H_c is equal to δ plus a small amount and and the gap thickness on the right is relatively speaking much smaller than the gap thickness on the left. Hence for an observer located at the centre of plates and looking toward the right, it looks like the gap is almost closed and it cannot readily be seen that this is actually a small gap as opposed to a closed off system. As a result, all the flow is now

moving to the left (which is also seen from equation (A.21) which places x_c, the divider between leftward moving and rightward moving flow, towards the right).

Therefore, physically or geometrically, for small times, near parallel plates behaviour is expected and flow moves through both directions. Meanwhile, for times close to the final time, flow only can move towards one end (i.e. towards the left end in Figure A.1 (b)).

Figure A.2 for a Newtonian system looks superficially like Figure 3.11 for a viscoplastic Bingham fluid (with Oldroyd number $Od = 0.3$ and various δ) in the sense that the non-parallel H_c exceeds the parallel H which in turn exceeds the non-parallel $H_c - \delta$. The difference of course is that for Figure A.2 the non-parallel plates touch whereas in Figure 3.11 motion stops at a finite film thickness. In order for plates to touch in a viscoplastic Bingham fluid it would be necessary to choose a different combination of Od and δ, specifically Od must be less than $\delta/4$.

As we have already noted, in a non-parallel case, and in the limit as H_c approaches δ, the remaining gap on the right hand end has almost closed completely. As a result, all flow is now towards the left (which, as has been mentioned, is also seen from equation (A.21) for Newtonian systems which then places x_c, the divider between leftward moving and rightward moving flow, at the far right hand end). A similar situation is also seen in the special case of viscoplastic Bingham systems which reach a steady state, with a very small but finite film thickness (i.e. $H_{cf} - \delta \ll 1$). These states have Od very slightly greater than $\delta/4$. Equation (3.38) then gives the final x_c value satisfying $x_{cf} \to 1$, such that all material is sheared toward the left.

A.3.2 Final Time for Plates to Touch

Figure A.2 only considered data for one particular δ value. Using analytical equation (A.24) we can however predict the final time for plates to touch in a Newtonian system for any δ value. Figure A.3 shows how final time in the squeeze film flow of a Newtonian fluid between non-parallel plates changes with the value of δ. As can be seen, the system will reach the final time sooner as δ increases. For very small δ, it turns out that equation (A.24) predicts t_f scales proportionally to δ^{-2}. Conceptually this is easy to understand. When δ is small, the system behaves similar to a parallel case, at least until H_c falls to a value on the order of δ. The parallel case equation (A.17) predicts an order δ^{-2} time for this to occur.

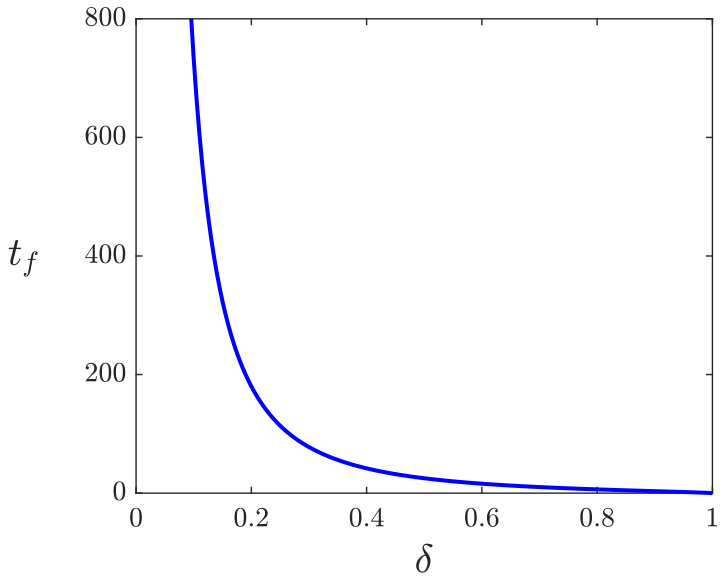

Figure A.3: Final time versus δ in Newtonian non-parallel system.

Thus the bigger δ becomes, the sooner the right hand end of the plates touch. On the other hand in the limit as $\delta \to 0$ the time for the plates to touch diverges as the parallel case is reached. A viscoplastic Bingham system can reach a final state in which plates do not touch at all, although in principle an arbitrarily long time is needed to attain that final state.

A.3.3 Torque Results

In Figure A.4, the graph of torque for a Newtonian fluid in terms of x_c is depicted. Here x_c according to equation (A.21) is the same as δ/H_c in the Newtonian case. Over time, H_c decreases, so x_c increases. Within Figure A.4 the value of Newtonian torque based on equation (A.27), increases comparatively slowly with x_c near $x_c = 0$, and it is only near $x_c = 1$ that torque increases very sharply eventually to reach unity.

For comparison we have also shown the yield stress contribution to torque in a Bingham fluid non-parallel case. Torque is again plotted against x_c, but this x_c is now no longer given by equation (A.21) but instead by (3.28), although this again gives x_c growing as H_c falls. The yield stress contribution to the torque or so called yield torque now obeys equation (3.32) and we can assume a case in which $Od = \delta/4$, so that at final steady state, the final x_c (now denoted x_{cf}) satisfies $x_{cf} \to 1$, corresponding to a case in which plates move and stop but almost touch. In this final state, torque is then only half the Newtonian torque. Note also that cases with even larger Od/δ than the one we have selected (which move and stop without nearly touching) would have smaller δ/H_c in the final state, hence smaller x_{cf}, and correspondingly smaller final torque in line with predictions of equation (3.33).

Another interesting comparison is in the small δ/H_c limit in which the Newtonian x_c is then δ/H_c as we have said, but the x_c used in the yield torque calculation via equation (3.28) is roughly half that. However the Newtonian torque is linear in the small parameter x_c, whereas the yield torque computed via equation (3.32) (for the specified Od/δ) is found to be quadratic in this small parameter. The Bingham yield stress contributions to the torque are therefore very small when δ/H_c is small, but can start to matter as H_c falls over time, such that δ/H_c grows, and hence x_c grows as well.

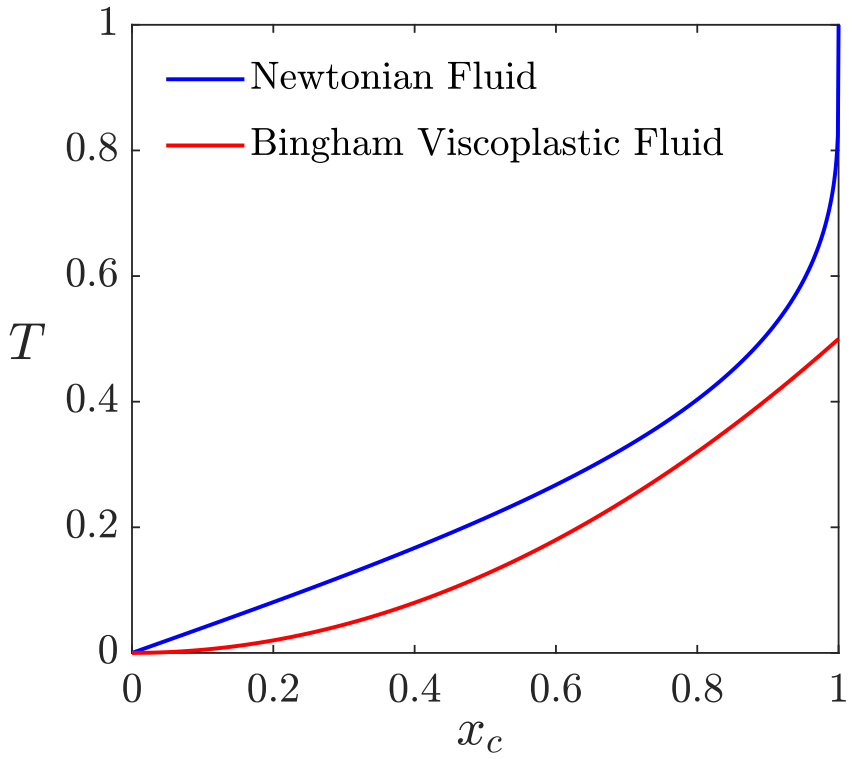

Figure A.4: Changes of torque in terms of x_c for Newtonian and Bingham fluids. In the Bingham case, we plot specifically the yield stress contribution to the torque.

Appendix B

Squeeze Film Flow of Viscoplastic Bingham Fluid between Parallel Plates

B.1 Methodology: Squeeze Film Flow of Bingham Fluid between Parallel Plates

In this section the parallel plate squeeze film flow of a viscoplastic Bingham fluid is discussed.

The geometry of squeeze film flow is similar to Figure 4.1 just with different rheology. The governing lubrication equations [25] for a yield stress fluid are discussed in the main body of the thesis, chapter 3, section 3.2.2. That analysis however concerned the non-parallel case. Here in the interests of completeness, we review step by step the analogous development for the parallel case. This is included specifically for the benefit of those readers who prefer to understand the parallel case first, before generalising to the non-parallel one.

The aim is to find the yield surface (or strictly speaking “fake yield surface” [72]) which is denoted as $y_{plug}(x)$. The yield surface will divide the film thickness into two regions, a yielded region (or strictly speaking “fully plastic” region [73]) in which $(y < y_{plug})$ and a plug region (or strictly speaking “pseudo-plug” region [19, 25, 31, 70]) in which $(y_{plug} < y < H(t)/2)$ and these regions are sketched in Figure 2.3. Due to the flow symmetry, only one quadrant of the flow domain is represented.

Taking the integral of equation (3.14) using a no slip boundary condition (i.e. $u = 0$ at $y = 0$), a velocity profile in the y direction can be deduced

$$u = \frac{\partial p}{\partial x}\frac{1}{2}y(y - H(t)) - Od\, y, \tag{B.1}$$

where recall Od is the Oldroyd number (the ratio between yield stress and imposed stress). The obtained velocity profile applies generally throughout the yielded region. In order to find the boundary between the yielded and plug regions, we use the fact that at the yield surface $(y = y_{plug})$, the shear rate is zero $(\partial u/\partial y = 0)$ or equivalently $|\tau_{xy}| = Od$. Therefore putting this condition into equation (3.14), the expression for the pressure gradient in the x direction can be determined

$$\frac{\partial p}{\partial x} = \frac{Od}{y_{plug} - \frac{H(t)}{2}}. \tag{B.2}$$

Now, via substitution of equation (B.2) in (B.1), the velocity profile for both yielded and plug regions is achievable

$$\begin{cases} u = \dfrac{Od}{2(y_{plug} - \frac{H(t)}{2})}y^2 - \dfrac{Od}{(y_{plug} - \frac{H(t)}{2})}y_{plug}y & \text{for} \quad y \leqslant y_{plug} \\ u_{plug} = -\dfrac{Od}{2(y_{plug} - \frac{H(t)}{2})}y_{plug}^2 & \text{for} \quad y_{plug} < y < \dfrac{H(t)}{2}. \end{cases} \tag{B.3}$$

Here, u and u_{plug} are the yielded and plug regions velocity profiles, respectively. Using the definition for the flow rate Q, an equation for the yield surface is

generated.

$$Q \equiv 2\left(\int_0^{y_{plug}} u\,\mathrm{d}y + \int_{y_{plug}}^{\frac{H(t)}{2}} u_{plug}\,\mathrm{d}y\right) = v_{top}x. \tag{B.4}$$

Inserting equation (B.3) in (B.4), taking the integral and after some algebra, the expression for the yield surface becomes [28]

$$y_{plug}^3 - \frac{3}{2}H(t)y_{plug}^2 - 3\frac{v_{top}x}{Od}y_{plug} + \frac{3}{2}\frac{v_{top}xH(t)}{Od} = 0. \tag{B.5}$$

This is a cubic equation for y_{plug} which in general can be tedious to solve exactly, so more convenient approaches to obtaining solutions are considered below. The fact that we encounter a non-linear equation here is a reflection of the non-linear rheology of a viscoplastic Bingham fluid. The equation only applies for $x \geq 0$ but that is all we need in the parallel plate case, as y_{plug} is symmetric about $x = 0$.

B.1.1 Solving for y_{plug}

As equation (B.5) is non-linear, typically numerical methods are employed to solve it. The typical way of solving it would be, starting from a guess of y_{plug} at any given x, using the Newton-Raphson method which gives a sequence of better approximations to the value of y_{plug}.

A suitable initial guess can be readily obtained. We rely on the observation that (at least in this parallel plate case) on symmetry grounds at $x = 0$ there can be no fluid motion either to left or right, hence no strain rate $\partial u/\partial y$ at any y. Hence at $x = 0$, we must have $y_{plug} = 0$.

Close to $x = 0$ then, y_{plug} must be small, i.e. $y_{plug} \ll H(t)/2$. The integral on the left hand side of (B.4) then evaluates to $u_{plug}H(t)$ which we set equal to $v_{top}x$, and with $u_{plug} \approx y_{plug}^2 Od/H(t)$ via (B.3). Therefore, the initial guess for

y_{plug} is

$$y_{plug}(x) \approx \sqrt{v_{top}x/Od}. \tag{B.6}$$

This gives a good approximation for y_{plug} at least for small x, and the Newton-Raphson approach then converges to the actual y_{plug} value. Equation (B.6) does not however apply uniformly for all x. Indeed for sufficiently large x, this equation might even predict a nonsense value of y_{plug} larger than $H(t)/2$.

Nonetheless, once we have solutions for y_{plug} for any particular x value, we can simply make a small increment in x, and use the y_{plug} value at one x value as an initial Newton-Raphson guess for y_{plug} at the next x value. Hence a profile of y_{plug} versus x all the way up to the end of the plate ($x = 1$) can be obtained.

Note that for sufficiently small Od (a system that is close to Newtonian), we anticipate that y_{plug} could be close to $H(t)/2$ over a significant domain of x. The Newtonian $\partial p/\partial x \equiv -12v_{top}x/H(t)^3$ is then recovered (this follows from equation (A.12)). If we substitute this into equation (B.2) for y_{plug} we find

$$y_{plug} \approx \frac{H(t)}{2} - \frac{H(t)^3 Od}{12v_{top}x}. \tag{B.7}$$

Regardless of whether we are in a regime in which equation (B.6) applies, or in which equation (B.7) applies, or whether we instead obtain solutions to the cubic equation (B.5) numerically, once we have values of $y_{plug}(x)$ we can evaluate how squeezing proceeds over time as follows.

B.1.2 Computing Film Thickness versus Time

So far our analysis has not differed from that of [28]. Now however we introduce a point of departure. Whereas [28] assumed a given constant v_{top} leading to a pre-specified H versus t relation, the difference here is that v_{top} is not constant and instead must be computed as part of the solution as was done by [30], and

this then affects H versus t.

We proceed as follows. Once y_{plug} versus x is determined, for any arbitrary v_{top}, we can integrate equation (B.2) to determine p versus x. Typically for $0 \leq x \leq 1$, we have

$$p(x) = \int_x^1 \frac{Od}{(-y_{plug}(x) + H(t)/2)} \, \mathrm{d}x. \tag{B.8}$$

This enforces a constraint $p = 0$ at $x = 1$. Given that $y_{plug}(x)$ is usually only known numerically, this integral needs to be done by quadrature (e.g. trapezoidal rule or Simpson's rule). We solve for $p(x)$ over the domain $0 \leq x \leq 1$ remembering that p is symmetric in the domain $-1 \leq x \leq 0$ at least in this parallel plate case.

Once p versus x is known, we evaluate the force $F = \int_{-1}^{1} p(x) \, \mathrm{d}x$ that this pressure field places on the plate: again this is determined by quadrature. This force now needs to be set to unity to match the applied force that is assumed constant and that is normalised to unity here.

Note that, as well as depending on x, the y_{plug} value also depends implicitly on Od, $H(t)$ and v_{top}, as follows from equation (B.5). Hence for any given Od and $H(t)$, imposing the constraint $F = 1$ implies a non-linear equation that defines v_{top}. Once v_{top} is determined, $H(t)$ can be updated via $\mathrm{d}H(t)/\mathrm{d}t = -v_{top}$.

In order to solve the non-linear equation for v_{top} we need a starting guess. An upper bound for v_{top} is the Newtonian value (see section A.1) which is $(H(t)^3)/8$ and which is only realised in the limit $Od \to 0$. Once v_{top} is found for any given Od at some particular $H(t)$, that same v_{top} value can be used as a starting guess for nearby values of $H(t)$ and/or Od.

Specifically the numerical routine that we used computed y_{plug} for at least 100 locations along the film, performed quadrature to obtain lubrication pressures

(and forces associated with those pressures). It then matched lubrication force to applied force to find v_{top} values, and updated $H(t)$ via Heun's method using an initial time step[1] of 0.5, although we found we could adapt to longer times as the squeezing proceeded and the squeezing rate slowed. Indeed, decreasing $H(t)$ and/or increasing Od causes v_{top} to fall. The issue we face in the parallel case is that for any finite Od (no matter how small) it is always possible to find a value of $H(t)$ at which v_{top} vanishes. All squeezing motion has now stopped and the force imposed on the plate is balanced by the force due to the yield stress of the fluid. This leads to a steady state $H(t)$ that we analyse shortly.

We also checked adequacy of the selected time step (set to 0.5) as follows. Heun's method was applied to a Newtonian system, and numerical data were compared with an analytical solution (given in section A.1). By time $t = 12$ (at which time the Newtonian $H(t)$ was half its original value), the difference between the numerical and analytical $H(t)$ was only 0.0002, an error we deemed acceptable. Systems with finite Oldroyd number evolve, if anything, more slowly than their Newtonian counterparts (i.e. smaller v_{top}), so if a time step of 0.5 was adequate for the Newtonian system, it would also be adequate in a case for which the Oldroyd number was finite.

B.1.3 Computing Contributions to the Force

The applied force (taken as unity here) is balanced by the lubrication force in the gap, which is comprised of a part associated with yield stresses plus a part associated with viscous stresses. In the final state, there is no viscous stress because there is no motion.

On the other hand, at very early times, viscous stresses are expected to be

[1] Although this selected time step might seem larger than expected, it should be remembered via equation (A.15) that the initial v_{top} in the Newtonian case is only 0.125 and the Bingham v_{top} is lower still. Hence the change in $H(t)$ over even the first time step is actually quite modest.

relevant, because any force associated with the yield stress is just a small fraction of the total. A transition is therefore possible between a situation in which the viscous forces are dominant and a situation in which the yield stress forces are dominant and finding which force dominates at which time depends on the Od number.

By computing the force that would be placed on the plate in the hypothetical situation in which $v_{top} = 0$ for any given H, the force associated with the yield stress (i.e. so called yield force) is obtained. Then the force associated with viscous stresses (i.e. viscous force) is calculated as the difference between the applied force and the yield force.

B.1.4 Steady State for Viscoplastic Bingham Fluid between Parallel Plates

For any given Oldroyd number, a final film thickness can be obtained. Indeed, for Od big enough, even the initial state, which is non-dimensionalized such that $H = 1$, leads to no motion. As alluded to earlier, in the present formulation like [30] but unlike [28], a constant squeezing force is considered to find the squeezing rate. Thus squeezing must eventually stop. Motion coming to a stop is equivalent to having $y_{plug} \to 0$ (or equivalently $y_{plug} \ll H/2$) for all x values. Thus, the plug region now fills effectively the entire gap. Putting $y_{plug} = 0$ in equation (B.2), $|\partial p/\partial x| = 2Od/H_f$. Here H_f is the final steady state film thickness. Using the above equation to find the pressure profile for positive and negative x directions, taking the integral of pressure profile over the whole length of the plate, the applied force is obtained as $F = 2Od/H_f$. Inserting $F = 1$ in this equation, we find, $H_f = 2Od$ which means that for a given Od the final steady state thickness is twice the Od number. Thus for small Od, we can squeeze the plates really quite close together before they stop moving.

As Od increases, the plates stop moving sooner, i.e. at larger H_f. Moreover a maximum Oldroyd number equal to $\frac{1}{2}$ is found for any squeezing to take place whatsoever: as $Od \rightarrow \frac{1}{2}$, even the initial plate separation $H = 1$ leads to no plate motion.

B.2 Results: Squeeze Film Flow of Bingham Fluid between Parallel Plates

In this section, the results obtained for the squeeze flow of viscoplastic Bingham between parallel plates are discussed. Again these are shown for completeness and to facilitate comparison with the non-parallel case results in the main body of the thesis, (e.g. chapter 3).

B.2.1 Yield Surface

The curves of yield surface y_{plug} with respect to x direction for the initial H value (i.e. $H = 1$) and different Od numbers, have been plotted in Figure B.1. As Od number decreases, the yield surface y_{plug} increases. For a case in which $Od = H/2$, which is the maximum Od number for which there is any motion at all for that specified H, we can deduce that the yield surface y_{plug} is zero everywhere since the whole flow field is a plug region. The viscoplastic Bingham fluid is now behaving as a rigid solid, and the yield stress is in balance with the imposed stress.

For large enough Od, there is no motion even in the initial state $H = 1$ which is the particular H value considered here. However, as Od number decreases closer to zero, more and more of the film yields, and the viscoplastic Bingham fluid starts to become more like a Newtonian fluid which yields over the entire film. Hence, as seen here, the value of y_{plug} will increase when the Od number

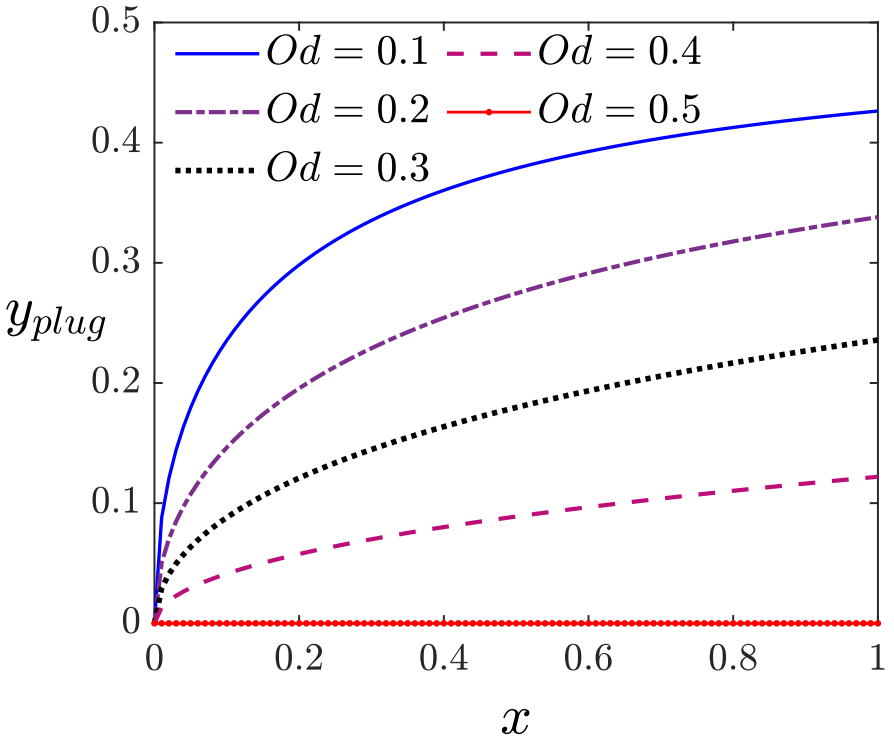

Figure B.1: Yield surfaces y_{plug} corresponding to $H = 1$ as functions of x for different Oldroyd numbers. Corresponding v_{top} values for different Od numbers at this H are as follows: $Od = 0.5$, $v_{top} \equiv 0$; $Od = 0.4$, $v_{top} = 0.0072$; $Od = 0.3$, $v_{top} = 0.0265$; $Od = 0.2$, $v_{top} = 0.0545$; $Od = 0.1$, $v_{top} = 0.0889$.

decreases. Note also that, even though just the case $H = 1$ has been considered here, decreasing H is qualitatively like increasing Od, i.e. it decreases y_{plug}.

B.2.2 Pressure Profile

The pressure profile p versus x for $H = 1$ (i.e. the initial film thickness) and different Oldroyd numbers is depicted in Figure B.2. As can be seen, when Od number decreases and becomes closer to zero, the pressure profile approaches a parabolic shape which is found in the Newtonian fluid. On the other hand, as the Od number approaches a maximum such that no motion occurs, the pressure profile asymptotes to a straight line which applies when the entirety of the fluid is in the plug region.

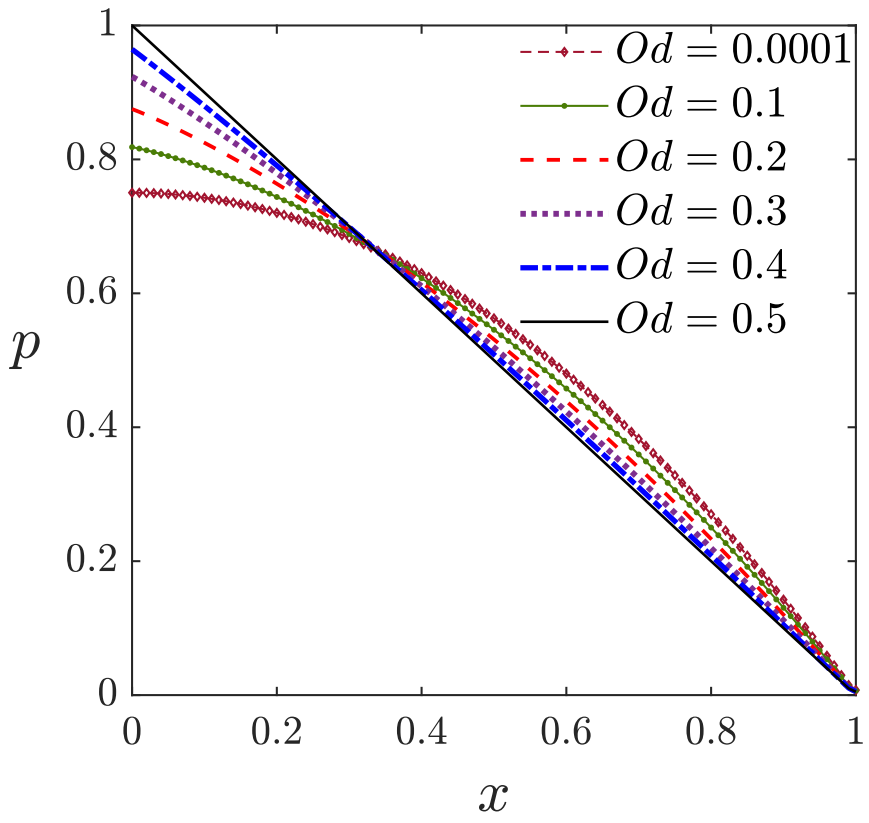

Figure B.2: Pressure profiles corresponding to $H = 1$ in terms of x for different Oldroyd numbers. Corresponding v_{top} values for different Od numbers at this H are as follows: $Od = 0.5$, $v_{top} \equiv 0$; $Od = 0.4$, $v_{top} = 0.0072$; $Od = 0.3$, $v_{top} = 0.0265$; $Od = 0.2$, $v_{top} = 0.0545$; $Od = 0.1$, $v_{top} = 0.0889$; $Od = 0.0001$, $v_{top} = 0.125$.

B.2.3 Velocity Profile

The horizontal velocity profile (u versus y) for $H = 1$ and different x locations with constant Od number ($Od = 0.2$) and $v_{top} = 0.0545$ is depicted in Figure B.3. In general, the horizontal velocity increases with x, both in the plug region and in the yielded region. This is because the total horizontal flow that this velocity profile must deliver increases with x. At the centre of the plates (near $x = 0$) the fraction of fluid in the plug region far exceeds that in the yielded region. This balance however shifts as x increases. Thus, at the centre $x = 0$, the plug region occupies the entire thickness but by moving to the right (increasing x), the yielded region grows because shear stress becomes greater than the yield stress over a significant part of the gap.

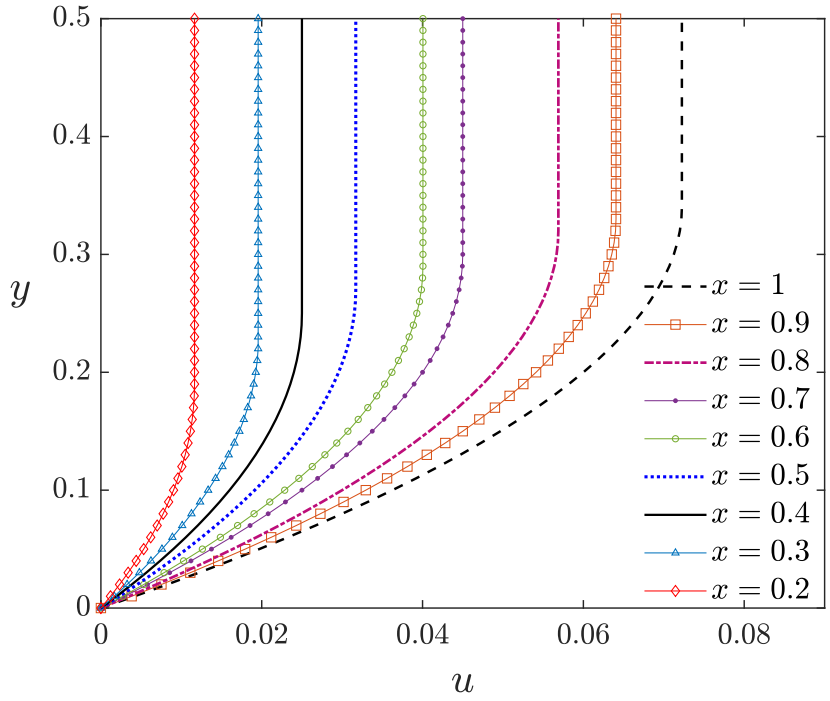

Figure B.3: Horizontal velocity profiles corresponding to $H = 1$ and $Od = 0.2$ at different x locations. Here $v_{top} = 0.0545$.

The horizontal velocity field at a constant location ($x = 0.5$) with different Oldroyd numbers for $H = 1$ is shown in Figure B.4. For small Oldroyd numbers, the velocity profile of a viscoplastic Bingham fluid exhibits similar behaviour to the parabolic profile of a Newtonian fluid. For bigger Od numbers, the velocity profile becomes a plug flow field with a uniform velocity over most of the width of the gap [19].

B.2.4 Film Thickness versus Time

From Figure B.5, which shows how film thickness H varies with time t, it can be seen that (at any given time) squeeze film thickness decreases with decreasing Od number, this being the dimensionless measure of the yield stress. At a certain maximum Od number, the plates never move at all since the plug region dominates the whole film thickness and the "fluid" behaves effectively as a rigid solid. Meanwhile, for small Od number, yield stress is small and the system

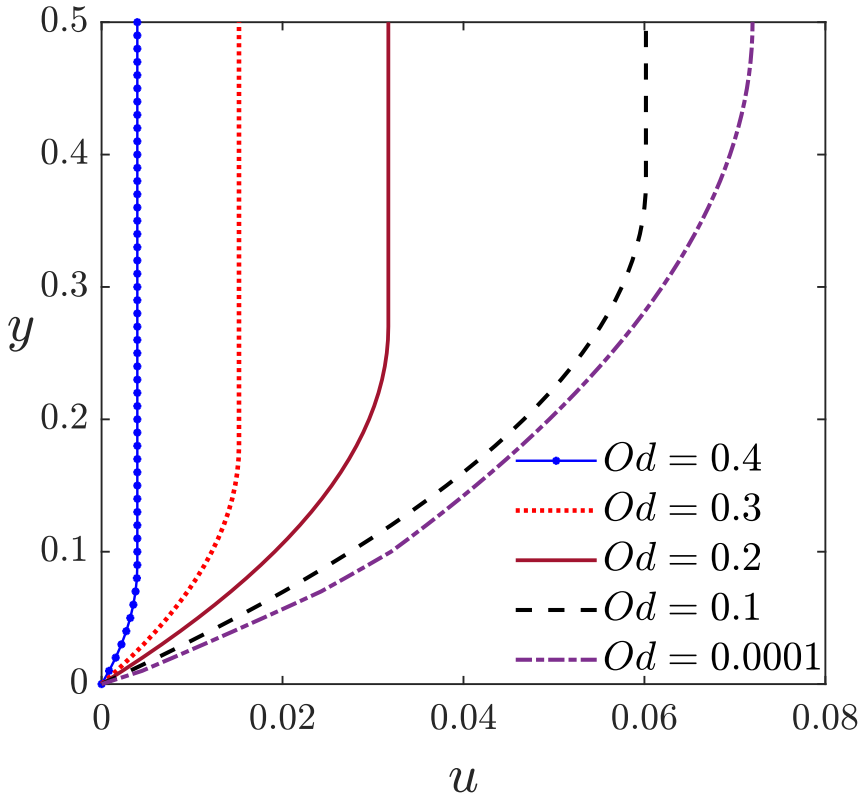

Figure B.4: Horizontal velocity profiles corresponding to $H = 1$ and $x = 0.5$ for different Od.

is much closer to the Newtonian case. For instance, when $Od = 0.0001$, the behaviour of H versus t is almost same as the analytical formula (equation (A.18)) in the Newtonian case. Moreover the final state at any finite Od number system corresponds to a final thickness $H_f = 2Od$.

Thus, the smaller the Od number, the smaller the final film thickness, the more the film can be squeezed before the yield stress alone is sufficient to stop the squeezing by balancing the force which is applied to the plate. In the case $Od \ll 1$, it takes at least a time $t \sim Od^{-2}$ before H is even close to this final value $2Od$. This follows since the $Od \ll 1$ case starts off close to the Newtonian case (see e.g. the case $Od = 0.0001$ in Figure B.5), whilst at very long times, the Newtonian system behaves as $H \sim 2\, t^{-1/2}$ (see equation (A.18)).

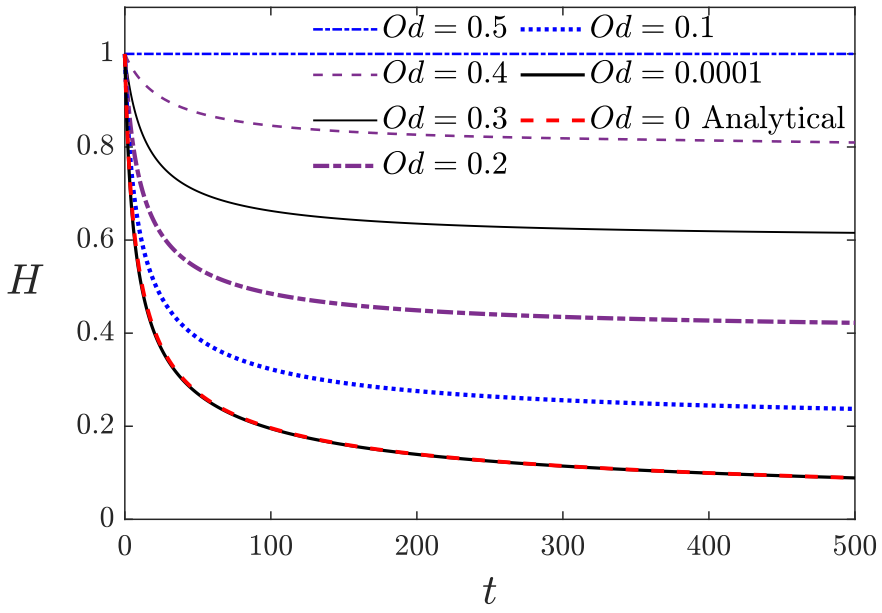

Figure B.5: Film thickness versus time for different Oldroyd numbers in a viscoplastic Bingham system with parallel plates.

B.2.5 Contributions to the Force

The total force comprises the viscous force and yield force (as mentioned in section B.1.3). The relative contributions that these make depends on the Oldroyd number Od. Figure B.6 shows the force contributions as time proceeds. For instance, for $Od = 0.2$, the yield force starts to dominate the viscous force even at early times. Meanwhile for smaller Oldroyd number (e.g. $Od = 0.02$), the viscous force accounts for almost all the force early on. Then as time goes on, the yield force increases as the viscous force decays. For each different Od number, there is a certain time at which the yield and viscous force curves cross over and this time is expected to scale proportionally to Od^{-2}.

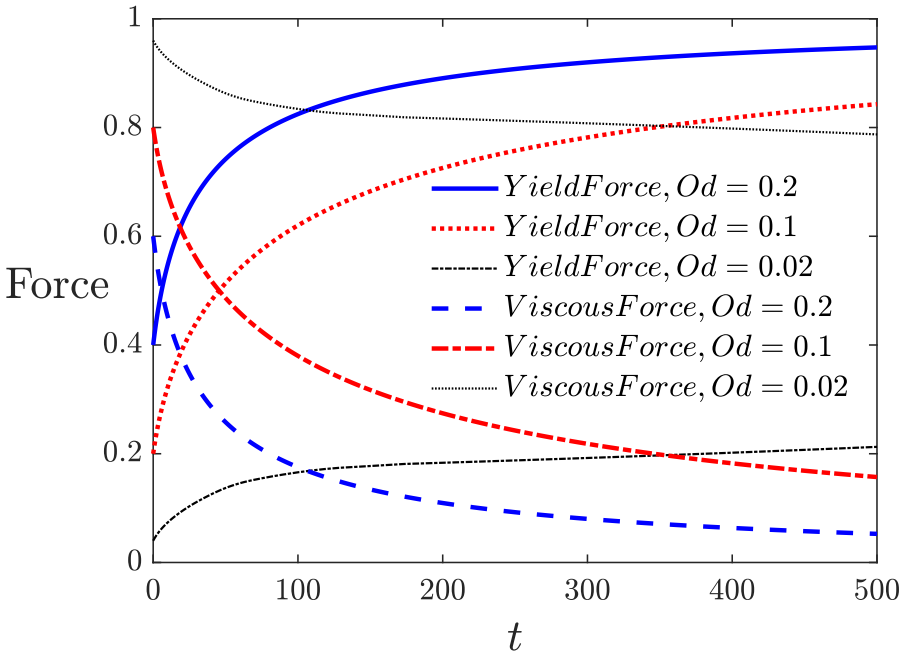

Figure B.6: Force contributions to the squeeze flow versus time for different Oldroyd numbers in the parallel geometry.

Appendix C

Published paper

The published paper [33] (J. non-Newtonian Fluid Mech., 305:104817), and associated supplementary material is reproduced in what follows. This is also available open access via

https://doi.org/10.1016/j.jnnfm.2022.104817

The published paper is based on the work of chapter 3, while the supplementary material is based on the work in appendix A and B.

An additional manuscript based on the work of chapter 4 has also been submitted to Eur. Phys. J. E. and is under peer review. This is also appended.

Journal of Non-Newtonian Fluid Mechanics 305 (2022) 104817

Contents lists available at ScienceDirect

Journal of Non-Newtonian Fluid Mechanics

journal homepage: www.elsevier.com/locate/jnnfm

Squeeze film flow of viscoplastic Bingham fluid between non-parallel plates

Elaheh Esmaeili *, Paul Grassia, Carlos Alejandro Torres Ulloa

Department of Chemical and Process Engineering, University of Strathclyde, 75 Montrose Street, Glasgow, G1 1XJ, UK

ARTICLE INFO

Keywords:
Squeeze film flow
Viscoplastic Bingham fluid
Oldroyd number
Non-parallel plates
Lubrication theory

ABSTRACT

Squeeze film flow of a viscoplastic Bingham fluid between non-parallel plates has been analysed. It is assumed that the force applied to the plates is known, therefore, their velocity must be found, and the film thickness decreases then as time proceeds. Moreover, for non-parallel plates, the position along the plates at which flow reverses direction is found as part of the solution. In the Newtonian limit, the thickness of the gap between the plates in the parallel system never quite reaches zero at any finite time, while for the non-parallel case a finite time can be obtained when the plates touch one another at a point. In squeeze flow of a viscoplastic Bingham fluid between parallel and non-parallel plates, under a fixed applied force, a final steady film thickness can sometimes be reached. This final thickness turns out to be sensitive not just to the plate tilt angle but also to the so called Oldroyd number which is defined as the ratio between yield stress and imposed stress. Nevertheless for squeeze film flow of Bingham viscoplastic fluid between non-parallel plates, the results show that other cases exist in which the lubrication force cannot always balance the applied force, leading to the plates approaching and touching at the narrowest end of the gap. Moreover torques that develop within the system have been analysed.

1. Introduction

Squeeze film flows [1] are flows in which a material is compressed between two approaching parallel or nearly parallel plane surfaces. They have myriad applications, including in areas such as engineering, biology, food industries, rheometry devices, compression moulding, papermaking, etc. [1–4]. Squeeze film flows of Newtonian and non-Newtonian fluids have been studied experimentally, theoretically and numerically. In particular, there is a comprehensive review [4] on squeeze flow theory and its applications in which a wide variety of materials such as Newtonian, viscoelastic and viscoplastic with different boundary conditions, i.e. perfect slip, no slip and partial slip at the sample-plate interfaces have been investigated.

Squeeze flow tests can be carried out either using a specified shear rate (constant displacement rate) or a specified shear stress (constant load). Thus, results can be in the form of relations between force–height, force–time and height–time depending on how the test is done [1,2,4,5]. Assuming a no slip condition between the sample and the plates, at fixed applied force, the shear rate in the squeeze film tends to fall as time proceeds (the Newtonian case implies that in fact). For viscoelastic fluids, this then means that elastic effects are likely to become less important over time [6] (the fluids behave closer to Newtonian). On the other hand, for a pseudo-plastic power law fluid say, it implies that the effective viscosity rises as time proceeds (the flow necessarily slows down relative to a Newtonian case) [2,4].

Indeed viscoplastic materials [7–9] are of special interest in squeeze film situations [3,4,10], since they flow as a fluid when the imposed stress is bigger than the yield stress but can be treated as a plug-like solid when the imposed stress is less than the yield stress. Therefore, the squeeze film flow field for a viscoplastic fluid is often considered to be divided into two regions [11–13], yielded (fluid) and plug (unyielding) region. The surface which separates yielded and plug regions is called the yield surface [14]. During squeeze film flow under constant load, as time proceeds, the yield surface would be expected to shift so that more and more of the flow domain is in the plug region and less of it is in the yielded region, until the yielded region disappears and the flow has stopped altogether, even whilst the squeeze film can remain at a finite thickness [3,5,15].

These flows are however less simple than it might first appear. When coupled with conventional lubrication theory applicable in small aspect ratios, they lead to an apparent paradox (the so called "lubrication paradox") [11,12,16,17]. Fig. 1 is predicted to have different horizontal velocities. Hence there is predicted to be a non-zero strain rate in the normal direction even in the (supposedly non-yielding) plug region, albeit this is of much smaller magnitude than the shear strain rate in the yielded region. The paradox has however been resolved by [18]. That analysis revealed [18,19] that the yielded region was in fact what was termed a "fully-plastic" region, in which even the dominant shear

* Corresponding author.
E-mail address: elaheh.esmaeili@strath.ac.uk (E. Esmaeili).

https://doi.org/10.1016/j.jnnfm.2022.104817
Received 29 October 2021; Received in revised form 15 April 2022; Accepted 21 April 2022
Available online 5 May 2022
0377-0257/© 2022 The Author(s). Published by Elsevier B.V. This is an open access article under the CC BY license (http://creativecommons.org/licenses/by/4.0/).

stress component exceeded the yield stress. On the other hand, the plug region was revealed to be merely a "pseudo-plug". When normal stresses (in addition to shear stresses) as well as perturbations over and above the leading order horizontal flow are taken into account, the "pseudo-plug" was found to be at a stress condition just slightly in excess of the yield stress. This then admitted the required non-zero strain rate there, which as mentioned, is smaller than the shear strain rate in the "fully-plastic" region. The "fully-plastic" and "pseudo-plug" regions were separated by what was termed a "fake yield surface". For the present work however it is sufficient to consider just the leading order horizontal flow and the pressure field that is associated with it. For simplicity then we continue to use the terminology "yielded", "plug" and "yield surface" rather than the terms "fully-plastic" "pseudo-plug" and "fake yield surface" [18,19].

As alluded to above, literature has been published on the squeeze film flow between parallel plates either with constant rate or constant load. The work done by [5], investigated the behaviour of a yield stress fluid between two parallel plates with a constant load, theoretically and experimentally. However, they have not dealt with the non-parallel plates geometry. The work of [13] meanwhile provided an asymptotic solution for the two-dimensional planar squeeze film flow of a viscoplastic medium and analytical solutions for the flow fields have been compared to numerical computations. We will make use of these solutions. Nonetheless the work done by [13] and likewise by [12], only investigated the squeeze flow of a viscoplastic fluid between parallel plates with a constant squeezing rate. This requires in particular that larger squeezing forces are applied as time proceeds, with the squeezing force needing to become arbitrarily large as the gap narrows.

Few studies have investigated non-parallel squeeze film flows. One study by [20] carried out the two-dimensional numerical simulation of the squeeze film flow of a viscoplastic fluid between two approaching circular cylinders. In another study conducted by [21], the peristaltic flow of a Herschel–Bulkley fluid is examined in an inclined tube. These studies have not however used the calculation procedure developed by [5] to establish under constant load conditions what the final state of such systems might be. Thus, in the present work, non-parallel squeeze flow of a viscoplastic Bingham fluid with an assumption of a fixed squeezing force (arguably more realistic than fixed squeezing rate which requires an ever increasing force) is developed. In the present work, the final state of the system is identified, and it is also considered how the squeezing rate varies with time (up to the final state). A number of features specific to non-parallel plates i.e. identifying the position along the plates at which flow direction reverses as well as evolution of torque, have also been described.

What has motivated the present study are applications in which a viscoplastic fluid is squeezed out of a complex shaped gap. One such example is foam-based papermaking in which a foam carrier fluid is squeezed out from a network of fibres [22]. There is no need for the fibres in the network to be aligned parallel. Often moreover, length of the fibres is significantly greater than the size of the bubbles in the foam [23], in which case it might be permitted to treat the bubbles, at least in a rough approximation, as if they were a continuum. Foam-based making is in fact a very complex system [22,24], and the problem to be solved here is admittedly just a highly idealised version of it.

The rest of this work is laid out as follows. Section 2 deals with methodology and introduces governing equations for non-parallel squeeze flow geometry. After that Section 3 deals with the results obtained from the investigated squeeze flow problem. Finally, Section 4 considers the conclusions from the present study.

2. Methodology

In what follows, Section 2.1 describes the squeeze film flow problem between non-parallel plates, Section 2.2 deals with torques and Section 2.3 considers final steady states. Following that, yield stress contributions to force and torque are discussed in Section 2.4.

2.1. Squeeze film flow of Bingham viscoplastic fluid between non-parallel plates

This section considers the squeeze flow of viscoplastic Bingham fluid between non-parallel plates. The analysis for a parallel, Newtonian squeeze film is well known in the literature [25]. However for completeness we have presented it in section S1 of the supplementary material. Moreover, the behaviour of a Newtonian fluid squeezed between non-parallel plates is reviewed in section S2 to facilitate comparison with the non-parallel viscoplastic Bingham case, particularly with regard to possible final states. The solution of squeeze film flow of a Bingham viscoplastic in the parallel case has been investigated by [5] and we provide the mathematical procedure in the supplementary material, section S3 again to support the non-parallel plate case in the present section.

In what follows, standard lubrication theory assumptions [25], i.e. planar geometry, thin geometry, incompressible fluid, negligible gravity, negligible inertia, no slip boundaries are considered to apply. We consider a gap of initial thickness $\hat{H}_{c_0}$ at the centre of the plates of length $2\hat{L}$. In Fig. 1 the top plate is moving downward with a time-varying velocity $\hat{v}_{top}$ under a constant applied force $\hat{F}_{app}$ (per unit distance transverse to the two-dimensional plane) thereby displacing the fluid, while the bottom plate is stationary. Moreover θ is the angle between the upper surface and the horizontal coordinate (it is assumed that the angle θ is small).

Governing lubrication equations [16] for a viscoplastic Bingham fluid are

$$-\partial\hat{p}/\partial\hat{x} + \partial\hat{\tau}_{xy}/\partial\hat{y} = 0 \tag{1}$$

$$\partial\hat{p}/\partial\hat{y} = 0 \tag{2}$$

$$\partial\hat{u}/\partial\hat{x} + \partial\hat{v}/\partial\hat{y} = 0. \tag{3}$$

Here $\hat{u}$ and $\hat{v}$ are velocities in $\hat{x}$ and $\hat{y}$ directions, $\hat{p}$ is pressure and $\hat{\tau}_{xy}$ denotes shear stress of the viscoplastic Bingham fluid which satisfies (see e.g. [9])

$$\begin{cases} \hat{\tau}_{xy} = \pm\tau_0 + \mu\hat{\dot{\gamma}} & \text{for} \quad |\hat{\tau}_{xy}| > \tau_0 \\ \hat{\dot{\gamma}} = 0 & \text{for} \quad |\hat{\tau}_{xy}| \leqslant \tau_0. \end{cases} \tag{4}$$

Here τ_0 is yield stress, $\hat{\dot{\gamma}} = \partial\hat{u}/\partial\hat{y}$ is shear rate and μ is fluid viscosity after yielding occurs. Here the $\pm\tau_0$ term is positive if $\hat{\dot{\gamma}} > 0$ and it is negative if $\hat{\dot{\gamma}} < 0$. The dimensional variables are denoted with a hat symbol and their dimensionless analogues (described later on) will have the hat symbol dropped.

2.1.1. Non-dimensionalisation of equations

We cast equations in dimensionless form. Horizontal lengths are scaled by $\hat{L}$, and vertical lengths are scaled by $\hat{H}_{c_0}$. Horizontal velocities are scaled by $\tilde{u} \equiv (\hat{F}_{app}/\mu)(\hat{H}_{c_0}^2/L^2)$, and vertical velocities are scaled by $\tilde{v} \equiv \hat{H}_{c_0}\tilde{u}/\hat{L}$. Times are scaled by $H_{c_0}/\tilde{v} \equiv \hat{L}/\tilde{u}$. Finally pressures are scaled by $\hat{F}_{app}/\hat{L}$: note that this has the correct units of pressure since $\hat{F}_{app}$ is taken as applied force per unit distance transverse to the two-dimensional calculation domain.

The dimensionless film thickness H is a function of both time t and x coordinate. We define δ as a rescaled angle, $\delta = \theta\hat{L}/\hat{H}_{c_0}$. Geometrically δ is the thickness change between the middle of the plate and one of the ends divided by the initial thickness in the middle. Thus, the dimensionless squeeze film thickness which varies with x-coordinate and time t, can be determined

$$H(x,t) = H_c(t) - \delta\, x \tag{5}$$

where $H_c(t)$ is film thickness at the centre of the plates.

We can define a dimensionless group, the Oldroyd number (Od) which represents the relative importance of yield stress effects and

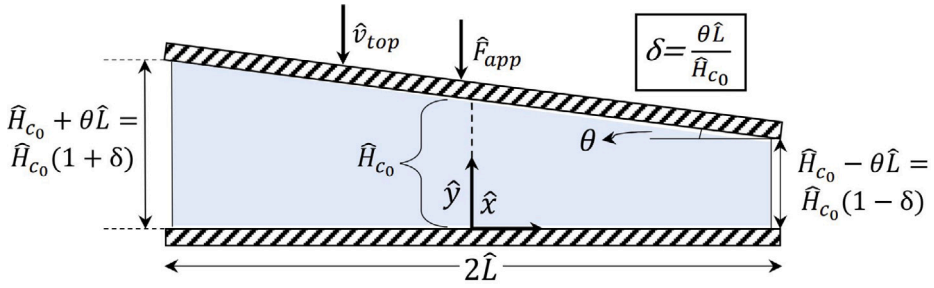

Fig. 1. Geometry of squeeze film flow between non-parallel plates.

imposed stress [14]. In our system, Oldroyd number can be defined as follows

$$Od = \frac{\text{Yield stress}}{\text{Imposed stress}} = \frac{\tau_0 \hat{L}^2}{\hat{H}_{c_0}\hat{F}_{app}}. \tag{6}$$

Suppose we make shear rate $\hat{\dot{\gamma}} \equiv \partial\hat{u}/\partial\hat{y}$ dimensionless on the scale $\tilde{u}/\hat{H}_{c_0}$ and shear stress $\hat{\tau}_{xy}$ dimensionless on the scale $\mu\tilde{u}/\hat{H}_{c_0}$. We deduce a dimensionless analogue of the constitutive equation

$$\begin{cases} \tau_{xy} = \pm Od + \dot{\gamma} & \text{for} \quad |\tau_{xy}| > Od \\ \dot{\gamma} = 0 & \text{for} \quad |\tau_{xy}| \leqslant Od. \end{cases} \tag{7}$$

Here the $\pm Od$ term is positive if $\dot{\gamma} > 0$ and is negative if $\dot{\gamma} < 0$. Recasting Eq. (1) in dimensionless form, integrating, and applying the boundary condition in which at $y = H(x,t)/2$, we have $\tau_{xy} = 0$, shear stress can be written, at least in regions in which the fluid is yielding, as below

$$\tau_{xy} = \frac{\partial p}{\partial x}\left(y - \frac{H(x,t)}{2}\right) = \pm Od + \dot{\gamma} = \pm Od + \frac{\partial u}{\partial y}. \tag{8}$$

In the non-parallel geometry, the point along the plates at which flow reverses such that the flow rate to either right or left is zero needs to be determined. This point will be denoted as x_c. The domain for solving the problem is divided into two sections $x > x_c$ and $x < x_c$ and we consider these in what follows.

2.1.2. Squeeze film flow for domain $x > x_c$

For the domain in which $x > x_c$, considering the fact that at the yield surface (denoted $y = y_{plug}$), shear rate is zero and shear stress is Od, using Eq. (8), pressure gradient with respect to x will be found

$$\frac{\partial p}{\partial x} = \frac{Od}{\left(y_{plug} - \frac{H(x,t)}{2}\right)}. \tag{9}$$

By substitution of Eq. (9) into (8), and from the Bingham fluid rheology, it is found that (in the yielded region $0 \leq y \leq y_{plug}$), $\tau_{xy} = \partial u/\partial y + Od$, thus, integrating and using the boundary condition in which at $y = 0$, $u = 0$, the velocity profile in the x direction for yielded and plug regions will be obtained.

$$\begin{cases} u = \dfrac{Od}{2(y_{plug} - \frac{H(x,t)}{2})}y^2 - \dfrac{Od}{(y_{plug} - \frac{H(x,t)}{2})}y_{plug}y & \text{for} \quad y \leqslant y_{plug} \\ u_{plug} = -\dfrac{Od}{2(y_{plug} - \frac{H(x,t)}{2})}y_{plug}^2 & \text{for} \quad y_{plug} < y < \dfrac{H}{2}. \end{cases} \tag{10}$$

The equation for flow rate Q established from the velocity profile for both plug and yielded regions is as follows

$$Q \equiv 2\left(\int_0^{y_{plug}} u\,\mathrm{d}y + \int_{y_{plug}}^{\frac{H(x,t)}{2}} u_{plug}\,\mathrm{d}y\right) = v_{top}(x - x_c). \tag{11}$$

Substitution of Eq. (10) into (11), taking the integral and making some manipulations, the final equation for y_{plug} for the domain $x > x_c$ will be generated. If $H(x,t)$ is substituted using Eq. (5) a cubic equation for y_{plug} now results

$$y_{plug}^3 - \frac{3}{2}(H_c(t) - \delta x)y_{plug}^2 - 3\frac{v_{top}(x - x_c)}{Od}y_{plug} + \frac{3}{2}\frac{v_{top}(H_c(t) - \delta x)(x - x_c)}{Od} = 0. \tag{12}$$

2.1.3. Squeeze film flow for domain $x < x_c$

In the domain, $x < x_c$, the flow and the shear stress have opposite sign from what they have for $x > x_c$. Working through the computation, we deduce

$$y_{plug}^3 - \frac{3}{2}(H_c(t) - \delta x)y_{plug}^2 + 3\frac{v_{top}(x - x_c)}{Od}y_{plug} - \frac{3}{2}\frac{v_{top}(H_c(t) - \delta x)(x - x_c)}{Od} = 0. \tag{13}$$

2.1.4. Solving for y_{plug}

The next step is to solve for the yield surface, y_{plug}, which is a function of position x, based on the two obtained Eqs. (12) and (13) for domains $x > x_c$ and $x < x_c$ respectively. To do so, a standard numerical method such as the Newton–Raphson technique is employed. Following an analogous procedure to that used for parallel plates (discussed in the supplementary material, section S3.1), assuming small values of $|x - x_c|$ and y_{plug}, a first guess for y_{plug} can be obtained. Specifically, based on the observation that at $x = x_c$ there can be no fluid motion either to left or right, hence there is no strain rate $\partial u/\partial y$ at any y. Hence at $x = x_c$, we must have $y_{plug} = 0$. For the domain $x > x_c$ but close to $x = x_c$, it follows that y_{plug} must be small, i.e. $y_{plug} \ll H(x,t)/2$. The integral within (11) then evaluates to $u_{plug}H(x,t)$ which we set equal to $v_{top}(x - x_c)$, with $u_{plug} \approx y_{plug}^2 Od/H(x,t)$ via (10). We can use analogous assumptions for the domain $x < x_c$, therefore, the initial guess for y_{plug} is

$$\begin{cases} y_{plug} = \sqrt{v_{top}(x - x_c)/Od} & \text{for} \quad x > x_c \\ y_{plug} = \sqrt{v_{top}(x_c - x)/Od} & \text{for} \quad x < x_c. \end{cases} \tag{14}$$

These only apply if they predict $y_{plug} \ll H(x,t)/2$. More generally we can have y_{plug} values up to $H(x,t)/2$. Nevertheless once we have the correct y_{plug} value at any given x, we can readily find it at a nearby x, using one y_{plug} value as an initial guess for the next. We end up with y_{plug} values for all x, provided H_c, v_{top} and x_c are given, and provided Od and δ are specified. The technique for finding v_{top}, x_c and ultimately squeeze film thickness H versus time t is described next.

2.1.5. Computing film thickness versus time

So far, the computational procedure for the constant load and constant rate systems have been similar. In this section, we proceed to find the force as a function of velocity, and hence the velocity required to deliver a constant load, and so we start to see a deviation between the constant load and constant rate systems.

Now, after finding y_{plug}, for the domain $x > x_c$, we have

$$p = \int_x^1 \frac{Od}{\frac{H(x,t)}{2} - y_{plug}}\,\mathrm{d}x. \tag{15}$$

Meanwhile for $x < x_c$ we have

$$p = \int_{-1}^{x} \frac{Od}{\frac{H(x,t)}{2} - y_{plug}}\,\mathrm{d}x. \tag{16}$$

The value of x_c needs to be chosen to ensure p is continuous at $x = x_c$. Once that is achieved (for any selected v_{top}) the value of v_{top} needs to be chosen to ensure $\int_{-1}^{1} p(x)\,\mathrm{d}x = 1$, the integral being readily computed numerically by quadrature. All this says is that in the dimensionless system considered here, the constant load is set to unity. We then evolve $H_c(t)$ according to $\mathrm{d}H_c(t)/\mathrm{d}t = -v_{top}$, with $H(x,t)$ then given by Eq. (5). To start the iteration at initial time, we need guesses of x_c and v_{top}. However we have guesses corresponding to the Newtonian case (see equations (S17) and (S18) in the supplementary material), and in general we expect that the Newtonian v_{top} provides an upper bound for the velocity in the viscoplastic Bingham fluid case. Once we have x_c and v_{top} values initially, we can then use x_c and v_{top} values at one time step as initial guesses for the subsequent time step.

2.2. Computing torque

In addition to computing film thickness versus time, the numerical scheme outlined above also allows us to track another quantity namely torque T. The scheme balances a lubrication force developed between the plates to an external applied force (which as mentioned is unity in the dimensionless system). However if the plates are tilted, a lubrication torque also develops and to keep the tilt angle fixed (as is assumed here) an external applied torque would be needed to balance it. We can however quantify the lubrication torque (per unit distance normal out of the two-dimensional plane) via $T = \int_{-1}^{1} x\,p(x)\,\mathrm{d}x$. Since p versus x is computed numerically at any instant in time, this torque can also be evaluated by quadrature.

The question we now ask is whether the plates ever come to rest at a finite film thickness (as is known to happen for a viscoplastic Bingham fluid in a parallel plate geometry as described in supplementary material section S3) or whether their right hand ends manage to touch (as happens for a Newtonian fluid between non-parallel plates as demonstrated in section S2). The question is addressed in the next section.

2.3. Steady state for viscoplastic Bingham fluid between non-parallel plates

This section develops the steady state solution for the system. The analogous approach for a yield stress fluid system in a parallel plate configuration is provided in section S3 and more specifically in section S3.4 of the supplementary material. In the parallel plate system, a steady state with a finite gap thickness is always found to exist. However in a non-parallel plate system, a steady state with a finite gap does not always exist. If there is no such steady state, then the plates eventually touch.

2.3.1. Conditions for steady state to exist

In the final state, the plug region fills the entire gap and the yield surface is at $y_{plug} = 0$. On the yield surface, there is a point now denoted $x = x_{cf}$ at which the dimensionless shear stress changes sign from $-Od$ to $+Od$. This x_{cf} is the final value of x_c (which typically denotes the point at which flow changes sign). However there is no flow at all in the final state, so what changes sign is now the shear stress.

We integrate the equation $\partial p/\partial x = \mp Od/((H_{cf} - \delta\,x)/2)$ applicable in the final steady state. Here H_{cf} is the assumed final thickness at the centre of the plates. Thus for $x > x_{cf}$, the pressure profile is determined

$$p(x) = \frac{2Od}{\delta}\ln\frac{H_{cf} - \delta x}{H_{cf} - \delta}. \tag{17}$$

For $x < x_{cf}$, the pressure profile is

$$p(x) = \frac{2Od}{\delta}\ln\frac{H_{cf} + \delta}{H_{cf} - \delta x}. \tag{18}$$

Since the pressure profile has to be continuous at $x = x_{cf}$, Eqs. (17) and (18) should be equal at this point

$$\frac{2Od}{\delta}\ln\frac{H_{cf} - \delta x_{cf}}{H_{cf} - \delta} = \frac{2Od}{\delta}\ln\frac{H_{cf} + \delta}{H_{cf} - \delta x_{cf}}. \tag{19}$$

Simplifying Eq. (19), a quadratic equation can be obtained

$$x_{cf}^2 - 2\frac{H_{cf}}{\delta}x_{cf} + 1 = 0. \tag{20}$$

Solving the quadratic Eq. (20) gives x_{cf} as a function of H_{cf} and δ

$$x_{cf} = \frac{H_{cf}}{\delta} - \sqrt{\frac{H_{cf}^2}{\delta^2} - 1}. \tag{21}$$

The force applied over the entire plate length can be calculated utilising the pressure profiles obtained above

$$\begin{aligned} F &= \int_{-1}^{x_{cf}} p(x)\mathrm{d}x + \int_{x_{cf}}^{1} p(x)\mathrm{d}x \\ &= \frac{2Od}{\delta}\left(\left(x_{cf} - \frac{H_{cf}}{\delta}\right)\ln\frac{H_{cf}^2 - \delta^2}{(H_{cf} - \delta x_{cf})^2} + 2x_{cf}\right). \end{aligned} \tag{22}$$

Substituting the obtained x_{cf} from Eq. (21) into (22), considerable simplification results, because the argument of the logarithmic term turns out to be unity, so the logarithm itself vanishes. Assuming the plates have stopped moving then, the force applied over the entire plate length turns out to be

$$F = 4\frac{Od}{\delta}\left(\frac{H_{cf}}{\delta} - \sqrt{\frac{H_{cf}^2}{\delta^2} - 1}\right) = \frac{4Od}{\delta}x_{cf}. \tag{23}$$

This force generated by the pressure profile must now be matched to the unit force applied to the plates, and conditions determined in which physically meaningful solutions for H_{cf} or equivalently for x_{cf} are obtained. Setting $F = 1$ we need to find combinations of Od and δ that admit solutions with $H_{cf} > \delta$ or equivalently with $x_{cf} < 1$. It is clear that to achieve this we require $4Od/\delta > 1$. Provided this condition is satisfied, the gap at the right hand end $H_{cf} - \delta$ is then finite.

2.3.2. Final steady state torque calculation

As well as computing a force in the steady state, we can also compute a torque. For a Bingham fluid in a non-parallel system this can be obtained by taking the integral $\int_{-1}^{1} x\,p(x)\,\mathrm{d}x$ using pressure profiles provided in Eqs. (17) and (18). For comparison, analysis of torque for a Newtonian fluid (albeit at unsteady state) has been done in the supplementary material, section S2.2, but here we focus on the steady Bingham case. We find

$$\begin{aligned} T_{steady} = \frac{Od}{2\delta^3}\Bigg(&2(H_{cf}^2 - \delta^2 x_{cf}^2)\ln\frac{(H_{cf} - \delta\,x_{cf})^2}{H_{cf}^2 - \delta^2} \\ &+ 4\,\delta\,x_{cf}H_{cf} + 2\delta^2(x_{cf}^2 - 1)\Bigg) \end{aligned} \tag{24}$$

where T_{steady} is the steady state torque and x_{cf} is a known function of H_{cf}/δ from Eq. (21). As before the logarithmic term vanishes (its argument is unity) and after some further algebra using Eq. (20), the steady state torque reduces to

$$T_{steady} = \frac{2Od}{\delta}x_{cf}^2. \tag{25}$$

However, from Eq. (23) in the final steady state we already know $(Od/\delta)x_{cf} = \frac{1}{4}$. Hence final torque is

$$T_{final} = x_{cf}/2. \tag{26}$$

This indicates that T_{final} depends on the film thickness at the right hand end $H_{cf} - \delta$ relative to the film thickness at the centre H_{cf}. For instance, a final state with a gap on the right hand end that is not too narrow relative to the centre (i.e. small δ/H_{cf}, hence small x_{cf}) leads to small

T_{final}. However a much narrower gap with plates almost touching when they stop (i.e. δ/H_{cf} close to unity, hence x_{cf} close to unity) leads to $T_{final} = \frac{1}{2}$. Note that this is only half the torque of the Newtonian system when it touches (see section S2.2 in supplementary material).

There is another way to interpret the torque obtained in Eq. (25). Rather than obtaining it at the final steady thickness H_{cf}, we can find torque at any instantaneous H_c. This allows us to estimate (at any instant) a yield stress contribution to both force and torque, the total force and torque being a sum of yield stress contributions and viscous contributions. This approach will be discussed in Section 2.4. However, when a steady state is reached, there is no motion, hence no viscous contribution, and so total force and torque arise entirely from yield stress contributions.

2.3.3. Maximum and minimum Oldroyd number

To proceed we next define a parameter called η which involves the ratio between the tilt angle and the Oldroyd number

$$\eta = \delta/(4Od). \tag{27}$$

Note that the bracketed term in Eq. (23) is always less than unity for any $H_{cf}/\delta > 1$, i.e. $x_{cf} < 1$ always. Hence in order to satisfy the constraint $F = 1$, it is essential to have $\eta < 1$. In other words for a specified Od there is a maximum δ at which a steady state solution with a finite thickness could exist (or equivalently for any δ, there is a minimum Oldroyd number, Od_{min}, for a steady state with a finite thickness to exist)

$$Od_{min} = \delta/4. \tag{28}$$

If $Od < Od_{min}$, the plates rather than reaching steady state instead must touch as they do in the Newtonian limit $Od \to 0$. It is only in the limit of parallel plates with $\delta \to 0$ that Od_{min} falls to zero. When plates are tilted, the narrow end of the gap is more effective at supplying force to the plates than the wider end is. The issue with increasing δ however is that the gap only remains narrow over a limited domain of x close to its right hand end. An increase in δ therefore must be accompanied by an increase in Od (effectively an increase in yield stress of the fluid) to ensure that Eq. (23) in the absence of any fluid motion is still able to satisfy $F = 1$.

If $\eta > 1$, there is no steady state in which the yield stresses in the fluid are able to balance the imposed unit force on the plates. The plates must always keep moving until their right hand ends touch, as happens in the Newtonian limit for instance. Moving plates always have $y_{plug} > 0$, and this leads to larger pressures p and larger forces F (due to those pressures) than a stationary plate case can deliver (via Eq. (23)). Hence moving plates can achieve $F = 1$ even with $\eta > 1$ even though stationary plates cannot.

In addition to Od_{min} given above, there is a maximum Oldroyd number, Od_{max}, at which $H_{cf} = 1$: at this Od_{max}, the plates will not move at all. Inserting $H_{cf} = 1$ in Eq. (23) and rearranging, Od_{max} which depends on δ turns out to be

$$Od_{max} = \frac{1 + \sqrt{1 - \delta^2}}{4}. \tag{29}$$

2.3.4. Phase diagram for permitted states of system

Fig. 2 shows the phase diagram in the Od versus δ plane in which there are three regions, "do not move"; "move and stop"; "move and touch". Although (at any fixed δ) there is both a Od_{min} and Od_{max} for the plates to move and stop, in the case of fixed Od, there is only a maximum δ value, δ_{max} say. However what happens at that δ_{max} depends on the value of Od. If $Od < \frac{1}{4}$, then δ_{max} corresponds to the plates moving and touching. However if $Od > \frac{1}{4}$, then δ_{max} corresponds to the plates not moving at all.

Generally speaking, the data for the unsteady state evolution are sensitive to both δ and Od number. However the final fate of the system (i.e. whether the plates stop without touching or whether instead they move and touch) is only dependent on the η value. Indeed, if $\eta < 1$, such that the final film thickness is non-zero, the final state is approached but an arbitrarily long time is needed to reach it at least in principle (qualitatively this is similar to the viscoplastic Bingham case in a parallel system). However, if $\eta > 1$, the gap falls to zero at the right hand end and a non-parallel viscoplastic Bingham system will behave instead more like a Newtonian non-parallel case. In the Newtonian case, the right hand ends of the plates touch in a finite time (see section S2).

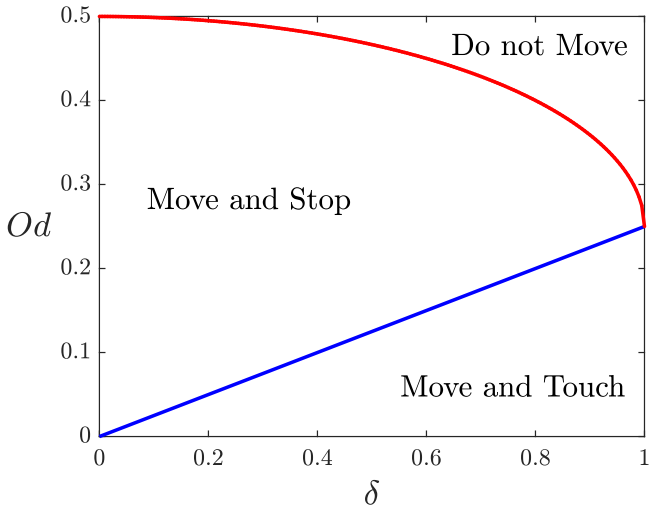

Fig. 2. Phase diagram in the Od vs δ plane for squeeze flow of viscoplastic Bingham fluid between non-parallel plates. In the "move and stop" and "do not move" regions, $\eta < 1$. In the "move and touch" region, $\eta > 1$.

2.3.5. Computing final film thickness

Having now identified the domain for which steady solutions are possible, we proceed to analyse the steady solutions further. Returning to Eq. (23) assuming $\eta < 1$, and imposing $F = 1$ we deduce

$$H_{cf} = \frac{\delta^2}{8Od} + 2Od. \tag{30}$$

For any Od number less than the maximum, a final H_{cf} less than unity can be determined. Now using this H_{cf} value, the point x_{cf} at which the viscoplastic stress switches sign can be defined. This can be determined via Eq. (21) and/or (23), and the result is

$$x_{cf} = \delta/(4Od) \equiv \eta. \tag{31}$$

Note that this steady state viscoplastic x_{cf} in general differs from the instantaneous Newtonian x_c given by Eq. (S17). Note also that as $\eta \to 1$, meaning the plates almost touch at their right hand ends once they have stopped moving, we find that $x_{cf} \to 1$, i.e. shearing in the final state is entirely towards the left. Furthermore, as already mentioned, in the non-parallel case torques can develop, and it turns out that final states with the largest x_{cf} also exhibit the largest torques. Indeed based on Eq. (26), torque is just $x_{cf}/2 = \eta/2$.

Rearranging Eq. (30) in terms of η gives $H_{cf}/(2Od)$ which is the average film thickness in the final state (at the centre of the plates) relative to the parallel case. This satisfies

$$\frac{H_{cf}}{2Od} = \eta^2 + 1. \tag{32}$$

Another important quantity, $(H_{cf} - \delta)/2Od$, which is the minimum film thickness (at the right hand end) in the final state relative to the parallel case, can be obtained

$$\frac{H_{cf} - \delta}{2Od} = (1 - \eta)^2. \tag{33}$$

The ratio between Eq. (33) and Eq. (32), $(H_{cf} - \delta)/H_{cf}$, is a measure of uniformity or otherwise of gap thicknesses such that it is zero if

polydisperse (the gaps at either end of the plates have different sizes) and unity if monodisperse (the gaps at either end have, in relative terms at least, the same thickness)

$$\frac{H_{cf}-\delta}{H_{cf}}=\frac{(1-\eta)^2}{\eta^2+1}. \tag{34}$$

To summarise Eqs. (32) and (33) give final film thicknesses in a tilted case relative to a parallel one. Meanwhile Eq. (34) tells us about the uniformity of final film thicknesses in the tilted case. These quantities depend on η, but not on Od and δ individually.

2.4. Yield force and yield torque calculation

For the Bingham parallel system presented in section S3.3 of supplementary material, we discuss a so called "yield force" contribution to the total force (the remainder of the total force being viscous force). The yield force is the force that would be developed with a given plate separation in the hypothetical case in which motion is stopped. Typically early on in the evolution, when plate separations are still quite large, yield force can be relatively small, meaning that total force is primarily viscous. However (see e.g. Figure S8) we show that over time eventually all the force becomes yield force. In this present section we explore the analogous behaviour for the non-parallel system.

Of course in the non-parallel case, in addition to defining a "yield force", we can also define a "yield torque". Again these both correspond at any given plate separation to the situation that occurs in the hypothetical case in which motion is stopped. The formulae we need are just (23) and (25), but using now the instantaneous H_c, albeit still computing x_c for this H_c value using (21). Of course the yield force and yield torque are not the same as the total force and total torque, since the totals include viscous contributions as well. Typically we can expect the yield force and yield torque to start out quite small, and only grow to match the total force and total torque in a situation in which the plates move and stop. On the other hand, if the plates instead move and touch (which can happen in a non-parallel system but not a parallel one), the yield force and yield torque might never match the total force and total torque.

3. Results and discussion

In the present section, results for a viscoplastic Bingham fluid in a non-parallel plate scenario are presented. We consider yield surfaces (Section 3.1), film thicknesses (Section 3.2), forces (Section 3.3), torques (Section 3.4) and final steady states (Section 3.5). The supplementary material, sections S4 and S5 focus primarily on results for the Newtonian fluid between parallel and non-parallel plates, and a viscoplastic Bingham fluid in a parallel plate configuration, respectively. Those results are useful for comparing and contrasting with the viscoplastic non-parallel case to be treated here, along with additional results which are presented in section S6.

3.1. Yield surface

The yield surface, y_{plug} versus x for $H_c = 1$ and $\delta = 0.2$ is shown in Fig. 3. This shows that y_{plug} for $x > x_c$ is not necessarily a monotonically increasing function of x, because y_{plug} has a maximum value of $H(x,t)/2$ and $H(x,t)$ is a decreasing function of x. Note that for $\delta = 0.2$, the maximum Od just slightly above $Od \approx 0.495$ is determined (via equation (29)). Close to this maximum Od number, y_{plug} is small.

For small Od however, y_{plug} is close to $H(x,t)/2$ (except very close to $x = x_c$ where $y_{plug} = 0$). For x just slightly greater than x_c, the value of y_{plug} increases very sharply at first (a consequence of the square root law in Eq. (14)), but for values of $Od = 0.1$ or less, y_{plug} reaches a maximum at a certain x, then, starts to decrease gradually.

The yield surface, y_{plug} versus x corresponding to $H_c = 1$ for different δ values and a constant $Od = 0.3$ is shown in Fig. 4. It is seen

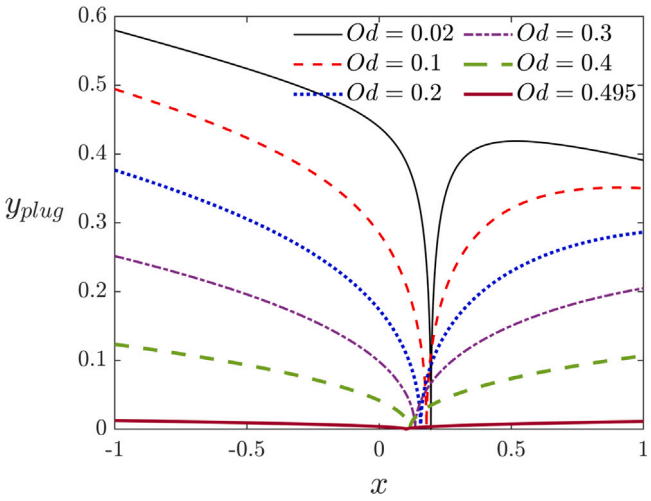

Fig. 3. Yield surfaces as functions of x corresponding to $H_c = 1$ and $\delta = 0.2$ for different Oldroyd numbers. Note that $Od = 0.495$ is close to the maximum Od number for the particular $\delta = 0.2$, so that $y_{plug} \ll 1$ when $H_c = 1$ in this case. The different Od values here have different v_{top} and x_c, values for which are reported in section S6.

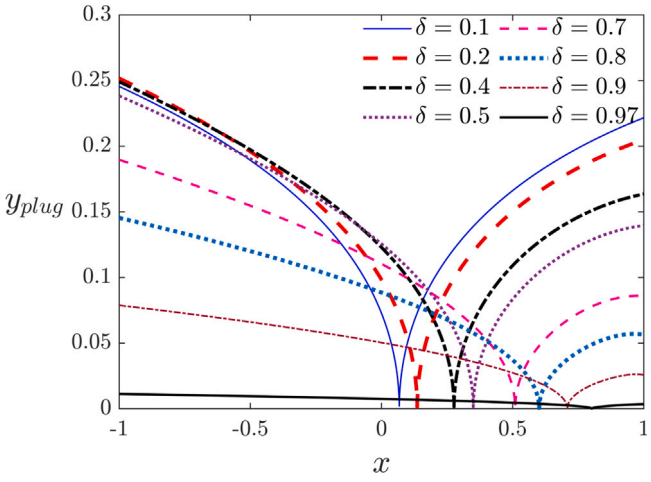

Fig. 4. Yield surfaces as functions of x corresponding to $H_c = 1$ and $Od = 0.3$ for different δ values. The different δ values here have different v_{top} and x_c, values for which are reported in section S6.

that, by increasing δ, the value of x_c increases and the yield surface becomes increasingly asymmetrical, tending to be thicker on the left hand side and thinner on the right hand side due to the geometrical constraint. For even larger δ however, y_{plug} can be small even on the left hand side, despite the wider gap there. This is due to v_{top} turning out to be small for these larger δ. Indeed by rearranging equation (29), a maximum value of δ (for the plates to move at all) just above 0.97 can be obtained for $Od = 0.3$.

Note that Figs. 3 and 4 tell us the locations of the plug region and yielded region, but not the velocities within each of those regions. Data for these velocities are however reported in section S6 in supplementary material.

Note moreover that Figs. 3 and 4 just consider one instant of time, i.e. the initial instant at which $H_c = 1$. The shapes of the yield surfaces can also be computed at later times with $H_c < 1$. However results are not presented here, because qualitatively the shapes are similar to those already seen in Figs. 3 and 4. The narrower the gap, the more impact the yield stress has upon the system, to the point that motion might stop altogether (as per Section 2.3). Hence decreasing H_c at fixed Od is similar, as far as shapes of yield surfaces are concerned, to increasing

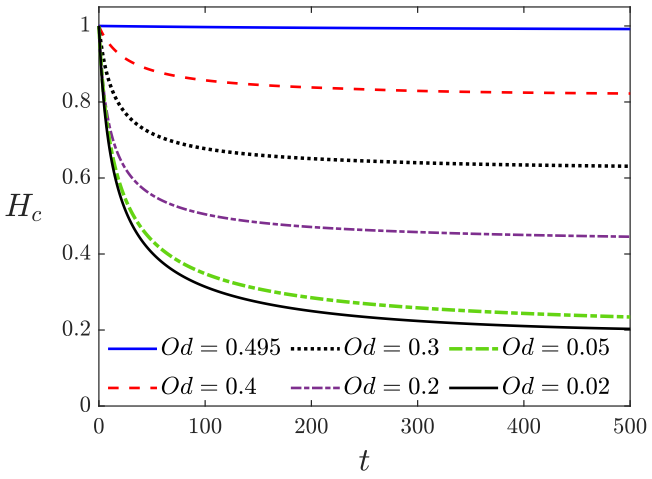

Fig. 5. Film thickness vs time for a constant $\delta = 0.2$ and different Oldroyd numbers.

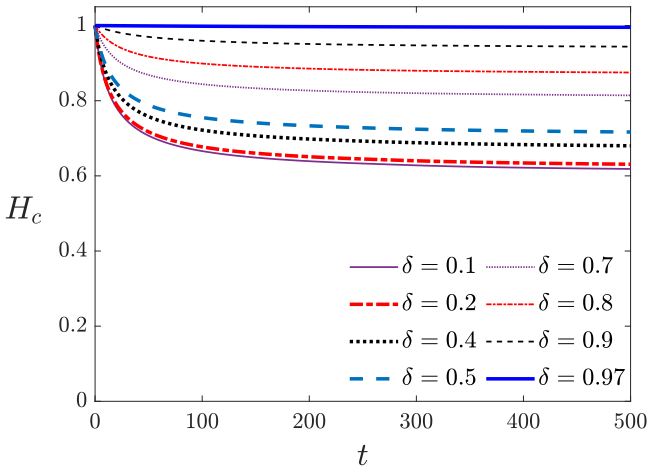

Fig. 6. Film thickness vs time corresponding to $Od = 0.3$ and different δ values.

Od at fixed H_c. Likewise the narrower the gap, the more impact a given tilt angle has upon the ratio of the film thickness between the right hand end and the centre. Hence decreasing H_c at fixed δ is similar, as far as shapes of yield surfaces are concerned, to increasing δ at fixed H_c. Instead of focussing on how y_{plug} varies with varying H_c, we therefore focus in what follows on how film thickness varies with time.

3.2. Film thickness versus time results

Changes of film thickness with respect to time for a constant $\delta = 0.2$ and various Od numbers are shown in Fig. 5. For the maximum $Od \approx 0.495$, the plates never move at all, whereas, for very small Od numbers (i.e. according to Eq. (28) for $Od < 0.05$ with this particular δ), the plates move and touch one another, and for all values of Od number in between, the plates move and stop at a final film thickness without touching one another at the right hand end. Assuming the plates move and stop without touching, Eq. (30) implies final film thickness is dependent not just on Od, but also on the ratio between tilt angle δ and Od number which appears in the definition of η in Eq. (27).

Film thickness versus time for different δ values and a constant $Od = 0.3$ is shown in Fig. 6. As δ increases, the final thickness H_{cf} increases. For any value of Od, there is a maximum value of δ beyond which the system stops moving. Using Eq. (29), the maximum δ value for a given Od number can be estimated (i.e. for $Od = 0.3$, a δ_{max} just slightly above 0.97 is achieved). All the δ values here are therefore less than the maximum. Hence, for all values of δ shown, the plates move, but also stop at final thickness since the value of η (see Eq. (27)) is also less than unity. However, for some cases (e.g. $\delta = 0.97$ or $\delta = 0.9$) the plates barely move before stopping.

A general comparison of film thickness versus time for squeeze film flow of a viscoplastic Bingham fluid with a constant $Od = 0.3$ between parallel non-parallel plates with different δ values is depicted in Fig. 7. In addition to that, changes of thickness at right hand ends of the plates (i.e. $H_c - \delta$) versus time for the two non-parallel cases are shown in the figure.

The difference between the final film thickness in the parallel case and the $\delta = 0.2$ non-parallel case is very small indeed, in line with the prediction of (30) which suggests this difference is second order in η and hence in δ. The difference with respect to the system with $\delta = 0.5$ is larger. Nonetheless, both the non-parallel systems shown here behave at least quantitatively analogous to the parallel case, with the gap at the right hand ends of the plates never reaching zero thickness as seen for the curves of $H_c - \delta$ (contrast this with section S4 in supplementary material and in particular Figure S3).

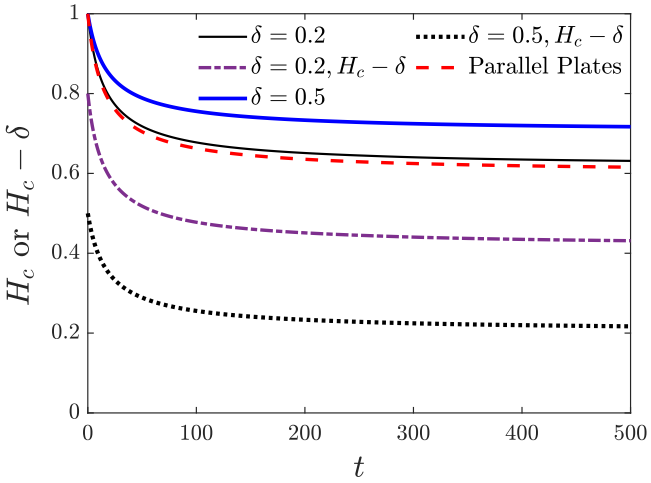

Fig. 7. Film thickness vs time corresponding to $Od = 0.3$ for parallel plates and non-parallel plates with δ values $\delta = 0.2$ and $\delta = 0.5$.

In Fig. 7 the parallel H_{cf} always lies between the non-parallel H_{cf} and the non-parallel $H_{cf} - \delta$, but is always further from the latter. This follows from Eq. (33) which suggests $H_{cf} - \delta$ is a first order quantity in η and hence first order in δ.

3.3. Contributions to the force

The force contributions (comprised of yield force and viscous force contributions summing to unity) as time proceeds for different Od values and $\delta = 0.2$ are shown in Fig. 8. The analogous result for the Bingham parallel system has been provided in the supplementary material, section S5.3.

For bigger Od numbers in the move and stop region (i.e. $Od = 0.2$, $Od = 0.1$), after relatively short times, yield force dominates the viscous force which is similar to the behaviour of the Bingham parallel system. However, for the smallest Od number considered (i.e. $Od = 0.02$) which is in the move and touch region, the yield force starts small, and despite it growing, it never approaches anywhere near unity. In fact when the plates eventually touch at right hand end of the gap the yield force can only ever reach $(4Od)/\delta$.

3.4. Torque results

Fig. 9 shows the numerically computed total torque (T; see Section 2.2) and also yield torque (T_{yield}; see Section 2.4) versus time for

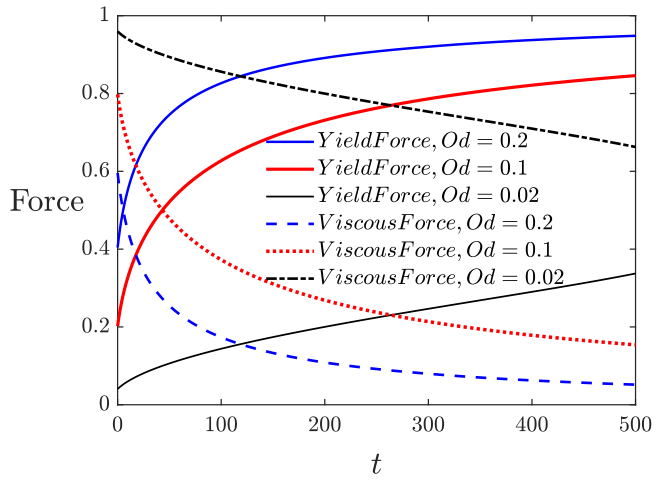

Fig. 8. Force contributions to the squeeze flow vs time for different Oldroyd numbers and $\delta = 0.2$ in the non-parallel geometry.

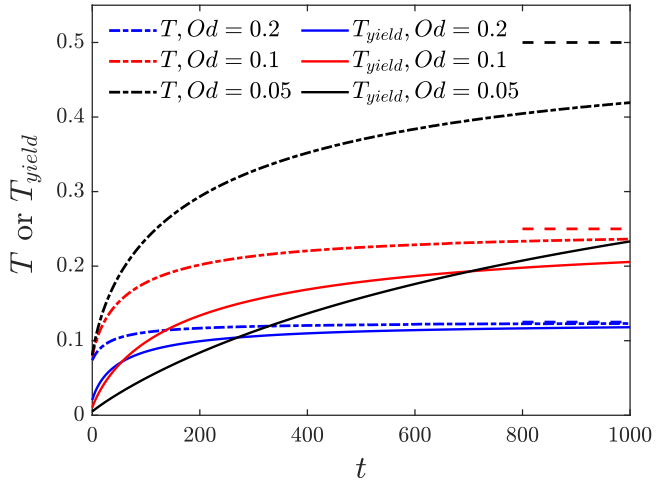

Fig. 9. Numerically computed total torque and also yield torque versus time for different Od numbers and $\delta = 0.2$. The horizontal dashed lines are the final torques attained in the limit of long times.

different Od numbers and a constant $\delta = 0.2$. From the figure, for each Od value the total torque is bigger than the yield torque and as time proceeds, the total torque and yield torque come closer together. For the largest Od number plotted (i.e. $Od = 0.2$), in fact total and yield torques are close together for almost all times. However, for the smallest Od number plotted (i.e. $Od = 0.05$), the yield torque starts off very small as mostly viscous torque is present initially and only by increasing the time, do the total and yield torques come closer together. Note that case $Od = 0.05$ with $\delta = 0.2$ has $\eta = 1$ so is on the boundary between the move and stop region and the move and touch region. Any smaller Od number will be in the move and touch region, and in such cases, the yield torque will never reach the same value as the total torque.

Another important point is that as Od decreases, the torque overall increases, whereas the yield torque starts off smaller but finishes larger due to the fact that the smaller the Od number, the greater the nonuniformity (average film thickness relative to film thickness on the right hand end) in the final state. This leads to a greater value of x_{cf}, and thus a larger final yield torque. Indeed the predicted final torque for each Od value is found via Eq. (26) and then given x_{cf} from Eq. (31), the final torque is found to be $T_{final} = \delta/(8Od)$. As seen in Fig. 9, the curves for each Od value are approaching the predicted final torque, although in the $Od = 0.05$ case, the approach is seen to be rather slow.

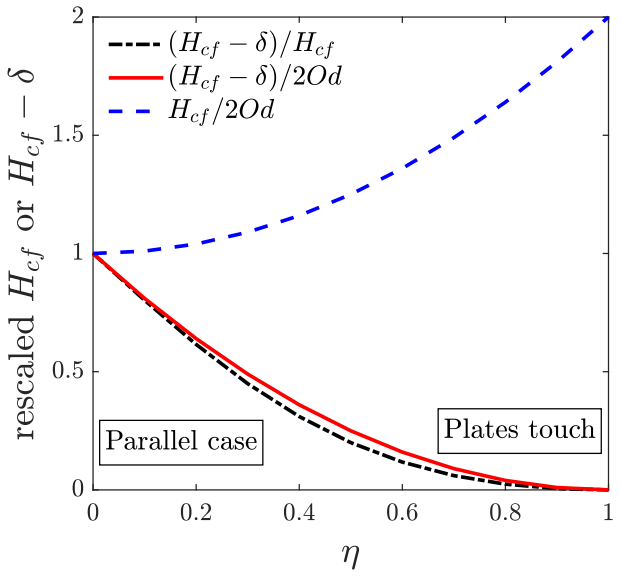

Fig. 10. Final film thicknesses in terms of $\eta = \delta/(4Od)$ values. The parallel case is $\eta = 0$ and the plates touch at $\eta = 1$.

This completes the discussion of torque in the Bingham fluid case, although a comparison between torques for Newtonian and Bingham fluids both as functions of x_c has been discussed in the supplementary material, Figure S5.

3.5. Steady states

In Fig. 10 plots are shown of $H_{cf}/(2Od)$ the average film thickness in the final steady state relative to the parallel case, $(H_{cf}-\delta)/(2Od)$ the minimum film thickness in the final state relative to the parallel case, and $(H_{cf} - \delta)/H_{cf}$ which is a measure of how uniform or nonuniform of film thicknesses are, specifically $(H_{cf}-\delta)/H_{cf}$ measures the ratio of the narrowest point to the average film thickness. All these quantities are plotted in terms of η (see Eqs. (32)–(34)), recalling that they are indeed functions only of η and not of Od and δ individually. In the case of the ratio $(H_{cf} - \delta)/H_{cf}$ in particular, note that as η increases, this ratio becomes smaller and hence the more polydisperse the system becomes in terms of film thickness, since the narrowest gap at the right hand end is then much thinner than the average thickness.

4. Conclusions

We considered a viscoplastic Bingham fluid squeezed between non-parallel plates (extending the work of [5] which considered merely the parallel geometry) under a fixed applied force (unlike the work of [13] which considered a fixed squeezing rate and parallel plates). We have also investigated the torque for the tilted plates.

Under a fixed applied force, a final film thickness can be found at which the plates stop moving. The final thickness is sensitive to Oldroyd number. A maximum Oldroyd number can be found beyond which the film thickness remains constant always without any squeezing whatsoever, due to the fact that the whole solution domain is in a plug region even at the initial instant. However, decreasing Oldroyd number allows the system to yield, and thereby reduce the film thickness as time increases. In a parallel system though, for any finite Oldroyd number, the two plates never touch even at infinite time. How the non-parallel, viscoplastic system which is considered here behaves depends, however, upon the ratio between the tilt angle, δ and the Oldroyd number, Od, this ratio appearing in the definition of a parameter $\eta \equiv \delta/(4Od)$.

If this ratio is small (i.e. $\eta < 1$), the behaviour is analogous to a viscoplastic Bingham fluid in a parallel configuration: squeezing stops while the gap is still finite. If this tilt angle to Oldroyd number ratio becomes too large (i.e. $\eta > 1$) however, the behaviour is more akin to a Newtonian fluid in a non-parallel configuration: the plates touch one another at a point. It is in the narrow part of the gap in which a viscoplastic Bingham fluid is best able to resist squeezing, but for a large tilt angle, the gap can only remain narrow over a very limited distance. Hence, with sufficient tilt, the applied force overcomes the yield stress even in the narrow part of the gap and drives the plates to touch. Moreover larger Oldroyd numbers lead to smaller η and hence more monodisperse film thicknesses.

Changing Oldroyd number also impacts on torque. Decreasing Od number increases the torque value, and torque also increases as time proceeds. In particular the torque is comprised of viscous and yield stress components. As Od decreases, the yield torque component is typically very small at early times as viscous torque dominates the yield torque. Then, as time proceeds and the system approaches a final state, the yield torque tends to dominate the viscous torque due to the fact that fluid is not moving in the final state.

Although we have managed to obtain model predictions here it is worth reflecting on the limitations of the model itself, that would also need to be overcome in future work. We have considered for simplicity a two-dimensional planar system (squeezing plates together). Squeezing together plates is however often a three-dimensional problem, as there will be many squeeze flow applications in which it is likely to be easier for fluid to escape by flowing in various directions during squeezing. Moreover we have ignored rotation of the plates. In reality the pressure field induced in the squeeze film, places not just a force on the plates (that balances the applied force) but also, as we have discussed, a torque. By balancing torque in addition to force it should be possible to deduce both a plate squeezing rate and a plate rotation rate. Rotation does however lead to a slightly more complicated flow field in the squeeze film (specifically equation (11) no longer applies). Here of course we have computed instead the torques that develop in the absence of rotation. Nevertheless the signs of those torques suggest that had rotation been permitted, it would have been such as to move the configuration closer to parallel as time evolved.

Declaration of competing interest

The authors declare that they have no known competing financial interests or personal relationships that could have appeared to influence the work reported in this paper.

Acknowledgments

The authors acknowledge support from EPSRC grant EP/V002937/1. E. Esmaeili also acknowledges support from a University of Strathclyde Student Excellence Award.

Appendix A. Supplementary sections

Supplementary material related to this article can be found online at https://doi.org/10.1016/j.jnnfm.2022.104817.

References

[1] D.F. Moore, A review of squeeze films, Wear 8 (4) (1965) 245–263.
[2] O.H. Campanella, M. Peleg, Squeezing flow viscometry for nonelastic semiliquid foods: Theory and applications, Crit. Rev. Food Sci. Nutr. 42 (3) (2002) 241–264.
[3] G.H. Meeten, Yield stress of structured fluids measured by squeeze flow, Rheol. Acta 39 (4) (2000) 399–408.
[4] J. Engmann, C. Servais, A.S. Burbidge, Squeeze flow theory and applications to rheometry: A review, J. Non-Newton. Fluid Mech. 132 (1–3) (2005) 1–27.
[5] G. Covey, B. Stanmore, Use of the parallel-plate plastometer for the characterisation of viscous fluids with a yield stress, J. Non-Newton. Fluid Mech. 8 (3–4) (1981) 249–260.
[6] G. Brindley, J.M. Davies, K. Walters, Elastico-viscous squeeze films. Part I, J. Non-Newton. Fluid Mech. 1 (1) (1976) 19–37.
[7] P. Coussot, Yield stress fluid flows: A review of experimental data, J. Non-Newton. Fluid Mech. 211 (2014) 31–49.
[8] P. Coussot, A.Y. Malkin, G. Ovarlez, Introduction: Yield stress – or 100 years of rheology, Rheol. Acta 56 (3) (2017) 161–162.
[9] D. Bonn, M.M. Denn, L. Berthier, T. Divoux, S. Manneville, Yield stress materials in soft condensed matter, Rev. Modern Phys. 89 (2017) 035005.
[10] B. Rabideau, C. Lanos, P. Coussot, An investigation of squeeze flow as a viable technique for determining the yield stress, Rheol. Acta 48 (2009) 517–526.
[11] G.G. Lipscomb, M.M. Denn, Flow of Bingham fluids in complex geometries, J. Non-Newton. Fluid Mech. 14 (1984) 337–346.
[12] D.N. Smyrnaios, J.A. Tsamopoulos, Squeeze flow of Bingham plastics, J. Non-Newton. Fluid Mech. 100 (1–3) (2001) 165–189.
[13] L. Muravleva, Squeeze plane flow of viscoplastic Bingham material, J. Non-Newton. Fluid Mech. 220 (2015) 148–161.
[14] J.G. Oldroyd, Two-dimensional plastic flow of a Bingham solid: A plastic boundary-layer theory for slow motion, Math. Proc. Camb. Phil. Soc. 43 (3) (1947) 383–395.
[15] G.H. Meeten, Effects of plate roughness in squeeze-flow rheometry, J. Non-Newton. Fluid Mech. 124 (1–3) (2004) 51–60.
[16] S.D.R. Wilson, Squeezing flow of a Bingham material, J. Non-Newton. Fluid Mech. 47 (1993) 211–219.
[17] I.A. Frigaard, D.P. Ryan, Flow of a visco-plastic fluid in a channel of slowly varying width, J. Non-Newton. Fluid Mech. 123 (1) (2004) 67–83.
[18] I. Walton, S. Bittleston, The axial flow of a Bingham plastic in a narrow eccentric annulus, J. Fluid Mech. 222 (1991) 39–60.
[19] N.J. Balmforth, R.V. Craster, A consistent thin-layer theory for Bingham plastics, J. Non-Newton. Fluid Mech. 84 (1) (1999) 65–81.
[20] A.R. Koblitz, S. Lovett, N. Nikiforakis, Viscoplastic squeeze flow between two identical infinite circular cylinders, Phys. Rev. Fluids 3 (2) (2018) 023301.
[21] K. Vajravelu, S. Sreenadh, V.R. Babu, Peristaltic transport of a Herschel–Bulkley fluid in an inclined tube, Int. J. Non-Linear Mech. 40 (1) (2005) 83–90.
[22] T. Hjelt, J.A. Ketoja, H. Kiiskinen, A.I. Koponen, E. Pääkkönen, Foam forming of fiber products: A review, J. Dispers. Sci. Technol. (2020) 1–37.
[23] V.J. Langlois, S. Hutzler, Dynamics of a flexible fibre in a sheared two-dimensional foam: Numerical simulations, Colloids Surf. A 534 (2017) 105–111.
[24] J. Lehmonen, E. Retulainen, J. Paltakari, K. Kinnunen-Raudaskoski, A. Koponen, Dewatering of foam-laid and water-laid structures and the formed web properties, Cellulose 27 (3) (2020) 1127–1146.
[25] O. Reynolds, IV. On the theory of lubrication and its application to Mr. Beauchamp Tower's experiments, including an experimental determination of the viscosity of olive oil, Philos. Trans. R. Soc. Lond. 177 (1886) 157–234.

Supplementary material: Squeeze film flow of viscoplastic Bingham fluid between non-parallel plates

Elaheh Esmaeili[a,*], Paul Grassia[a], Carlos Alejandro Torres Ulloa[a]

[a]*Department of Chemical and Process Engineering, University of Strathclyde, 75 Montrose Street, Glasgow, G1 1XJ, UK*

Abstract

This supplementary section reviews standard lubrication theory for Newtonian fluids (section S1) including cases in a non-parallel plate configuration (section S2). It then extends to consider the case of a viscoplastic Bingham fluid in a parallel configuration (section S3). Some additional results (over and above the results presented in the main text) for squeeze film flows of both Newtonian (section S4) and viscoplastic Bingham fluids (section S5 and section S6) are then presented. All of these supplementary sections support the analysis of squeeze film flow of a viscoplastic Bingham fluid between non-parallel plates that is presented in the main text.

S1. Squeeze Film Flow of Newtonian Fluid between Parallel Plates

In this section, the analysis for a parallel, Newtonian squeeze film will be reviewed. The governing lubrication equations for squeeze film flow of a Newtonian fluid are [1]

$$-\partial\hat{p}/\partial\hat{x} + \mu\,\partial^2\hat{u}/\partial\hat{y}^2 = 0 \tag{S1}$$

$$\partial\hat{p}/\partial\hat{y} = 0 \tag{S2}$$

$$\partial\hat{u}/\partial\hat{x} + \partial\hat{v}/\partial\hat{y} = 0 \tag{S3}$$

where $\hat{x}$ and $\hat{y}$ are coordinates along and across the lubrication layer, $\hat{u}$ and $\hat{v}$ are corresponding velocity components, $\hat{p}$ is pressure and μ is viscosity.

Dimensionless analogues of these equations, making variables dimensionless on

*Corresponding author.
Email address: elaheh.esmaeili@strath.ac.uk (Elaheh Esmaeili)

scales identified in the main text are

$$\partial p/\partial x = \partial^2 u/\partial y^2 \tag{S4}$$

$$\partial p/\partial y = 0 \tag{S5}$$

$$\partial u/\partial x + \partial v/\partial y = 0. \tag{S6}$$

Geometry of the squeeze film flow specifically between parallel plates is shown in Figure S1.

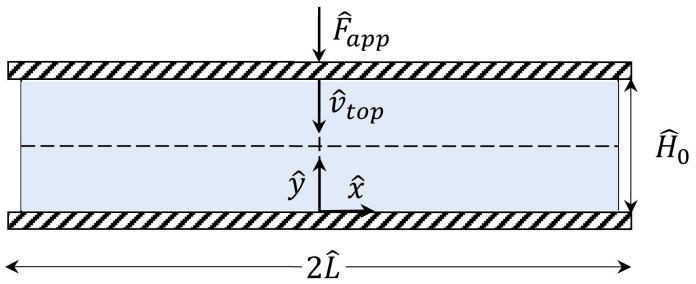

Figure S1: Geometry of squeeze film flow between parallel plates.

The solution of equations (S4), (S5) and (S6) now follows a standard procedure for a Newtonian squeeze film [2, 3]. From equation (S5) we find that the pressure is a function of x coordinate, thus, $p = p(x)$. Using the no slip boundary conditions $u = 0$ at $y = 0$ and $y = H(t)$, equation (S4) can be solved to obtain the velocity u in the horizontal direction

$$u = \frac{1}{2}\frac{\partial p}{\partial x} y(y - H(t)). \tag{S7}$$

Via the continuity equation (S6), the vertical velocity component at the top of the film, v_{top} can be determined

$$v_{top} = -\frac{H(t)^3}{12}\frac{\partial^2 p}{\partial x^2}. \tag{S8}$$

Note the sign convention adopted here: we define v_{top} to be a positive quantity, so that $v_{top}(t) \equiv -v|_{y=H(t)}$. The flow rate between the plates can be expressed as

$$Q \equiv \int_0^{H(t)} u \, \mathrm{d}y = \int_0^{H(t)} \frac{1}{2}\frac{\partial p}{\partial x} y(y - H(t)) \, \mathrm{d}y = -\frac{H(t)^3}{12}\frac{\partial p}{\partial x}. \tag{S9}$$

We also know that, $Q = v_{top}x$, in which recall v_{top} is considered as a positive quantity. Thus, using also boundary conditions in which at $x = -1$ and $x = 1$, $p = 0$, we can obtain the pressure distribution in the squeeze film

$$p(x) = \frac{6v_{top}}{H(t)^3}(1 - x^2). \tag{S10}$$

We now define F as the force (per unit distance out of the two-dimensional plane) that this pressure field places on the upper plate. This is obtained by integration of the pressure field along the plates

$$F = \int_{-1}^{1} p(x)\,\mathrm{d}x = \frac{8v_{top}}{H(t)^3}. \tag{S11}$$

We can define the velocity of the upper plate, v_{top} as a derivative of film thickness, $H(t)$. With our sign convention

$$v_{top} = -\mathrm{d}H(t)/\mathrm{d}t. \tag{S12}$$

The force F imposed by the pressure field on the plate must balance the applied force that sets up the squeeze film flow in the first place. However because of the way we have non-dimensionalized the system (the relevant scales are given in the main text), this applied force is simply unity. It then follows from equation (S11) that $v_{top} = H(t)^3/8$. Via equation (S12) it then follows

$$t = 4\left(\frac{1}{H(t)^2} - 1\right). \tag{S13}$$

This rearranges to

$$H(t) = (1 + t/4)^{-1/2}. \tag{S14}$$

S2. Squeeze Film Flow of Newtonian Fluid between non-Parallel Plates

Now, we will investigate the behaviour of squeeze film flow between two non-parallel plates, still for a Newtonian fluid. In the parallel case, section S1, on symmetry grounds, it was found that the dimensionless flow rate Q vanishes at the half way point along the plates, i.e. at $x = 0$. However, we cannot use that same assumption for non-parallel plates. Therefore, we must find the point at which the flow rate will be zero. This point will be denoted as x_c. The flow rate Q can still be defined in terms of the integral of the horizontal velocity equation (S7) over the film

thickness which gives equation (S9). However the flow rate for non-parallel plates is $Q = v_{top}(x - x_c)$ where, as before, the sign convention is such that v_{top} is positive. Moreover, H within that equation now depends on x (not just on t). Hence, using the equations (S9) and (5), the pressure gradient is

$$\frac{\partial p}{\partial x} = \frac{12 v_{top}(x_c - x)}{(H_c(t) - \delta\, x)^3}. \tag{S15}$$

Here $H_c(t)$ is the separation at the centre of the plates, and δ is the rescaled tilt angle. Note that when H_c is close to δ and also x is close to unity, such that the gap at the right hand end of the plates is narrow, large pressure gradients are seen near $x = 1$. This means that as x decreases from unity, sharp rises in pressure are seen in the narrow part of the gap. Integration of equation (S15) using the boundary conditions in which at $x = -1$ and $x = 1$, the pressure is equal to zero, the pressure distribution and also x_c can be determined after some algebra

$$p(x) = \frac{6 v_{top}(1 - x^2)}{H_c(t)^3 \left(1 - \frac{\delta}{H_c(t)} x\right)^2}. \tag{S16}$$

$$x_c = \delta / H_c(t). \tag{S17}$$

Note that in the limit of $\delta \to 0$ this reduces back to the parallel plate case as we expect. On the other hand for a fixed δ, as $H_c(t)$ falls over time, it is clear that x_c grows. When $H_c(t)$ falls towards the value δ, the plates come into contact at the right hand end, since in that case $H|_{x\to 1} \equiv H_c(t) - \delta$ approaches zero. In that limit, $x_c \to 1$, implying that all the flux $Q = v_{top}(x - x_c)$ is to the left with $x < x_c$ and none of it flows out the narrow gap to the right. Returning to a general value of $\delta / H_c(t)$, the force F which the pressure distribution places on the upper plate can be obtained by integrating equation (S16) which leads to

$$F = \frac{24 v_{top}}{H_c(t)\delta^2} \left(\frac{H_c(t)}{2\delta} \ln \frac{1 + \frac{\delta}{H_c(t)}}{1 - \frac{\delta}{H_c(t)}} - 1 \right). \tag{S18}$$

A differential equation for $H_c(t)$ versus t can now be derived by recognising that this force F due to the pressure field must be balanced to the unit force imposed externally on the plate. Setting $F = 1$ and $v_{top} = -\mathrm{d}H_c(t)/\mathrm{d}t$ leads to after some

algebra

$$t = \frac{12}{\delta^3}\bigg((H_c - \delta)\ln(1 - \frac{\delta}{H_c}) - (1-\delta)\ln(1-\delta) \\ - (H_c + \delta)\ln(\frac{\delta}{H_c} + 1) + (\delta + 1)\ln(\delta + 1)\bigg). \quad \text{(S19)}$$

This is an implicit equation for H_c given t. It is easy to check by inspection that $H_c \to 1$ as $t \to 0$. At other times, we cannot in general invert this expression to obtain an explicit analytic formula for H_c in terms of t. However there is still a limiting case that we can analyse as discussed below.

S2.1. Asymptotic Behaviour in Limit $\delta/H_c \to 1$

In this section, the special case in which the two plates touch at one end is considered. In equation (S19), if we take the limit $\delta/H_c \to 1$, a final time t_f at which the plates touch (i.e. H_c equals δ) can be calculated:

$$t_f = \frac{12}{\delta^3}\bigg(- (1-\delta)\ln(1-\delta) - 2\,\delta\ln(2) + (\delta+1)\ln(\delta+1)\bigg). \quad \text{(S20)}$$

Details of how t_f behaves are deferred until section S4. For now however we note that t_f is finite, i.e. the plates touch in finite time, unlike the parallel case given by equation (S14) which requires infinite time for the plates to touch.

Of interest also is to find out how H_c varies with time close to this final time. Within equation (S18) we know that the term $\ln(1 - \delta/H_c(t))$ goes to infinity when $H_c(t)$ approaches δ. Hence, consulting equation (S18) with $F = 1$ and $v_{top} = -\mathrm{d}H_c(t)/\mathrm{d}t$, it follows that $\mathrm{d}H_c(t)/\mathrm{d}t$ approaches zero at $t = t_f$, even though the final time is already obtained as a finite quantity.

Therefore, an asymptotic analysis is required to establish the behaviour of film thickness for times close to the final time. A parameter called ϵ is defined such that $\epsilon(t) \equiv 1 - \delta/H_c(t)$ with $\epsilon \ll 1$ in cases of interest. In this limit $\epsilon \ll 1$ we have $H_c(t) \approx \delta + \delta\,\epsilon(t)$. It follows via equation (S18) that

$$\delta\frac{\mathrm{d}\epsilon(t)}{\mathrm{d}t} \approx \frac{\mathrm{d}H_c(t)}{\mathrm{d}t} \approx \frac{\delta^3}{24\ln\epsilon}. \quad \text{(S21)}$$

As expected $\mathrm{d}H_c(t)/\mathrm{d}t$ approaches zero in the limit as $\epsilon \to 0$, but the approach to zero is exceedingly slow, so tiny velocities are only reached for exceedingly small ϵ.

When ϵ is small this gives at leading order

$$t \approx t_f - \frac{24}{\delta^2}\epsilon \ln(1/\epsilon) \quad \text{for} \quad \epsilon \ll 1. \tag{S22}$$

Starting then from any time t at which ϵ is small but finite, the subsequent time interval $t_f - t$ that must elapse for the plates to touch scales not proportionally to ϵ but rather proportionally to $\epsilon \ln(1/\epsilon)$ which is significantly greater than ϵ. The time interval $t_f - t$, whilst shrinking as ϵ shrinks, is therefore surprisingly long.

To summarize, even though having a very narrow gap tends to imply a very slow approach to the final state (e.g. $v_{top} = H(t)^3/8$ in the parallel case), in the tilted case, the gap only manages to be exceedingly narrow over a very short distance in x (at the far right hand end), so v_{top} is large enough that plates still touch in finite time. That said, the approach to the final state still remains surprisingly slow.

S2.2. Torque Calculation

Tilted systems are associated with non-zero torques. In this section the analysis for investigating the torque is considered. Torque (per unit distance out of the two-dimensional plane) is evaluated as the integral along the plates $\int_{-1}^{1} x\, p(x)\, \mathrm{d}x$. Thus, for Newtonian fluid in the non-parallel system, we can compute a dimensionless torque that is analogous to the dimensionless force formula, equation (S18). Since v_{top} is defined by setting the dimensionless lubrication force to unity, we can evaluate v_{top} and substitute it in, to obtain a torque expression wholly in terms of $\delta/H_c(t)$. Equivalently the torque can be expressed in terms of x_c since by equation (S17), $\delta/H_c(t)$ is the same as x_c in the Newtonian case. We find

$$T = \int_{-1}^{1} x\, p(x) \mathrm{d}x = \frac{H_c(t)^2 \left((3 - \frac{\delta^2}{H_c(t)^2}) \ln \frac{1+\frac{\delta}{H_c(t)}}{1-\frac{\delta}{H_c(t)}} - 6\frac{\delta}{H_c(t)} \right)}{4\delta^2 \left(\frac{H_c(t)}{2\delta} \ln \frac{1+\frac{\delta}{H_c(t)}}{1-\frac{\delta}{H_c(t)}} - 1 \right)}. \tag{S23}$$

In the limit of $x_c \to 0$ (i.e. $\delta/H_c(t)$ to zero), this gives zero torque (as expected). Also in the limit of $x_c \to 1$ (i.e. $\delta/H_c(t)$ to unity), it gives unit torque. Physically this implies that the lubrication pressure field (and hence the lubrication force) is highly concentrated in the neighbourhood of $x_c = 1$.

S3. Squeeze Film Flow of Bingham Fluid between Parallel Plates

In this section the parallel plate squeeze film flow of a viscoplastic Bingham fluid is discussed. The general analysis is based on the work of [4, 5], but compared to [5]

a different situation is considered. In [5], squeezing force is analysed with a constant squeezing velocity, while we are investigating a constant squeezing force to find the rate of squeeze action, as per [4].

The geometry of squeeze film flow is similar to Figure S1 just with different rheology. The governing lubrication equations [6] for a yield stress fluid are discussed in the main text, section 2.1. Obviously the analysis in the main text concerned the non-parallel case. Here in the interests of completeness, we review step by step the analogous development for the parallel case. This is included specifically for the benefit of those readers who prefer to understand the parallel case first, before generalising to the non-parallel one.

The aim is to find the yield surface (or strictly speaking "fake yield surface") which is denoted as $y_{plug}(x)$. The yield surface will divide the film thickness into two regions, a yielded region (or strictly speaking "fully plastic" region) in which ($y < y_{plug}$) and a plug region (or strictly speaking "pseudo-plug" region) in which ($y_{plug} < y < H(t)/2$) and these regions are shown in Figure S2. Due to the flow symmetry, only one quadrant of the flow domain is represented.

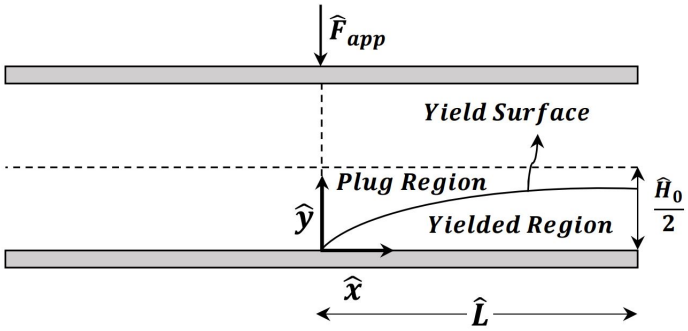

Figure S2: Schematic representation of the flow structure showing yielded and plug regions. The sketch shows the case for the initial film thickness, $\hat{H} = \hat{H}_0$, but generalizes to any other $\hat{H}$.

Taking the integral of equation (8) using a no slip boundary condition (i.e. $u = 0$ at $y = 0$), a velocity profile in the y direction can be deduced

$$u = \frac{\partial p}{\partial x}\frac{1}{2}y(y - H(t)) - Od\, y, \tag{S24}$$

where recall Od is the Oldroyd number (the ratio between yield stress and imposed stress as defined in the main text). The obtained velocity profile applies generally throughout the yielded region. In order to find the boundary between the yielded and plug regions, we use the fact that at the yield surface ($y = y_{plug}$), the shear rate

is zero ($\partial u/\partial y = 0$) or equivalently $|\tau_{xy}| = Od$. Therefore putting this condition into equation (8), the expression for the pressure gradient in the x direction can be determined

$$\frac{\partial p}{\partial x} = \frac{Od}{y_{plug} - \frac{H(t)}{2}}. \tag{S25}$$

Now, via substitution of equation (S25) in (S24), the velocity profile for both yielded and plug regions is achievable

$$\begin{cases} u = \dfrac{Od}{2(y_{plug} - \frac{H(t)}{2})} y^2 - \dfrac{Od}{(y_{plug} - \frac{H(t)}{2})} y_{plug} y & \text{for} \quad y \leqslant y_{plug} \\ u_{plug} = -\dfrac{Od}{2(y_{plug} - \frac{H(t)}{2})} y_{plug}^2 & \text{for} \quad y_{plug} < y < \dfrac{H(t)}{2}. \end{cases} \tag{S26}$$

Here, u and u_{plug} are the yielded and plug regions velocity profiles, respectively. Using the definition for the flow rate Q, an equation for the yield surface is generated.

$$Q \equiv 2\left(\int_0^{y_{plug}} u \, \mathrm{d}y + \int_{y_{plug}}^{\frac{H(t)}{2}} u_{plug} \, \mathrm{d}y\right) = v_{top} x. \tag{S27}$$

Inserting equation (S26) in (S27), taking the integral and after some algebra, the expression for the yield surface becomes [5]

$$y_{plug}^3 - \frac{3}{2} H(t) y_{plug}^2 - 3\frac{v_{top} x}{Od} y_{plug} + \frac{3}{2}\frac{v_{top} x H(t)}{Od} = 0. \tag{S28}$$

This is a cubic equation for y_{plug} which in general can be tedious to solve exactly, so more convenient approaches to obtaining solutions are considered below. The fact that we encounter a non-linear equation here is a reflection of the non-linear rheology of a viscoplastic Bingham fluid. The equation only applies for $x \geq 0$ but that is all we need in the parallel plate case, as y_{plug} is symmetric about $x = 0$.

S3.1. Solving for y_{plug}

As equation (S28) is non-linear, typically numerical methods are employed to solve it. The typical way of solving it would be, starting from a guess of y_{plug} at any given x, using the Newton-Raphson method which gives a sequence of better approximations to the value of y_{plug}.

A suitable initial guess can be readily obtained. We rely on the observation that (at least in this parallel plate case) on symmetry grounds at $x = 0$ there can be no

fluid motion either to left or right, hence no strain rate $\partial u/\partial y$ at any y. Hence at $x = 0$, we must have $y_{plug} = 0$.

Close to $x = 0$ then, y_{plug} must be small, i.e. $y_{plug} \ll H(t)/2$. The integral on the left hand side of (S27) then evaluates to $u_{plug}H(t)$ which we set equal to $v_{top}x$, and with $u_{plug} \approx y_{plug}^2 Od/H(t)$ via (S26). Therefore, the initial guess for y_{plug} is

$$y_{plug}(x) \approx \sqrt{v_{top}x/Od}. \tag{S29}$$

This gives a good approximation for y_{plug} at least for small x, and the Newton-Raphson approach then converges to the actual y_{plug} value. Equation (S29) does not however apply uniformly for all x. Indeed for sufficiently large x, this equation might even predict a nonsense value of y_{plug} larger than $H(t)/2$.

Nonetheless, once we have solutions for y_{plug} for any particular x value, we can simply make a small increment in x, and use the y_{plug} value at one x value as an initial Newton-Raphson guess for y_{plug} at the next x value. Hence a profile of y_{plug} versus x all the way up to the end of the plate ($x = 1$) can be obtained.

Note that for sufficiently small Od (a system that is close to Newtonian), we anticipate that y_{plug} could be close to $H(t)/2$ over a significant domain of x. The Newtonian $\partial p/\partial x \equiv -12v_{top}x/H(t)^3$ is then recovered (this follows from equation (S8)). If we substitute this into equation (S25) for y_{plug} we find

$$y_{plug} \approx \frac{H(t)}{2} - \frac{H(t)^3 Od}{12v_{top}x}. \tag{S30}$$

Regardless of whether we are in a regime in which equation (S29) applies, or in which equation (S30) applies, or whether we instead obtain solutions to the cubic equation (S28) numerically, once we have values of $y_{plug}(x)$ we can evaluate how squeezing proceeds over time as follows.

S3.2. Computing Film Thickness versus Time

So far our analysis has not differed from that of [5]. Now however we introduce a point of departure. Whereas [5] assumed a given constant v_{top} leading to a prespecified H versus t relation, the difference here is that v_{top} is not constant and instead must be computed as part of the solution as was done by [4], and this then affects H versus t.

We proceed as follows. Once y_{plug} versus x is determined, for any arbitrary v_{top}, we can integrate equation (S25) to determine p versus x. Typically for $0 \leq x \leq 1$,

we have

$$p(x) = \int_x^1 \frac{Od}{(-y_{plug}(x) + H(t)/2)}\,\mathrm{d}x. \tag{S31}$$

This enforces a constraint $p = 0$ at $x = 1$. Given that $y_{plug}(x)$ is usually only known numerically, this integral needs to be done by quadrature (e.g. trapezoidal rule or Simpson's rule). We solve for $p(x)$ over the domain $0 \le x \le 1$ remembering that p is symmetric in the domain $-1 \le x \le 0$ at least in this parallel plate case.

Once p versus x is known, we evaluate the force $F = \int_{-1}^{1} p(x)\,\mathrm{d}x$ that this pressure field places on the plate: again this is determined by quadrature. This force now needs to be set to unity to match the applied force that is assumed constant and that is normalised to unity here.

Note that, as well as depending on x, the y_{plug} value also depends implicitly on Od, $H(t)$ and v_{top} as follows from equation (S28). Hence for any given Od and $H(t)$, imposing the constraint $F = 1$ implies a non-linear equation that defines v_{top}. Once v_{top} is determined, $H(t)$ can be updated via $\mathrm{d}H(t)/\mathrm{d}t = -v_{top}$.

In order to solve the non-linear equation for v_{top} we need a starting guess. An upper bound for v_{top} is the Newtonian value (see section S1) which is $(H(t)^3)/8$ and which is only realised in the limit $Od \to 0$. Once v_{top} is found for any given Od at some particular $H(t)$, that same v_{top} value can be used as a starting guess for nearby values of $H(t)$ and/or Od.

Specifically the numerical routine that we used computed y_{plug} at least 100 locations along the film, performed quadrature to obtain lubrication pressures (and forces associated with those pressures). It then matched lubrication force to applied force to find v_{top} values, and updated $H(t)$ via Heun's method using an initial time step[1] of 0.5, although we found we could adapt to longer times as the squeezing proceeded and the squeezing rate slowed. Indeed, decreasing $H(t)$ and/or increasing Od causes v_{top} to fall. The issue we face in the parallel case is that for any finite Od (no matter how small) it is always possible to find a value of $H(t)$ at which v_{top} vanishes. All squeezing motion has now stopped and the force imposed on the plate is balanced by the force due to the yield stress of the fluid. This leads to a steady state $H(t)$ that we analyse shortly.

We also checked adequacy of the selected time step (set to 0.5) as follows. Heun's method was applied to a Newtonian system, and numerical data were compared with an analytical solution (given in section S1). By time $t = 12$ (at which time the

[1]Although this selected time step might seem larger than expected, it should be remembered via equation (S11) that the initial v_{top} in the Newtonian case is only 0.125 and the Bingham v_{top} is lower still. Hence the change in $H(t)$ over even the first time step is actually quite modest.

Newtonian $H(t)$ was half its original value), the difference between the numerical and analytical $H(t)$ was only 0.0002, an error we deemed acceptable. Systems with finite Oldroyd number evolve, if anything, more slowly than their Newtonian counterparts (i.e. smaller v_{top}), so if a time step of 0.5 was adequate for the Newtonian system, it would also be adequate in a case for which the Oldroyd number was finite.

S3.3. Computing Contributions to the Force

The applied force (taken as unity here) is balanced by the lubrication force in the gap, which is comprised of a part associated with yield stresses plus a part associated with viscous stresses. In the final state, there is no viscous stress because there is no motion.

On the other hand, at very early times, viscous stresses are expected to be relevant, because any force associated with the yield stress is just a small fraction of the total. A transition is therefore possible between a situation in which the viscous forces are dominant and a situation in which the yield stress forces are dominant and finding which force dominates at which time depends on the Od number.

By computing the force that would be placed on the plate in the hypothetical situation in which $v_{top} = 0$ for any given H, the force associated with the yield stress (i.e. so called yield force) will be obtained. Then the force associated with viscous stresses (i.e. viscous force) is calculated as the difference between the applied force and the yield force.

S3.4. Steady State for Viscoplastic Bingham Fluid between Parallel Plates

For any given Oldroyd number, a final film thickness can be obtained. Indeed, for Od big enough, even the initial state, which is non-dimensionalized such that $H = 1$, leads to no motion. As alluded to earlier, in the present formulation like [4] but unlike [5], a constant squeezing force is considered to find the squeezing rate. Thus squeezing must eventually stop. Motion coming to a stop is equivalent to having $y_{plug} \to 0$ (or equivalently $y_{plug} \ll H/2$) for all x values. Thus, the plug region now fills effectively the entire gap. Putting $y_{plug} = 0$ in equation (S25)

$$|\partial p/\partial x| = 2Od/H_f. \tag{S32}$$

Here H_f is the final steady state film thickness. Using the above equation to find the pressure profile for positive and negative x directions, taking the integral of pressure profile over the whole length of the plate, the applied force is obtained

$$F = \int_{-1}^{1} p(x)\,\mathrm{d}x = \int_{-1}^{0} \frac{2Od}{H_f}(1+x)\mathrm{d}x + \int_{0}^{1} \frac{2Od}{H_f}(1-x)\mathrm{d}x = \frac{2Od}{H_f}. \tag{S33}$$

Inserting $F = 1$ in above equation, we find, $H_f = 2Od$ which means that for a given Od the final steady state thickness is twice the Od number. Thus for small Od, we can squeeze the plates really quite close together before they stop moving. As Od increases, the plates stop moving sooner, i.e. at larger H_f. Moreover a maximum Oldroyd number equal to $\frac{1}{2}$ is found for any squeezing to take place whatsoever: as $Od \to \frac{1}{2}$, even the initial plate separation $H = 1$ leads to no plate motion.

S4. Results: Newtonian Fluid between Parallel & non-Parallel Plates

The main text section 3 focussed primarily on results for the viscoplastic Bingham fluid in non-parallel plate configurations. In the present section, in the interests of completeness and for comparison, analogous results for a Newtonian fluid are presented.

S4.1. Film Thickness versus Time

In Figure S3 changes of film thickness versus time are shown. For parallel plates (equation (S14)), film thickness decreases with time and the most rapid changes occur at early times and then film thickness changes slowly with subsequent time. Indeed, in the parallel case, the plates only come into contact in the limit of infinite time which means that theoretically the film thickness never quite reaches zero [2, 3].

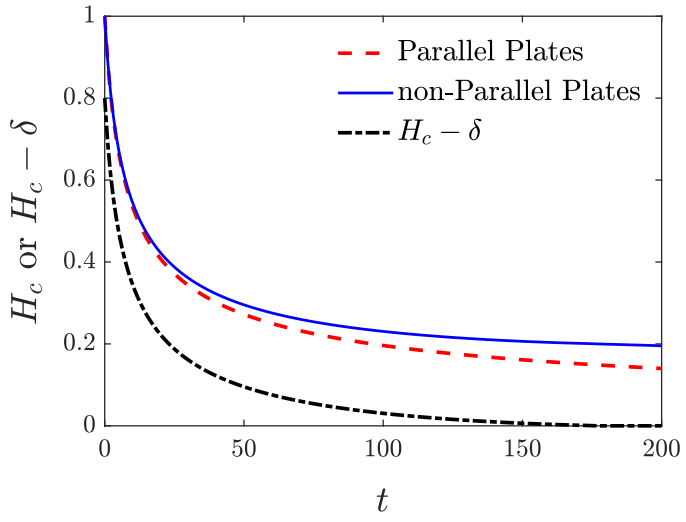

Figure S3: Profile of film thickness vs time. For non-parallel plates, δ was set to 0.2.

However, in the case of non-parallel plates, H_c reaches its final value δ when time is still finite. The parallel case can be a good approximation to the non-parallel case for sufficiently large values of film thickness, i.e. provided H_c much larger than δ. It is only when H_c falls to comparable magnitude to δ that the non-parallel case differs notably from the parallel one. In that situation, the film thickness on the right hand end $H_c - \delta$ is much smaller in relative terms than the film thickness at the centre H_c.

Figure S3 for a Newtonian system looks superficially like Figure 7 in the main text for a viscoplastic Bingham fluid (with Oldroyd number $Od = 0.3$ and various δ) in the sense that the non-parallel H_c exceeds the parallel H which in turn exceeds the non-parallel $H_c - \delta$. The difference of course is that for Figure S3 the non-parallel plates touch whereas in Figure 7 motion stops at a finite film thickness. In order for plates to touch in a viscoplastic Bingham fluid it would be necessary to choose a different combination of Od and δ, specifically Od must be less than $\delta/4$.

In a non-parallel case, and in the limit as H_c approaches δ, the remaining gap on the right hand end has almost closed completely. As a result, all flow is now towards the left (which is also seen from equation (S17) for Newtonian systems which places x_c, the divider between leftward moving and rightward moving flow, at the far right hand end). A similar situation is also seen in the special case of viscoplastic Bingham systems which reach a steady state, with a very small but finite film thickness (i.e. $H_{cf} - \delta \ll 1$). These states have Od very slightly greater than $\delta/4$. Equation (31) in the main text then gives the final x_c value satisfying $x_{cf} \to 1$, such that all material is sheared toward the left.

S4.2. Final Time for Plates to Touch

Figure S3 only considered data for one particular δ value. Using analytical equation (S20) we can however predict the final time for plates to touch in a Newtonian system for any δ value. Figure S4 shows how final time in the squeeze film flow of a Newtonian fluid between non-parallel plates changes with the value of δ. As can be seen, the system will reach the final time sooner as δ increases. For very small δ, it turns out that equation (S20) predicts t_f scales proportionally to δ^{-2}. Conceptually this is easy to understand. When δ is small, the system behaves similar to a parallel case, at least until H_c falls to a value on the order of δ. The parallel case equation (S13) predicts an order δ^{-2} time for this to occur.

Thus the bigger δ becomes, the sooner the right hand end of the plates touch. On the other hand in the limit as $\delta \to 0$ the time for the plates to touch diverges as the parallel case is reached. A viscoplastic Bingham system can reach a final state in which plates do not touch at all, although in principle an arbitrarily long time is needed to attain that final state.

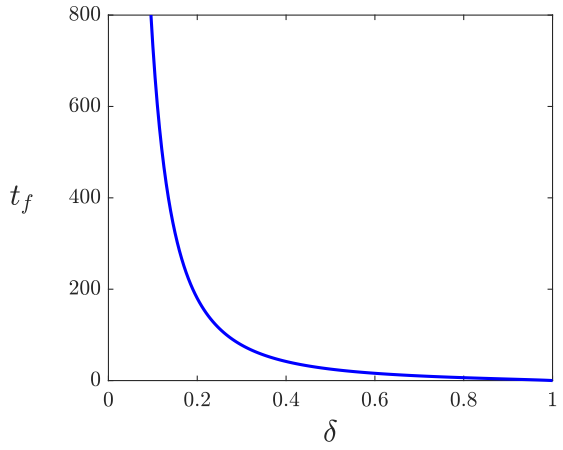

Figure S4: Final time vs δ in Newtonian non-parallel system.

S4.3. Torque Results

In Figure S5, the graph of torque for a Newtonian fluid in terms of x_c is depicted. Here x_c according to equation (S17) is the same as δ/H_c in the Newtonian case.

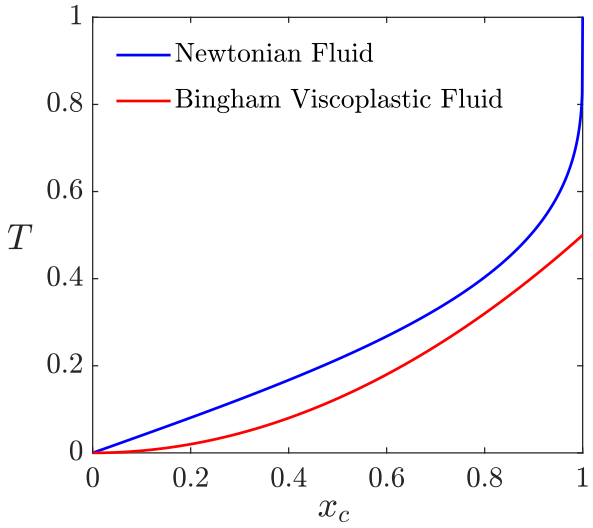

Figure S5: Changes of torque in terms of x_c for Newtonian and Bingham fluids.

Over time, H_c decreases, so x_c increases. The value of Newtonian torque based

on equation (S23), increases comparatively slowly with x_c near $x_c = 0$, and it is only near $x_c = 1$ that torque increases very sharply eventually to reach unity.

For comparison we have also shown the yield stress contribution to torque in a Bingham fluid non-parallel case. Torque is again plotted against x_c, but this x_c is now no longer given by equation (S17) but instead by (21), although this again gives x_c growing as H_c falls over time. The yield stress contribution to the torque or so called yield torque now obeys equation (25) and we assume a case in which $Od = \delta/4$, so that at final steady state, the final x_c (now denoted x_{cf}) satisfies $x_{cf} \to 1$, corresponding to a case in which plates move and stop but almost touch. In this final state, torque is then only half the Newtonian torque. Note also that cases with even larger Od/δ than the one we have selected (which move and stop without nearly touching) would have smaller δ/H_c in the final state, hence smaller x_{cf}, and correspondingly smaller final torque in line with predictions of equation (26).

Another interesting comparison is in the small δ/H_c limit in which the Newtonian x_c is then δ/H_c as we have said, but the x_c used in the yield torque calculation via equation (21) is roughly half that. However the Newtonian torque is linear in the small parameter x_c, whereas the yield torque computed via equation (25) (for the specified Od/δ) is quadratic in this small parameter. The Bingham yield stress contributions to the torque are therefore very small when δ/H_c is small, but can start to matter as H_c falls over time, such that δ/H_c grows, and hence x_c grows as well.

S5. Results: Squeeze Film Flow of Bingham Fluid between Parallel Plates

In this section, the results obtained for the squeeze flow of viscoplastic Bingham between parallel plates are discussed. Again these are shown for completeness and to facilitate comparison with the non-parallel case results in the main text.

S5.1. Yield Surface

The curves of yield surface y_{plug} with respect to x direction for the initial H value (i.e. $H = 1$) and different Od numbers, have been plotted in Figure S6. As Od number decreases, the yield surface y_{plug} increases. For the special case in which $Od = H/2$, which is the maximum Od number for which there is any motion at all for any specified H, we see that yield surface y_{plug} is zero everywhere since the whole flow field is a plug region. The viscoplastic Bingham fluid is now behaving as a rigid solid, and the yield stress is in balance with the imposed stress.

For large enough Od, there is no motion even in the initial state $H = 1$. However, as Od number decreases closer to zero, more and more of the film yields, and the

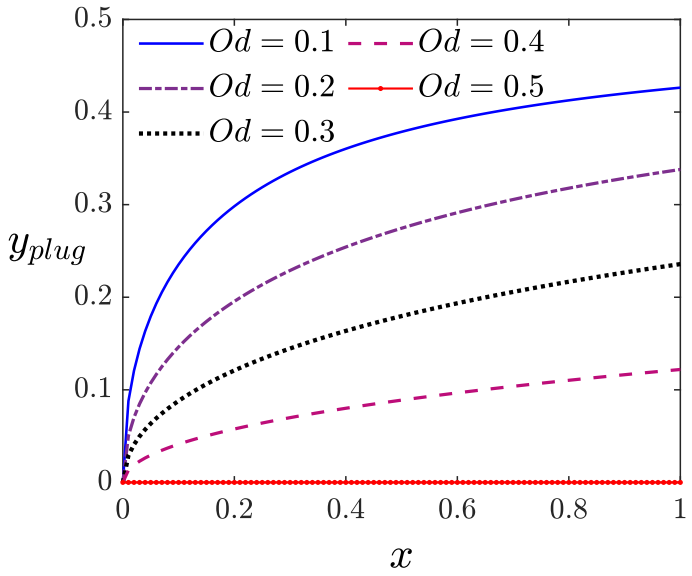

Figure S6: Yield surfaces y_{plug} corresponding to $H = 1$ as functions of x for different Oldroyd numbers. Corresponding v_{top} values for different Od numbers at this H are as follows: $Od = 0.5, v_{top} \equiv 0$; $Od = 0.4, v_{top} = 0.0072$; $Od = 0.3, v_{top} = 0.0265$; $Od = 0.2, v_{top} = 0.0545$; $Od = 0.1, v_{top} = 0.0889$.

viscoplastic Bingham fluid starts to become more like a Newtonian fluid which yields over the entire film. Hence, as seen here, the value of y_{plug} will increase when the Od number decreases. Note also that, even though just the case $H = 1$ has been considered here, decreasing H is qualitatively like increasing Od, i.e. it decreases y_{plug}.

S5.2. Film Thickness versus Time

From Figure S7, which shows how film thickness H varies with time t, it can be seen that (at any given time) squeeze film thickness decreases with decreasing Od number, this being the dimensionless measure of the yield stress. For maximum Od number, the plates never move at all since the plug region dominates the whole film thickness and the "fluid" behaves effectively as a rigid solid. Meanwhile, for small Od number, yield stress is small and the system is much closer to the Newtonian case. For instance, when $Od = 0.0001$, the behaviour of H versus t is almost same as the analytical formula (equation (S14)) in the Newtonian case. Moreover the final state of the finite Od number system corresponds to a final thickness $H_f = 2Od$.

Thus, the smaller the Od number, the smaller the final film thickness, the more

the film can be squeezed before the yield stress alone is sufficient to stop the squeezing by balancing the force which is applied to the plate. In the case $Od \ll 1$, it takes at least a time $t \sim Od^{-2}$ before H is even close to this final value $2Od$. This follows since the $Od \ll 1$ case starts off close to the Newtonian case (see e.g. the case $Od = 0.0001$ in Fig S7), whilst at very long times, the Newtonian system behaves as $H \sim 2\,t^{-1/2}$ (see equation (S14)).

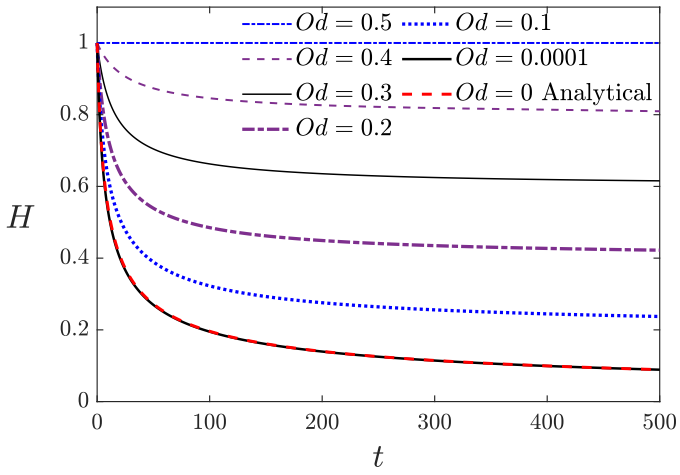

Figure S7: Film thickness vs time for different Oldroyd numbers in a viscoplastic Bingham system with parallel plates.

S5.3. Contributions to the Force

The total force comprises the viscous force and yield force (as per section S3.3). The relative contributions that these make depends on the Oldroyd number Od. Figure S8 shows the force contributions as time proceeds. For instance, for $Od = 0.2$, the yield force starts to dominate the viscous force even at early times. Meanwhile for smaller Oldroyd number (e.g. $Od = 0.02$), the viscous force accounts for almost all the force early on. Then as time goes on, the yield force increases as the viscous force decays. For each different Od number, there is a certain time at which the yield and viscous force curves cross over and this time is expected to scale proportionally to Od^{-2}.

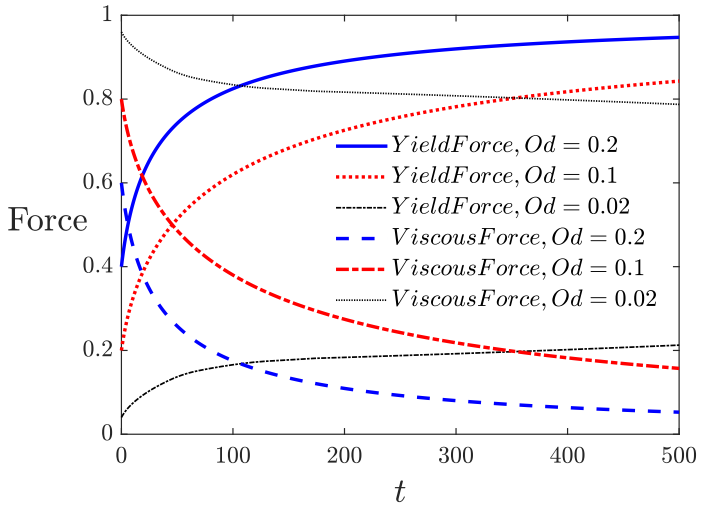

Figure S8: Force contributions to the squeeze flow vs time for different Oldroyd numbers in the parallel geometry.

S6. Additional Results: Squeeze Film Flow of Bingham Fluid between non-Parallel Plates

In this section we report some additional results for a Bingham fluid squeezed between non-parallel plates to supplement those already given in section 3. Figure 3 and Figure 4 in the main text plot values of shapes of yield surfaces for various combinations of Od and δ. To compute these shapes it is necessary to know v_{top} and x_c. Relevant values are reported in Table S1 and Table S2.

Od	v_{top}	x_c
0.495	6×10^{-5}	0.1023
0.4	0.0064	0.1168
0.3	0.0248	0.1360
0.2	0.052	0.1573
0.1	0.0853	0.1793
0.02	0.1145	0.1961

Table S1: Values of v_{top} and x_c for the case $\delta = 0.2$ and various Od. These v_{top} and x_c values correspond to the initial instant at which $H_c = 1$, and are needed to compute yield surfaces.

δ	v_{top}	x_c
0.1	0.06774	0.0260
0.2	0.0248	0.1360
0.4	0.01995	0.2763
0.5	0.01654	0.3498
0.7	0.00851	0.5096
0.8	0.00447	0.6009
0.9	0.00115	0.7083
0.97	2×10^{-5}	0.8013

Table S2: Values of v_{top} and x_c for the case $Od = 0.3$ and various δ. These v_{top} and x_c values correspond to the initial instant at which $H_c = 1$, and are needed to compute yield surfaces.

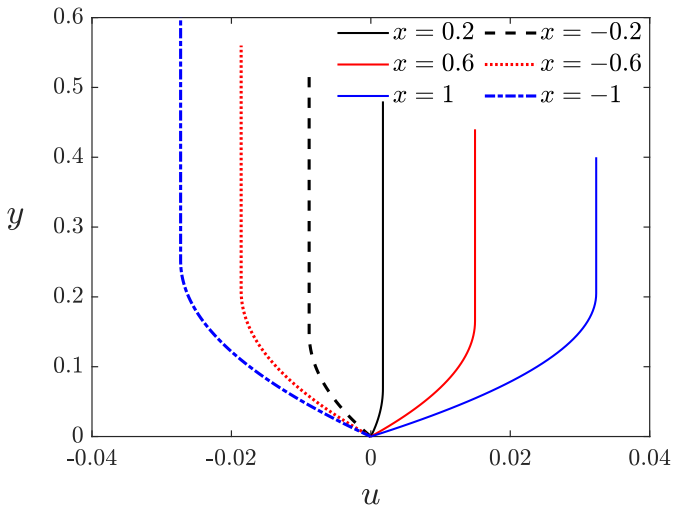

Figure S9: Velocity profiles for the case $Od = 0.3$ and $\delta = 0.2$ at different x locations.

Note that in addition to computing shapes of yield surfaces as Figure 3 and Figure 4 already do, it is also of interest to know the velocity fields both in the yielded and plug regions. Figure S9 shows the plots of velocity profiles u vs y at various x values. Provided $x > x_c$, these can be computed using equation (10) in the main text. If $x < x_c$, the profile is given by the negative of equation (10).

In Figure S9 we consider the case $\delta = 0.2$ and $Od = 0.3$, a parameter combination which occurs in both Figure 3 and Figure 4. Velocity profiles at the initial instant of time are plotted at $x = 0.2$, $x = 0.6$ and $x = 1.0$, and also at $x = -0.2$, $x = -0.6$ and

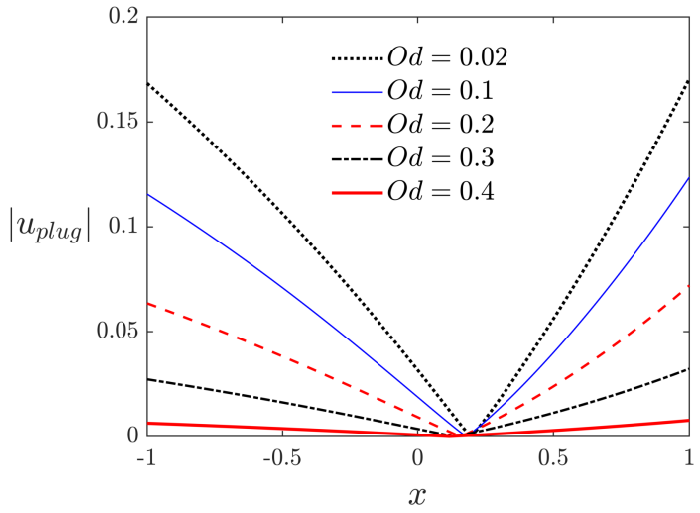

Figure S10: Profiles of $|u_{plug}|$ vs x for $\delta = 0.2$ and various Od. Data are determined at the initial instant (such that $H_c = 1$).

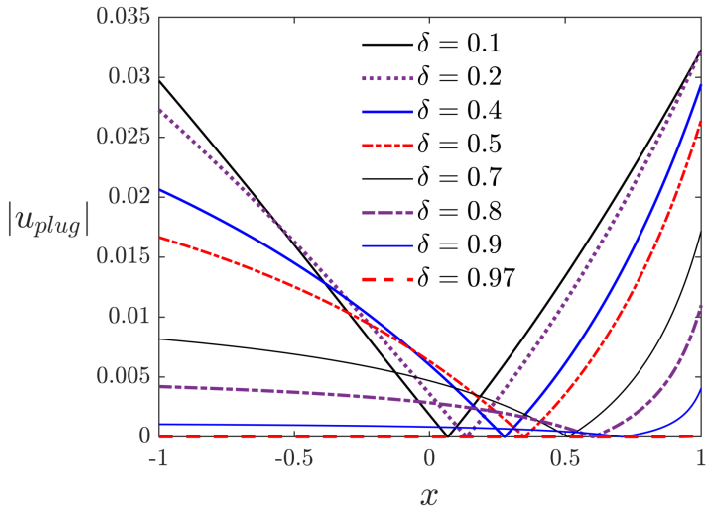

Figure S11: Profiles of $|u_{plug}|$ vs x for $Od = 0.3$ and various δ. Data are determined at the initial instant (such that $H_c = 1$).

$x = -1.0$. According to Table S1 and Table S2 the value of x_c is $x_c \approx 0.1360$. What we see then is that as x moves away from x_c in either direction, velocities increase in

magnitude in general and also a higher proportion of the flow profile is in the yielded region and less of it is in the plug region.

Another effect evident in Figure S9 is that, at any given value of $|x|$, there is more flux to the left than to the right (owing to x_c being positive). However this does not always manifest in a higher u_{plug} value on the left as Figure S10 and Figure S11 show. The larger flux to the left is also delivered over a larger vertical distance, and this impacts on the velocity.

References

[1] O. Reynolds, IV. On the theory of lubrication and its application to Mr. Beauchamp Tower's experiments, including an experimental determination of the viscosity of olive oil, Philosophical Transactions of the Royal Society of London 177 (1886) 157–234.

[2] D. F. Moore, A review of squeeze films, Wear 8 (4) (1965) 245–263.

[3] O. H. Campanella, M. Peleg, Squeezing flow viscometry for nonelastic semiliquid foods: Theory and applications, Critical Reviews in Food Science and Nutrition 42 (3) (2002) 241–264.

[4] G. Covey, B. Stanmore, Use of the parallel-plate plastometer for the characterisation of viscous fluids with a yield stress, Journal of non-Newtonian Fluid Mechanics 8 (3–4) (1981) 249–260.

[5] L. Muravleva, Squeeze plane flow of viscoplastic Bingham material, Journal of non-Newtonian Fluid Mechanics 220 (2015) 148–161.

[6] S. Wilson, Squeezing flow of a Bingham material, Journal of non-Newtonian Fluid Mechanics 47 (1993) 211–219.

Eur. Phys. J. E manuscript No.
(will be inserted by the editor)

Asymptotic Behaviour Approaching Final State of Viscoplastic Bingham Fluid Squeezed between Parallel Plates

Elaheh Esmaeili [a,1], **Paul Grassia** [b,1]

[1] *Department of Chemical and Process Engineering, University of Strathclyde, James Weir Building, 75 Montrose Street, Glasgow, G1 1XJ, UK*

Received: date / Accepted: date

Abstract There are flows of viscoplastic Bingham fluids in which motion decays to zero in finite time typically after a load is removed: a final state is thereby reached after finite time. Analogous flows of Newtonian fluids need however an infinite time for motion to decay to zero. In this work, a flow of a Bingham fluid squeezed between two parallel plates is considered with the plates subject to a constant load. This admits a final state without any motion despite the load remaining present. Asymptotic analysis close to that final state is considered, which reveals that in the squeeze film configuration, a Bingham fluid requires an infinite (rather than a finite time) to stop moving. That said, the decay of the motion of the Bingham fluid is still shown to be asymptotically much faster than that of the equivalent Newtonian fluid.

1 Introduction

Viscoplastic fluids (i.e. fluids that exhibit a yield stress including as examples gels, muds, pastes, emulsions and foams) form one of the classes of fluids of interest in the field of soft matter/non-Newtonian fluid mechanics [10]. Even more generally, viscoelastoplastic fluids may exhibit yield stress behaviour also [4]. Nonetheless the archetype of yield stress fluids remains the viscoplastic Bingham fluid which has been first modelled by [5]. There is a large volume of published studies exploring the rheological behaviour of yield stress fluids in general and Bingham fluids in particular [6, 9, 10, 15, 25–27]. It was already identified by [5] that a viscoplastic material will only start to flow after an imposed stress exceeds a yield stress. A corollary of this however is that, when the material is flowing but the stress is decaying over time, the flow will necessarily stop once stress everywhere falls below the yield stress. Via techniques of [16], a remarkable characteristic of Bingham fluids is therefore that, in finite time, they can stop dead (and their velocity can hence go to zero) due to the aforementioned yield stress effects [7, 17]. This typically happens when the cause of the flow (the driving force) is removed, so that the flow slows and eventually ceases. Meanwhile, for Newtonian fluids in analogous flows [30], the velocity fields go to zero only in the limit of infinite time. In view of this difference, a number of quantitative and qualitative analyses have been performed to establish the finite time decay of viscoplastic Bingham fluids in various geometries and under various conditions [1, 19, 29, 38].

Returning to consider fluids in general (not just viscoplastic ones), there are of course many different geometries in which rheology can be studied [3], e.g. steady shear flows, oscillatory shear flows, extensional flows, flows through channel expansions and contractions. One particularly simple geometry to set up however is a squeeze film flow, originally studied by [32] in the context of lubrication theory [31], but also useful for studying interactions between a fluid and the solid that bounds it [33, 34]. Squeeze film flows have moreover been investigated using various types of fluids [12, 24], Newtonian or non-Newtonian. In a squeeze film situation, fluid inertia tends to be insignificant [31], so if a driving force (e.g. a load on the squeeze film) were to be removed, the flow would in principle stop immediately (regardless of the fluid's rheology). Hence a driving force must be applied to continue to have any flow. That said, absence of flow does not necessarily imply absence of a driving force, if the fluid in question happens to be viscoplastic.

It is possible also to distinguish between a squeeze film flow with a constant squeezing rate (see e.g. [28]) or with a constant applied squeezing force (also known as a constant load case, see e.g. [23]). In the latter case, flow tends to slow

[a] e-mail: elaheh.esmaeili@strath.ac.uk
[b] e-mail: paul.grassia@strath.ac.uk (corresponding author)

down over time even for a Newtonian fluid [32]. This happens because, as the gap becomes narrow, pressures can develop within it that are sufficient to match the applied force despite having a lower shear stress and hence a lower flow velocity along the gap also.

In the case of squeeze film flows of yield stress fluids, many of the results in literature (see e.g. [20, 28, 36]) are for constant rate rather than constant load. A question of interest in studies like those is therefore how the load must vary as the constant rate squeezing proceeds. To determine this, it is necessary to establish, given the kinematics associated with the constant rate squeezing, how the stress field varies both across and along the gap. The stresses then determine lubrication pressures and lubrication forces that ultimately match the varying load. The stresses are however such that fluid in certain regions of the gap (typically close to the plates) is in a yielded plastic region, whereas fluid elsewhere in the gap (typically midway across and midway along the gap) is more plug-like [28]. A yield surface between these regions must be found as part of the solution of the problem. Sometimes the terms "fully plastic region", "pseudo-plug region" and "fake yield surface" are used (see [2, 39] for full details), reflecting the fact that even the nominally plug-like region also yields to a certain extent. However distinctions like those are not central to the arguments that follow.

One issue with constant rate studies though is that it is not possible to interrogate long time behaviour. For constant rate, by definition, we always know exactly what the plate separation is at any instant in time, and we know that there is always a finite time at which the plates come into contact. Hence we cannot ask questions about how yield stresses in particular might cause flow to come to a stop, nor about how the squeeze film flow behaves if and when it is close to stopping. To address questions like those, a constant load (i.e. constant applied squeezing force) must be considered. In fact the solution procedure for determining the squeeze film flows of yield stress fluids at constant rate [28] can be readily adapted to the constant load case also, merely with an extra step of identifying the instantaneous squeezing rate for any instantaneous gap thickness. Despite the similarity in procedure, what is however different as we explain next, is the final state of the system, i.e. whether the plates touch at the end of the process or not.

Squeeze film flow of a yield stress fluid between parallel plates and subject to a constant applied squeezing force has been studied by [11]. As already alluded to, the shear stress decays as the gap between the plates decreases: in more and more of the gap, the shear stress decays below the yield stress. The study of [11] accordingly identified that for a viscoplastic Bingham fluid, the flow can cease at a finite final gap thickness even though the load is not removed. In that final state, the gap between the plates remains finite, and yield stresses alone cause sufficient pressure to develop so as to balance applied force. This feature which makes yield stress fluids attractive for lubrication applications, potentially also mitigating against complications associated with lubricating gaps with rough surfaces [22].

The work of [11] was recently extended by [14]. This showed that the final steady state of a viscoplastic Bingham fluid squeezed between non-parallel plates is qualitatively similar to the parallel plate case, provided the tilt angle remains less than a certain threshold value, albeit the threshold value itself is sensitive to yield stress. This then echoes a more general finding of [18], namely that static (i.e. non-flowing) states of yield stress fluids can be rather common in many different geometries, and are not always trivial to analyse.

Returning specifically to the squeeze film case, although the final steady states under constant load are known, and although [11, 14] also considered unsteady state evolution numerically, what these works did not consider are the details of how the unsteady state solution approaches the final state. Specifically it was not established whether the unsteady state reaches the final state in finite time and then stops dead, or whether this final state is only reached in the limit of infinite time. This therefore is the question we address here. What we will find is that the viscoplastic Bingham fluids do not actually stop dead in a squeeze film, but instead they take an infinite time to reach the final state. However, the way in which they approach the final state is faster than for a Newtonian fluid. In yield stress fluids, what we will demonstrate is that the difference between instantaneous gap thickness at any time t and final gap thickness decays proportionally to t^{-1}, whereas for a Newtonian fluid this decays instead proportionally to $t^{-1/2}$.

Thus what we discover in the present work therefore is that, for a yield stress fluid, there is more than one way to cut off motion quickly. One way, as already alluded to, is cutting off motion in finite time (e.g. by removing a driving force). The other way is still to require infinite time for motion to stop, but even so, for motion to decay faster than for the analogous Newtonian fluid. This paper explores the latter type of behaviour specifically for a viscoplastic Bingham fluid squeezed between parallel plates. Similar results turn out also to apply for a non-parallel plate case, but the mathematical analysis is rather more complicated. We focus just on the simpler, i.e. parallel plate case here, but details of the non-parallel case can be found in a thesis prepared by one of us [13].

The rest of this work is laid out as follows. Section 2 presents the methodology that we deploy to analyse the approach of a squeeze film flow to steady state. After that section 3 presents squeeze film results for viscoplastic Bingham fluids with different yield stresses, assuming constant load and focussing particularly on late times. Finally section 4 offers conclusions.

2 Methodology

This methodology section is laid out as follows. Section 2.1 describes the governing equations for a viscoplastic Bingham fluid in squeeze film geometry. In section 2.2 we identify a key dimensionless group that governs system behaviour. Variables are cast in dimensionless form in section 2.3. After that section 2.4 considers a yield surface within the squeeze film. Section 2.5 then identifies the final state of the squeeze flow. Following that in section 2.6, gap thicknesses close to a final state are discussed. Up until section 2.6, the methodology merely reviews existing techniques for determining squeeze film flows of yield stress fluids such as e.g. [14] also reviewed. After this section however, novel aspects of the methodology are introduced. Section 2.7 for instance determines lubrication pressure and lubrication force close to a final state. This then enables us to determine, close to that final state, the speed of approach of the plates enclosing a squeeze film (section 2.8) and subsequently the evolution of the gap between them (section 2.9).

2.1 Governing equations

In the system studied here depicted in Figure 1, we have parallel plates of length $2\hat{L}$, with a viscoplastic Bingham fluid in between them. A fixed force $\hat{F}_{app}$ (or more specifically, since we consider a two-dimensional system, force per unit length in the direction normal to the plane of Figure 1) is applied on the upper plate. This moves downward with a time varying velocity, $\hat{v}_{top}$. The initial thickness of the gap between the plates is $\hat{H}_0$. The instantaneous thickness is $\hat{H}$.

In what follows, standard lubrication theory assumptions [32] (i.e. planar two-dimensional geometry, gap thickness much smaller than length along the gap, incompressible fluid, negligible gravity, negligible inertia, no slip boundaries) are considered to apply. Governing lubrication equations for a viscoplastic Bingham fluid now become [40]

$$-\frac{\partial \hat{p}}{\partial \hat{x}}+\frac{\partial \hat{\tau}_{xy}}{\partial \hat{y}}=0 \tag{1}$$

$$\frac{\partial \hat{p}}{\partial \hat{y}}=0 \tag{2}$$

$$\frac{\partial \hat{u}}{\partial \hat{x}}+\frac{\partial \hat{v}}{\partial \hat{y}}=0. \tag{3}$$

Here $\hat{u}$ and $\hat{v}$ are velocities in $\hat{x}$ and $\hat{y}$ directions, $\hat{p}$ is pressure and $\hat{\tau}_{xy}$ denotes shear stress of the viscoplastic Bingham fluid. The Bingham model (see e.g. [5, 6]) is characterized by two parameters namely a viscosity and yield stress. If the magnitude of shear stress is less than the yield stress, the Bingham material behaves as a solid. On the other hand, when the shear stress exceeds the yield stress, the material behaves instead akin to a viscous fluid [5, 8, 11, 35, 37]. Specifically for a viscoplastic Bingham fluid, shear stress obeys the constitutive equation

$$\begin{cases} \hat{\tau}_{xy}=\pm\tau_y+\mu_p\hat{\dot{\gamma}} & \text{for} \quad |\hat{\tau}_{xy}|>\tau_y \\ \hat{\dot{\gamma}}=0 & \text{for} \quad |\hat{\tau}_{xy}|\leqslant\tau_y. \end{cases} \tag{4}$$

Here τ_y is yield stress, $\hat{\dot{\gamma}}=\partial\hat{u}/\partial\hat{y}$ is shear rate and μ_p is Bingham fluid viscosity after yielding occurs. Here the $\pm\tau_y$ term is positive if $\hat{\dot{\gamma}}>0$ and it is negative if $\hat{\dot{\gamma}}<0$. Many of the variables are denoted here with a hat symbol. This is to indicate that they are dimensional variables which also have dimensionless analogues (to be used later on, with the hat symbol dropped).

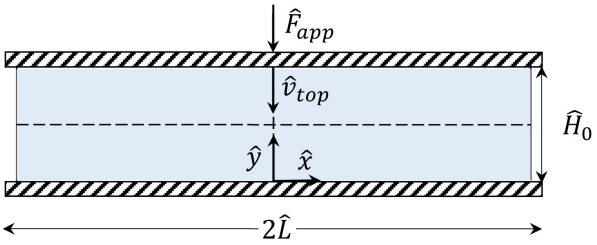

Fig. 1 Geometry of squeeze film flow of viscoplastic Bingham fluid between parallel plates.

2.2 Oldroyd number

The lubrication force that develops in the gap between the plates must match the applied force. In order of magnitude terms, we estimate the lubrication pressure as being order $\hat{F}_{app}/\hat{L}$ and the gradient of the pressure as being order $\hat{F}_{app}/\hat{L}^2$. Momentum balance requires that the pressure gradient should match the divergence of the shear stress (see equation (1)). If the shear stress has a typical value $\hat{\tau}$, then in order of magnitude terms its divergence (at least in the initial configuration with gap thickness $\hat{H}_0$) will be order $\hat{\tau}/\hat{H}_0$. It follows then that $\hat{\tau}$ will be an order $\hat{H}_0\hat{F}_{app}/\hat{L}^2$ quantity.

Suppose now that the Bingham fluid has a yield stress τ_y. As in [14], we define an Oldroyd number Od as

$$Od\equiv\tau_y\hat{L}^2/(\hat{H}_0\hat{F}_{app}). \tag{5}$$

Effectively this is the ratio between the yield stress τ_y and the typical imposed shear stress $\hat{H}_0\hat{F}_{app}/\hat{L}^2$, at least assuming a shear stress corresponding to the initial gap thickness. If $Od\ll 1$, then the yield stress is much smaller than the typical shear stress needed to balance applied force. The system must yield, leading then to viscous stresses over and above the yield stress. However as the gap narrows, the shear stress $\hat{\tau}$ required to balance the applied force falls likewise, becoming only order $\hat{H}\hat{F}_{app}/\hat{L}^2$ instead of $\hat{H}_0\hat{F}_{app}/\hat{L}^2$. Eventually $\hat{\tau}$ falls to a value commensurate with the yield stress τ_y.

2.3 Non-dimensionalization of equations

Equations are now expressed in dimensionless form. Horizontal lengths are scaled by $\hat{L}$, whereas vertical lengths are scaled by $\hat{H}_0$. Meanwhile horizontal velocities are scaled by $\tilde{u} \equiv (\hat{F}_{app}/\mu_p)(\hat{H}_0^2/\hat{L}^2)$, and vertical velocities are scaled by $\tilde{v} \equiv \hat{H}_0\tilde{u}/\hat{L}$. Times are scaled by $\hat{H}_0/\tilde{v} \equiv \hat{L}/\tilde{u}$. Pressures are scaled by $\hat{F}_{app}/\hat{L}$, which has units of pressure since $\hat{F}_{app}$ is taken as applied force per unit distance transverse to the two-dimensional calculation domain. We make shear rate $\hat{\dot{\gamma}} \equiv \partial\hat{u}/\partial\hat{y}$ dimensionless on the scale $\tilde{u}/\hat{H}_0$ and shear stress $\hat{\tau}_{xy}$ dimensionless on the scale $\mu_p\tilde{u}/\hat{H}_0$.

All variables from here onward are dimensionless. The dimensionless analogues of equations (1)–(3) have the same form as the originals merely with the hat symbols dropped. Meanwhile the dimensionless analogue of the constitutive equation (4) is

$$\begin{cases} \tau_{xy} = \pm Od + \dot{\gamma} & \text{for} \quad |\tau_{xy}| > Od \\ \dot{\gamma} = 0 & \text{for} \quad |\tau_{xy}| \leqslant Od. \end{cases} \tag{6}$$

Here the $\pm Od$ term is positive if $\dot{\gamma} > 0$ and is negative if $\dot{\gamma} < 0$.

2.4 Determining the yield surface

We now work towards identifying the location of the yield surface, which recall separates plastic and plug regions. The analysis follows the approach of [28]. Integrating the dimensionless analogue of equation (1), and applying the boundary condition in which at $y = H(t)/2$, we have $\tau_{xy} = 0$, shear stress is obtained. At least in regions in which the fluid is yielding, this can then be related to shear rate

$$\tau_{xy} = \frac{\partial p}{\partial x}\left(y - \frac{H(t)}{2}\right) = \pm Od + \dot{\gamma} = \pm Od + \frac{\partial u}{\partial y}. \tag{7}$$

Taking the integral of equation (7) using a no slip boundary condition (i.e. $u = 0$ at $y = 0$), a velocity profile across the y direction can be deduced

$$u = \frac{\partial p}{\partial x}\frac{1}{2}y(y - H(t)) - Od\, y. \tag{8}$$

This velocity profile applies throughout the yielded plastic region. In the plug region, we have instead $u = u_{plug}$, where u_{plug} is a value to be determined. The boundary between the plastic region and the plug region, defines the yield surface $y = y_{plug}$. We use the fact that at the yield surface, the shear rate is zero ($\partial u/\partial y = 0$) or equivalently $|\tau_{xy}| = Od$. Therefore putting this condition into equation (7), the expression for the pressure gradient in the x direction can be determined

$$\mathrm{d}p/\mathrm{d}x = -Od/(-y_{plug}(x) + H/2), \tag{9}$$

which applies for $x > 0$, but has a sign change when $x < 0$. Now, via substitution of equation (9) into (8), the velocity profile for both yielded plastic and plug regions is obtained

$$u = \begin{cases} -\dfrac{Od}{2(\frac{H(t)}{2} - y_{plug})}y^2 + \dfrac{Od}{(\frac{H(t)}{2} - y_{plug})}y_{plug}y \\ \qquad\qquad \text{for} \quad y \leqslant y_{plug} \\ \dfrac{Od}{2(\frac{H(t)}{2} - y_{plug})}y_{plug}^2 \equiv u_{plug} \\ \qquad\qquad \text{for} \quad y_{plug} < y < \dfrac{H(t)}{2}, \end{cases} \tag{10}$$

which again applies for $x > 0$, but switches sign if $x < 0$. The velocity field in the domain $H(t)/2 < y < H(t)$ is symmetric with that in the domain $0 < y < H(t)/2$ which is given here. Note that, amongst other things, equation (10) specifies u_{plug}, provided y_{plug} is known.

Using the definition for the flow rate $Q \equiv 2\int_0^{H(t)/2} u\,\mathrm{d}y$, along with equation (3), we can deduce $\partial Q/\partial x = v_{top}$, where v_{top} is the velocity at which the top plate moves relative to the bottom plate. The sign convention adopted here is that downward motion of the top plate corresponds to positive v_{top}. It now follows

$$Q \equiv 2\left(\int_0^{y_{plug}} u\,\mathrm{d}y + \int_{y_{plug}}^{\frac{H(t)}{2}} u_{plug}\,\mathrm{d}y\right) = v_{top}x. \tag{11}$$

Inserting equation (10) into (11), taking the integral and after some algebra, the expression for the yield surface y_{plug} becomes [28]

$$y_{plug}^3 - \frac{3}{2}H(t)y_{plug}^2 - 3\frac{v_{top}|x|}{Od}y_{plug} + \frac{3}{2}\frac{v_{top}|x|H(t)}{Od} = 0. \tag{12}$$

One issue with solving the above equation for y_{plug} is that v_{top} is a priori unknown. In order to determine the plate velocity v_{top}, in general we need to proceed iteratively as [14] explained. For any assumed value of v_{top} and any position x along the plates and any given Oldroyd number Od, it is possible to identify the location of a yield surface $y_{plug}(x)$. In any case once the yield surface is identified for an assumed v_{top}, it is possible to deduce the lubrication pressure field developed in the gap (obtained via equation (9)), and hence the lubrication force: further details of pressures and lubrication forces that we compute are given later on, see section 2.7. The value of v_{top} then generally needs to be adjusted iteratively until the lubrication force balances the applied force. In fact in the dimensionless system considered here, forces have been scaled in such a fashion that the dimensionless applied force is effectively unity.

Another complication however is that equation (12), determining y_{plug} for any given v_{top}, x and Od, is a cubic equation that is rather awkward to solve [14]. Here however we

are specifically interested in systems approaching close to their final state. In this limit, small v_{top} is expected. For small v_{top}, the second and fourth terms on the left hand side of equation (12) dominate, with the first and third terms becoming smaller (which is easily verified a posteriori). It then follows [14] that

$$y_{plug} \approx \sqrt{|x| v_{top}/Od}. \tag{13}$$

For small v_{top} what this equation means is that $y_{plug}(x)$ is small, i.e. the yield surface at $y_{plug}(x)$ and its symmetric partner at $H - y_{plug}(x)$ are both close to the plates. Most of the gap is then in the plug region, and most of the fluid flux out of the gap is carried by the plug, with very little flux contribution from the plastic region. It follows that the flux now satisfies $Q \approx u_{plug} H$ with $u_{plug} \approx Od\, y_{plug}^2/H$ in equation (10). Using equation (11), we can thereby deduce equation (13). This approximate formula for $y_{plug}(x)$ was originally obtained by [14] for a general v_{top} but just in the neighbourhood of $x = 0$. However when v_{top} is small, as happens when the final state is approached, this same formula for y_{plug} applies now for a general x.

2.5 Final state

In the present formulation similar to [11] but unlike [28], a constant squeezing force is applied to determine the squeezing rate. Squeezing must however eventually stop. For any given Oldroyd number, a final gap thickness (denoted H_f) can be obtained. Indeed, for large enough values of Od, we will see that even the initial state, which is non-dimensionalized here such that $H = 1$, leads to no motion.

When motion comes to a stop that is equivalent to having $y_{plug} \to 0$ (or equivalently $y_{plug} \ll H/2$) for all x values. Thus, the plug region now fills essentially the entire gap. Putting $y_{plug} = 0$ and $H = H_f$ in equation (9)

$$|\mathrm{d}p/\mathrm{d}x| = 2Od/H_f, \tag{14}$$

with $\mathrm{d}p/\mathrm{d}x$ being positive if $x < 0$ and negative if $x > 0$. In addition, $p = 0$ at $x = \pm 1$.

Force is obtained by integrating the pressure profile

$$F = \int_{-1}^{1} p(x)\,\mathrm{d}x = \int_{-1}^{0} \frac{2Od}{H_f}(1+x)\,\mathrm{d}x + \int_{0}^{1} \frac{2Od}{H_f}(1-x)\,\mathrm{d}x = \frac{2Od}{H_f}. \tag{15}$$

Inserting $F = 1$ in the above equation, we find $H_f = 2Od$. Thus at any given Od the final steady state thickness is just twice the Od number. For small Od, it is possible to squeeze plates really quite close together before they stop moving. As Od increases though, the plates stop moving at a rather larger H_f. Moreover a maximum Oldroyd number equal to $\frac{1}{2}$ is found in order for any squeezing to take place whatsoever: as $Od \to \frac{1}{2}$, there can be no plate motion even at the initial plate separation $H = 1$.

Systems with $Od \geq 1/2$ do not yield at all, but systems with $Od < 1/2$ evolve from $H = 1$ initially to $H_f = 2Od$ at steady state. Newtonian systems, which have Od zero by definition, permit the plates to approach arbitrarily close together, i.e. $H_f \to 0$.

Having determined the final state, what we describe next is how to perturb the system for H close to H_f.

2.6 Gap thicknesses close to the final state

Thus far we have identified the final state of the squeeze film flow, but have not determined how rapidly flow comes to a stop. To determine that, what needs to be established is how v_{top} varies as a function of H. We then know that

$$\mathrm{d}H/\mathrm{d}t = -v_{top}, \tag{16}$$

the negative sign here arising from the sign convention that plates approaching one another are considered to have positive v_{top}. After finding v_{top} for any given H, we can solve for how H evolves with time t. Clearly v_{top} is identically zero in the final state when $H = H_f$, but the question here is how v_{top} behaves for $H > H_f$, and in particular for H just slightly greater than H_f. Based on arguments presented in [18, 19], the flow of yield stress fluids tends to slow to a stop more quickly than Newtonian fluids do. This then could also impact on the functional form of v_{top} versus H.

For parallel plates with a Newtonian system (originally tackled by [32] but summarised in dimensionless form in [14]), final gap thickness H_f is zero, and velocity $\mathrm{d}H/\mathrm{d}t$ turns out to be $-H^3/8$. The Newtonian solution for H is then

$$H = (1 + t/4)^{-1/2} \tag{17}$$

meaning that at long times

$$H \sim 2t^{-1/2}. \tag{18}$$

For parallel plates with a viscoplastic yield stress fluid, final gap thickness H_f is non-zero as we have seen. It is convenient then to write

$$H(t) \equiv H_f + \Delta H(t), \tag{19}$$

where $\Delta H(t)$ (the difference in gap thickness from the final state) must eventually decay towards zero. For a Bingham fluid, we will show shortly as one of the main novel contributions of this work (see section 2.8), that in the asymptotic limit when ΔH is small, the value of $\mathrm{d}\Delta H/\mathrm{d}t$ is proportional to $-\Delta H^2$. This still takes an infinite time for ΔH to reach zero, and hence an infinite time for H to reach the

final state H_f (see section 2.9). However because it involves a quadratic ΔH^2 not a cubic $H^3/8$, the approach is faster than the purely viscous Newtonian case. In addition, in the viscoplastic Bingham fluid case, the value of $\mathrm{d}\Delta H/\mathrm{d}t$ also turns out (again see section 2.8) to depend on Oldroyd number Od, and part of our aim here is to elucidate how Od impacts upon the time to approach the steady state.

2.7 Determining the pressure field and lubrication force

Having found a formula for y_{plug} (equation (12) or more specifically equation (13) close to the final state), we can now determine the pressure field in the gap. Pressure for $x > 0$ obeys equation (9) and for $x < 0$, it is similar, merely with opposite sign. Physically this is simply a momentum balance, with pressure gradient matched to the divergence of the shear stress. The divergence of the shear stress is then computed on the basis that shear stress vanishes on the centreline of the gap, but equals the yield stress on the yield surface [28].

Close to the final state, in the asymptotic limit of small ΔH and small v_{top}, we Taylor expand the pressure gradient, for $x > 0$

$$\frac{\mathrm{d}p}{\mathrm{d}x} \approx -\frac{2Od}{H_f}\left(1 - \frac{\Delta H}{H_f} + \frac{2y_{plug}(x)}{H_f}\right) \tag{20}$$

with an analogous equation for $x < 0$, solely with opposite sign. This equation implies that having finite ΔH makes the magnitude of the pressure gradient slightly smaller (meaning the lubrication pressure is less able to resist the imposed pressure). Meanwhile having finite y_{plug} makes the magnitude of the pressure gradient slightly bigger (meaning the lubrication pressure is more able to resist the imposed pressure).

Integrating equation (20), after substituting from equation (13) and imposing conditions that $p = 0$ at $x = \pm 1$, we find

$$p(x) \approx \frac{2Od}{H_f}\left((1-|x|) - \frac{\Delta H}{H_f}(1-|x|) + \frac{4\sqrt{v_{top}/Od}}{3H_f}(1-|x|\sqrt{|x|})\right). \tag{21}$$

In the above equation, the first term is dominant and gives the final pressure field, making a positive contribution to the pressure. The second term has a negative contribution to the pressure due to the fact that when the gap is still thick, the pressure may be rather weak, but it can become stronger and support the force applied on the system when the gap thickness is smaller. The third term has a positive contribution to the pressure, since the system is able to yield in order to increase the pressure to sustain the applied force. We integrate this pressure field $p(x)$ over the whole domain $-1 \le x \le 1$ to find the lubrication force F which is comprised of three terms as follows

$$F \approx \frac{2Od}{H_f} - \frac{2Od}{H_f^2}\Delta H(t) + \frac{16Od}{5H_f^2}\sqrt{\frac{v_{top}}{Od}}. \tag{22}$$

2.8 Determining speed of approach of the plates

In equation (22) the lubrication force F, must match the applied force, which is normalised to unity in the dimensionless system being considered here. However the first term on the right hand side, which is the force in the final state, is also necessarily unity (as equation (15) already found). In order to keep $F = 1$, the second and third terms on the right hand side are required to be equal. Thus

$$v_{top} \approx \frac{25}{64} Od\, \Delta H(t)^2. \tag{23}$$

We recall also (see equation (16)) that $\mathrm{d}H(t)/\mathrm{d}t = -v_{top}$ and hence

$$\frac{\mathrm{d}\Delta H(t)}{\mathrm{d}t} \approx -\frac{25}{64} Od\, \Delta H(t)^2. \tag{24}$$

As already stated earlier, the value of $\mathrm{d}\Delta H/\mathrm{d}t$ is indeed proportional to $-\Delta H(t)^2$.

The above equation is well known in chemistry and chemical engineering albeit in a different context. It is in fact entirely analogous to the equation that arises for the evolution of reactant concentration for a second order reaction [21] provided reactants are supplied in stoichiometric amounts (neither of them in excess). This then leads to a relatively slow decay because both reactants become exhausted simultaneously, thereby slowing the reaction rate significantly. This is then a rather slower decay than the late-time exponential decay which arises when one reactant is supplied in excess, meaning that just one of them becomes exhausted. On the other hand, the decay is still faster than for a third order reaction in stoichiometric amounts, which is the analogue of equations (17) and (18). We also observe that the Oldroyd number Od within equation (24) is analogous to a second order kinetic rate constant. Hence decreasing Od tends to slow down the decay.

2.9 Evolution of plate separation

The gap between the plates $H(t)$ can now be determined remembering here that $\Delta H(t) \equiv H(t) - H_f$ with H_f given by equation (15). The solution of equation (24) for ΔH versus t is obtained as

$$\Delta H \approx \frac{\Delta H_1}{(25/64)Od\,(t-t_1)\,\Delta H_1 + 1} \tag{25}$$

where ΔH_1 is any value at which ΔH is small, and then t_1 is the time at which ΔH reaches ΔH_1. Equation (25) cannot be extrapolated for t values much earlier than t_1, because ΔH would then be predicted to grow, whereas the derivation leading up to equation (24) was an asymptotic analysis that assumed small ΔH. On the other hand, for $t > t_1$, the equation should be reliable. Moreover in the limit when $t \gg t_1$ and $(25/64)Od\,(t-t_1)\,\Delta H_1 \gg 1$, we find a very simple formula

$$\Delta H \sim 64/(25Od\,t). \tag{26}$$

It follows then that the approach to the final state for the yield stress fluid requires an infinite time and, at any instant in time, the state of the system is sensitive only to the value of Od number (i.e. ratio between yield stress and imposed stress).

In addition to the analytical approximations described above, we can also compute $\Delta H(t) \equiv H(t) - H_f$ versus t numerically (details of the numerical procedure are already discussed in [14] so are not reproduced here). If we plot those data on a log-log graph, then based on equation (26) a slope -1 is expected for long times. Although this is still an algebraic decay (rather than an exponential one), even so it is faster than the decay of the Newtonian case, given by equation (17) and then reducing to equation (18), namely $H \sim 2t^{-1/2}$ in the long time limit. Plotting the Newtonian system on a log-log graph will give a slope of $-1/2$, indicating a more gradual decay than happens for a slope of -1.

3 Results and Discussion

In what follows, sections 3.1–3.2 deal with evolution of squeeze film gap thickness, and sections 3.3–3.4 deal with difference between gap thickness and final gap thickness.

3.1 Squeeze film gap thickness versus time

Figure 2 shows the profiles of gap thickness (computed numerically using the procedure of [14]) versus logarithmic time for a viscoplastic Bingham fluid with different Od values, and also for a Newtonian fluid with $Od = 0$. As seen, for small Oldroyd numbers, the curves will stay close to the Newtonian curve (i.e. $Od = 0$) up to a comparatively long time. Meanwhile the curves for larger Od numbers deviate from the Newtonian graph sooner. In addition to that, gap thickness for each Od number eventually approaches $H_f \equiv 2Od$ at long enough time. Note though that this value is approached sooner as Od increases.

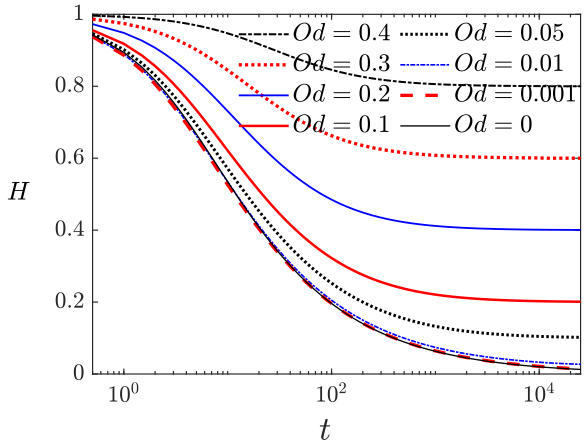

Fig. 2 Gap thickness H against logarithmic time t for different Od values.

3.2 Gap thickness versus rescaled time

The timescale that is of interest in this system is order $1/Od^2$, which can be deduced as follows. For small enough Od, systems should start off following Newtonian behaviour (equation (17) and eventually equation (18), $H \sim 2t^{-1/2}$). However that behaviour must cease once equation (18) predicts H values comparable with H_f (with $H_f \equiv 2Od$ itself given by equation (15)). This of course happens when $t \sim 1/Od^2$. We can however rescale time (from t to $Od^2\,t$) in an effort to obtain a universal behaviour for different Od values. We also rescale the gap thickness (plotting H/H_f instead of just H). Thus Figure 3 presents rescaled logarithmic gap thickness H/H_f against rescaled logarithmic time $Od^2\,t$ for various Od numbers.

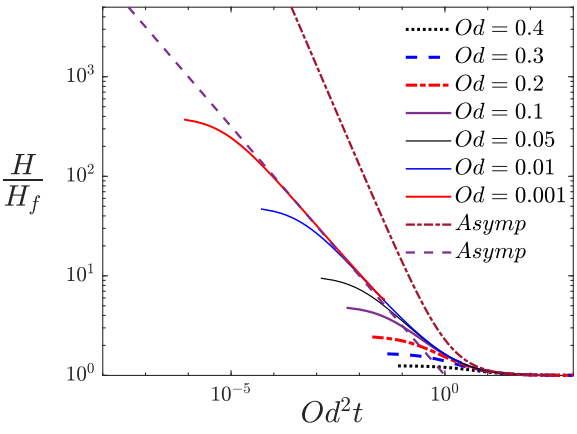

Fig. 3 Logarithmic ratio of gap thickness to final state gap thickness H/H_f in terms of rescaled logarithmic $Od^2\,t$ for different Od values. Long time asymptotic formulae given respectively by equations (27) (dash-dot curve) and (28) (dashed line) are also plotted.

As seen, each curve now starts off at a different location for each Oldroyd number, but at sufficiently large $Od^2 t$ they all collapse together onto a single master curve. In fact since the initial H is unity whereas $H_f \equiv 2Od$, it follows that the initial H/H_f is $(2Od)^{-1}$. Therefore, as Od decreases, the initial H/H_f is larger, whilst the master curve is likewise attained at a larger H/H_f value and hence at a smaller $Od^2 t$.

Using equations (15), (19) and (26) a possible asymptotic form for a master curve can be deduced

$$H/H_f \sim 1 + 32/(25Od^2 t), \tag{27}$$

which is plotted within Figure 3. Obviously though, this formula presents issues for the case $Od \ll 1$, because we then also need very long times t to prevent $Od^2 t$ from being vanishingly small. If times are not sufficiently long, then the $Od \ll 1$ case should follow instead the Newtonian equations (17)–(18), not equation (26). If a system with $Od \ll 1$ satisfies, at least temporarily, equation (18) instead of equation (26), we can deduce an asymptotic formula

$$H/H_f \sim (Od^2 t)^{-1/2}. \tag{28}$$

This is also plotted in Figure 3.

What is apparent is that equation (27) does not give a good fit to H/H_f over a wide domain of H/H_f values, whereas equation (28) evidently does, particularly when Od is small. The issue with equation (27) is that the analysis leading to it is based on an assumption that ΔH is rather smaller than H_f and hence $H/H_f \equiv 1 + \Delta H/H_f$ can never be much larger than unity if the formula is to be valid.

3.3 Difference in gap thickness versus time

Figure 4 presents both numerical and analytical ΔH (i.e. the difference in gap thickness from the final state) on a logarithmic scale in terms of logarithmic time for different Oldroyd numbers. Here the numerical ΔH is computed using the methodology of [14], whereas the analytical ΔH is obtained using equation (25). Values of ΔH_1 and t_1 to use within equation (25) were themselves read off from the numerical data: see values in Table 1. Equation (25) is however insensitive to which combination of ΔH_1 and t_1 is chosen, provided we select a combination with ΔH_1 rather smaller than H_f. This is certainly the case in Table 1 when $Od = 0.2$, $Od = 0.1$ or $Od = 0.05$. For $Od = 0.01$ or $Od = 0.001$ this is more difficult to achieve however, as it would require very long t_1 values, so we have opted in those cases for ΔH_1 values just slightly smaller than H_f.

Gap thickness for $Od = 0$ (i.e. Newtonian fluid) decreases with a slope of $-1/2$ in Figure 4, at least at long times. Meanwhile subtracting H_f from H to obtain ΔH moves the curves for the viscoplastic Bingham fluid below the Newtonian case.

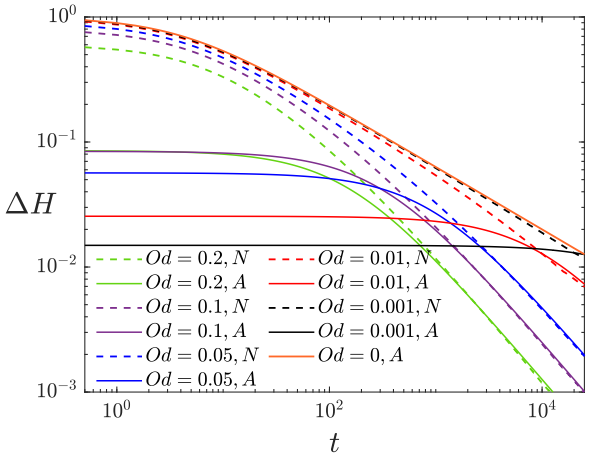

Fig. 4 Numerical (N) and Analytical (A) values of logarithmic ΔH against logarithmic t for different Od values.

Od	ΔH_1	$\Delta H_1/H_f$	t_1	$Od^2 t_1$
0.001	0.0013	0.65	40000	0.04
0.01	0.01277	0.6385	10000	1
0.05	0.01044	0.1044	4000	10
0.1	0.00913	0.04565	2500	25
0.2	0.00483	0.012075	2500	100

Table 1 Values of ΔH_1 and t_1 used for each Od.

In the Bingham fluid case, by plotting numerical and analytical ΔH values against time, we see that discrepancies arise at early times, but for times greater than t_1, the analytical predictions and numerical data tend to agree. As Od decreases however, we need to select longer and longer times before agreement is attained. Indeed for $Od = 0.001$, the numerical and analytical data are only just starting to agree at the very largest timescales we have considered.

For $Od = 0.2$, $Od = 0.1$, $Od = 0.05$, we see in Figure 4 good agreement between numerical and analytical formulae for ΔH less than about 2×10^{-2}, which matches with the notion that $\Delta H/H_f$ needs to be small for the analytical formulae to work well, remembering here that $H_f = 2Od$. Smaller Od values e.g. $Od = 0.01$ and $Od = 0.001$, in principle should require even smaller ΔH values before the analytical formula starts to be reliable. Judging the quality of the analytical formula for these smaller Od is however less straightforward for the following reason. By construction we fit the analytical formula to the numerical data at t_1 and ΔH_1, and so what we must verify is that the formula continues to fit well for $t \gg t_1$ and $\Delta H \ll \Delta H_1$, but that then needs data out to very long times. Nonetheless, as Table 1 makes apparent, when Od is small, meaning that H_f is also small, it is not easy to reach a ΔH_1 that is itself much smaller than H_f.

From Figure 4, ΔH for all values of Od number decays towards zero as time proceeds, and moreover the curves at long times appear to acquire a slope of -1 as expected based on equation (26). For bigger Od numbers, this regime is at-

tained sooner. For small Od on the other hand, the curves follow the Newtonian case (slope $-1/2$) for quite some time, before deviating towards a slope -1.

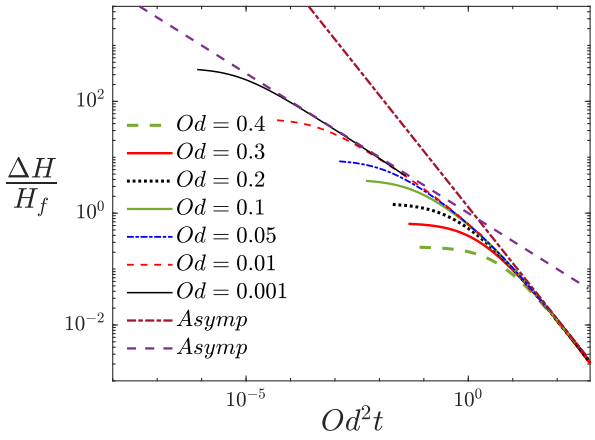

Fig. 5 Numerical values of rescaled logarithmic $\Delta H/H_f$ in terms of rescaled logarithmic Od^2t for different Od values. Long time asymptotic formulae given respectively by equations (28) (dashed line) and (29) (dash-dot line) are also plotted.

3.4 Difference in gap thickness versus rescaled time

Figure 5 shows the rescaled logarithmic gap thickness namely $\Delta H/H_f$ (computed numerically) against rescaled logarithmic time Od^2t for different Oldroyd numbers. Recall also the basis for this rescaling: the characteristic timescale to approach close to the final state is expected to be on the order of $1/Od^2$.

In Figure 5, all of the plots do appear to collapse together at sufficiently long times. At very short times of course there are discrepancies: the value of ΔH can never exceed $1-2Od$ and so $\Delta H/H_f$ can never exceed $(2Od)^{-1}-1$. Focussing on asymptotics at much longer times though, the analogue of equation (27) is

$$\Delta H/H_f \sim 32/(25Od^2t). \tag{29}$$

This is plotted on Figure 5. It does fit the data when Od^2t is sufficiently large and $\Delta H/H_f$ is sufficiently small. On the other hand, it does not fit the data well for larger $\Delta H/H_f$.

To attain large values of $\Delta H/H_f$ (well in excess of unity) we require small Od. Data with small Od (e.g. $Od = 0.001$, $Od = 0.01$) do collapse together in Figure 5 but they collapse onto the Newtonian formula given by equation (28), also plotted on Figure 5. Even though equation (28) gives H/H_f rather than $\Delta H/H_f$, they are essentially the same when $\Delta H/H_f$ is large.

4 Conclusions

Viscoplastic fluids (e.g. gels, muds, pastes, emulsions, foams) are of interest because, amongst other properties, they can stop flowing much more suddenly than Newtonian fluids do. Studies on these types of fluids in the past have identified that they have the capacity to stop dead in finite time, if a driving force or a load is removed. However viscoplastic fluids can also stop moving, even when a load is maintained. In this work we looked at a squeeze film problem to explore such behaviour. What we have found is that yield stress fluids in a squeeze film require infinite time to stop, but even so their motion still decays faster than what happens with Newtonian fluids. Specifically we see a decay in the difference between instantaneous squeeze film gap thickness and final gap thickness scaling inversely with time. The Newtonian analogue however scales inversely with square root of time.

The decay towards the final thickness in yield stress fluids depends also on the Oldroyd number Od, which measures the ratio between the yield stress and the initial applied stress. For larger Od numbers i.e. larger yield stresses, the decay towards the final state is faster than for smaller Od numbers. This implies an advantage of selecting fluids with larger Od in lubrication applications: squeeze films approach a final gap thickness more rapidly, and then remain at that thickness. On the other hand, smaller values of Od lead to the system behaving, for quite some time, similar to a Newtonian fluid with its slower decay. It is then only at very long times with very small gap thicknesses that the faster than Newtonian decay in rate of squeezing becomes evident. Although the results presented here concern parallel squeeze films, it turns out they also extend to the non-parallel case (see thesis work of one of us [13] for details), albeit the calculations are less simple to perform than for the parallel case.

Statements and declarations

Competing interests

The authors have no competing interests to declare.

Funding

The authors acknowledge support from EPSRC research grant EP/V002937/1. E. Esmaeili also acknowledges support from a University of Strathclyde Student Excellence Award.

Authorship contributions

Authorship contributions are as follows: E. Esmaeili: conception of the work; acquisition, analysis and interpretation

of data; drafting the manuscript; P. Grassia: conception of the work; funding acquisition; supervision; interpretation of data; critical revision of the manuscript for important intellectual content. Both authors approved the final version of manuscript. Both authors agree to be accountable for all aspects of the work in ensuring that questions related to the accuracy or integrity of any part of the work are appropriately investigated and resolved.

Data availability

In this article, asymptotic analytical formulae have been given within the body of the article itself. These are compared with numerical data generated by algorithms described in [14]. The numerical datasets analysed here (numerical predictions for squeeze film gap thickness versus time) are available in the supplementary material (as a comma separated value file, time in the first column and gap thickness for various Oldroyd numbers in the remaining columns).

References

1. Alba K, Frigaard IA (2016) Dynamics of the removal of viscoplastic fluids from inclined pipes. Journal of non-Newtonian Fluid Mechanics 229:43–58, doi: 0.1016/j.jnnfm.2016.01.006
2. Balmforth NJ, Craster RV (1999) A consistent thin-layer theory for Bingham plastics. Journal of non-Newtonian Fluid Mechanics 84(1):65–81, doi: 10.1016/S0377-0257(98)00133-5
3. Barnes HA, Hutton JF, Walters K (1989) An introduction to rheology, 1st edn. Elsevier, Amsterdam
4. Bénito S, Bruneau CH, Colin T, Gay C, Molino F (2008) An elasto-visco-plastic model for immortal foams or emulsions. European Physical Journal E 25:225–251, doi: 10.1140/epje/i2007-10284-2
5. Bingham EC (1922) Fluidity and plasticity, vol 2. McGraw Hill, New York
6. Bonn D, Denn MM, Berthier L, Divoux T, Manneville S (2017) Yield stress materials in soft condensed matter. Reviews of Modern Physics 89:035005, doi: 10.1103/RevModPhys.89.035005
7. Chatzimina M, Georgiou GC, Argyropaidas I, Mitsoulis E, Huilgol RR (2005) Cessation of Couette and Poiseuille flows of a Bingham plastic and finite stopping times. Journal of non-Newtonian Fluid Mechanics 129(3):117–127, doi: 10.1016/j.jnnfm.2005.07.001
8. Coussot P (2005) Rheometry of pastes, suspensions, and granular materials: Applications in industry and environment. John Wiley & Sons, Hoboken, NJ, doi: 10.1002/0471720577
9. Coussot P (2014) Yield stress fluid flows: A review of experimental data. Journal of non-Newtonian Fluid Mechanics 211:31–49, doi: 10.1016/j.jnnfm.2014.05.006
10. Coussot P, Malkin AY, Ovarlez G (2017) Introduction: Yield stress – or 100 years of rheology. Rheologica Acta 56(3):161–162, doi: 10.1007/s00397-017-1003-6
11. Covey GH, Stanmore BR (1981) Use of the parallel-plate plastometer for the characterisation of viscous fluids with a yield stress. Journal of non-Newtonian Fluid Mechanics 8(3–4):249–260, doi: 10.1016/0377-0257(81)80024-9
12. Engmann J, Servais C, Burbidge AS (2005) Squeeze flow theory and applications to rheometry: A review. Journal of non-Newtonian Fluid Mechanics 132(1–3):1–27, doi: 10.1016/j.jnnfm.2005.08.007
13. Esmaeili E (2022) Squeeze film flow of viscoplastic bingham fluids. PhD thesis, Submitted to University of Strathclyde
14. Esmaeili E, Grassia P, Torres Ulloa CA (2022) Squeeze film flow of viscoplastic Bingham fluid between non-parallel plates. Journal of non-Newtonian Fluid Mechanics 305:104817, doi: 10.1016/j.jnnfm.2022.104817
15. Frigaard IA (1998) Stratified exchange flows of two Bingham fluids in an inclined slot. Journal of non-Newtonian Fluid Mechanics 78(1):61–87, doi: 10.1016/S0377-0257(98)00059-7
16. Glowinski R (1984) Numerical methods for nonlinear variational problems. Springer-Verlag, Berlin, Heidelberg, New York, Tokyo
17. Huilgol RR, Mena B, Piau JM (2002) Finite stopping time problems and rheometry of Bingham fluids. Journal of non-Newtonian Fluid Mechanics 102(1):97–107, doi: 10.1016/S0377-0257(01)00166-5
18. Karimfazli I, Frigaard IA (2016) Flow, onset and stability: Qualitative analysis of yield stress fluid flow in enclosures. Journal of non-Newtonian Fluid Mechanics 238:224–232, doi: 10.1016/j.jnnfm.2016.06.005
19. Karimfazli I, Frigaard IA, Wachs A (2015) A novel heat transfer switch using the yield stress. Journal of Fluid Mechanics 783:526–566, doi: 10.1017/jfm.2015.511
20. Koblitz AR, Lovett S, Nikiforakis N (2018) Viscoplastic squeeze flow between two identical infinite circular cylinders. Physical Review Fluids 3(2):023301, doi: 10.1103/PhysRevFluids.3.023301
21. Laidler KJ (1987) Chemical kinetics, 2nd edn. McGraw Hill, New York
22. Lorenz B, Persson BNJ (2010) Time-dependent fluid squeeze-out between solids with rough surfaces. European Physical Journal E 32:281–290, doi: 10.1140/epje/i2010-10625-0
23. Meeten GH (2000) Yield stress of structured fluids measured by squeeze flow. Rheologica Acta 39(4):399–408, doi: 10.1007/s003970000071

24. Moore DF (1965) A review of squeeze films. Wear 8(4):245–263, doi: 10.1016/0043-1648(65)90001-3
25. Mosolov PP, Miasnikov VP (1965) Variational methods in the theory of the fluidity of a viscous-plastic medium. Journal of Applied Mathematics and Mechanics 29(3):545–577, doi: 10.1016/0021-8928(65)90063-8
26. Mosolov PP, Miasnikov VP (1966) On stagnant flow regions of a viscoplastic medium in pipes. Journal of Applied Mathematics and Mechanics 30(4):841–854, 10.1016/0021-8928(66)90035-9
27. Mosolov PP, Miasnikov VP (1967) On qualitative singularities of the flow of a viscoplastic medium in pipes. Journal of Applied Mathematics and Mechanics 31(3):609–613, doi: 10.1016/0021-8928(67)90055-X
28. Muravleva L (2015) Squeeze plane flow of viscoplastic Bingham material. Journal of non-Newtonian Fluid Mechanics 220:148–161, doi: 10.1016/j.jnnfm.2015.01.012
29. Palabiyik I, Olunloyo B, Fryer PJ, Robbins PT (2014) Flow regimes in the emptying of pipes filled with a Herschel-Bulkley fluid. Chemical Engineering Research and Design 92(11):2201–2212, doi: 10.1016/j.cherd.2014.01.001
30. Papanastasiou T, Georgiou G, Alexandrou AN (2021) Viscous fluid flow. CRC Press, Boca Raton, FL, doi: 10.1201/9780367802424
31. Pinkus O, Sternlicht B (1961) Theory of hydrodynamic lubrication. McGraw Hill, New York
32. Reynolds O (1886) IV. On the theory of lubrication and its application to Mr. Beauchamp Tower's experiments, including an experimental determination of the viscosity of olive oil. Philosophical Transactions of the Royal Society of London 177:157–234, doi: 10.1098/rstl.1886.0005
33. Rognon P, Gay C (2008) Soft dynamics simulation. 1. Normal approach of two deformable particles in a viscous fluid and optimal-approach strategy. European Physical Journal E 27:253–260, doi: 10.1140/epje/i2008-10378-3
34. Rognon P, Gay C (2009) Soft dynamics simulation. 2. Elastic spheres undergoing a T1 process in a viscous fluid. European Physical Journal E 30:291–301, doi: 10.1140/epje/i2009-10528-1
35. Scott Blair GW (1933) On the nature of "yield-value". Physics 4(3):113–118, doi: 10.1063/1.1745163
36. Smyrnaios DN, Tsamopoulos JA (2001) Squeeze flow of Bingham plastics. Journal of non-Newtonian Fluid Mechanics 100(1–3):165–189, doi: 10.1016/S0377-0257(01)00141-0
37. Tichy JA (1991) Hydrodynamic lubrication theory for the Bingham plastic flow model. Journal of Rheology 35(4):477–496, doi: 10.1122/1.550231
38. Wachs A, Frigaard IA (2016) Particle settling in yield stress fluids: Limiting time, distance and applications. Journal of non-Newtonian Fluid Mechanics 238:189–204, doi: 10.1016/j.jnnfm.2016.09.002
39. Walton IC, Bittleston SH (1991) The axial flow of a Bingham plastic in a narrow eccentric annulus. Journal of Fluid Mechanics 222:39–60, doi: 10.1017/S002211209100099X
40. Wilson SDR (1993) Squeezing flow of a Bingham material. Journal of non-Newtonian Fluid Mechanics 47:211–219, doi: 10.1016/0377-0257(93)80051-C